Aus der Augenklinik und Poliklinik
der Universitätsmedizin der Johannes Gutenberg-Universität Mainz

Die Unterscheidung von Myopie und Glaukom anhand der Optischen Kohärenztomographie

Habilitationsschrift
zur Erlangung der venia legendi
für das Fach
Augenheilkunde

Universitätsmedizin der Johannes Gutenberg-Universität Mainz

vorgelegt von

Dr. med. Jasmin Rezapour
aus Landau in der Pfalz

Mainz 2025

Für meine Alice

Wissenschaftliche Originalpublikationen der kumulativen Habilitationsschrift

I. **Rezapour J**, Bowd C, Dohleman J, Belghith A, Proudfoot JA, Chrisopher M, Hyman L, Jonas JB, Fazio MA, Weinreb RN, Zangwill LM; *The influence of axial myopia on optic disc characteristics of glaucoma eyes;* Scientific reports; 2021; Apr 23;11(1):8854. doi: 10.1038/s41598-021-88406-1. PMID: 33893383 11:8854.
(Habilitationswert: B)

II. **Rezapour J**, Bowd C, Dohleman J, Belghith A, Proudfoot JA, Chrisopher M, Hyman L, Jonas JB, Fazio MA, Weinreb RN, Zangwill LM; *Bruch's membrane opening detection accuracy in healthy and glaucoma eyes with and without high myopia in an American and Korean cohort;* American Journal of Ophthalmology; 2022; May;237:221-234. doi: 0.1016/j.ajo.2021.11.030. Epub 2021 Dec 10. PMID: 34902327.
(Habilitationswert: A)

III. **Rezapour J,** Tran AQ, Bowd C, El-Nimri NW, Belghith A, Christopher M, Brye N, Proudfoot JA, Dohleman J, Fazio MA, Jonas JB, Weinreb RN, Zangwill LM; *Comparison of Optic Disc Ovality Index and Rotation Angle Measurements in Myopic Eyes Using Photography and OCT based Techniques*; Frontiers in Medicine; 2022 Jun 24;9:872658. doi: 10.3389/fmed.2022.872658. PMID: 35814778; PMCID: PMC9263212
(Habilitationswert: B)

IV. **Rezapour J**, Bowd C, Dohleman J, Belghith A, Proudfoot JA, Christopher M, Hyman L, Jonas JB, Penteado RC, Moghimi S, Hou H, Fazio MA, Weinreb RN, Zangwill LM; *Macula structural and vascular differences in glaucoma eyes with and without high axial myopia. British Journal of Ophthalmology;* 2023; Sep;107(9):1286-1294. doi: 10.1136/bjophthalmol-2021-320430. Epub 2022 Jun 20. PMID: 35725293.
(Habilitationswert: A)

V. **Rezapour J**, Walker E, Belghith A, Bowd C, Fazio MA, Jiravarnsirikul A, Hyman L, Jonas JB, Weinreb RN, Zangwill LM; *Diagnostic accuracy of optic nerve head and macula OCT parameters for detecting glaucoma in eyes with and without high axial myopia;* American Journal of Ophthalmology; 2024; Oct;266:77-91. doi: 10.1016/j.ajo.2024.04.022. Epub 2024 May 15. PMID: 38754801.
(Habilitationswert: A)

Inhaltsverzeichnis

1. Einleitung in die Thematik

Mit zunehmender Prävalenz und schätzungsweise 5 Milliarden Betroffenen (die Hälfte der Weltbevölkerung) bis zum Jahr 2050,[1] wird angesichts des erhöhten Risikos für visusbedrohende Augenerkrankungen wie myope Makulopathie, myope choroidale Neovaskularisation, Netzhautablösung und insbesondere Glaukom, die weltweite medizinische und ökonomische Belastung durch die Myopie zunehmen. Aus epidemiologischen Studien ist bekannt, dass Myopie das Risiko, am Primären Offenwinkelglaukom (POWG) zu erkranken, um das 2- bis 3-fache erhöht.[2] Einige Studien zeigen, dass die hohe Myopie (definiert anhand des sphärischen Äquivalents [SÄ] ≤ -6.0 Dioptrien [D] oder einer Achsenlänge [AL] > 26,0mm), von der ca. 1 Milliarde Menschen betroffen sein werden, das Risiko sogar um das 6-fache erhöhen kann.[1, 3]

Die Ursachen für das erhöhte Risiko sind bis heute noch nicht vollständig geklärt, Studien zeigen jedoch eine Minderperfusion im Bereich der peripapillären Choriokapillaris.[4] Die Choriokapillaris wird von den kurzen hinteren Ziliararterien versorgt, die ebenfalls die Lamina cribrosa versorgen. Mikrovaskuläre Defekte der Choriokapillaris könnten daher mit einer Minderperfusion der Lamina cribrosa und somit mit einem erhöhten Glaukomrisiko assoziiert sein.[4-7]

Die Myopie erhöht nicht nur das Risiko für POWG, sondern erschwert auch die klinische Diagnose des Glaukoms (Abbildungen 1a und 1b).

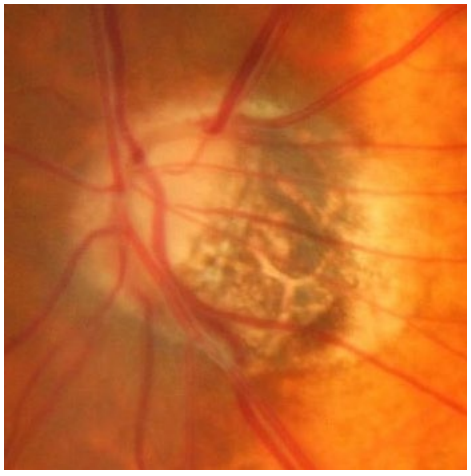

Abbildung 1a. Darstellung der Papille bei einem hoch-myopen Auge (AL=28,3mm) mit Glaukom

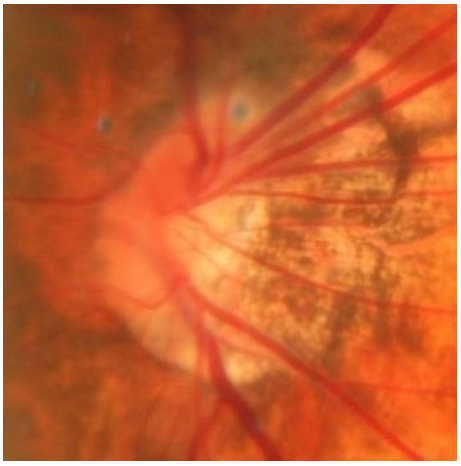

Abbildung 1b. Darstellung der Papille bei einem hoch-myopen Auge (AL=28,5mm) ohne Glaukom

Durch die axiale Elongation des Bulbus entstehen Veränderungen am hinteren Pol, einschließlich des Sehnervenkopfes (Papilla nervi optici), die eine Verkippung, Rotation, veränderte Konfiguration sowie eine vergrößerte peripapilläre Atrophiezone der Papille zur Folge haben können.[8, 9] Einige dieser Veränderungen sind häufig auch mit dem Glaukom assoziiert, andere maskieren glaukomatöse Veränderungen, sodass einerseits die klinische Diagnose eines Glaukoms erschwert wird und es andererseits auch zur Fehldiagnose eines Glaukoms bei gesunden myopen Personen kommen kann und diese in der Folge übertherapiert werden.

Seit mehr als zwei Jahrzehnten hat sich die Optische Kohärenztomographie (OCT) in der Augenheilkunde etabliert. Insbesondere in der Diagnostik und Verlaufskontrolle des Glaukoms hat sich dieses bildgebende Verfahren, welches den strukturellen Verlust der retinalen Nervenfaserschicht (RNFL) objektivierbar und reproduzierbar erfassen kann und auf dem Prinzip der niederkohärenten Interferometrie beruht, bewährt.[10] Die Fähigkeit der Differenzierung von gesunden und glaukomatösen Augen wird durch eine integrierte normative Datenbank ermöglicht, die alters- und ethnizitätsgematchte Messwerte enthält.[11]

Allerdings enthalten die normativen Datenbanken der verschiedenen OCT-Hersteller keine myopen Augen und es ist wenig über die Messgenauigkeit der Instrumente bei myopen Augen bekannt.

Das Verständnis der Anatomie des hoch-myopen Auges ist von entscheidender Bedeutung, um besser zwischen myopen und glaukomatösen Veränderungen zu unterscheiden. Dies ermöglicht eine frühzeitige Glaukomdiagnose bei myopen Menschen und kann letztendlich die medizinische Versorgung einer weltweit wachsenden Bevölkerungsgruppe verbessern.

Im Rahmen der vorliegenden kumulativen Habilitationsschrift werden anhand der fünf vorgelegten Publikationen die morphologischen Eigenschaften nicht-myoper, moderat-myoper und hoch-myoper Augen mit und ohne Glaukom untersucht und Parameter zu deren Charakterisierung entwickelt. Diese Parameter verbessern das Verständnis der Auswirkungen der axialen Elongation auf den Sehnervenkopf sowie die Makula und unterstützen schließlich eine bessere Differenzierung von glaukomatösen und myopen Veränderungen. Die Ergebnisse der vorliegenden Publikationen könnten als Grundlage für weitere Forschungsarbeiten dienen, um das Glaukom bei myopen Menschen rechtzeitig zu diagnostizieren und eine frühzeitige

Therapie einzuleiten. Zudem könnten diese Ergebnisse dazu beitragen, den Anteil der Patienten zu reduzieren, die fälschlicherweise mit einem Glaukom diagnostiziert wurden, um eine Übertherapie zu vermeiden und letztendlich die Lebensqualität zu verbessern.

2. Darstellung der Ergebnisse

2.1. Charakterisierung von glaukomatösen Augen mit und ohne hohe Myopie

2.1.1 OCT-Parameter der Papille und Makula

Papillenbefunde können durch die klinische Untersuchung charakterisiert werden, unterliegen jedoch einer subjektiven, nicht reproduzierbaren Beurteilung. Mittels der OCT können die anatomischen Eigenschaften sowohl der Papille als auch der Makula reproduzierbar und auf Basis anatomisch präziser Landmarken erfasst werden. Gleichzeitig ist das Verständnis der Verteilungsmuster etablierter Papillen- und Makula-OCT-Parameter bei myopen Augen im Vergleich zu nicht-myopen Augen erforderlich, um myopiebedingte Veränderungen besser von glaukomatösen Veränderungen unterscheiden zu können.

Dazu haben wir Papillen- und Makula-OCT-Parameter von Glaukom-Augen mit und ohne hohe Myopie ausgewertet und die Ergebnisse in ***Publikation I***[12] und ***Publikation IV***[13] *veröffentlicht*. In ***Publikation I*** wurden zudem neuartige Papillen-Parameter etabliert, die auf objektiven Landmarken basieren, die mittels der OCT erfasst wurden. Einige Berechnungen wurden anhand von selbst programmierten Modellen einer künstlichen Intelligenz durchgeführt.

In **Publikation *I*** wurden 452 Augen von 277 Glaukompatienten anhand der Achsenlänge (AL) in folgende Gruppen unterteilt:

Keine Myopie (AL < 24,0 mm; 145 Augen)

Moderate Myopie (24 mm < AL ≤ 26,0 mm; 214 Augen)

Hohe Myopie (AL > 26,0 mm; 93 Augen)

Mit Hilfe der Spectralis® OCT-Software wurden die peripapilläre retinale Nervenfaserschichtdicke (RNFL) und die Bruch'sche Membranöffnung (BMO) – minimale Randsaumbreite (engl. BMO-MRW) automatisiert gemessen.

Die neuartigen Papillen-Parameter Ovalitätsindex, Verkippungswinkel und Rotationswinkel werden mit der Standard-OCT-Software nicht gemessen. Für diese Berechnungen haben wir die BMO-Grenze als objektive Landmarke verwendet, anstelle der üblicherweise verwendeten klinischen Papillengrenze.

Die BMO-Punkte wurden mit Hilfe der eigens programmierten „SALSA“-Software (San Diego Automated Layer Segmentation Algorithm) segmentiert. Um den BMO-Ovalitätsindex zu erhalten, wurde der kürzeste BMO-Durchmesser durch den längsten geteilt. Dabei entsprach ein Wert näher an 1 einer runderen Konfiguration und ein Wert näher an 0 einer ovaleren Konfiguration.

Zur Berechnung des BMO-Verkippungswinkels (gemessen in Grad) wurden jeweils zwei Punkte, die das Ende der Bruch-Membran (BMB) und der BMO definieren, markiert (Abbildung 2a) und die BMB-Ebene sowie die BMO-Ebene in ein 3D-Koordinatensystem projiziert. Der BMO-Verkippungswinkel entsprach dem Winkel zwischen den Normalenvektoren der beiden Ebenen (Abbildung 2b). Zur Berechnung des BMO-Rotationswinkels (gemessen in Grad) wurden die BMO-Punkte auf eine BMO-Referenzebene projiziert und der Rotationswinkel relativ zur Fovea berechnet

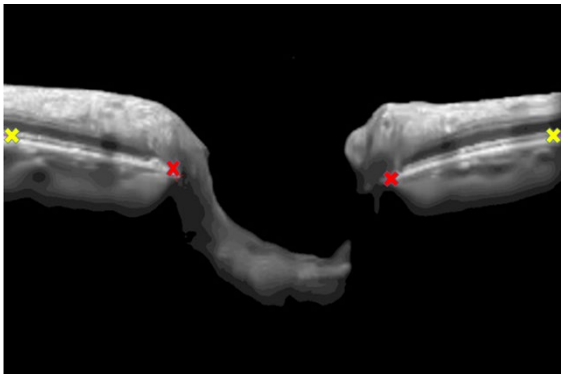

Abbildung 2a. Papillen-OCT-B-Scans mit automatisierter Markierung der Bruch’schen Membranöffnung (BMO, rote Kreuze) und dem Ende der Bruch-Membran (BMB, gelbe Kreuze)

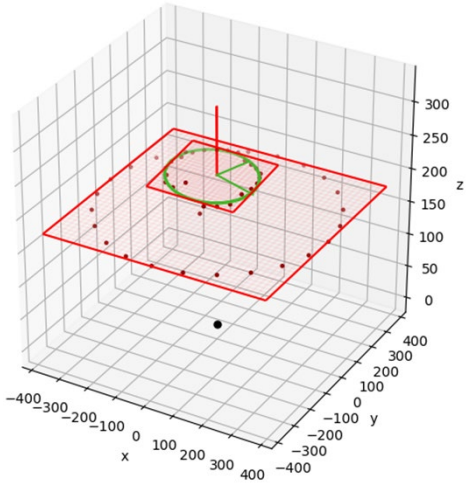

Abbildung 2b. Projektion der BMO-Ebene (grüne Ellipse) und der BMB-Ebene in ein Koordinatensystem zur Berechnung des BMO-Verkippungswinkels anhand der Normalenvektoren

Die Ergebnisse wurden für Alter und Schweregrad des Glaukoms (gemessen als mittlere Standardabweichung des Gesichtsfeldes; VFMD; *engl. visual field mean deviation*) adjustiert. Der mittlere BMO-Ovalitätsindex war für hoch-myope Augen (0,85 [95% CI: 0,84; 0,87]) statistisch signifikant kleiner als für moderat-myope (0,89 [95% CI: 0,88; 0,90]) und nicht-myope Augen (0,88 [95% CI: 0,86; 0,89]) ($p<0,003$). Der mittlere BMO-Verkippungswinkel war bei hoch-myopen Augen statistisch signifikant größer (3,4° [95% CI: 3,1; 3,8]) im Vergleich zu moderat-myopen (2,0° [95% CI: 1,8; 2,2]) und nicht-myopen Augen (1,7° [95% CI: 1,5; 2,0]) ($p<0,001$). Es gab keine

statistisch signifikanten Unterschiede zwischen den verschiedenen Myopiegruppen für den mittleren BMO-Rotationswinkel, die globale und sektorielle RNFL-Dicke und die BMO-MRW (alle p-Werte > 0,1), mit Ausnahme der temporalen RNFL (58,8 µm [55,4; 62,3] p=0,029) und der superonasalen BMO-MRW (192,0 µm [175,3; 208,8] p=0,003). Zusammenfassend konnte gezeigt werden, dass hoch-myope Papillen eine ovalere Konfiguration aufweisen und stärker verkippt sind.

Zur Untersuchung der Makula-OCT-Parameter bei Glaukom-Augen mit und ohne hohe Myopie wurden 438 Augen von 270 Glaukompatienten nach der oben beschriebenen Klassifizierung in drei Myopiegruppen eingeteilt, mit 163 Augen in der nicht-myopen Gruppe, 218 Augen in der moderat-myopen Gruppe und 57 Augen in der hoch-myopen Gruppe. Die Ergebnisse werden in ***Publikation IV*** dargestellt.

Mit Hilfe der Spectralis® OCT-Software wurden horizontale „Posterior-Pole“ („P-Pole“) Scans der Makula mit einer Fläche von 30°x25° (6x6 mm) durchgeführt. Die retinale Schichtdicke der inneren plexiformen Ganglienzellschicht (GCIPL), der makulären RNFL sowie des Ganglienzellkomplexes (GCC, bestehend aus der GCIPL und der makulären RNFL) wurden entsprechend der sektoriellen Einteilung der Early Treatment Diabetic Retinopathy Study[14] gemessen (siehe ***Publikation IV***).[13]

Das Verteilungsmuster der globalen und sektoriellen GCIPL-Dicke und der GCC-Dicke war in allen drei Myopiegruppen ähnlich (alle p-Werte > 0,17). Die globale makuläre RNFL sowie alle Sektoren der makulären RNFL waren in der hoch-myopen Gruppe nicht-signifikant dicker (alle p-Werte < 0,137) und signifikant dicker im äußeren superioren Ringsektor (p=0,013) (Abbildung 3).

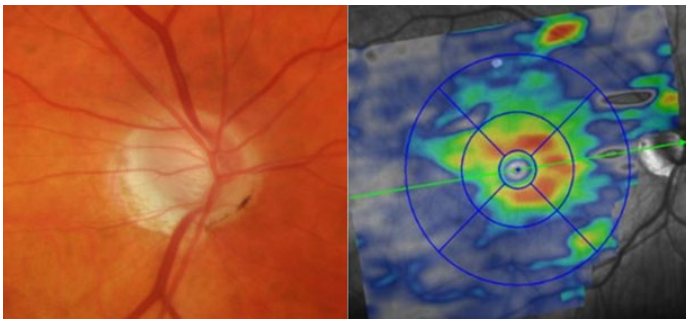

Abbildung 3. Illustration einer hoch-myopen glaukomatösen Papille (links im Bild) und der korrespondierenden Makula-OCT(„Posterior Pole“-Scan) (rechts im Bild) mit Reduktion der Ganglienzellschicht temporal unten

2.1.1.2 Vergleichbarkeit von Papillen-Parametern gemessen mit Hilfe der OCT und Papillen-Fotos

Die Papillenmorphologie wurde bereits in zahlreichen Publikationen anhand von Parametern wie dem Ovalitätsindex, dem Verkippungswinkel und dem Rotationswinkel (in der Literatur auch als Torsionswinkel bezeichnet) charakterisiert und quantifiziert.[8, 15-18] Allerdings wurden diese Parameter in den bisherigen Studien manuell auf zweidimensionalen Fundusfotos gemessen.

Aufgrund der unterschiedlichen Methodik zur Berechnung der gleichen Papillenparameter haben wir untersucht, ob diese miteinander vergleichbar sind (**Publikation *III).***[19] Hierzu haben wir Papillenparameter, die anhand von OCT-Landmarken berechnet wurden, mit Papillenparameter, die anhand der klinischen Beurteilung von zweidimensionalen Fundusfotos berechnet wurden, verglichen.

175 gesunde Augen und 146 Glaukomaugen wurden anhand der Achsenlänge in die oben definierten Myopiegruppen eingeteilt, wobei 56 Augen der Gruppe ohne Myopie, 58 Augen der Gruppe mit moderater Myopie und 32 Augen der hoch-myopen Gruppe zugeordnet wurden. Zur manuellen Berechnung von Papillenparametern wurde die Bildverarbeitungssoftware ImageJ® verwendet. ImageJ® ermöglicht eine halbautomatisierte Bildbearbeitung und -analyse. Zur Berechnung des Ovalitätsindex auf Basis der Fundusfotos wurde die klinische Papillengrenze manuell mit der ImageJ®-Software markiert und die kleinste Achse durch die größte Achse dividiert, die jeweils von der Software ermittelt wurde (Abbildung 4) (Details siehe ***Publikation III)***. Die OCT-basierte Methodik zur Berechnung des Ovalitätsindex wurde bereits in Kapitel 2.1.1 (**Publikation *I***) erläutert.

Die manuelle Markierung der klinischen Papillengrenze sowie die Ermittlung der größten und kleinsten Achse dienten ebenfalls als Grundlage für die Berechnung des fotobasierten Rotationswinkels. Der Rotationswinkel wurde definiert als der Winkel zwischen der größten Achse und einer vertikalen Achse (Abbildung 4*)* (Details siehe ***Publikation III)***. Die OCT-basierte Methodik zur Berechnung des Rotationswinkels wurde bereits in Kapitel 2.1.1 (**Publikation *I***) erläutert.

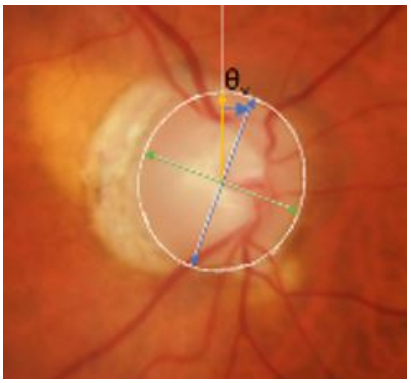

Abbildung 4. Papillenfoto mit manueller Markierung der klinischen Papillengrenze (weißer Kreis) sowie automatisierter Ermittlung der größten (blauer Pfeil) und kleinsten Achse (grüner Pfeil) und Ermittlung des Rotationswinkels (θ, zwischen gelbem und blauem Pfeil)

Der auf Fundusfotos basierende Ovalitätsindex betrug im Durchschnitt 0,89 für nicht-myope Augen, 0,90 für moderat-myope Augen und 0,85 für hoch-myope Augen (VFMD und altersgematcht: p=0,002).

Der OCT-basierte Ovalitätsindex betrug durchschnittlich 0,88 für nicht-myope Augen, 0,88 für moderat-myope Augen und 0,84 für hoch-myope Augen (VFMD und altersgematcht: p=0,008).

Es konnte gezeigt werden, dass zwar eine signifikante, aber sehr schwache Korrelation zwischen fotobasierten und OCT-basierten Messungen für alle Augen bestand (R^2=0,26; p<0,001).

Der auf Fundusfotos basierende Rotationswinkel betrug durchschnittlich 15,2° für nicht-myope Augen, 19,9° für moderat-myope Augen und 20,9° für hoch-myope Augen (p=0,078).

Der OCT-basierte Rotationswinkel lag durchschnittlich bei 35,9° für nicht-myope Augen, 34,4° Grad für moderat-myope Augen und 33,7° für hoch-myope Augen (p=0,83).

Es gab keine signifikante Korrelation zwischen fotobasierten und OCT-basierten Messungen des Rotationswinkels (R^2-Werte von 0,00 [nicht-myop] bis 0,03 [hoch-myop], alle p≥0,33).

2.1.1.3 Evaluation der Messgenauigkeit der OCT bei hoch-myopen Augen

Aufgrund der in Kapitel 2.1.1 (***Publikation I***) beschriebenen morphologischen Veränderungen der hoch-myopen Papille ist die Glaukomdiagnose oft schwierig und nicht präzise. Diese strukturellen Veränderungen stellen ebenfalls eine große Herausforderung für die Diagnose und Verlaufskontrolle des Glaukoms mittels OCT dar.

Die akkurate Messung der peripapillären RNFL und auch der BMO-MRW mittels OCT basiert auf der korrekten Lokalisation der BMO. In ***Publikation II***[20] haben wir untersucht, wie präzise die OCT-basierte Lokalisation der BMO bei hoch-myopen Augen ist und wie hoch die Wahrscheinlichkeit von nicht lokalisierbaren BMO-Punkten ist. Außerdem wurde untersucht, welche Parameter mit einer Messungenauigkeit der BMO assoziiert sind.

In dieser Studie wurden 551 gesunde und glaukomatöse Augen von 344 Probanden einer amerikanischen und koreanischen Studienpopulation anhand ihrer Achsenlänge in eine Gruppe ohne hohe Myopie (AL≤26mm; 438 Augen) und eine Gruppe mit hoher Myopie (AL>26mm; 113 Augen) eingeteilt.

In der Gruppe der gesunden Augen ohne axiale Myopie wurden bei 106 Augen (87,6 %) die BMO-Punkte durch die OCT-Software automatisch korrekt lokalisiert, bei 13 Augen (10,7 %) mussten die BMO-Punkte manuell korrigiert werden und bei 2 Augen (1,7 %) konnten die BMO-Punkte nicht lokalisiert werden. Bei gesunden Augen mit hoher axialer Myopie wurden die BMO-Punkte hingegen bei 18 Augen (54,5 %) automatisch korrekt lokalisiert, bei 12 Augen (36,4 %) konnten sie manuell korrigiert werden und bei 3 Augen (9,1 %) waren die BMO-Punkte nicht lokalisierbar.

In der Glaukomgruppe ohne hohe Myopie waren die BMO-Punkte bei 186 Augen (58,7 %) automatisch korrekt lokalisiert, bei 121 Augen (38,2 %) manuell korrigierbar und bei 10 Augen (3,2 %) nicht lokalisierbar, während in der Glaukomgruppe mit hoher axialer Myopie die BMO-Punkte bei 14 Augen (30,0 %) automatisch korrekt lokalisiert wurden, bei 44 Augen (55,0 %) manuell korrigiert werden konnten und bei 12 Augen (15,0 %) nicht lokalisierbar waren.

Der Anteil nicht lokalisierbarer BMO bei Augen mit hoher Myopie war signifikant höher als bei Augen ohne hohe Myopie, sowohl in der gesunden Gruppe (9,1 % vs. 1,7 %; p=0,17) als auch in der Glaukomgruppe (15,0 % vs. 3,2 %; p=0,005) (Abbildung 5).

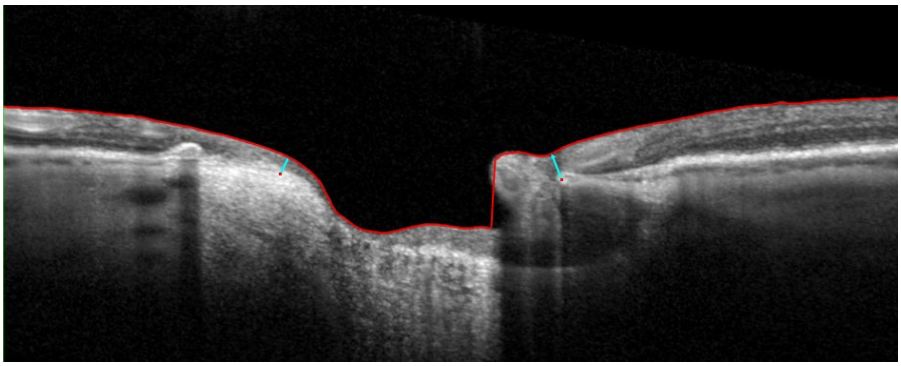

Abbildung 5. Papillen-OCT-B-Scan einer hoch-myopen Papille mit inkorrekter Lokalisation der BMO (roter Punkt, links im Bild)

In univariaten Regressionsanalysen war die Achsenlänge (sowohl als kontinuierliche als auch als kategoriale Variable) ein starker Prädiktor für Ungenauigkeiten der BMO-Lokalisation. Augen mit hoher Myopie hatten ein 3-fach höheres Risiko ($p<0,001$) für eine initiale Fehllokalisation der BMO. Weitere Parameter für ein erhöhtes Risiko einer BMO-Ungenauigkeit waren ein kleinerer BMO-Ovalitätsindex (eine ovalere BMO-Konfiguration), ein größerer BMO-Verkippungswinkel, eine größere BMO-Fläche und eine geringere globale BMO-MRW (Details siehe ***Publikation II***).[20] In multivariaten Regressionsanalysen waren die Achsenlänge, der BMO-Ovalitätsindex und der BMO-Verkippungswinkel signifikante Prädiktoren für eine BMO-Lokalisationsungenauigkeit (Details siehe ***Publikation II***).[20]

Eine qualitative Auswertung der OCT-B-Scans der 27 Augen mit nicht lokalisierbarer BMO zeigte, dass bei hoch-myopen Augen die BMO häufiger im temporalen Sektor (43,5 %) als im nasalen Sektor (26,3 %) nicht lokalisiert werden konnte und dass 80 % der Augen eine klinisch sichtbare peripapilläre Atrophiezone aufwiesen. In der Gruppe nicht hoch-myoper Augen war der Anteil gleichmäßig auf den temporalen (27,1 %) und nasalen Sektor (26,3 %) verteilt und bei 30,3 % der Augen konnte die BMO aufgrund von Gefäßverschattungen nicht korrekt lokalisiert werden.

2.1.2 Vaskuläre Parameter und peripapilläre und makuläre Aderhautdicke

Frühere OCT-Angiographie (OCTA)-Studien zeigten eine starke Assoziation zwischen der makulären Kapillardichte und dem Schweregrad des Glaukoms.[21, 22] Die OCTA ist eine Weiterentwicklung der OCT, mit der Fähigkeit der non-invasiven Darstellung der Gefäße der Netzhaut und Aderhaut. Um die Verteilungsmuster der makulären Gefäßdichte sowie der makulären und peripapillären Aderhautdicke bei myopen Augen und die Assoziation dieser Parameter mit Myopie und Glaukom besser zu

verstehen, haben wir diese Parameter in ***Publikation I***[12] *und* ***Publikation IV***[23] untersucht.

Details zur Studienpopulation wurden bereits in Kapitel 2.1.1 beschrieben. Die oberflächliche makuläre Gefäßdichte wurde mittels der Avanti-AngioVue® OCTA (Optovue, Inc.) analysiert und anhand eines 3x3 mm² großen, foveazentrierten Makula-Scans gemessen. Es wurden die gesamte Gefäßdichte, die des temporalen, superioren, nasalen und inferioren Sektors sowie die parafoveale Gefäßdichte berechnet. Die parafoveale Gefäßdichte wurde innerhalb eines auf die Fovea zentrierten Ringes mit einem Innendurchmesser von 1 mm und einem Außendurchmesser von 2,5 mm berechnet.

Da die Aderhautdicke in der Standardsoftware der OCT-Hersteller nicht verfügbar ist, wurde eine hauseigene, auf Deep Learning basierende Software entwickelt, der „San Diego Automated Layer Segmentation Algorithm-Deep (SALSA-Deep)“.[12] Hierfür wurden der Bruch Membran/Retinaler Pigmentepithel-Komplex sowie die posteriore Begrenzung der Aderhaut von einem geschulten Grader (JR) manuell segmentiert und als Grundlage für das Training eines neuronalen Netzwerkes verwendet (Details siehe ***Publikationen I*** und ***IV***).[12, 13]

In ***Publikation IV*** konnte tendenziell eine höhere oberflächliche Gefäßdichte bei nicht-myopen Augen im Vergleich zu hoch-myopen Augen gezeigt werden. Eine statistische Signifikanz wurde jedoch nur im nasalen Sektor erreicht (44,4 % [34,6; 45,3] und 43,1 % [41,2; 45,0], p=0,0049). Die makuläre Aderhautdicke war in allen Sektoren bei hoch-myopen Augen signifikant dünner (alle p-Werte<0,001) und lag in der nicht-myopen Gruppe zwischen 125,4 µm und 191,2 µm, in der moderat-myopen Gruppe zwischen 107,5 µm und 188,9 µm und in der hoch-myopen Gruppe zwischen 70,8 µm und 145,4 µm (Details siehe ***Publikation IV***).
Die peripapilläre Aderhautdicke war bei hoch-myopen Augen ebenfalls signifikant dünner als bei moderat- und nicht-myopen Augen (p<0,001) (Abbildung 6a und 6b). Die sektoralen Verteilungsmuster waren bei nicht-myopen, moderat-myopen und hoch-myopen Augen ähnlich und waren im inferotemporalen Sektor am dünnsten (106,5 µm vs. 95,1 µm vs. 82,7 µm) und im superonasalen Sektor am dicksten (152,8 µm vs. 140,9 µm vs. 128,7 µm) (Details siehe ***Publikation I***).[12]

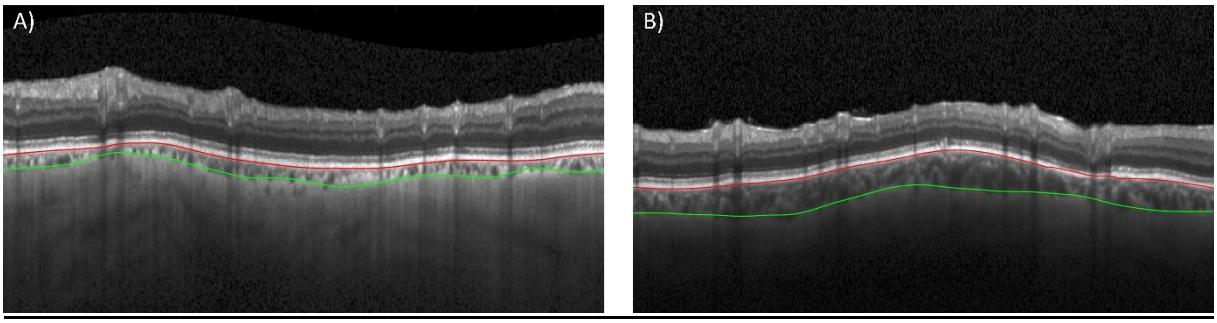

Abbildung 6. Segmentierung der peripapillären Aderhautdicke (zwischen roter und grüner Markierung) eines hochmyopen (6A) und nicht-myopen Auges (6B)

2.1.3 Assoziation von OCT-Parametern und OCTA-Parametern mit Myopie und Glaukom

Um klinisch relevante Parameter für die Glaukomdiagnose bei stark kurzsichtigen Augen zu identifizieren, wurde in ***Publikation I*** und ***IV*** die Beziehung zwischen der Dicke verschiedener papillärer und makulärer Netzhautschichten, neuartigen papillären OCT-Parametern, der Gefäßdichte (sVD) der Makula und der peripapillären und makulären Aderhautdicke mit der Myopie (gemessen anhand der Achsenlänge) und dem Schweregrad des Glaukoms (VFMD) untersucht.

In der multivariaten Regressionsanalyse zeigte der BMO-Verkippungswinkel eine statistisch signifikante, aber schwache bis moderate Assoziation mit der Achsenlänge (R^2=10,4%; p<0,001) und keine signifikante Assoziation mit der VFMD (R^2=0,9%; p=0,072), während der BMO-Ovalitätsindex und der BMO-Rotationswinkel keine statistisch signifikante Assoziation mit der Achsenlänge (p=0,289 und p=0,947) und der VFMD (p=0,307 und p=0,489) zeigten.
Betrachtet man die in der OCT messbaren papillären und makulären Netzhautschichten, so konnte gezeigt werden, dass die peripapilläre RNFL nicht statistisch signifikant mit der Achsenlänge assoziiert war (R^2=0%; p=0,966), außer im temporalen Sektor (R^2=2,1%; p=0,006), jedoch in allen Sektoren eine starke statistisch signifikante Assoziation mit der VFMD aufwies (R^2 zwischen 7,3 % und 25,9 %; alle p-Werte<0,001). Auch die BMO-MRW zeigte eine starke statistisch signifikante Assoziation mit der VFMD (R^2 zwischen 10,6 % und 23,8 %; alle p-Werte<0,001) und keine statistisch signifikante Assoziation mit der Achsenlänge, außer im superonasalen und inferonasalen Sektor (R^2=1,9%; p=0,012 bzw. R^2=1.2%; p=0,046).[12]

Sowohl die peripapilläre als auch die makuläre Aderhautdicke waren nicht statistisch signifikant mit der VFMD assoziiert (alle p-Werte>0,6), zeigten jedoch in allen Sektoren eine statistisch signifikante Assoziation mit der Achsenlänge. Mit zunehmender Achsenlänge war die Aderhautdicke signifikant dünner (R^2 zwischen 4,0 % und 19,8 %; alle p-Werte<0,001).[12, 13]
Alle untersuchten makulären Netzhautparameter wie GCIPL, GCC und makuläre RNFL waren statistisch signifikant mit dem Glaukomschweregrad und nicht mit Myopie assoziiert. Die makuläre RNFL zeigte eine statistisch signifikante Assoziation mit der VFMD in allen Sektoren außer dem inneren nasalen und temporalen Sektor (p>0,088) (Details siehe ***Publikation IV***).[13]

Die makuläre Gefäßdichte war statistisch signifikant, jedoch nur schwach mit der Achsenlänge assoziiert (R^2≤2,7%; p<0,04) und zeigte eine starke statistisch signifikante Assoziation mit schlechterer VFMD (R^2 zwischen 17,2 % und 33,5 %; alle p-Werte<0,001).[13]

2.2 Charakterisierung von gesunden und glaukomatösen Augen mit und ohne hohe Myopie

2.2.1 OCT-Parameter der Papille und Makula bei gesunden und glaukomatösen Augen mit und ohne hohe Myopie

Um genauere diagnostische Parameter zur Differenzierung von Myopie und Glaukom zu identifizieren, ist es erforderlich, sowohl Glaukomaugen als auch gesunde Augen mit und ohne hohe Myopie zu untersuchen. In ***Publikation V***[24] wurden Probanden ohne Glaukom rekrutiert, um strukturelle Unterschiede zu identifizieren und die diagnostische Wertigkeit von Papillen- und Makula-OCT-Parametern zur Identifikation von Glaukom in hoch-myopen Augen zu analysieren.

Insgesamt wurden 885 Glaukomaugen und 767 gesunde Augen in diese Studie eingeschlossen und die Einteilung in die drei Myopiegruppen erfolgte, wie oben beschrieben, anhand der Achsenlänge. Alle p-Werte wurden für Alter, VFMD und Bildqualität adjustiert. Details zur OCT-Diagnostik wurden bereits in Kapitel 2.1.1 (***Publikation I*** und ***IV***)[12, 13] erläutert.

In allen drei Myopiegruppen waren die Werte der globalen peripapillären RNFL und der BMO-MRW bei den gesunden Augen statistisch signifikant höher als bei den Glaukomaugen (alle p-Werte≤0,01). Alle globalen und sektoriellen GCIPL-Werte waren in den drei Myopiegruppen bei gesunden Augen ebenfalls statistisch signifikant dicker als bei Glaukomaugen (alle p-Werte≤0,013), außer im nasalen Sektor, wo keine statistische Signifikanz bei nicht-myopen und moderat-myopen Augen bestand (p≥0,211). Unabhängig von der Myopiegruppe und der Diagnose wiesen alle Augen die dickste GCIPL im inneren superioren Sektor und die dünnste GCIPL im äußeren inferioren Sektor auf. Die globale makuläre RNFL war in allen drei Myopiegruppen bei gesunden Augen statistisch signifikant dicker als bei Glaukomaugen (p<0,001), mit Ausnahme des inneren Rings bei nicht-myopen und moderat-myopen Augen (insbesondere des inneren nasalen Sektors in der Gruppe ohne Myopie und des inneren temporalen Sektors in der Gruppe mit moderater Myopie) (Details siehe Abbildungen 1 bis 4, **Publikation *V***).[24]

2.2.2 Diagnostische Genauigkeit von OCT-Parametern der Papille und Makula

Die diagnostische Genauigkeit der Glaukomerkennung wurde anhand der Fläche (AUC, *engl.* „area under the curve“) unter der ROC-Kurve (*engl.* „receiver operating characteristic“) quantifiziert. Alle AUC-Werte wurden für Alter, VFMD und Bildqualität adjustiert (Details siehe ***Publikation V***).[24]

Die diagnostische Genauigkeit für die Erkennung von Glaukom variierte je nach spezifischem Papillen-OCT-Parameter, Sektor und Myopiegruppe.

Bei hoch-myopen Augen war die diagnostische Genauigkeit für die globale peripapilläre RNFL (AUC=0,95) und die inferotemporale peripapilläre RNFL (AUC=0,91) am höchsten. Bei nicht-myopen und moderat-myopen Augen war die diagnostische Genauigkeit für die globale BMO-MRW (AUC=1,00 bzw. 0,97) am höchsten. Bei hoch-myopen Augen war die diagnostische Genauigkeit für die BMO-MRW geringer (AUC=0,89). Die diagnostische Genauigkeit der sektoriellen peripapillären RNFL bei hoch-myopen Augen war am höchsten (AUC-Werte reichten von 0,74 bis 0,91), gefolgt von nicht-myopen Augen und moderat-myopen Augen (AUC-Werte reichten von 0,64 bis 0,83 bzw. von 0,63 bis 0,83) (Details siehe Tabelle 2 und 3, ***Publikation V***).[24]

Die diagnostische Genauigkeit der Makula-OCT-Parameter variierte ebenfalls nach Sektor und Myopiegruppe. In allen Myopiegruppen war die diagnostische Genauigkeit der GCIPL höher als die der makulären RNFL, mit Ausnahme der äußeren nasalen und äußeren inferioren Sektoren. Bei hoch-myopen Augen war die diagnostische Genauigkeit der globalen GCIPL sowie der inneren und äußeren Ringsektoren der GCIPL höher (AUC=0,91; 0,90 und 0,91) als die der globalen makulären RNFL und der inneren und äußeren Ringsektoren der makulären RNFL (AUC=0,84; 0,71 und 0,89).

Die diagnostische Genauigkeit für GCIPL und die makuläre RNFL war tendenziell niedriger bei nicht- und moderat-myopen Augen (AUC-Werte reichten von 0,59 bis 0,83 bzw. von 0,52 bis 0,80) im Vergleich zu hoch-myopen Augen (AUC-Werte reichten von 0,52 bis 0,92) (Details siehe Tabelle 4, Tabelle 5 und Abbildung 5, ***Publikation V***).[24]

3.Übergreifende Diskussion

3.1 Diagnostischer Fallstrick Myopie und Glaukom

Myope, insbesondere hoch-myope Patienten, stellen bis heute eine große Herausforderung in der Diagnostik und Therapie des Glaukoms dar. Durch die morphologischen Veränderungen im Rahmen der axialen Elongation ist die klinische Diagnose des Glaukoms erschwert und bildgebende Verfahren wie die OCT können nur bedingt eingesetzt werden. Dies liegt zum einen daran, dass hoch-myope Augen nicht in den Referenzdatenbanken der verschiedenen Instrumenten-Softwares enthalten sind, zum anderen ist die Interpretation der Messwerte aufgrund der besonderen Verteilungsmuster erschwert. Auch über die Messgenauigkeit der OCT bei myopen Augen liegen bisher nur wenige Informationen vor.

Um unser Verständnis der Anatomie des myopen Auges zu erweitern und insbesondere die Differenzierung zum Glaukom zu verbessern, ist es zunächst erforderlich, den Einfluss der Myopie auf die Morphologie der Papille und Makula zu klären.

In den vorliegenden Publikationen haben wir zunächst Glaukomaugen unterschiedlicher Achsenlänge untersucht und Unterschiede in der Morphologie der Papille und Makula mittels OCT-Messungen untersucht. Diese Ergebnisse tragen zu einem besseren Verständnis der Anatomie des hoch-myopen Auges bei.

Da in älteren Publikationen andere Messmethoden zur Charakterisierung der Papille verwendet wurden, haben wir zudem untersucht, inwieweit verschiedene Messmethoden miteinander verglichen werden können und wie zuverlässig die OCT-Diagnostik bei hoch-myopen Augen ist.

Abschließend haben wir die OCT-Parameter bei gesunden und glaukomatösen Augen mit unterschiedlichen Achsenlängen untersucht und die diagnostische Genauigkeit dieser Parameter beurteilt.

3.2 Strukturelle Papillen- und Makula-OCT-Parameter und deren Assoziation mit Myopie und Glaukom

In ***Publikation I und IV*** wurden Glaukomaugen mit und ohne hohe Myopie anhand von OCT-Parametern charakterisiert und die Assoziation mit Myopie und Glaukom untersucht.

Publikation I unterscheidet sich von den meisten vorangegangenen Studien dadurch, dass automatisierte Vermessungen der Papille durchgeführt wurden. Als Landmarke diente die BMO und nicht wie in früheren Publikationen die klinische Papillengrenze. Die BMO kann nur mittels der OCT erfasst werden. Der Vorteil liegt in der Objektivierbarkeit sowie der Reproduzierbarkeit der Messwerte, während die klinische Papillengrenze der subjektiven Beurteilung unterliegt und insbesondere bei myopen Papillen eine hohe Messvariabilität zwischen den Untersuchenden besteht. Außerdem sind bis heute keine festen anatomischen Grenzstrukturen bzw. Landmarken für die Beurteilung der klinischen Papillengrenze bekannt.

In unserer Arbeit konnte gezeigt werden, dass Glaukomaugen mit hoher Myopie im Vergleich zu nicht-myopen Augen einen höheren BMO-Verkippungswinkel und einen niedrigeren BMO-Ovalitätsindex aufwiesen, d. h. myopen Papillen waren stärker verkippt und ovaler. Es wird vermutet, dass der Grad der Papillenverkippung ein Hinweis auf anatomische und biomechanische Veränderungen des Sehnervs während der axialen Elongation sein könnte, weshalb dieser Parameter unter anderem die erhöhte Prävalenz des Glaukoms erklären könnte.[25, 26] Im Gegensatz zum Ovalitätsindex zeigte der Verkippungswinkel eine schwache bis moderate Assoziation mit der Achsenlänge. Die Ergebnisse der bisherigen Studien sind inkonsistent und einige Studien zeigten eine Assoziation zwischen der (erhöhten) Achsenlänge und dem Grad der Ovalität.[27-33] Allerdings wurde der Grad der Ovalität in den meisten Studien anhand der klinischen Papillengrenze auf Papillenfotos erfasst.[8, 30, 32-34] Um ein besseres Verständnis der zugrundeliegenden Anatomie zu erhalten, wurde in unserer Publikation eine automatisierte Auswertung von OCT-Scans vorgenommen. Zudem variierte die Definition der Myopie in den meisten Studien erheblich. In vielen Publikationen wurde die Myopie anhand des sphärischen Äquivalents und nicht anhand der Achsenlänge definiert. Nakanishi et al. untersuchten in ihrer Arbeit den Ovalitätsindex sowohl anhand der klinischen Papillengrenze als auch anhand der BMO-Grenze und stellten fest, dass der Ovalitätsindex, gemessen anhand der

klinischen Papillengrenze, mit der Achsenlänge assoziiert war, jedoch nicht gemessen anhand der BMO-Grenze.[35] Auch histopathologische Untersuchungen von hoch-myopen Augen zeigten, dass die BMO-Grenze nicht ovaler war als bei nicht-myopen Augen.[9] Diese Ergebnisse stimmen mit unseren Ergebnissen, dass es keine Assoziation zwischen dem BMO-basierten Ovalitätsindex und der Achsenlänge gab, überein.

Wir fanden heraus, dass hoch-myope Papillen stärker verkippt waren und dass der BMO-basierte Verkippungswinkel mit der Achsenlänge, aber nicht mit dem Glaukom assoziiert war. Dies impliziert, dass ein höherer Grad der Verkippung charakteristisch für die Myopie und kein Indikator für das Vorliegen eines Glaukoms ist.

Die vorliegenden Ergebnisse sind mit der vorhandenen Literatur schwer vergleichbar, da der Verkippungswinkel unterschiedlich definiert wurde. In einigen Publikationen wurde nicht der tatsächliche Verkippungswinkel gemessen, sondern der Ovalitätsindex als Indikator für die Verkippung definiert.[8, 33, 34] In anderen Studien wurde der Verkippungswinkel indirekt gemessen, indem die klinische Papillengrenze auf das OCT-Nervenfaserhöhenprofil projiziert wurde.[28, 30, 36, 37] Auch diese Ergebnisse können nicht mit unseren Resultaten verglichen werden, da hier die dreidimensionale Information fehlt, die durch die direkte Messung von OCT-Scans verfügbar ist.

BMO-Rotationswinkel, globale RNFL und globale BMO-MRW waren in allen drei Myopiegruppen gleich und zeigten keine signifikante Assoziation mit der Achsenlänge, mit Ausnahme des temporalen RNFL-Sektors und des superonasalen BMO-MRW-Sektors.

Unsere Ergebnisse für den BMO-Rotationswinkel, wie auch für den BMO-Ovalitätindex und den BMO-Verkippungswinkel, können nicht mit den Ergebnissen aus der vorliegenden Literatur verglichen werden, da in unserer Arbeit eine dreidimensionale Messung des Rotationswinkels anhand von OCT-Scans erfolgte. In der Literatur wird der Rotationswinkel, häufig auch als „Torsionswinkel“ bezeichnet, anhand von zweidimensionalen Fundusfotos gemessen, indem der Winkel zwischen der größten Achse der Papille und einem vertikalen Meridian gemessen wird.[8, 28-31, 36] Insbesondere bei hoch-myopen Augen kann es bei der Abschätzung der größten Achse der Papille auf zweidimensionalen Fundusfotos aufgrund des schrägen Einblicks auf die Papille zu leichten Abweichungen von der tatsächlichen Größe kommen.[38] In unserer Studie war der BMO-Rotationswinkel weder mit der

Achsenlänge noch mit der VFMD assoziiert und ist daher weder für die Myopie noch für das Glaukom charakteristisch.

Um die Zuverlässigkeit etablierter Papillen-OCT-Parameter wie der peripapillären RNFL und der BMO-MRW zu evaluieren, haben wir diese in den verschiedenen Myopiegruppen gemessen und untersucht, ob eine Assoziation mit der Achsenlänge und dem Glaukom besteht.

Für beide Parameter gab es keine statistisch signifikanten Unterschiede zwischen den drei Myopiegruppen und es konnte keine Assoziation mit der Achsenlänge gezeigt werden. Sowohl die RNFL als auch die BMO-MRW zeigten eine starke statistisch signifikante Assoziation mit dem Schweregrad des Glaukoms (VFMD). Allerdings sollte bei der Interpretation der RNFL und der BMO-MRW das im Vergleich zu emmetropen Augen unterschiedliche sektorielle Verteilungsmuster berücksichtigt werden.[15, 39] In unserer Analyse nahm die temporale RNFL-Dicke mit zunehmender Achsenlänge zu und die nasale BMO-MRW ab, was sich mit den Ergebnissen anderer Publikationen deckt, in denen eine dickere RNFL im temporalen Sektor nachgewiesen werden konnte. Es ist anzunehmen, dass diese Umverteilung des Nervenfaserprofils unter anderem durch die Verkippung des Sehnervenkopfes bei myopen Augen erklärt werden kann.[15, 39] Da die Referenzdatenbanken der unterschiedlichen OCT-Hersteller keine hoch-myopen Augen enthalten, kann dies zu einer höheren Rate falsch positiver Ergebnisse führen.[40, 41]

Aufgrund der unterschiedlichen Verteilungsmuster in der Papillen-OCT und des Fehlens hoch-myoper Augen in den OCT-Referenzdatenbanken haben wir in ***Publikation IV*** makuläre Parameter zur Differenzierung von Myopie und Glaukom untersucht. Mit ca. 50 % aller retinalen Ganglienzellen in der Fovea bietet sich die Untersuchung der Makula für die Glaukomdiagnostik an.[42] Zudem betreffen die morphologischen Veränderungen durch die axiale Elongation primär den Sehnervenkopf, sodass die makuläre Region für die Glaukomdiagnostik bei hoch-myopen Augen besser geeignet sein könnte. Allerdings sind die topographischen Verteilungsmuster der verschiedenen Netzhautschichten bei myopen Augen ebenfalls noch nicht gut untersucht. Um das topographische Profil besser zu verstehen, haben wir Makula-OCT-Parameter wie die innere plexiforme Schicht (GCIPL) und den Ganglienzellkomplex (GCC) sowie die makuläre RNFL-Dicke analysiert und ihre Assoziation mit Myopie und Glaukom untersucht.

Unsere Ergebnisse zeigten, dass Makula-OCT-Parameter für die Diagnose und das Monitoring des Glaukoms bei myopen Patienten hilfreich sein könnten, da diese Parameter stark signifikant mit dem Glaukom, nicht jedoch mit der Myopie assoziiert waren. Sowohl die GCIPL als auch der GCC zeigten eine starke statistisch signifikante Assoziation mit dem Glaukom und keine Assoziation mit der Myopie (gemessen anhand der Achsenlänge). Die makuläre RNFL zeigte eine schwache, aber statistisch signifikante Assoziation mit der Myopie und eine moderate statistisch signifikante Assoziation mit dem Glaukom. Yang et al. zeigten bereits die hohe diagnostische Genauigkeit der GCIPL bei nicht-myopen Patienten mit vergleichbaren Ergebnissen zur peripapillären RNFL.[43] Diese Ergebnisse konnten von anderen Autoren auch für myope Patienten bestätigt werden. Shoji et al. zeigten sogar, dass die GCIPL bei myopen Patienten eine höhere diagnostische Genauigkeit aufwies als die peripapilläre RNFL.[44] In einer weiteren Studie zeigten die gleichen Autoren, dass der Ganglienzellkomplex ebenfalls eine hohe diagnostische Genauigkeit bei myopen und nicht-myopen Patienten aufwies und dass der Ganglienzellkomplex nicht mit Myopie assoziiert war.[45] Wir haben in unserer Arbeit den Ganglienzellkomplex mit der OCT-Software von zwei unterschiedlichen Instrumentenherstellern (Spectralis® von Heidelberg Engineering und Avanti-AngioVue® von Optovue, Inc.) gemessen und konnten ähnliche Ergebnisse zeigen. Sowohl unsere Ergebnisse als auch die Daten aus der Literatur[44-46] implizieren, dass die Makula-Parameter, insbesondere die GCIPL und der Ganglienzellkomplex, weniger empfindlich auf strukturelle Veränderungen im Rahmen der axialen Elongation reagieren und für das Glaukom-Screening bei hoch-myopen Patienten geeignet sein könnten. Allerdings wurden weder in unserer noch in den vorliegenden Studien gesunde hoch-myope Augen eingeschlossen.

3.3 Vaskuläre Papillen- und Makula-Parameter und deren Assoziation mit Myopie und Glaukom

In einigen Studien konnte bereits ein Zusammenhang zwischen dem Glaukomschweregrad und der mittels der OCTA gemessenen kapillären Gefäßdichte im Bereich der Makula gezeigt werden.[21, 22] Zudem wird vermutet, dass die peripapilläre und makuläre Aderhautdicke bei myopen Augen verdünnt sein könnte.[47-50] Allerdings ist bisher wenig über die lokalen Verteilungsmuster der Gefäßdichte und

Aderhautdicke bei hoch-myopen Augen und deren Zusammenhang mit der Myopie bekannt.

In ***Publikation IV*** wurde die topographische Verteilung der makulären Gefäßdichte bei nicht-myopen, moderat-myopen und hoch-myopen Augen sowie die Assoziation der Gefäßdichte mit Myopie und Glaukom untersucht. Das Verteilungsmuster der Gefäßdichte war in den drei Myopiegruppen im Allgemeinen sehr inkonsistent, mit einer Tendenz zur höheren Gefäßdichte bei nicht-myopen Augen im Vergleich zu moderat- und hoch-myopen Augen. Eine statistische Signifikanz konnte jedoch nur im nasalen Sektor nachgewiesen werden. Zudem konnten eine statistisch signifikante, moderate Assoziation der Gefäßdichte mit dem Glaukomschweregrad und eine statistisch signifikante, aber schwache Assoziation der Gefäßdichte mit Myopie gezeigt werden. Die Ergebnisse in der Literatur sind sehr widersprüchlich. Diese Widersprüche können zum Teil durch Unterschiede in der Studienpopulation und der OCTA-Aufnahme erklärt werden. Beispielsweise wurde in unserer Publikation ein 3x3 mm großes Scanareal mit der OCTA untersucht, während Yang et al. in ihrer Publikation ein doppelt so großes Scanareal (6x6 mm) untersuchten.[51] Ein größeres Scanareal kann zum einen empfindlicher für Bildartefakte sein, zum anderen können Reduktionen der Gefäßdichte auch in weiter peripheren Regionen detektiert werden.[51] Obwohl eine schwache Assoziation zwischen Myopie und der Gefäßdichte besteht, implizieren unsere Ergebnisse, dass die oberflächliche Gefäßdichte für das Glaukommonitoring von myopen Augen hilfreich sein könnte.

In ***Publikation I*** und ***IV*** wurde zudem die Aderhautdicke von nicht-myopen, moderat-myopen und hoch-myopen Augen untersucht. Wir konnten zeigen, dass mit zunehmender Achsenlänge sowohl die peripapilläre als auch die makuläre Aderhautdicke in allen Sektoren abnahm, und bestätigten damit die bisherigen Ergebnisse in der Literatur.[47-49, 52, 53] Ähnlich den Resultaten von Ho et al. war auch in unserer Arbeit die makuläre Aderhautdicke in allen drei Myopiegruppen im nasalen Sektor am geringsten.[52] Die peripapilläre Aderhautdicke war im inferioren Sektor am kleinsten. Zudem konnten wir in beiden Publikationen eine starke signifikante Assoziation zwischen der Aderhautdicke und der Achsenlänge und keine Assoziation zwischen der Aderhautdicke und dem Glaukom zeigen. In unseren Arbeiten ist eine geringe Aderhautdicke charakteristisch für eine hohe Myopie und nicht geeignet, um gesunde Augen von glaukomatösen Augen zu differenzieren. Die Rolle der

Aderhautdicke im Zusammenhang mit dem Glaukom ist noch nicht abschließend geklärt. Einige Autoren nehmen an, dass Regionen mit einer dünnen Aderhaut empfindlicher auf Tensioschwankungen reagieren und somit ein erhöhtes Glaukomrisiko aufweisen.[47, 54, 55] Die beiden vorliegenden Publikationen zeichnen sich dadurch aus, dass die Berechnung der Aderhautdicke nicht anhand manueller Segmentierungen erfolgte, sondern mit Hilfe einer künstlichen Intelligenz („SALSA-deep"),[12, 13] die an einer Stichprobe manuell segmentierter OCT-RNFL-Ringscans (JR) trainiert wurde. Zum Zeitpunkt der Veröffentlichung waren die vorliegenden Publikationen die ersten Arbeiten, die eine künstliche Intelligenz zur Segmentierung der Aderhautdicke bei hoch-myopen Augen einsetzten.

3.4 OCT-Messgenauigkeit bei hoch-myopen Augen und Vergleichbarkeit von Papillen-Parametern anhand unterschiedlicher Messmethoden

Aus unseren Ergebnissen der ***Publikation I*** geht hervor, dass morphologische Veränderungen des Sehnervenkopfes aufgrund der axialen Elongation die Glaukomdiagnostik mittels der OCT erschweren könnten. Da die normativen Datenbanken der OCT-Hersteller keine hoch-myopen Augen enthalten, ist die Interpretation der RNFL-Ergebnisse bei hoch-myopen Augen limitiert. Wir konnten in dieser Publikation demonstrieren, dass die temporale RNFL-Dicke mit zunehmender Achsenlänge zunahm und stark mit der Achsenlänge assoziiert war. Dies führt zu einer „Temporalisierung" des RNFL-Profils im Vergleich zu gesunden nicht-myopen Augen und damit zu einer teilweise fehlerhaften Auswertung durch die Instrumenten-Software.[56-58] Darüber hinaus wurde in einer kürzlich durchgeführten Studie mit myopen Augen verdeutlicht, dass es bedeutend ist, RNFL-Messungen relativ zum anatomisch korrekten Papillenzentrum zu beurteilen. Es wurde demonstriert, dass sich die peripapilläre RNFL-Dicke, die in einem festen Abstand vom Zentrum der Bruch'schen Membranöffnung (BMO) gemessen wurde, signifikant von der RNFL-Dicke unterschied, die relativ zum klinischen Papillenzentrum gemessen wurde.[59]

Die größte Herausforderung besteht jedoch darin, dass die exakte Position der BMO bei hoch-myopen Augen nicht immer korrekt lokalisiert werden kann. Der primäre strukturelle Parameter für die Diagnose und das Monitoring eines Glaukoms ist die peripapilläre RNFL. Diese kann jedoch nicht exakt gemessen werden, wenn die BMO nicht korrekt lokalisiert wird. Das Zentrum der BMO-Konfiguration wird von OCT-

Instrumenten zur exakten Definition des Papillenzentrums und zur Berechnung der peripapillären RNFL verwendet.[59] Zudem wird die BMO zur Berechnung der BMO-MRW („Bruch's membrane opening minimum rim width"), die den minimalen Abstand der BMO zur Membrana limitans interna darstellt, ebenfalls in der Glaukomdiagnostik verwendet und weist je nach Studie eine ähnliche diagnostische Genauigkeit wie die peripapilläre RNFL auf.[60]

Die korrekte Lokalisierung der BMO ist daher für die genaue Messung und Interpretation glaukomatöser RNFL-Defekte unerlässlich. Aufgrund der morphologischen Veränderungen der Papille bei axialer Myopie kann dies jedoch eine Herausforderung darstellen.[61]

Aufgrund der oben beschriebenen Herausforderungen und insbesondere der zunehmenden Myopieprävalenz in asiatischen Ländern haben wir in ***Publikation II*** die OCT-gestützte automatische BMO-Erkennung und die Wahrscheinlichkeit einer nicht nachweisbaren BMO in einer gemischten amerikanischen und koreanischen Kohorte von gesunden Probanden und Glaukompatienten mit und ohne hohe Myopie untersucht. Darüber hinaus wurden anatomische Merkmale zur Prädiktion der Lokalisationsgenauigkeit der BMO evaluiert.

Die Ungenauigkeit der BMO-Lokalisierung (manuell korrigierbare BMO und nicht erkennbare BMO) war sowohl bei gesunden Personen, als auch bei Glaukompatienten mit hoher Myopie signifikant höher, als bei Personen ohne hohe Myopie. Diese Ergebnisse wurden ebenfalls von Zheng et al. bestätigt.[61] In den multivariaten Regressionsanalysen waren eine längere Achsenlänge, eine ovalere BMO-Konfiguration, ein größerer BMO-Verkippungswinkel und das Vorliegen einer hohen axialen Myopie signifikant mit einer ungenauen BMO-Lokalisierung assoziiert. Diese Ergebnisse verdeutlichen, dass insbesondere anatomische Merkmale, die mit der Achsenmyopie assoziiert sind, mit einer ungenaueren BMO-Lokalisation einhergehen. Diese Resultate deuten darauf hin, dass bei hoch-myopen Augen eine qualitative Überprüfung und eine manuelle Korrektur der BMO-Lokalisation, was im klinischen Alltag meist nicht möglich ist, von entscheidender Bedeutung ist, um eine Fehlinterpretation der OCT-Ergebnisse zu vermeiden. Eine korrekte BMO-Lokalisation ist sowohl für die Evaluation der BMO-MRW als auch der peripapillären RNFL erforderlich. Wenn aufgrund einer ungenauen BMO-Lokalisation das BMO-Zentrum nicht identifiziert werden kann, werden die peripapillären RNFL-Messungen im

Vergleich zur normativen Referenzdatenbank des Instruments nicht korrekt berechnet und somit fälschlicherweise als innerhalb oder außerhalb des Referenzdatenbereichs interpretiert. Die qualitative Auswertung der OCT-Scans ergab, dass die nicht-lokalisierbaren BMO-Punkte bei hoch-myopen Augen häufiger in den temporalen Sektoren zu finden waren, was sich unter anderem durch den erhöhten Verkippungswinkel und das Vorliegen einer peripapillären Atrophiezone im temporalen Bereich der Papille erklären lässt. Auch diese Ergebnisse stimmen mit denen von Zheng et al.[61] überein.

Die Gründe für die fehlerhafte BMO-Lokalisierung durch die Standard-OCT-Software sind wahrscheinlich zum Teil auf die anatomischen Unterschiede bei stark myopen Augen[62] und auf die Tatsache zurückzuführen, dass die Segmentierungsalgorithmen nicht für hoch-myope Augen entwickelt wurden. Allerdings ist auch zu beachten, dass die finale korrekte BMO-Lokalisierung durch die Software von der initialen korrekten BMO-Lokalisierung durch den Instrumenten-Bediener abhängt. Wenn dieser erste Schritt aufgrund mangelnder Expertise mit hoch-myopen Augen fehlerhaft durchgeführt wird, ist die finale Segmentierung durch die Software inakkurat.

Zusammenfassend verdeutlichen die Ergebnisse der ***Publikation II,*** dass nicht nur die klinische Papillendiagnostik bei hoch-myopen Augen erschwert ist, sondern auch diagnostische Verfahren wie die OCT aufgrund von Segmentierungsfehlern und fehlenden hoch-myopen Augen in Referenzdatenbanken nur eingeschränkt anwendbar sind.

Bei der Beschreibung und Charakterisierung der morphologischen Veränderungen bei hoch-myopen Augen sollte die zugrundeliegende Methodik berücksichtigt werden, um die Vergleichbarkeit der Ergebnisse unterschiedlicher Studien zu gewährleisten. In der Vergangenheit hat eine Vielzahl von Studien die Anatomie des Sehnervenkopfes bei myopen Augen anhand von Parametern wie der Ovalität der Papillenkonfiguration sowie der Verkippung und Verdrehung (aus dem engl. „*torsion*“) der Papille beschrieben. In diesen Studien wurden diese Parameter jedoch manuell auf der Grundlage von zweidimensionalen Fundusfotografien oder der Projektion der Fundusfotografien auf OCT-Scans gemessen. Diese Methodik hat den Nachteil, dass sie nicht auf objektiven anatomischen Landmarken wie der BMO beruht, sondern auf der subjektiven Beurteilung der klinischen Papillengrenze.

Wir haben in ***Publikation III*** untersucht, ob die manuelle Vermessung des Ovalitätsindexes (in der Literatur oft auch als Verkippung bezeichnet) und der Verdrehung/Torsion (in unserer Arbeit als „Rotation“ bezeichnet) des Sehnervenkopfes, basierend auf der klinischen Papillengrenze anhand von Fundusfotos, mit der automatisierten Vermessung, basierend auf der BMO anhand von OCT-Scans, verglichen werden kann.

In der Literatur wurden automatisierte und manuelle Methoden der Papillendiagnostik bisher nicht miteinander verglichen. Wir konnten in unserer Arbeit eine statistisch signifikante, aber schwache Korrelation zwischen der manuellen und automatisierten Messung des Ovalitätsindexes und keine Korrelation zwischen der manuellen und automatisierten Messung der Papillenrotation zeigen. Wir haben die Hypothese aufgestellt, dass die objektive Charakterisierung der Papille von grundlegender Bedeutung ist, um die Hürden bei der Glaukomdiagnostik bei Augen mit hoher Myopie zu reduzieren. Das Konzept der präzisen Charakterisierung des Sehnervenkopfes könnte zur Identifizierung von Merkmalen führen, die spezifisch mit der Myopie oder dem Glaukom assoziiert sind und Kliniker in der Unterscheidungsfindung unterstützen.

Deshalb haben wir in ***Publikation I*** Methoden entwickelt, die eine objektive Charakterisierung des Sehnervenkopfes ermöglichen. Obwohl einige dieser Parameter (Ovalitätsindex/Verkippung, Rotation) bereits zuvor beschrieben wurden, verdeutlichen die Ergebnisse von ***Publikation III*** jedoch, dass zwei- und dreidimensionale Messungen der gleichen Parameter nicht austauschbar sind. Es wurde bereits berichtet, dass Papillenmerkmale, die auf der klinischen Papillengrenze auf Fundusfotos basieren, wenig mit denen korrelieren, die auf der BMO auf OCT-Scans basieren.[63] Der Ovalitätsindex wurde in ***Publikation III*** sowohl zweidimensional manuell als auch dreidimensional automatisiert in der hoch-myopen Gruppe am kleinsten (ovalere Konfiguration) gemessen, was mit zweidimensionalen Messungen in der Literatur übereinstimmt.[28-33, 64] In unserer Studie gab es jedoch nur eine schwache Korrelation zwischen den beiden unterschiedlichen Messmethoden. Der Rotationswinkel war in unserer Studie in der hoch-myopen Gruppe größer, allerdings nur bei der manuellen Messung und nicht bei der dreidimensionalen Messung auf Basis der OCT-Scans. Auch in der Literatur war der zweidimensionale, manuell gemessene Rotationswinkel bei hoch-myopen Augen größer.[28-31] Eine wichtige Erklärung für die Diskrepanz in den Ergebnissen des Rotationswinkels könnte der

dreidimensionale Ansatz in ***Publikation I*** und ***III*** im Gegensatz zum zweidimensionalen Ansatz in ***Publikation III*** und in der Literatur sein. Die dreidimensionale Messung basiert auf der mit Hilfe der OCT dargestellten BMO, die insbesondere bei hoch-myopen Augen stark von der klinischen Papillengrenze abweicht, wie auch Chauhan et al. in ihrer Arbeit demonstrierten.[60] In OCT-Studien wurde zudem festgestellt, dass insbesondere bei myopen Augen die Bruch-Membran über die klinische Papillengrenze hinausreicht und relativ zur anterioren Sklerakanalöffnung nach temporal versetzt ist und daher auf Fundusfotos nicht sichtbar ist.[38, 60, 62, 63].

Basierend auf den Ergebnissen von ***Publikation III*** und der Tatsache, dass die klinische Papillengrenze bei myopen Augen oft nicht mit der BMO-Grenze übereinstimmt, sollte die Charakterisierung des Sehnervenkopfes auf objektiven Landmarken basieren, die mittels der OCT identifiziert werden können.

3.5 Diagnostische Genauigkeit von OCT-Parametern zur Differenzierung von Myopie und Glaukom

Um die diagnostische Genauigkeit der OCT-Parameter zur Differenzierung von Myopie und Glaukom zu evaluieren, wurden in ***Publikation V*** neben Glaukompatienten auch gesunde Probanden eingeschlossen.

Die diagnostische Genauigkeit der einzelnen Parameter in ***Publikation V*** variierte stark zwischen den einzelnen Myopiegruppen. Im Allgemeinen zeigten die peripapilläre RNFL und die GCIPL die höchste diagnostische Genauigkeit bei hoch-myopen Augen und die BMO-MRW bei moderat-myopen und nicht-myopen Augen. Da die peripapilläre RNFL fast alle Axone der Ganglienzellen repräsentiert, ist sie ein etablierter Marker zur Unterscheidung von gesunden und glaukomatösen Augen bei nicht-myopen Augen. Aufgrund der morphologischen Veränderungen in der Papillenregion bei myopen Augen war jedoch bisher unklar, inwieweit die peripapilläre RNFL und die BMO-MRW bei nicht-emmetropen Augen zuverlässig sind.[65] Die diagnostische Genauigkeit der peripapillären RNFL war in der hoch-myopen Gruppe am höchsten, während sie für die BMO-MRW in der nicht-myopen und moderat-myopen Gruppe am höchsten war. Möglicherweise reagieren Parameter des neuroretinalen Randsaums wie die BMO-MRW empfindlicher auf Veränderungen der axialen Elongation als die peripapilläre RNFL. Aufgrund dieser Veränderungen war

bisher auch unklar, ob makuläre Parameter eine höhere diagnostische Genauigkeit haben als Papillen-Parameter. Unsere Ergebnisse in ***Publikation IV*** veranschaulichten, dass makuläre Parameter wie die GCIPL-Schicht und der Ganglienzellkomplex (GCC) mit Glaukom, aber nicht mit Myopie assoziiert waren. In ***Publikation V*** waren jedoch GCIPL und GCC der diagnostischen Genauigkeit der perpipapillären RNFL bei hoch-myopen Augen nicht überlegen. Betrachtet man die spezifischen Sektoren innerhalb der einzelnen Parameter genauer, so hatte innerhalb der peripapillären RNFL der inferotemporale Sektor die höchste diagnostische Stärke, wie auch Choi et al. in ihrer Studie zeigten.[65]

Innerhalb der GCIPL-Sektoren wiesen der innere inferiore, der innere temporale und der äußere temporale Sektor die höchste diagnostische Genauigkeit auf, was mit den Ergebnissen von Takayama et al. übereinstimmt, die zeigten, dass die Region inferotemporal zur Fovea am frühesten von glaukomatösen Veränderungen betroffen ist. Die peripapilläre RNFL umfasst nahezu alle Axone der retinalen Ganglienzellen, während die perifoveale Region nur Informationen von den dort befindlichen Ganglienzellen enthält, was die Überlegenheit der RNFL gegenüber der GCIPL erklären könnte.[66, 67]

Sowohl für die peripapilläre RNFL als auch für die GCIPL ist die unterschiedliche diagnostische Stärke der einzelnen Sektoren auffällig und verdeutlicht, dass diese lokalen Differenzen bei der klinischen Interpretation der Ergebnisse berücksichtigt werden sollten. Die insgesamt sehr hohe diagnostische Stärke sowohl für die peripapilläre RNFL als auch für die GCIPL könnte unter anderem durch unser Studiendesign erklärt werden. Hoch-myope Augen durchliefen einen separaten „Gradingprozess“, um möglichst wenige Grenzfälle einzuschließen, wodurch hoch-myope Augen mit unklarer Diagnose ausgeschlossen wurden. Dies hat zur Folge, dass die diagnostische Stärke für alle Parameter in dieser Studie relativ hoch ist.

3.6 Schlussfolgerung

In der vorliegenden kumulativen Habilitationsschrift wurden Forschungsergebnisse zur bildgebenden Diagnostik von Myopie und Glaukom zusammengetragen. Ziel der vorliegenden Publikationen war es, die Morphologie hoch-myoper Augen mittels

bildgebender Verfahren wie der OCT und der OCTA zu charakterisieren, die diagnostische Zuverlässigkeit der bildgebenden Verfahren zu evaluieren und schließlich objektive Parameter zur Differenzierung von Myopie und Glaukom zu identifizieren.

Zu diesem Zweck haben wir in ***Publikation I*** die Anatomie des Sehnervenkopfes mittels neuer objektiver, OCT-basierter Parameter analysiert und die Assoziation dieser Parameter mit Myopie und Glaukom untersucht. Einige dieser Papillen-Parameter wie der Ovalitätsindex, der BMO-Verkippungswinkel und der BMO-Rotationswinkel wurden mit selbst entwickelten, automatisierten Modellen berechnet. Die Messung der peripapillären Aderhautdicke erfolgte mit Hilfe von Deep-Learning-Modellen, die anhand einer manuell ausgewerteten Stichprobe trainiert wurden. Hoch-myope Papillen waren ovaler, stärker verkippt und wiesen eine geringere Aderhautdicke auf. Der Rotationswinkel, die peripapilläre RNFL und die BMO-MRW waren innerhalb der Myopiegruppen ähnlich, mit Ausnahme der temporalen peripapillären RNFL und der nasalen BMO-MRW, die ebenfalls signifikant mit der Myopie assoziiert waren. Der Verkippungswinkel, der Ovalitätsindex und die geringe Aderhautdicke charakterisieren die myope Papille und sind im Gegensatz zur peripapillären RNFL und BMO-MRW mit Ausnahme der oben genannten Sektoren nicht zur Glaukomdiagnostik geeignet.

Da die oben genannten Parameter auf OCT-Landmarken wie der BMO basieren, haben wir im Rahmen der Berechnungen mehrere tausend OCT-Scans von hoch-myopen Augen evaluiert und eine Häufung von Segmentierungsfehlern festgestellt. Wir haben daher in ***Publikation II*** OCT-Scans qualitativ und quantitativ auf Segmentierungsfehler ausgewertet und konnten feststellen, dass die Rate der Segmentierungsfehler bei hoch-myopen Augen signifikant höher war und dass Parameter, die für Myopie charakteristisch sind, wie die zunehmende Achsenlänge, eine größere Ovalität und ein größerer Verkippungswinkel, signifikant mit Segmentierungsfehlern assoziiert waren.

Die in ***Publikation I*** berechneten Papillenparameter wurden zum Teil bereits in der Literatur beschrieben. Allerdings wurden diese Parameter in der Literatur bisher manuell anhand der klinischen Papillengrenze berechnet, die auf zweidimensionalen Fundusfotos identifiziert wurde. Wir haben diese Methodik in ***Publikation III*** mit unserer automatisierten, dreidimensionalen, OCT-basierten Technik verglichen, bei

der die klinische Papillengrenze durch die objektive BMO-Grenze ersetzt wurde. Es bestand keine Korrelation zwischen dem klinisch gemessenen zweidimensionalen Ovalitätsindex und Rotationswinkel und der automatisierten dreidimensionalen Messung, was verdeutlicht, dass gleiche Parameter mit unterschiedlicher Messmethodik nicht austauschbar sind.

Da die Papille aufgrund der axialen Elongation starken morphologischen Veränderungen unterliegen kann und etablierte Parameter wie die RNFL und die BMO-MRW aufgrund von Segmentierungsfehlern und fehlenden myopen Augen in den OCT-Referenzdatenbanken fehlerhaft berechnet werden könnten, ist unklar, inwieweit die RNFL und die BMO-MRW zur Differenzierung von Myopie und Glaukom geeignet sind. Daher wurden in ***Publikation IV*** sowohl vaskuläre OCTA-Parameter als auch strukturelle OCT-Parameter der Makula bei hoch-myopen Augen gemessen und deren Assoziation mit Myopie und Glaukom untersucht. Die Ergebnisse dieser Arbeit zeigten, dass insbesondere die GCIPL und GCC für die Unterscheidung zwischen Myopie und Glaukom geeignet sein könnten, da beide Parameter nicht mit der Myopie, aber signifikant mit dem Glaukom assoziiert waren.

In ***Publikation V*** wurden neben Glaukomaugen auch gesunde Augen mit und ohne hohe Myopie eingeschlossen und die OCT-Parameter der Papille und der Makula hinsichtlich der topographischen Verteilung in den einzelnen Gruppen analysiert sowie die diagnostische Stärke der OCT-Parameter zur Differenzierung von Myopie und Glaukom evaluiert. Die Ergebnisse verdeutlichen, dass sowohl die peripapilläre RNFL als auch die GCIPL eine hohe diagnostische Stärke für die Differenzierung von Myopie und Glaukom haben und dass diese Ergebnisse in größeren Publikationen bestätigt werden müssen.

Zusammenfassend leistet die vorliegende Arbeit einen umfassenden Beitrag zum besseren Verständnis von Myopie und Glaukom, analysiert spezifische Eigenschaften beider Krankheitsbilder, bewertet die diagnostischen Möglichkeiten kritisch und trägt zur besseren Differenzierung beider Krankheitsbilder bei. Aufgrund der diagnostischen Herausforderungen der bildgebenden Verfahren bei hoch-myopen Augen besteht weiterhin großer Forschungsbedarf auf diesem Gebiet.

4. In der Habilitationsschrift zusammengefasste Publikationen

Publikation I

Rezapour J, Bowd C, Dohleman J, Belghith A, Proudfoot JA, Chrisopher M, Hyman L, Jonas JB, Fazio MA, Weinreb RN, Zangwill LM; The influence of axial myopia on optic disc characteristics of glaucoma eyes; Scientific reports; 2021; Apr 23;11(1):8854. doi: 10.1038/s41598-021-88406-1. PMID: 33893383 11:8854.

scientific reports

Check for updates

OPEN

The influence of axial myopia on optic disc characteristics of glaucoma eyes

Jasmin Rezapour[1,2], Christopher Bowd[1], Jade Dohleman[1], Akram Belghith[1], James A. Proudfoot[1], Mark Christopher[1], Leslie Hyman[3], Jost B. Jonas[4], Massimo A. Fazio[5,6], Robert N. Weinreb[1] & Linda M. Zangwill[1]✉

This study characterizes differences in glaucomatous eyes with and without high axial myopia using custom automated analysis of OCT images. 452 eyes of 277 glaucoma patients were stratified into non (n = 145 eyes), mild (n = 214 eyes), and high axial myopia (axial length (AL) > 26 mm, n = 93 eyes). Optic disc ovality index, tilt and rotation angle of Bruch's membrane opening (BMO) and peripapillary choroidal thickness (PCT) were calculated using automated and deep learning strategies. High myopic optic discs were more oval and had larger BMO tilt than mild and non-myopic discs (both $p < 0.001$). Mean PCT was thinnest in high myopic eyes followed by mild and non-myopic eyes ($p < 0.001$). BMO rotation angle, global retinal nerve fiber layer (RNFL) thickness and BMO-minimum rim width (MRW) were similar among groups. Temporal RNFL was thicker and supranasal BMO-MRW was thinner in high myopic eyes. BMO tilt and PCT showed moderate and temporal RNFL and nasal BMO-MRW showed weak but significant associations with AL in multivariable analyses (all $p < 0.05$). Large BMO tilt angle and thin PCT are characteristics of highly myopic discs and were not associated with severity of glaucoma. Caution should be exercised when using sectoral BMO-MRW and RNFL thickness for glaucoma management decisions in myopic eyes.

There is consistent evidence that the prevalence of myopia has markedly increased. Persons with high myopia are also more likely to have primary open angle glaucoma than non-highly myopic individuals. Specifically, the prevalence of myopia is increasing from approximately 1.4 billion worldwide in 2010, to an estimated 5 billion by 2050[1]. In addition, a meta-analysis of 7 studies suggests individuals with myopia are 2.5 times more likely to have glaucoma than those without myopia[2]. It is unclear why myopia increases the risk of glaucoma, but it is likely related to a greater susceptibility of the optic nerve head to glaucoma damage through a variety of mechanisms. For example, it has been discussed that a thinner lamina cribrosa in myopic eyes makes it more susceptible due to a steepening of the pressure gradient[3], and combined with secondary enlargement of the optic nerve head from myopia and elongation and thinning of the peripapillary scleral flange, it may increase an individual's risk for developing glaucoma[3–6]. Moreover, the diagnosis of glaucoma often is challenging in high myopes as the appearance of the myopic optic nerve head, with its higher degree of tilt and possibly oval shape and torsion mimics glaucomatous optic disc damage making the diagnosis of glaucoma difficult in high myopes[7–10]. It follows that the myopic optic disc may mistakenly be interpreted as glaucoma resulting in possible overdiagnosis and overtreatment of glaucoma in non-glaucomatous myopes[11]. Hence, the study of morphological features of the myopic optic disc can improve our understanding of the relationship between myopia and glaucoma.

In the majority of studies, ovality index, disc tilt and torsion measurements have been evaluated based on qualitative review of fundus photographs relative to the clinical disc margin. These studies report inconsistent results with respect to the association of these parameters with axial length[7–9,12–18]. The problem with a photograph-based approach to measure the ovality index, disc tilt or torsion is that landmarks such as the clinical disc

[1]Hamilton Glaucoma Center, Shiley Eye Institute, Viterbi Family Department of Ophthalmology, University of California, San Diego, 9500 Gilman Drive, La Jolla, CA 92093-0946, USA. [2]Department of Ophthalmology, University Medical Center of the Johannes Gutenberg University, Mainz, Germany. [3]Wills Eye Hospital, Thomas Jefferson University, Philadelphia, PA, USA. [4]Department of Ophthalmology, Medical Faculty Mannheim, Heidelberg University, Mannheim, Germany. [5]Department of Ophthalmology and Vision Science, School of Medicine, The University of Alabama At Birmingham, Birmingham, AL, USA. [6]Department of Biomedical Engineering, School of Engineering, The University of Alabama At Birmingham, Birmingham, AL, USA. ✉email: lzangwill@health.ucsd.edu

margin are subjective and not based on the actual three-dimensional anatomy of the optic disc[19–21]. Furthermore, there is evidence that with increasing axial length the Bruch's membrane opening (BMO) anatomy is less likely to be represented by the clinical disc margin so that a two-dimensional photography-based assessment does not reflect the true disc configuration in all aspects[22]. An advantage of using optical coherence tomography (OCT) imaging to measure ovality index, tilt and torsion is that an objective identification and measurement of these features relative to the BMO, is possible[23].

The objective of this study is to improve our understanding of the morphological characteristics of the glaucomatous optic disc in axial highly myopic and non-myopic eyes. We measured standard optic disc parameters including retinal nerve fiber layer (RNFL) thickness and BMO-MRW (minimum rim width) as well as partially novel features, BMO tilt, BMO torsion, BMO ovality and peripapillary choroidal thickness (PCT) based on custom image processing and deep learning analysis of OCT scans relative to the BMO.

Methods

Participants. This cross-sectional study included all glaucoma patients enrolled in the Diagnostic Innovations in Glaucoma Study (DIGS; clinicaltrials.gov identifier NCT00221897) with axial length, visual field measurements and good quality spectral domain (SD)-OCT of the optic nerve head (ONH) using radial circle (RC) scans. The institutional review board of the University of California San Diego approved the study methods, which are in accordance with HIPAA regulations and according to the Declaration of Helsinki, written informed consent was obtained from all participants. A detailed description of the study design has been published previously[24]. Subjects were ≥ 18 years old and had open anterior chamber angles. All participants received a complete ophthalmologic examination including refractometry and assessment of best-corrected visual acuity, standard automated perimetry (Humphrey Field Analyzer; 24–2 Swedish interactive thresholding algorithm [SITA] standard; Carl-Zeiss Meditec), Goldmann applanation tonometry, gonioscopy, dilated fundus examination, central corneal thickness (CCT) measurement by ultrasound pachymetry (DGH Technology, Inc., Exton, PA), coherence interferometry measurement of the axial length (IOLMaster, Carl Zeiss Meditec, Dublin, CA), and simultaneous stereophotography and SD-OCT of the optic disc and macula.

The definition of primary open angle glaucoma was based on the DIGS conventional "gold standard" of visual field loss and photograph-based optic disc damage[24]. Stereo photograph-based optic disc damage was defined as focal or diffuse narrowing of the neuroretinal rim, and/or detection of retinal nerve fiber layer (RNFL) defects characteristic of glaucoma as based on a masked assessment by two trained observers. Two experts (JR and CB) graded photographs after a high myopia optic disc grading training with a senior consultant (JBJ) with expertise in myopia and glaucoma. Stereo photograph-based optic disc damage was defined by consensus between both graders. In case of disagreement, diagnosis was defined by adjudication by the senior consultant.

The Visual Field Assessment Center (VisFACT) Reading Center completed the quality control of all visual fields according to standard protocols and unreliable visual fields were excluded[24]. Standard automated perimetry glaucomatous visual field damage was defined as two repeatable and reliable visual field tests (rate of fixation losses and false negatives and false positives responses of < 33%) with a glaucoma hemifield test (GHT) outside normal limits and/ or a pattern standard deviation (PSD) with a p value of < 0.05 with a similar defect on consecutive abnormal tests[24].

Axial myopia categories. Axial elongation can lead to morphological changes of the optic disc and the fundus[25,26]. Myopia defined by the refractive error does not always imply axial elongation that can lead to the morphological changes mentioned above. At the same time cataract surgery or refractive procedures might lead to a refractive change in eyes that are axially elongated but do no longer appear to be (highly) myopic as defined by refractive error. This is also confirmed by the distribution of the spherical equivalent in our study population (Table 1). This study assessed the morphological changes of the optic disc in association with axial length and for these reasons myopia was defined by axial length and not by refractive error. Based on population-based studies[2,27], axial myopia groups were defined as follows:

- No axial myopia: axial length ≤ 24.0 mm
- Mild axial myopia: 24.0 mm < axial length ≤ 26.0 mm
- High axial myopia: axial length > 26.0 mm

Image acquisition. The Spectralis OCT was used to obtain 24 high-resolution optic nerve head (ONH) radial scans and 3 retinal nerve fiber layer (RNFL) circle scans centred on the optic nerve head using the ONH radical circle (ONHRC) scan from the Glaucoma Module Premier Edition software (version 6.10; Heidelberg Engineering Inc, Heidelberg, Germany). Heidelberg Engineering Spectralis standard software was used to calculate BMO area, BMO-MRW and RNFL thickness. Images were electronically transferred for quality assessment to the Imaging Data Evaluation and Analysis (IDEA) Center. OCT images were reviewed for accurate BMO segmentation in the radial B-scans and accurate internal limiting membrane (ILM), RNFL and Bruch's membrane (BM) segmentation in the circle scans. If needed, these automated segmentations were manually corrected according to standard IDEA Reading Center protocols. Poor quality images (quality score < 15) or those with BMO segmentation failure that could not be manually corrected were excluded.

The BMO-MRW, defined as the shortest distance from the BMO point to the ILM[28], was automatically computed by instrument software for each radial scan and averaged for all 24 scans. Circumpapillary RNFL thickness

	No myopia 81 (145 eyes)	Mild myopia 128 (214 eyes)	High myopia 68 (93 eyes)	*p* value (age-adjusted)
Age	77.2 (74.7, 79.6)	73.0 (71.1, 74.9)	65.6 (62.6, 68.7)	$<0.001^{1,2,3}$
Sex (% Female)	65.4%	43.0%	47.1%	$0.005^{1,2}$
Race				
European descent	67.9%	68.8%	66.2%	0.410
African descent	23.5%	17.2%	13.2%	
Asian descent	7.4%	12.5%	17.6%	
Other/unknown	1.2%	1.6%	2.9%	
AL (mm)	23.4 (23.3, 23.5)	24.8 (24.7, 24.9)	26.7 (26.5, 26.8)	$<0.001^{1,2,3}$ ($<0.001^{1,2,3}$)
[a]SE (D)	0.21 (−0.24, 0.66)	−1.36 (−1.74, −0.98)	−3.49 (−4.06, −2.92)	$<0.001^{1,2,3}$ ($<0.001^{1,2,3}$)
[b]CCT (µm)	533.6 (525.4, 541.8)	534.5 (527.7, 541.4)	529.6 (519.4, 539.9)	0.788 (0.774)
VF MD (dB)	−6.09 (−7.41, −4.77)	−6.90 (−7.99, −5.81)	−7.34 (−8.91, −5.76)	0.450 (0.083^{2})
[c]IOP (mmHg)	14.1 (13.2, 15.1)	13.9 (13.1, 14.7)	13.3 (12.1, 14.4)	0.514 (0.046^{2})
[d]BMO area (mm^2)	2.11 (2.01, 2.20)	2.12 (2.04, 2.20)	2.18 (2.06, 2.30)	0.608 (0.954)

Table 1. Glaucoma patient and eye characteristics by myopia group. Results are presented as mean (95% confidence interval) or percentage. Race was compared using a chi-squared test. Continuous variables were compared using ANOVA (for age) or linear mixed models (for eye level data). No myopia: AL ≤ 24.0 mm; Mild myopia: AL: > 24 mm and ≤ 26.0 mm; High myopia: AL > 26.0 mm. Missing 66[a], 14[b], 2[c], and 28[d] values. [1]No versus Mild Myopia $p < 0.05$; [2]No versus High Myopia $p < 0.05$; [3]Mild versus High Myopia $p < 0.05$. AL, axial length; BMO, Bruch's membrane opening; CCT, central corneal thickness; IOP (intraocular pressure); SE, spherical equivalent; VF MD, visual field mean deviation.

was measured from the 3 circle scans obtained at approximately 3.5 mm, 4.1 mm and 4.7 mm diameter using instrument software. For this study RNFL thickness measurements were based on the 3.5 mm diameter circle scan.

Measurement of optic disc BMO ovality, tilt and rotation. Optic disc ovality, tilt and rotation were automatically calculated on the BMO points using custom San Diego Automated Layer Segmentation Algorithm (SALSA) software[29], as Spectralis software does not provide these measurements. It should be noted that the custom calculations were not based on the clinical disc margin but on the BMO. With this novel method we utilize the term BMO rotation[19] instead of using the more commonly used term disc "torsion". By using "rotation" we aim to characterize the purely anatomical characteristics of the BMO-based disc margin, contrary to "torsion", which implies shearing deformations of the peripapillary and ONH tissue, which can only be proven by histological examinations. To calculate these three parameters, two BM boundary (BMB) points of the BM at the edges of each of the 24 radial B-scan (furthest peripheral pixels on each BM edge of a B-scan in total two BMB points per B-scan and two BMO points per B-scan were calculated (Fig. 1A). Details of the calculations are provided in the Supplemental Material.

The ovality index was calculated by dividing the shortest diameter of the BMO by the longest diameter. The major and minor axes were defined as the longest and shortest diameter of the fitted BMO ellipse.

BMO tilt angle (measured in degrees) was defined as the angle between BMO plane and BMB plane normal vectors. After transforming the coordinates in the 3D rectangular space, one 2D plane was fit to the BMB points and one to the BMO points using linear least squares method (Fig. 1B). BMO tilt angle was calculated by assessing the angle between their normal vectors.

To calculate the BMO rotation angle (measured in degrees), each BMO point was projected onto the BMO reference plane and used to fit a two-dimensional ellipse to the points in the reference plane. The orientation and ovality of the fit ellipse was used to compute the BMO rotation angle and ovality index, respectively (Fig. 2).

BMO ovality, tilt and rotation validation. Automated BMO ovality index measurement was validated manually (JR) for reliability in a randomly chosen subset of 50 non-, mild- and high axial myopic eyes and showed good performance. To validate the BMO tilt and rotation measurements described above we independently assessed both the segmentation and quantification algorithms by reprocessing the ONHRC scans with a commercially available auto-segmentation software (ReflectivityTM; AbyssProcessing, Singapore)[30] and then calculating the same 3D morphological parameters described in the methods with a custom algorithm based developed by MAF in Mathematica (Wolfram Research, Urbana, Illinois). It should be noted that the cross-validation method used a fixed distance of 1700 µm from the center of the BMO to determine the reference points for the tilt calculation.

Measurement of peripapillary choroidal thickness using SALSA-deep. As Spectralis software does not provide choroidal thickness measurements, custom software (SALSA-deep) was developed using a deep learning strategy, BCDU-Net[29] to segment the RNFL circle scan (3.5 mm diameter) of the ONHRC (Supplemental Figure 2) to identify the BM and the posterior boundary of the choroid to calculate choroidal thick-

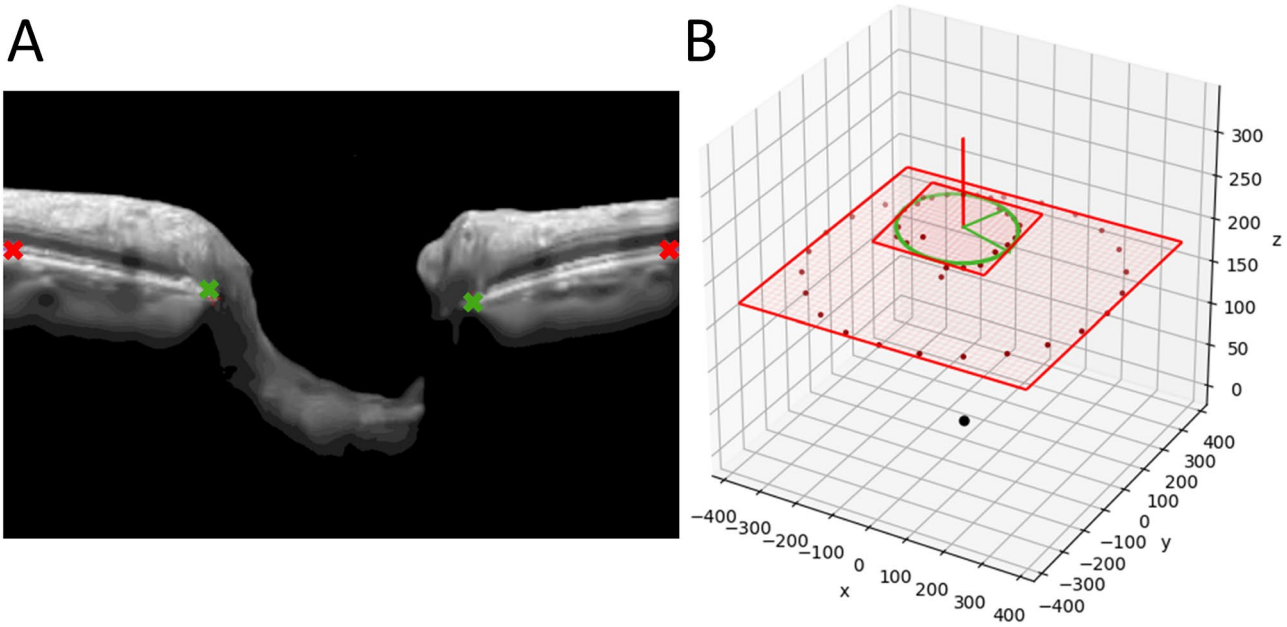

Figure 1. 3D rectangular coordinate space illustrating the BMO fit plane, the BMB fit plane and the corresponding BMB- and BMO points derived from OCT B-scans to calculate tilt and ovality index. (**A**) SALSA-segmented optic disc B-scan demonstrating 2 BMO points (green) and 2 BMB points (red) used to project on the rectangular coordinate space to calculate BMO ovality index, tilt and rotation angle. (**B**) The green ellipse represents the fit BMO ellipse and the smaller red rectangle represents the fit BMO plane. The larger red rectangle represents the fit BMB plane, calculated from the BMB ellipse (red dots inside the larger red rectangle). The red vector from the center of the fit ellipse represents the normal vector to the fit ellipse and helps to illustrate the tilt. The black point represents the origin of the coordinate system. The two green vectors from the center of the fit ellipse are the semi-major and semi-minor axes used to calculate the BMO ovality index calculated as the minor BMO axis divided by the major BMO axis. Abbreviations: BMB, Bruch's membrane boundary; BMO, Bruch's membrane opening; SALSA, San Diego Automated Layer Segmentation Algorithm.

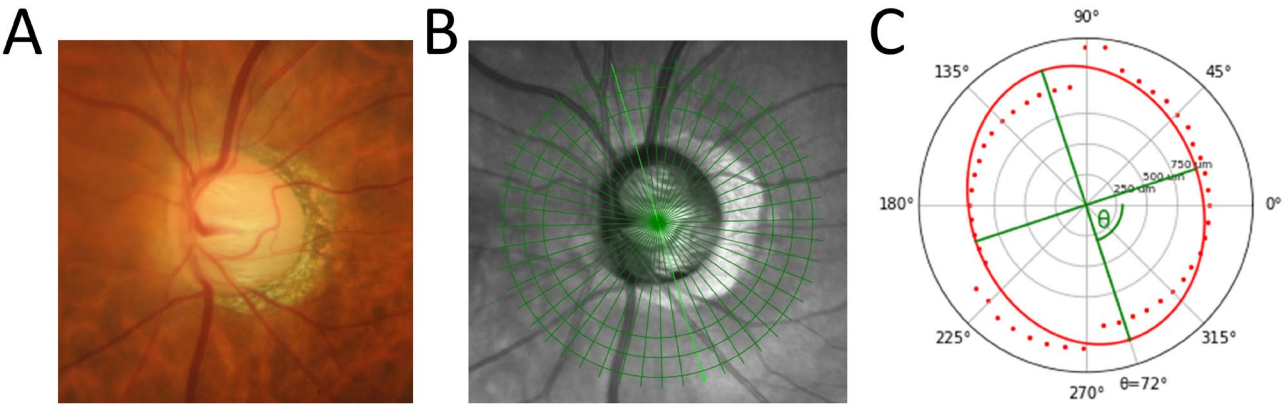

Figure 2. Case illustration of BMO ovality index (0.82) and BMO rotation angle (72.4°) measurement in a highly myopic left eye (AL = 26.1 mm). The photograph (**A**) and OCT infrared image (**B**) of the optic disc are shown on the left and the corresponding BMO ovality and rotation measurement (**C**) is illustrated on the right image. The red dots indicate the BMO points. The red ellipse represents the fit ellipse based on the BMO points. The green vectors indicate the shortest and longest diameter of the BMO ellipse and are defined as major and minor axis to calculate the BMO ovality index. The BMO rotation angle is defined as the angle between the semimajor axis and the temporal axis (0°, horizontal axes of the en face OCT image), adjusted for variation in individual anatomies based on the FoBMOc angle. Abbreviations: BMO, Bruch's membrane opening; FoBMOc, Fovea BMO center; OCT, optical coherence tomography.

ness. Details of how BCDU-Net an extension of U-Net, bi-directional ConvLSTM was applied is available in the Supplemental Material. Peripapillary choroidal thickness (PCT) was defined as the perpendicular distance between the posterior border of the BM and the posterior boundary of the choroid. Global and sectoral PCT was calculated for temporal, superotemporal, inferotemporal, nasal, superonasal, and inferonasal sectors. The automated deep learning strategy was articulated as follow: First, a trained grader (JR) manually segmented the BM and the posterior boundary of the choroid in circle scans of the ONHRC scan in the Spectralis software (version 6.10; Heidelberg Engineering Inc, Heidelberg, Germany). This subset of eyes was used as the ground truth to train a BCDU-Net deep convolutional neural network model. In total, 385 eyes of 190 non axial myopic, mild axial myopic subjects, and 15 eyes of 10 high axial myopic subjects were used to train the model. Scans with poor quality (quality score < 15 dB) were excluded from the segmentation process.

The automated deep learning BCDU-Net based choroidal segmentation of each RNFL circle scan was reviewed for accuracy (JR). The RNFL scans of 21 eyes were not available for segmentation due to low image quality. The overall performance of the deep learning segmentation algorithm was very good with 379/384 (98.7%) scans considered accurately segmented and included in the analysis. In addition, the proportion of eyes with good quality choroidal segmentation was over 95% in each of the myopia groups (no myopia: 135/139 [97.1%], mild myopia: 203/207 [98.1%] and high myopia: 41/43, [95.4%]).

Statistical analyses. Statistical analysis was conducted using categorical data to compare between axial myopia groups and continuous data to analyze an association between different ocular parameters and axial length. Data is presented as mean (95% confidence interval) and count (percentage) for continuous and categorical variables, respectively. The statistical significance of comparisons between patient-level characteristics across myopia groups was determined by analysis of variance (ANOVA) for continuous variables and chi-squared tests for categorical variables. For eye-level characteristics, mean and confidence interval estimates were derived from linear mixed effects models, with a random intercept to account for within-subject correlation. Overall significance across myopia category was determined from these models using F-tests, with denominator degrees of freedom computed via Satterthwaite's method. Significance of pairwise comparisons of myopia groups was determined similarly by t-tests of regression parameters with degrees of freedom calculated via Satterthwaite's method. Univariate and age and VF MD adjusted models were fit to evaluate the association between axial length and ocular parameters of interest. Similar univariate and multivariate (adjusted for age and axial length) regression models were fit to evaluate the association between VF MD and ocular parameters. R-squared values were computed via the methods of Edwards el. al, with partial R-squared computed for the fixed effect of interest in age and VF MD multivariate models[31]. Pearson correlation coefficient was applied to assess correlation between BMO ovality index, BMO tilt and BMO rotation. All statistical analyses were performed using the R (version 3.5.2)[32]. We consider p values less than 0.05 to indicate statistical significance throughout.

Results

Four hundred fifty-two glaucoma eyes of 277 patients were included with 145 eyes (81 patients) in the no axial myopia group, 214 eyes (128 patients) in the mild axial myopia group and 93 eyes (68 patients) in the high axial myopia group (Table 1). Mean (95% [CI]) age (years) in the high axial myopia group was significantly younger (65.6 [62.6, 68.7]) compared to the mild (73.0 [71.1, 74.9]) and no axial myopia (77.2 [74.7, 79.6]) group ($p < 0.001$). The proportion of individuals of Asian descent was higher (17.6%) and of African descent lower (13.2%) in the high axial myopia group, compared to the mild and no axial myopia group ($p = 0.410$). Mean (95% [CI]) spherical equivalent was significantly lower in high axial myopes (−3.49 [−4.06, −2.92]) compared to mild (−1.36 [−1.74, −0.98]) and non-myopes (0.21 [−0.24, 0.66]) (age adjusted $p < 0.001$). There was no significant difference in mean visual field mean deviation (MD) ($p = 0.450$), IOP ($p = 0.514$), central corneal thickness (CCT) ($p = 0.788$) and BMO area (age adjusted $p = 0.608$) between the three groups.

OCT optic disc parameters. A total of 21 eyes were excluded from the analysis for not meeting image quality criteria of ONHRC scans (quality score > 15 dB or ONHRC segmentation failure) with 9/145 (6.2%), 7/214 (3.3%) and 5/46 (10.9%) eyes excluded from the no-, mild- and high axial myopia group, respectively. Excluded eyes were significantly younger (mean age = 62.7 years, $p = 0.009$), had a higher axial length (mean = 25.1 mm, $p = 0.032$) and a worse VF MD (mean = −14.3 dB, $p = 0.001$) than included eyes.

BMO morphometrics (ovality index and tilt angle) and choroidal thickness differed by axial myopia group. BMO rotation angle, global and sectoral RNFL thickness values and global and sectoral BMO-MRW values except in the temporal sector for the RNFL and the superonasal sector for the BMO-MRW did not differ significantly between the axial myopia groups. These results along with age- and VF MD adjusted p values are presented in Table 2. Specifically, the BMO of high axial myopes was significantly more oval (0.85 [0.84, 0.87]) compared to no axial myopes (0.88 [0.86, 0.89]) and mild axial myopes (0.89 [0.88, 0.90]; $p < 0.005$), but this difference is small and may not be clinically important. The BMO also was significantly more titled in high myopes (3.4° [3.1, 3.8]) compared to mild myopes (2.0° [1.8, 2.2]) and no myopes (1.7° [1.5, 2.0]; $p < 0.001$). In contrast to global and other sectoral RNFL and BMO-MRW thickness values, in multivariable analysis in the high myopia group temporal RNFL thickness was significantly thicker and the superonasal BMO-MRW was significantly thinner compared to the no myopia group.

Global and sectoral PCT values were also significantly thinner in highly axial myopic eyes compared to mild axial myopic eyes and non-axial myopic eyes. The sectoral thickness pattern of the PCT was similar across no-, mild- and high myopic groups with the PCT thinnest in the inferotemporal sector (106.5 μm vs. 95.1 μm vs. 82.7 μm, respectively) and thickest in the superonasal sector (152.8 μm vs. 140.9 μm vs. 128.7, respectively) (Table 2).

	No myopia	Mild myopia	High myopia	*p* value (Age and VF MD adjusted *p* value)
BMO morphometrics	77 (128 eyes)	118 (185 eyes)	51 (61 eyes)	
Ovality index	0.88 (0.86, 0.89)	0.89 (0.88, 0.90)	0.85 (0.84, 0.87)	$0.003^{2,3}$ (0.007^{3})
Tilt angle (°)	1.7 (1.4, 2.0)	2.0 (1.8, 2.2)	3.4 (3.1, 3.8)	$<0.001^{2,3}$ ($<0.001^{2,3}$)
Rotation angle (°)	36.1 (32.6, 39.7)	35.0 (32.1, 37.9)	36.7 (31.4, 42.0)	0.818 (0.803)
RNFL thickness (µm)	81 (145 eyes)	128 (214 eyes)	68 (93 eyes)	
Global	67.1 (64.2, 70.0)	65.2 (62.8, 67.6)	67.5 (64.0, 70.9)	0.427 (0.419)
Temporal	52.6 (49.7, 55.5)	54.6 (52.2, 56.9)	58.8 (55.4, 62.3)	$0.024^{2,3}$ ($0.029^{2,3}$)
Superotemporal	85.9 (80.9, 90.9)	81.5 (77.4, 85.7)	85.2 (79.2, 91.3)	0.332 (0.284)
Inferotemporal	89.9 (83.6, 96.1)	82.8 (77.6, 87.9)	89.2 (81.7, 96.7)	0.135 (0.139)
Nasal	57.6 (54.8, 60.4)	58.0 (55.7, 60.3)	57.7 (54.3, 61.1)	0.972 (0.934)
Superonasal	77.4 (73.0, 81.7)	72.2 (68.6, 75.8)	71.4 (66.1, 76.7)	0.122 (0.120)
Inferonasal	73.4 (69.0, 77.9)	68.1 (64.5, 71.7)	70.3 (65.1, 75.6)	0.162 (0.227)
BMO-MRW (µm)	80 (142 eyes)	124 (204 eyes)	59 (78 eyes)	
Global	199.1 (188.8, 209.4)	192.4 (183.8, 201.0)	188.0 (174.8, 201.2)	0.387 (0.392)
Temporal	148.9 (140.4, 157.5)	148.3 (141.1, 155.4)	155.6 (144.6, 166.6)	0.513 (0.784)
Superotemporal	179.4 (166.4, 192.3)	162.6 (151.8, 173.4)	170.9 (154.2, 187.5)	0.128^{1} (0.102^{1})
Inferotemporal	182.4 (167.6, 197.3)	177.2 (164.7, 189.6)	178.5 (159.4, 197.7)	0.856 (0.945)
Nasal	226.2 (212.7, 239.7)	228.8 (217.5, 240.0)	211.1 (193.7, 228.5)	0.226 (0.262)
Superonasal	226.9 (213.9, 239.9)	206.6 (195.7, 217.5)	192.0 (175.3, 208.8)	$0.004^{1,2}$ ($0.003^{1,2}$)
Inferonasal	243.9 (228.9, 258.9)	224.2 (211.7, 236.7)	217.0 (197.6, 236.4)	$0.052^{1,2}$ (0.121)
Choroidal thickness (µm)	76 (135 eyes)	126 (203 eyes)	47 (61 eyes)	
Global	135.8 (125.4, 146.2)	122.3 (113.9, 130.8)	109.8 (96.4, 123.1)	$0.006^{1,2}$ ($<0.001^{1,2,3}$)
Temporal	140.8 (129.0, 152.6)	121.0 (111.5, 130.6)	95.0 (79.6, 110.5)	$<0.001^{1,2,3}$ ($<0.001^{1,2,3}$)
Superotemporal	152.5 (140.3, 164.6)	136.6 (126.8, 146.5)	114.1 (98.2, 130.0)	$0.001^{1,2,3}$ ($<0.001^{1,2,3}$)
Inferotemporal	106.5 (97.2, 115.8)	95.1 (87.5, 102.6)	82.7 (70.6, 94.8)	$0.007^{1,2}$ ($<0.001^{1,2,3}$)
Nasal	142.7 (130.9, 154.4)	131.4 (121.8, 140.9)	128.6 (113.3, 144.0)	0.207 ($0.029^{1,2}$)
Superonasal	152.8 (140.2, 165.4)	140.9 (130.7, 151.1)	128.7 (112.1, 145.2)	0.062^{2} ($0.003^{1,2}$)
Inferonasal	111.2 (101.3, 121.1)	100.7 (92.7, 108.7)	100.0 (87.0, 112.9)	0.181 ($0.020^{1,2}$)

Table 2. Optic disc parameters by myopia group. Results are presented as mean (95% confidence interval). Significance is determined by linear mixed models. No myopia: AL ≤ 24.0 mm; Mild myopia: AL: > 24 mm and ≤ 26.0 mm; High myopia: AL > 26.0 mm. BMO-MRW, Bruch's membrane opening minimum rim width; ONH, optic nerve head; RNFL, retinal nerve fiber layer; VF MD, visual field mean deviation. [1]No versus Mild Myopia $p < 0.05$; [2]No versus High Myopia $p < 0.05$; [3]Mild versus High Myopia $p < 0.05$.

Not all optic nerve head parameters that differed across myopic groups were significantly associated with axial length (Fig. 3). Specifically, in multivariable models adjusted for age and VF MD (Table 3), there was a significant (all $p < 0.001$) but weak to moderate linear association (semi-partial R^2) between axial length and the BMO tilt angle ($R^2 = 10.4\%$) and global ($R^2 = 8.5\%$) and sectoral PCT with R^2 values ranging from 4.0% in the nasal sector to 15.8% in the temporal sector. BMO ovality index (R^2 =0.4%, $p = 0.289$), BMO rotation angle ($R^2 = 0.0\%$, $p = 0.947$), global RNFL thickness (0.0%, $p = 0.966$) and BMO-MRW (0.3%, $p = 0.294$) were not significantly associated with axial length in linear models. However, a weak, significant association between axial length and RNFL thickness in the temporal sector ($R^2 = 2.1\%$, $p = 0.006$, respectively) and BMO-MRW in the superonasal and inferonasal sectors ($R^2 = 1.9\%$, $p = 0.012$ and $R^2 = 1.2\%$, $p = 0.046$, respectively) was found.

In multivariable regression models adjusted for age and axial length we found global and sectoral RNFL and BMO-MRW to be significantly (semi-partial R^2) associated with VF MD (Table 4 and Fig. 4) with R^2 values ranging from 7.3% to 25.9%, and 10.6% to 23.8%, respectively. BMO tilt angle (0.9%, $p = 0.072$) and global (0%, $p = 0.659$) and sectoral PCT (all $p > 0.127$) were not associated with VF MD in univariate and multivariate regression models.

We found relatively weak associations among the 3 BMO morphometrics. Specifically, BMO ovality index was negatively correlated with the BMO tilt angle ($r = -0.23$, $p < 0.001$), and was positively correlated with BMO rotation angle ($r = 0.16$, $p = 0.007$). BMO tilt angle was negatively correlated with BMO rotation angle ($r = -0.12$, $p = 0.028$).

To validate our results, we also evaluated the association of the BMO parameters with myopia using ovality index, tilt angle and rotation angle calculated by the independent validation method. The independent method showed similar associations between ovality index, tilt and rotation angle and myopic group and axial length as obtained using SALSA described above (data not shown).

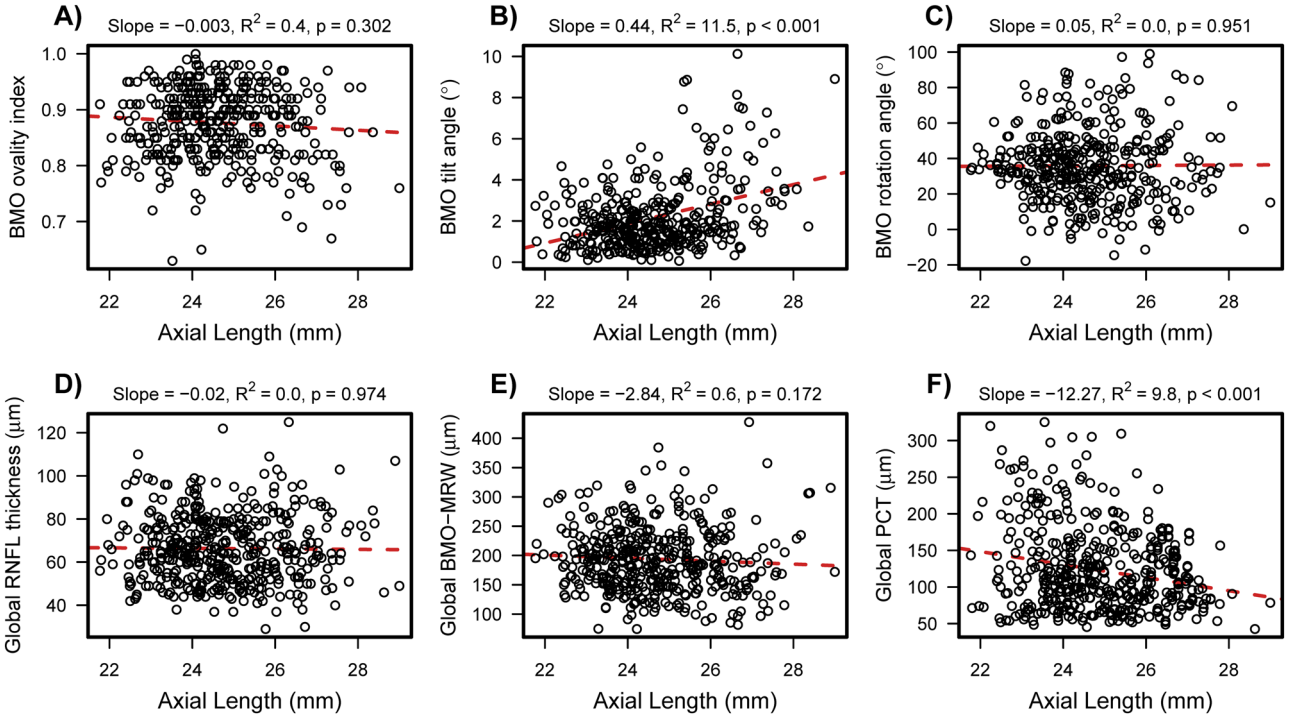

Figure 3. Scatter plots demonstrating association between axial length and ocular characteristics. Significant albeit relatively weak associations were found between axial length and BMO tilt angle (**B**) and PCT (**F**) in multivariate (adjusted for age and VF MD) regression analysis. No significant associations were found between axial length and BMO ovality index (**A**), BMO rotation angle (**C**), global RNFL thickness (**D**) and global BMO-MRW (**E**), respectively. Abbreviations: BMO, Bruch's membrane opening; MRW, minimum rim width; PCT, peripapillary choroidal thickness; RNFL, retinal nerve fiber layer.

Discussion

This study was unique in that it compared automated OCT-BMO based optic disc characteristics and deep learning assessed PCT of glaucoma eyes with no, mild and high axial myopia with similar severity of glaucoma (based on VF MD) and did not base these measurements on the subjective assessment using a photograph based clinical disc margin. We found that larger BMO tilt angle, lower BMO ovality index and thinner global PCT were associated with increased axial myopia while BMO rotation angle, global and sectoral RNFL thickness and BMO-MRW (except in the temporal, superonasal and inferonasal sectors) were not. This information can be used to inform the clinical management of glaucoma in myopic eyes and can contribute to the understanding of the pathophysiology of the myopic glaucoma eye.

There is evidence that the tilted configuration of the optic disc in myopic eyes is associated with a skewed outlet of the optic nerve from the globe during eyeball elongation[33]. Shearing deformations associated with remodelling of the connective tissue in myopic eyes may also be a factor contributing to the increased tilt[34]. Myopic eyes might therefore be more susceptible to IOP changes due to this anatomic- and tissue biomechanical variation, contributing to higher prevalence of glaucoma among myopic eyes. For this reason, indices that capture this phenomena, such as 1) optic disc ovality index, 2) tilt and 3) rotation have been suggested as possible explanatory factors for the higher prevalence of glaucoma in myopic eyes compared to non-myopic eyes.

Results from previous studies are inconsistent, with some but not all studies reporting an association between axial length and optic disc ovality index[7–9,12,15,16,35]. In most prior studies ovality measurements were based on the clinical disc margin observed in fundus photographs[12–16]. In the current study we utilized custom automated analysis of OCT images to provide objective characterization of glaucoma eyes based on the underlying anatomy across a range of axial lengths. Furthermore, the definition and extent of myopia differed across studies with some reports using spherical equivalent, rather than using the axial length[9,35]. In one of the few studies that included high myopes and used OCT to quantify ovality, Nakanishi et al.[7] reported an association between axial length and the clinical disc margin based ovality index but not between axial length and the BMO margin based ovality index. Additionally, histological studies have reported the BMO in highly myopic eyes to be circular and not more oval than in non-highly myopic eyes[36]. These results are consistent with our results of no association with BMO based ovality index and axial length.

We also found that objective BMO-based tilt angle was associated with axial length, but not associated with VF MD indicating that larger BMO tilt angles are characteristic of eyes with long axial length and are unrelated to glaucoma. BMO tilt is therefore less likely to be useful to distinguish between healthy and glaucomatous eyes with the same axial length. It is challenging to compare our results to previous findings as the methods for measuring tilt varied across studies. Several studies defined a low ovality index as an indicator for disc tilt, rather

	N	Univariate regression[a]		Multivariable regression Age and VF MD adjusted[a]	
	Patients (Eyes)	Estimate (95% CI)	R^2 (*p* value)	Estimate (95% CI)	Semi-partial R^2 (*p* value)
Age	277 (452)	− 0.37 (− 0.63, − 0.11)	0.3 (0.006)	− 0.37 (− 0.63, − 0.11)	0.3 (0.005)
VF MD	277 (452)	− 0.30 (− 0.84, 0.23)	0.4 (0.262)	− 0.64 (− 1.20, − 0.08)	1.4 (0.026)
BMO morphometrics	246 (374)				
Ovality index		− 0.004 (− 0.009, 0.001)	0.7 (0.135)	− 0.003 (− 0.009, 0.003)	0.4 (0.289)
Tilt angle (°)		0.45 (0.33, 0.57)	13.4 (< 0.001)	0.42 (0.29, 0.55)	10.4 (< 0.001)
Rotation angle (°)		− 0.18 (− 1.78, 1.42)	0.0 (0.829)	− 0.06 (− 1.76, 1.65)	0.0 (0.947)
RNFL thickness (µm)	277 (452)				
Global		− 0.04 (− 1.21, 1.13)	0.0 (0.946)	0.02 (− 1.05, 1.10)	0.0 (0.966)
Temporal		1.70 (0.53, 2.87)	2.3 (0.005)	1.71 (0.49, 2.93)	2.1 (0.006)
Superotemporal		− 0.32 (− 2.37, 1.72)	0.0 (0.756)	− 0.36 (− 2.22, 1.50)	0.0 (0.707)
Inferotemporal		− 0.98 (− 3.51, 1.55)	0.2 (0.448)	− 0.50 (− 2.80, 1.80)	0.1 (0.670)
Nasal		0.01 (− 1.12, 1.15)	0.0 (0.981)	0.02 (− 1.15, 1.19)	0.0 (0.968)
Superonasal		− 1.29 (− 3.05, 0.47)	0.6 (0.151)	− 1.40 (− 3.20, 0.39)	0.6 (0.127)
Inferonasal		− 1.54 (− 3.32, 0.24)	0.8 (0.092)	− 1.34 (− 3.09, 0.41)	0.6 (0.135)
BMO-MRW (µm)	263 (424)				
Global		− 1.95 (− 6.31, 2.41)	0.2 (0.382)	− 2.22 (− 6.37, 1.92)	0.3 (0.294)
Temporal		2.69 (− 0.92, 6.30)	0.7 (0.146)	1.73 (− 1.92, 5.39)	0.3 (0.353)
Superotemporal		− 1.79 (− 7.28, 3.70)	0.1 (0.524)	− 3.31 (− 8.44, 1.81)	0.5 (0.206)
Inferotemporal		− 0.21 (− 6.50, 6.07)	0.0 (0.948)	− 0.59 (− 6.51, 5.33)	0.0 (0.846)
Nasal		− 2.78 (− 8.52, 2.96)	0.3 (0.344)	− 2.16 (− 8.05, 3.72)	0.2 (0.472)
Superonasal		− 6.78 (− 12.29, − 1.27)	1.7 (0.017)	− 6.97 (− 12.38, − 1.56)	1.9 (0.012)
Inferonasal		− 7.09 (− 13.40, − 0.77)	1.4 (0.029)	− 6.26 (− 12.39, − 0.13)	1.2 (0.046)
Choroid thickness (µm)	249 (399)				
Global		− 9.29 (− 14.00, − 4.58)	5.0 (< 0.001)	− 12.93 (− 17.61, − 8.25)	9.1 (< 0.001)
Temporal		− 15.31 (− 20.58, − 10.04)	10.3 (< 0.001)	− 19.67 (− 24.89, − 14.46)	15.8 (< 0.001)
Superotemporal		− 11.91 (− 17.38, − 6.44)	6.1 (< 0.001)	− 15.91 (− 21.37, − 10.44)	10.0 (< 0.001)
Inferotemporal		− 8.99 (− 13.18, − 4.81)	5.9 (< 0.001)	− 12.57 (− 16.72, − 8.43)	10.8 (< 0.001)
Nasal		− 5.99 (− 11.29, − 0.68)	1.7 (0.028)	− 9.46 (− 14.78, − 4.13)	4.0 (< 0.001)
Superonasal		− 7.67 (− 13.36, − 1.99)	2.4 (0.009)	− 11.53 (− 17.24, − 5.82)	5.1 (< 0.001)
Inferonasal		− 4.81 (− 9.26, − 0.36)	1.6 (0.035)	− 8.09 (− 12.57, − 3.62)	4.1 (< 0.001)

Table 3. The association of ocular characteristics with axial length. BMO-MRW, Bruch's membrane opening minimum rim width; CI, confidence interval; ONH, optic nerve head; RNFL, retinal nerve fiber layer; VF MD, visual field mean deviation. [a]Linear mixed models slope estimates (with 95% confidence intervals) from univariate and multivariable models adjusted for age and VF MD.

than measuring the actual degree angle of the disc tilt[12–14]. Other studies measured optic disc tilt calculated by projecting the clinical disc margin on the OCT ONH height profile and measuring the angle corresponding to where the disc margin and the height profile meet[8,16,18,37]. Park et al. reported that the clinical disc margin from photographs based tilt angle was greater in glaucoma eyes than in healthy eyes with similar axial length, concluding that glaucomatous eyes have more prominent optic disc morphological changes[18]. These definitions of ONH tilt angle are problematic because three-dimensional (i.e. z-axis) information is not utilized.

Utilizing an objective three-dimensional approach, we found rotation angles were similar across the three myopia groups and were not associated with axial length or VF MD. Again, it is challenging to compare results across studies due to methodological differences as the degree of optic disc rotation (often referred to as "torsion") has been traditionally based on evaluation of two-dimensional clinical fundus photographs by determining the angle between the long optic disc axis and the vertical meridian[7–9,14,16–18]. In this study, we differentiate between "tilt angle" which refers to the optic disc tilt and corresponding BMO rotated around a vertical axis, and "rotation angle" which refers to the rotation around a sagittal axis[38,39]. Optic disc diameters, in particular the long optic disc axis of the optic disc can easily be overestimated in a two-dimensional assessment, because of the slightly oblique view of the optic disc[22]. Studies using the clinical disc margin suggest that the rotation angle is more affected by glaucoma than myopia[8,18]. In contrast to these 2 studies which used two-dimensional definitions of rotation, we found no significant association between three-dimensional BMO rotation angle and VF MD in univariate and multivariate regression analysis. Other authors that applied a three-dimensional approach to assess optic disc rotation angle found the rotation angle to be associated with shorter axial length.

Consistent with our strategy of using the anatomically based BMO ellipse to measure ovality index, tilt and rotation, other studies have also confirmed the importance of utilizing OCT measurements to characterize the

	N	Univariate regression[a]		Multivariable regression Age and axial length adjusted[a]	
	Patients (Eyes)	Estimate (95% CI)	R^2 (p value)	Estimate (95% CI)	Semi-partial R^2 (p value)
Age	277 (452)	0.009 (−0.007, 0.026)	0.0 (0.267)	0.010 (−0.007, 0.027)	0.0 (0.248)
Axial length	277 (452)	−0.000 (−0.009, 0.008)	0.0 (0.921)	−0.002 (−0.011, 0.007)	0.0 (0.651)
BMO morphometrics	246 (374)				
Ovality index		−0.001 (−0.002, 0.000)	0.4 (0.242)	−0.001 (−0.001, 0.000)	0.3 (0.307)
Tilt angle (°)		−0.02 (−0.05, 0.00)	0.7 (0.100)	−0.02 (−0.04, 0.00)	0.9 (0.072)
Rotation angle (°)		0.10 (−0.21, 0.41)	0.1 (0.517)	0.11 (−0.20, 0.42)	0.1 (0.489)
RNFL thickness (µm)	277 (452)				
Global		1.09 (0.91, 1.26)	25.0 (<0.001)	1.07 (0.89, 1.25)	23.7 (<0.001)
Temporal		0.60 (0.40, 0.80)	7.2 (<0.001)	0.60 (0.40, 0.80)	7.3 (<0.001)
Superotemporal		1.95 (1.64, 2.26)	26.2 (<0.001)	1.90 (1.59, 2.21)	24.6 (<0.001)
Inferotemporal		2.43 (2.05, 2.80)	27.0 (<0.001)	2.41 (2.03, 2.79)	25.9 (<0.001)
Nasal		0.60 (0.41, 0.80)	7.9 (<0.001)	0.59 (0.39, 0.79)	7.4 (<0.001)
Superonasal		1.09 (0.79, 1.39)	10.6 (<0.001)	1.05 (0.74, 1.35)	9.6 (<0.001)
Inferonasal		1.34 (1.05, 1.62)	16.2 (<0.001)	1.31 (1.02, 1.60)	15.2 (<0.001)
BMO-MRW (µm)	263 (424)				
Global		3.78 (3.13, 4.44)	23.1 (<0.001)	3.74 (3.08, 4.39)	22.3 (<0.001)
Temporal		2.29 (1.72, 2.86)	12.3 (<0.001)	2.24 (1.66, 2.81)	11.7 (<0.001)
Superotemporal		4.97 (4.15, 5.79)	25.0 (<0.001)	4.85 (4.03, 5.67)	23.8 (<0.001)
Inferotemporal		5.43 (4.48, 6.38)	23.0 (<0.001)	5.36 (4.40, 6.32)	22.1 (<0.001)
Nasal		3.44 (2.50, 4.39)	10.8 (<0.001)	3.44 (2.49, 4.39)	10.6 (<0.001)
Superonasal		4.21 (3.33, 5.09)	17.5 (<0.001)	4.14 (3.26, 5.02)	16.8 (<0.001)
Inferonasal		4.89 (3.86, 5.92)	17.6 (<0.001)	4.86 (3.82, 5.89)	17.3 (<0.001)
Choroid thickness (µm)	249 (399)				
Global		0.27 (−0.30, 0.85)	0.1 (0.353)	0.13 (−0.44, 0.69)	0.0 (0.659)
Temporal		0.07 (−0.65, 0.78)	0.0 (0.856)	−0.17 (−0.85, 0.51)	0.0 (0.630)
Superotemporal		0.35 (−0.38, 1.08)	0.2 (0.346)	0.14 (−0.57, 0.85)	0.0 (0.705)
Inferotemporal		−0.14 (−0.68, 0.39)	0.0 (0.600)	−0.29 (−0.81, 0.24)	0.2 (0.286)
Nasal		0.70 (0.02, 1.39)	0.7 (0.046)	0.53 (−0.15, 1.21)	0.4 (0.127)
Superonasal		0.42 (−0.33, 1.18)	0.2 (0.275)	0.22 (−0.52, 0.97)	0.1 (0.557)
Inferonasal		0.16 (−0.43, 0.76)	0.1 (0.596)	0.01 (−0.58, 0.60)	0.0 (0.963)

Table 4. The association of ocular characteristics with VF MD. BMO-MRW, Bruch's membrane opening minimum rim width; CI, confidence interval; ONH, optic nerve head; RNFL, retinal nerve fiber layer; VF MD, visual field mean deviation. [a]Linear mixed models slope estimates (with 95% confidence intervals) from univariate and multivariable models adjusted for age and axial length.

optic disc[7,19,22,40]. For instance Dai et al.[22] demonstrated the discrepancy between the inaccurately short disc diameter measurements (particularly the horizontal disc diameter) by two-dimensional clinical disc margin assessment compared to three-dimensional OCT measurements in myopic and non-myopic eyes. The difference between the two-dimensional and three-dimensional disc diameter measurements increased with increasing axial length, suggesting that disc diameters based on two-dimensional clinical disc measurements may not be accurate for highly myopic eyes[22].

With excellent performance and reproducibility, OCT assessed RNFL thickness is widely used to detect glaucoma[41,42]. However, it is known that myopia can lead to a significant number of healthy eyes being classified as glaucoma (false-positives) based on comparison to the pattern of RNFL measurements in normative/reference databases of healthy eyes[43–45]. BMO-MRW is proposed as a more stable diagnostic marker to detect glaucoma[23]. Chauhan et al. reported a higher sensitivity at 95% specificity of BMO-MRW compared to RNFL thickness[23]. We found similar global RNFL thickness and BMO-MRW across the three myopia groups, and no significant association with axial length. However, the temporal RNFL thickness increased with increasing axial length and the supra-nasal BMO-MRW sector decreased with increasing axial length. Our results confirm previous reports that the pattern of RNFL thickness and BMO-MRW is different in myopic compared to non-myopic eyes, with myopic eyes often having a temporally located peak RNFL thickness[46,47]. resulting in a higher rate of false positives based on comparisons to normative/reference databases[43,48]. For glaucoma management decisions, RNFL and BMO-MRW values in the temporal and nasal sectors should be interpreted with caution as these sectors show a significant but weak association with axial length.

The role of choroidal vasculature in pathologies such as glaucoma and myopia has been previously investigated[49–52]. According to most clinical studies[49–51,53] the peripapillary choroidal thickness (PCT) decreases

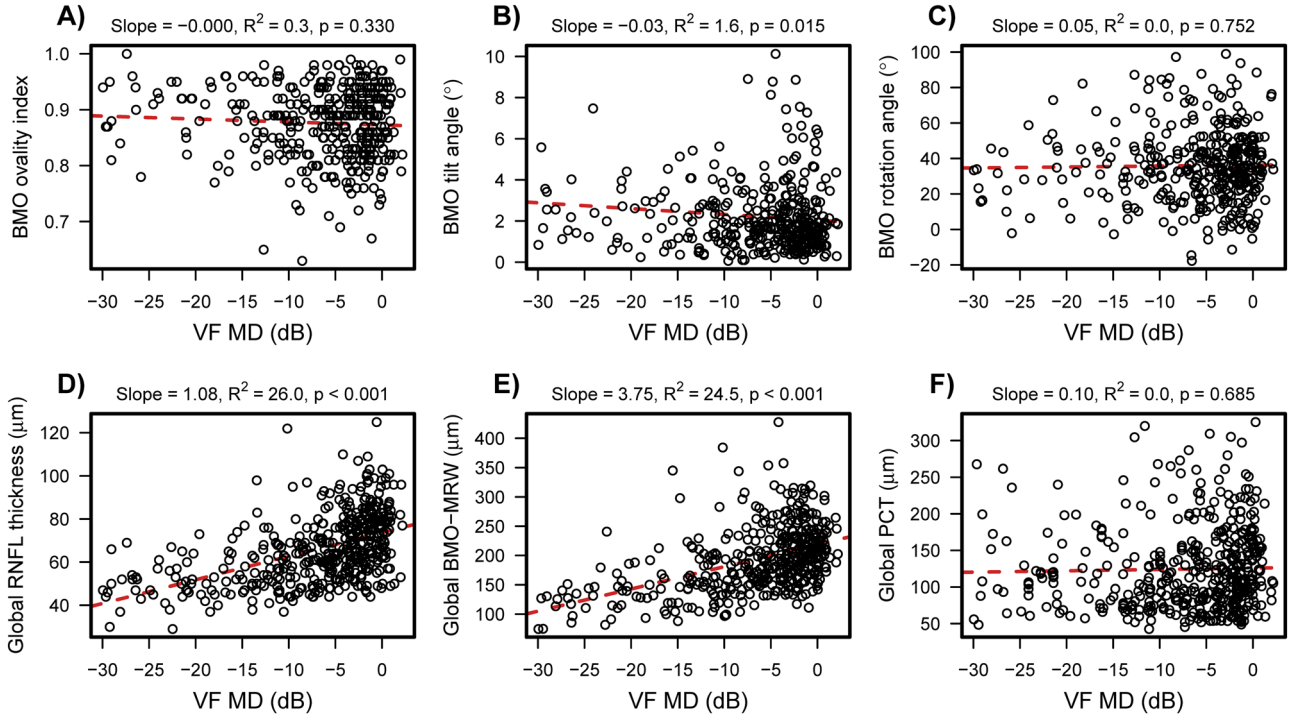

Figure 4. Scatter plots demonstrating association between VF MD and ocular characteristics. Significant associations were found between VF MD and RNFL (**D**) and BMO-MRW (**E**) in multivariate (adjusted for age and axial length) regression analysis. No significant association were found between VF MD and BMO ovality index (**A**), BMO tilt angle (**B**), BMO rotation angle (**C**) and global PCT (**F**), respectively. Abbreviations: BMO, Bruch's membrane opening; MRW, minimum rim width; PCT, peripapillary choroidal thickness; RNFL, retinal nerve fiber layer; VF MD, visual field mean deviation.

significantly with axial elongation, while an association between axial length and the thickness of the choriocapillaris is still in discussion[54]. As the choroidal vasculature provides the blood supply of the ONH[55], it is hypothesized that regions with thin choroid are associated with decreased choriocapillaris blood flow and may contribute to the optic disc region being more susceptible to elevated IOP[49,56,57]. We showed a decrease of the PCT with increasing axial length, which is likely due in part to the stretching of choroidal and retinal tissue with axial elongation. Consistent with other studies, we found the inferior sector has the thinnest PCT[49,52,56]. We found global and sectoral PCT to be associated with axial length but not with VF MD, which suggests that thin choroid is rather a characteristic of an axial highly myopic eye than a glaucomatous eye.

Deep learning strategies recently have revolutionized medical and ophthalmic research and enable diseases prediction and image segmentation[58]. We previously measured choroidal thickness using SALSA[59]. The SALSA strategy worked reasonably well, but had a relatively high rate of eyes excluded due to poor segmentation. In the current study we implemented automatized deep learning strategies (SALSA-deep) choroidal layer segmentation in OCT RNFL circle scans. To the best of our knowledge this is the first study utilizing BCDU-Net deep learning-based OCT choroid segmentation in highly myopic glaucoma eyes to assess PCT. SALSA deep did not require a large number of manually segmented scans for its ground truth and resulted in a smaller proportion of eyes excluded due to poor segmentation. A limitation of this approach using RNFL circle scans is that it might not represent choroidal thickness throughout the optic nerve head.

A strength of this study is that we investigated the relationship between axial myopia and optic disc morphology in two ways, by categorizing axial myopia status into three groups and by including axial length as a continuous variable. Both analyses are important. The categorized analysis of axial myopia has the advantage of providing clinicians with clear topographic optic nerve head information regarding the challenging subset of highly myopic eyes, a group whose optic nerve head features are difficult to interpret. Using axial length to define myopia groups instead of using the spherical equivalent, has advantages as it represents better the size of the eye and its axial elongation, then spherical equivalent which changes after cataract and refractive surgery[37], which is also confirmed by the results in Table 1. However, it should be noted that there are emmetropic eyes, as defined by spherical equivalent, in the mild myopia group. It is therefore important to distinguish between myopia that is defined by refractive error and axial myopia that is defined by axial length and to further keep in mind that spherical equivalent and axial myopia do not correlate strongly in all eyes.

Another study strength is that we used the BMO, an objective anatomical landmark, as the reference plane for analysis of the optic disc morphology instead of the clinical disc margin. Furthermore, we validated the sensitivity of the automated BMO parameters measurements with an independent method and found similar results. In addition, the baseline characteristics of the three glaucoma myopia groups including IOP and the severity of

disease (VF MD) were similar across the three groups so that the differences we found among the three groups were more likely due to the different axial lengths and not due to the severity of glaucoma.

Our study includes several potential limitations. First, the mean axial length in the high myopic group was 26.7 mm. We therefore cannot make generalizations about eyes with longer axial length. Second, due to relatively higher prevalence of high myopia in young patients, the high myopia group was significantly younger. For this reason, we incorporated multivariate analysis that adjusted for age. Third, the anatomic features of high myopic optic discs, make accurate BMO segmentation and detection difficult. We therefore meticulously reviewed the BMO segmentation of the radial scans for the BMO-MRW measurement and adjusted the BMO placement accordingly. In addition, to minimize the effect of inaccurate SALSA BMO segmentation, we fit an ellipse to the BMO plane for the custom calculation of ovality index, tilt and rotation. Fourth, myopia was defined by axial length but the axial length measurement was not repeated and evaluated for reproducibility. However, previous studies have reported that IOLMaster measurements show good repeatability and accuracy for axial length assessment[60].

In summary, using objective and anatomically based OCT measurements, we found that glaucoma eyes with highly myopic optic discs were characterized by larger BMO tilt and smaller PCT, and these parameters were not associated with severity of glaucoma (visual field mean deviation). Furthermore, caution should be exercised when using sectoral BMO-MRW and RNFL thickness for glaucoma management decisions in myopic eyes as the pattern varies with axial length.

Data availability

The data that support the findings of this study are available from the corresponding author upon reasonable request.

Received: 19 October 2020; Accepted: 5 April 2021
Published online: 23 April 2021

References

1. Weale, R. A. Epidemiology of refractive errors and presbyopia. *Surv. Ophthalmol.* **48**, 515–543 (2003).
2. Marcus, M. W., de Vries, M. M., Junoy Montolio, F. G. & Jansonius, N. M. Myopia as a risk factor for open-angle glaucoma: a systematic review and meta-analysis. *Ophthalmology* **118**, 1989–1994. https://doi.org/10.1016/j.ophtha.2011.03.012 (2011).
3. Jonas, J. B. Role of cerebrospinal fluid pressure in the pathogenesis of glaucoma. *Acta Ophthalmol.* **89**, 505–514. https://doi.org/10.1111/j.1755-3768.2010.01915.x (2011).
4. Xu, L., Wang, Y., Wang, S., Wang, Y. & Jonas, J. B. High myopia and glaucoma susceptibility the Beijing Eye Study. *Ophthalmology* **114**, 216–220. https://doi.org/10.1016/j.ophtha.2006.06.050 (2007).
5. Jonas, J. B. & Budde, W. M. Optic nerve damage in highly myopic eyes with chronic open-angle glaucoma. *Eur. J. Ophthalmol.* **15**, 41–47 (2005).
6. Xu, L. *et al.* Characteristics of highly myopic eyes: the Beijing Eye Study. *Ophthalmology* **114**, 121–126. https://doi.org/10.1016/j.ophtha.2006.05.071 (2007).
7. Nakanishi, H. *et al.* Association of Bruch's membrane opening and optic disc morphology to axial length and visual field defects in eyes with primary open-angle glaucoma. *Graefe's Arch. Clin. Exp. Ophthalmol. = Albrecht von Graefes Archiv fur klinische und experimentelle Ophthalmologie* **256**, 599–610. https://doi.org/10.1007/s00417-017-3874-8 (2018).
8. Choi, J. A., Park, H. Y., Shin, H. Y. & Park, C. K. Optic disc tilt direction determines the location of initial glaucomatous damage. *Invest. Ophthalmol. Vis. Sci.* **55**, 4991–4998. https://doi.org/10.1167/iovs.14-14663 (2014).
9. How, A. C. *et al.* Population prevalence of tilted and torted optic discs among an adult Chinese population in Singapore: the Tanjong Pagar Study. *Arch. Ophthalmol. (Chicago, Ill.: 1960)* **127**, 894–899. https://doi.org/10.1001/archophthalmol.2009.134 (2009).
10. You, Q. S., Xu, L. & Jonas, J. B. Tilted optic discs: The Beijing Eye Study. *Eye (Lond.)* **22**, 728–729. https://doi.org/10.1038/eye.2008.87 (2008).
11. Hsu, C. H., Chen, R. I. & Lin, S. C. Myopia and glaucoma: sorting out the difference. *Curr. Opin. Ophthalmol.* **26**, 90–95. https://doi.org/10.1097/icu.0000000000000124 (2015).
12. Tay, E. *et al.* Optic disk ovality as an index of tilt and its relationship to myopia and perimetry. *Am. J. Ophthalmol.* **139**, 247–252. https://doi.org/10.1016/j.ajo.2004.08.076 (2005).
13. Seol, B. R., Park, K. H. & Jeoung, J. W. Optic disc tilt and glaucoma progression in myopic glaucoma: A longitudinal match-pair case-control study. *Invest. Ophthalmol. Vis. Sci.* **60**, 2127–2133. https://doi.org/10.1167/iovs.18-25839 (2019).
14. Park, H. L., Kim, Y. C., Jung, Y. & Park, C. K. Vertical disc tilt and features of the optic nerve head anatomy are related to visual field defect in myopic eyes. *Sci. Rep.* **9**, 3485. https://doi.org/10.1038/s41598-019-38960-6 (2019).
15. Zhao, X. J. *et al.* Correlations between the optic nerve head morphology and ocular biometrics in highly myopic eyes. *Int. J. Ophthalmol.* **11**, 997–1001. https://doi.org/10.18240/ijo.2018.06.17 (2018).
16. Takasaki, H., Higashide, T., Takeda, H., Ohkubo, S. & Sugiyama, K. Relationship between optic disc ovality and horizontal disc tilt in normal young subjects. *Jpn. J. Ophthalmol.* **57**, 34–40. https://doi.org/10.1007/s10384-012-0193-9 (2013).
17. Hwang, Y. H., Yoo, C. & Kim, Y. Y. Characteristics of peripapillary retinal nerve fiber layer thickness in eyes with myopic optic disc tilt and rotation. *J. Glaucoma* **21**, 394–400. https://doi.org/10.1097/IJG.0b013e3182182567 (2012).
18. Park, H. Y., Choi, S. I., Choi, J. A. & Park, C. K. Disc torsion and vertical disc tilt are related to subfoveal scleral thickness in open-angle glaucoma patients with myopia. *Invest. Ophthalmol. Vis. Sci.* **56**, 4927–4935. https://doi.org/10.1167/iovs.14-15819 (2015).
19. Wang, Y. X. *et al.* Peripapillary scleral bowing increases with age and is inversely associated with peripapillary choroidal thickness in healthy eyes. *Am. J. Ophthalmol.* https://doi.org/10.1016/j.ajo.2020.03.050 (2020).
20. Hong, S. W. *et al.* Glaucoma specialist optic disc margin, rim margin, and rim width discordance in glaucoma and glaucoma suspect eyes. *Am. J. Ophthalmol.* **192**, 65–76. https://doi.org/10.1016/j.ajo.2018.04.022 (2018).
21. Reis, A. S. *et al.* Optic disc margin anatomy in patients with glaucoma and normal controls with spectral domain optical coherence tomography. *Ophthalmology* **119**, 738–747. https://doi.org/10.1016/j.ophtha.2011.09.054 (2012).
22. Dai, Y., Jonas, J. B., Ling, Z. & Sun, X. Ophthalmoscopic-Perspectively Distorted Optic Disc Diameters and Real Disc Diameters. *Invest. Ophthalmol. Vis. Sci.* **56**, 7076–7083. https://doi.org/10.1167/iovs.14-16033 (2015).
23. Chauhan, B. C. *et al.* Enhanced detection of open-angle glaucoma with an anatomically accurate optical coherence tomography-derived neuroretinal rim parameter. *Ophthalmology* **120**, 535–543. https://doi.org/10.1016/j.ophtha.2012.09.055 (2013).
24. Sample, P. A. *et al.* The African Descent and Glaucoma Evaluation Study (ADAGES): design and baseline data. *Archives of ophthalmology (Chicago, Ill.: 1960)* **127**, 1136–1145. https://doi.org/10.1001/archophthalmol.2009.187 (2009).

25. Jonas, J. B., Ohno-Matsui, K. & Panda-Jonas, S. Optic Nerve Head Histopathology in High Axial Myopia. *J. Glaucoma* **26**, 187–193. https://doi.org/10.1097/IJG.0000000000000574 (2017).
26. Shen, L. *et al.* Scleral and choroidal volume in relation to axial length in infants with retinoblastoma versus adults with malignant melanomas or end-stage glaucoma. *Graefe's Arch. Clin. Exp. Ophthalmol. = Albrecht von Graefes Archiv fur klinische und experimentelle Ophthalmologie* **254**, 1779–1786. https://doi.org/10.1007/s00417-016-3345-7 (2016).
27. Wang, Y. *et al.* Optic disc size in a population based study in northern China: the Beijing Eye Study. *Br. J. Ophthalmol.* **90**, 353–356. https://doi.org/10.1136/bjo.2005.081521 (2006).
28. Kromer, R. & Spitzer, M. S. Bruch's membrane opening minimum rim width measurement with SD-OCT: A method to correct for the opening size of Bruch's membrane. *J Ophthalmol* **2017**, 8963267. https://doi.org/10.1155/2017/8963267 (2017).
29. Belghith, A. *et al.* Does the location of Bruch's membrane opening change over time? Longitudinal analysis using san diego automated layer segmentation algorithm (SALSA). *Invest. Ophthalmol. Vis. Sci.* **57**, 675–682. https://doi.org/10.1167/iovs.15-17671 (2016).
30. Krishna Devalla, S. *et al.* A deep learning approach to digitally stain optical coherence tomography images of the optic nerve head (2017). arXiv:1707.07609.
31. Edwards, L. J., Muller, K. E., Wolfinger, R. D., Qaqish, B. F. & Schabenberger, O. An R2 statistic for fixed effects in the linear mixed model. *Stat. Med.* **27**, 6137–6157. https://doi.org/10.1002/sim.3429 (2008).
32. Team, R. C. R: A language and environment for statistical computing. (2013).
33. Rada, J. A., Shelton, S. & Norton, T. T. The sclera and myopia. *Exp. Eye Res.* **82**, 185–200. https://doi.org/10.1016/j.exer.2005.08.009 (2006).
34. Grytz, R., Yang, H., Hua, Y., Samuels, B. C. & Sigal, I. A. Connective tissue remodeling in myopia and its potential role in increasing risk of glaucoma. *Curr. Opin. Biomed. Eng.* **15**, 40–50 (2020).
35. Guo, Y. *et al.* Optic Disc Ovality in Primary School Children in Beijing. *Invest. Ophthalmol. Vis. Sci.* **56**, 4547–4553. https://doi.org/10.1167/iovs.15-16590 (2015).
36. Wang, Y. X., Panda-Jonas, S. & Jonas, J. B. Optic nerve head anatomy in myopia and glaucoma, including parapapillary zones alpha, beta, gamma and delta: Histology and clinical features. *Prog. Retinal Eye Res.* https://doi.org/10.1016/j.preteyeres.2020.100933 (2020).
37. Hosseini, H. *et al.* Measurement of the optic disc vertical tilt angle with spectral-domain optical coherence tomography and influencing factors. *Am. J. Ophthalmol.* **156**, 737–744. https://doi.org/10.1016/j.ajo.2013.05.036 (2013).
38. Fan, Y. Y., Jonas, J. B., Wang, Y. X., Chen, C. X. & Wei, W. B. Horizontal and vertical optic disc rotation. The Beijing Eye Study. *PLoS ONE* **12**, e0175749. https://doi.org/10.1371/journal.pone.0175749 (2017).
39. Jonas, J. B. *et al.* Parapapillary Gamma Zone and Axial Elongation-Associated Optic Disc Rotation: The Beijing Eye Study. *Invest. Ophthalmol. Vis. Sci.* **57**, 396–402. https://doi.org/10.1167/iovs.15-18263 (2016).
40. Marsh-Tootle, W. L. *et al.* Optic nerve tilt, crescent, ovality, and torsion in a multi-ethnic cohort of young adults with and without myopia. *Invest. Ophthalmol. Vis. Sci.* **58**, 3158–3171. https://doi.org/10.1167/iovs.16-20860 (2017).
41. Leung, C. K. *et al.* Retinal nerve fiber layer imaging with spectral-domain optical coherence tomography: a variability and diagnostic performance study. *Ophthalmology* **116**, 1257–1263, 1263 e1251–1252, doi:https://doi.org/10.1016/j.ophtha.2009.04.013 (2009).
42. Leung, C. K. *et al.* Retinal nerve fiber layer imaging with spectral-domain optical coherence tomography: analysis of the retinal nerve fiber layer map for glaucoma detection. *Ophthalmology* **117**, 1684–1691. https://doi.org/10.1016/j.ophtha.2010.01.026 (2010).
43. Vernon, S. A., Rotchford, A. P., Negi, A., Ryatt, S. & Tattersal, C. Peripapillary retinal nerve fibre layer thickness in highly myopic Caucasians as measured by Stratus optical coherence tomography. *Br. J. Ophthalmol.* **92**, 1076–1080. https://doi.org/10.1136/bjo.2007.127571 (2008).
44. Biswas, S., Lin, C. & Leung, C. K. Evaluation of a myopic normative database for analysis of retinal nerve fiber layer thickness. *JAMA ophthalmology* **134**, 1032–1039. https://doi.org/10.1001/jamaophthalmol.2016.2343 (2016).
45. Yamashita, T. *et al.* Relationship between supernormal sectors of retinal nerve fibre layer and axial length in normal eyes. *Acta Ophthalmol.* **92**, e481-487. https://doi.org/10.1111/aos.12382 (2014).
46. Hwang, Y. H., Yoo, C. & Kim, Y. Y. Myopic optic disc tilt and the characteristics of peripapillary retinal nerve fiber layer thickness measured by spectral-domain optical coherence tomography. *J. Glaucoma* **21**, 260–265. https://doi.org/10.1097/IJG.0b013e31820719e1 (2012).
47. Kim, M. J., Lee, E. J. & Kim, T. W. Peripapillary retinal nerve fibre layer thickness profile in subjects with myopia measured using the Stratus optical coherence tomography. *Br. J. Ophthalmol.* **94**, 115–120. https://doi.org/10.1136/bjo.2009.162206 (2010).
48. Kim, Y. W. & Park, K. H. Diagnostic accuracy of three-dimensional neuroretinal rim thickness for differentiation of myopic glaucoma from myopia. *Invest. Ophthalmol. Vis. Sci.* **59**, 3655–3666. https://doi.org/10.1167/iovs.18-24283 (2018).
49. Gupta, P. *et al.* Peripapillary choroidal thickness in young Asians with high myopia. *Invest. Ophthalmol. Vis. Sci.* **56**, 1475–1481. https://doi.org/10.1167/iovs.14-15742 (2015).
50. Flores-Moreno, I., Lugo, F., Duker, J. S. & Ruiz-Moreno, J. M. The relationship between axial length and choroidal thickness in eyes with high myopia. *Am. J. Ophthalmol.* **155**, 314–319 e311, doi:https://doi.org/10.1016/j.ajo.2012.07.015 (2013).
51. Yang, H. *et al.* Factors influencing optical coherence tomography peripapillary choroidal thickness: a multicenter study. *Invest. Ophthalmol. Vis. Sci.* **60**, 795–806. https://doi.org/10.1167/iovs.18-25407 (2019).
52. Huang, W. *et al.* Peripapillary choroidal thickness in healthy Chinese subjects. *BMC Ophthalmol.* **13**, 23. https://doi.org/10.1186/1471-2415-13-23 (2013).
53. Harb, E. *et al.* Choroidal thickness profiles in myopic eyes of young adults in the correction of myopia evaluation trial cohort. *Am. J. Ophthalmol.* **160**, 62–71 e62, doi:https://doi.org/10.1016/j.ajo.2015.04.018 (2015).
54. Holbach, L., Jonas, J. & Panda-Jonas, S. Choriocapillaris thickness and density in high myopia. *Acta Ophthalmol.* https://doi.org/10.1111/j.1755-3768.2019.5482 (2019).
55. Hayreh, S. S. Blood supply of the optic nerve head. *Ophthalmologica. Journal international d'ophtalmologie. International journal of ophthalmology. Zeitschrift fur Augenheilkunde* **210**, 285–295, doi:https://doi.org/10.1159/000310727 (1996).
56. Tanabe, H., Ito, Y. & Terasaki, H. Choroid is thinner in inferior region of optic disks of normal eyes. *Retina (Philadelphia, PA.)* **32**, 134–139. https://doi.org/10.1097/IAE.0b013e318217ff87 (2012).
57. Hirooka, K. *et al.* Evaluation of peripapillary choroidal thickness in patients with normal-tension glaucoma. *BMC Ophthalmol.* **12**, 29. https://doi.org/10.1186/1471-2415-12-29 (2012).
58. Shen, D., Wu, G. & Suk, H. I. Deep learning in medical image analysis. *Annu. Rev. Biomed. Eng.* **19**, 221–248. https://doi.org/10.1146/annurev-bioeng-071516-044442 (2017).
59. Mundae, R. S. *et al.* A longitudinal analysis of peripapillary choroidal thinning in healthy and glaucoma subjects. *Am. J. Ophthalmol.* **186**, 89–95. https://doi.org/10.1016/j.ajo.2017.10.025 (2018).
60. Lam, A. K., Chan, R. & Pang, P. C. The repeatability and accuracy of axial length and anterior chamber depth measurements from the IOLMaster. *Ophth. Physiol. Opt.* **21**, 477–483. https://doi.org/10.1046/j.1475-1313.2001.00611.x (2001).

Acknowledgements
DIGS: EY11008, EY19869, EY14267, EY027510, EY026574, EY029058, P30EY022589; UCSD School of Medicine Summer Research Fellowship; and participant retention incentive grants in the form of glaucoma medication at no cost from Novartis/Alcon Laboratories Inc, Allergan, Akorn, and Pfizer Inc. An Unrestricted grant from Research to Prevent Blindness (New York, NY).

Author contributions
J.R. conceptualized the study, was involved in the development of the methodology and drafted the original manuscript, C.B. was involved in the development of the methodology and revision of the manuscript, J.D. was responsible for the development of custom software, A.B. was responsible for the development of custom software, J.A.P. was responsible for data curation and the statistical analysis, M.C. was involved in the development of the methodology and custom software, L.H. was involved in the conceptualization of the study and editing of the manuscript, J.B.J was involved in the conceptualization of the study and editing of the manuscript, M.A.F. was involved in the development custom validation software and editing of the manuscript, R.N.W edited the manuscript, L.M.Z provided the resources and supervision for the study, and was involved in the conceptualization of the study, development of the methodology and in editing the manuscript. All authors reviewed the manuscript.

Funding
J.R.: Research Fellowship Grant of the German Research Foundation (DFG) (Grant-Nr: RE4155/1–1) and German Ophthalmological Society (DOG) Grant. C.B., J.D., A.B., J.A.P., M.C., L.H., J.B.J: None. M.A.F.: NEI/NIH, R01EY026574, African Descent and Glaucoma Evaluation (ADAGEs) IV: Alterations of the lamina cribrosa in progression). R.N.W.: Aerie Pharmaceuticals, Allergan, Eyenovia, Implantdata, Unity (consultant); Heidelberg Engineering, Carl Zeiss Meditec, Centervue, Bausch and Lomb, Genentech, Konan Medical, National Eye Institute, Optos, Optovue, Research to Prevent Blindness (New York, NY) (research support). L.M.Z.: Carl Zeiss Meditec, Heidelberg Engineering, National Eye Institute, Optovue, Topcon Medical System Inc. (research support).

Competing interests
JR: No competing interests CB: No competing interests JD: No competing interests AB: No competing interests JAP: No competing interests MC: No competing interests LH: No competing interests JBJ: No competing interests MAF: No competing interests LMZ: Research support and/or equipment from: Heidelberg Engineering, Carl Zeiss Meditec, Optovue, Topcon, Inc. RNW: Consultant: Aerie Pharmaceuticals, Allergan, Eyenovia, Implantdata; Unity. Financial Support: Heidelberg Engineering, Carl Zeiss Meditec, Konan, Optovue, Genentech, Optos, Centervue, Bausch&Lomb; Patent: Toromedes, Carl Zeiss Meditec.

Additional information
Supplementary Information The online version contains supplementary material available at https://doi.org/10.1038/s41598-021-88406-1.

Correspondence and requests for materials should be addressed to L.M.Z.

Reprints and permissions information is available at www.nature.com/reprints.

Publisher's note Springer Nature remains neutral with regard to jurisdictional claims in published maps and institutional affiliations.

Publikation II

Rezapour J, Bowd C, Dohleman J, Belghith A, Proudfoot JA, Chrisopher M, Hyman L, Jonas JB, Fazio MA, Weinreb RN, Zangwill LM; *Bruch's membrane opening detection accuracy in healthy and glaucoma eyes with and without high myopia in an American and Korean cohort;* American Journal of Ophthalmology; 2022; May;237:221-234. doi: 0.1016/j.ajo.2021.11.030. Epub 2021 Dec 10. PMID: 34902327.

Bruch Membrane Opening Detection Accuracy in Healthy Eyes and Eyes With Glaucoma With and Without Axial High Myopia in an American and Korean Cohort

JASMIN REZAPOUR, JAMES A. PROUDFOOT, CHRISTOPHER BOWD, JADE DOHLEMAN, MARK CHRISTOPHER, AKRAM BELGHITH, SUZANNE M. VEGA, KERI DIRKES, MIN HEE SUH, JOST B. JONAS, LESLIE HYMAN, MASSIMO A. FAZIO, RUTI SELLA, NATALIE A. AFSHARI, ROBERT N. WEINREB, AND LINDA M. ZANGWILL

• PURPOSE: To determine the predictors of Bruch membrane opening (BMO) location accuracy and the visibility of the BMO location in glaucoma and healthy individuals with and without axial high myopia.

• DESIGN: Cross-sectional study.

• METHODS: Healthy eyes and eyes with glaucoma from an American study and a Korean clinic population were classified into 2 groups: those with no axial high myopia (axial length [AL] <26 mm) and those with axial high myopia (AL ≥26 mm). The accuracy of the automated BMO location on optic nerve head Spectralis optical coherence tomography radial scans was assessed by expert reviewers.

• RESULTS: Four hundred thirty-eight non–highly myopic eyes (263 subjects) and 113 highly myopic eyes (81 subjects) were included. In healthy eyes with and without axial high myopia, 9.1% and 1.7% had indiscernible BMOs while 54.5% and 87.6% were accurately segmented, respectively. More than a third (36.4%) and 10.7% of eyes with indiscernible BMOs were manually correctable (respectively, $P = .017$). In eyes with glaucoma with and without high myopia, 15.0% and 3.2% had indiscernible BMOs, 55.0% and 38.2% were manually corrected, and 30.0% and 58.7% were accurately segmented without the need for manual correction (respectively, $P = .005$). Having axial high myopia, a larger AL, a larger BMO tilt angle, a lower BMO ovality index (more oval), and a glaucoma diagnosis were significant predictors of BMO location inaccuracy in multivariable logistic regression analysis.

• CONCLUSIONS: As BMO location inaccuracy was 2.4 times more likely in eyes with high axial myopia regardless of diagnosis, optical coherence tomography images of high myopes should be reviewed carefully, and when possible, BMO location should be corrected before using optic nerve head scan results for the clinical management of glaucoma. (Am J Ophthalmol 2022;237: 221–234. © 2021 Elsevier Inc. All rights reserved.)

AJO.com Supplemental Material available at AJO.com.
Accepted for publication November 29, 2021.

From the Hamilton Glaucoma Center (J.R., J.A.P., C.B., J.D., M.C., A.B., S.M.V., K.D., R.S., N.A.A., R.N.W., L.M.Z.), Shiley Eye Institute, Viterbi Family Department of Ophthalmology, University of California, San Diego, La Jolla, California, USA; Department of Ophthalmology (J.R.), University Medical Center of the Johannes Gutenberg University Mainz, Mainz, Germany; Department of Ophthalmology (M.H.S.), Haeundae Paik Hospital, Inje University College of Medicine, Busan, South Korea; Department of Ophthalmology (J.B.J.), Medical Faculty Mannheim, Ruprecht-Karls-University Heidelberg, Heidelberg, Germany; Institute of Molecular and Clinical Ophthalmology Basel (J.B.J.), Basel, Switzerland; Institute of Clinical and Scientific Ophthalmology and Acupuncture Jonas & Panda (J.B.J.), Heidelberg, Germany; Wills Eye Hospital (L.H.), Thomas Jefferson University, Philadelphia, Pennsylvania, USA; Department of Ophthalmology and Vision Science (M.A.F.), School of Medicine, The University of Alabama at Birmingham, Birmingham, Alabama, USA; Department of Biomedical Engineering (M.A.F.), School of Engineering, The University of Alabama at Birmingham, Birmingham, Alabama, USA; Department of Ophthalmology (R.S.), Rabin Medical Center, Petah Tikva, Israel; Sackler Faculty of Medicine (R.S.), Tel Aviv University, Tel Aviv, Israel

Inquiries to Linda M. Zangwill, Shiley Eye Institute/Hamilton Glaucoma Center, Viterbi Family Department of Ophthalmology, University of California, San Diego, 9500 Gilman Dr, La Jolla, CA 92093-0946, USA.; e-mail: lzangwill@health.ucsd.edu

EARLY GLAUCOMA DETECTION IS OF THE UTMOST importance to slow down or even stop disease progression in this chronic and potentially vision-threatening disease.[1] Structural loss in the optic nerve head (ONH) is often visible before perimetric visible visual field (VF) defects occur.[2,3] Optical coherence tomography (OCT) enables objective structural loss detection and is the standard of care along with VF testing for detecting glaucoma and monitoring its progression.

Glaucoma diagnosis based on clinical optic disc examination in (highly) myopic eyes can be difficult because of morphologic changes such as disc tilt and enlarged peripapillary areas that mimic glaucomatous ONH characteristics.[4,5] Structural changes associated with myopia also pose significant challenges to diagnose and monitor glaucoma using OCT. For example, the diagnostic accuracy of peripapillary retinal nerve fiber layer (RNFL) measurements in high myopes based on comparison to commercial OCT refer-

0002-9394/$36.00
https://doi.org/10.1016/j.ajo.2021.11.030

ence database of healthy non–highly myopic eyes has been shown to be lower because of the temporalization of the location of the RNFL peaks, leading to a misclassification of sectoral values as outside normal limits based on measurements from healthy eyes.[6–8] In addition, a recent study of myopic eyes highlighted the importance of assessing RNFL measurements relative to an anatomically accurate ONH center because sectoral circumpapillary RNFL (cpRNFL) thickness measured at fixed distances from the center of the Bruch membrane opening (BMO) were significantly different from those measured relative to the center of the clinical disc margin identified on infrared fundus image (ie, en face images).[9] These challenges are compounded by the difficulty in identifying the location of the BMO in highly myopic eyes.

The BMO is an important anatomic feature that is used by OCT instruments to define the ONH center to determine the location of RNFL thickness measurements at predetermined diameters in the circumpapillary retina.[9] RNFL thickness is the primary structural parameter used for detecting glaucoma and monitoring its progression. Moreover, the BMO also is used to measure the neuroretinal rim and the BMO-minimum rim width (MRW, defined as the shortest distance between the BMO and the internal limiting membrane). The diagnostic accuracy for glaucoma detection of the BMO-MRW is reportedly similar to or better than that of RNFL thickness and confocal scanning laser ophthalmoscope neuroretinal rim measurements, and BMO-MRW change over time has been shown to vary by race.[10–16] BMO location also is used to differentiate between different types of peripapillary atrophy (PPA), as β- and γ-PPA, and has been investigated as a biomarker to distinguish between myopia and glaucoma.[17–20]

Correct BMO localization is therefore necessary for appropriate representation of the ONH in OCT scans and is essential for the accurate measurement and interpretation of glaucomatous optic nerve and RNFL damage. Identifying the BMO in eyes with high axial myopia can be challenging[21] in part because of the differences in the appearance of the ONH, with highly myopic eyes having a greater degree of tilt and ovality than nonmyopic eyes.[22,23] With the increasing prevalence of myopia,[24–26] especially in Asian populations,[27] and given that myopia is a risk factor for glaucoma,[28–32] it is important to determine the accuracy of BMO detection in highly myopic eyes.

The objective of this study is to estimate the accuracy of OCT-based automated BMO detection and the likelihood of indiscernible BMOs in an American and Korean cohort of healthy subjects and patients with glaucoma with and without high myopia. In addition, anatomic features predictive of location accuracy and indiscernible BMOs are evaluated.

METHODS

Patients with glaucoma and healthy subjects from the Diagnostic Innovations in Glaucoma Study (clinicaltrials.gov identifier NCT00221897) and a Korean clinic population from Haeundae Paik Hospital (Busan, South Korea) were included in this cross-sectional study.

Study methods were approved by the Institutional Review Board of the University of California San Diego and adhered to the tenets of the Declaration of Helsinki and the Health Insurance Portability and Accountability Act. Methods also were approved by the Institutional Review Board of Haeundae Paik Hospital and written informed consent of the participants was waived. A detailed description of the Diagnostic Innovations in Glaucoma Study design has been published elsewhere.[33]

Participants were excluded if they had a history of intraocular surgery (except for cataract surgery or glaucoma surgery), secondary causes for glaucoma, VFs caused by other ocular or systemic diseases, significant cognitive impairment, or an inability to perform VF examinations reliably.[33]

Study subjects were ≥18 years of age and had open anterior chamber angles at study entry. All participants underwent a complete ophthalmologic examination including best-corrected visual acuity and refractive error assessment, standard automated perimetry (Humphrey Field Analyzer; 24-2 Swedish interactive thresholding algorithm; Carl Zeiss Meditec), intraocular pressure (IOP) measurement (Goldmann applanation tonometry), gonioscopy, dilated fundus examination, central corneal thickness measured with ultrasound pachymetry (DGH Technology, Inc, Exton, Pennsylvania, USA), coherence interferometry measurement of the axial length (AL; IOLMaster, Carl Zeiss Meditec, Dublin, California, USA), simultaneous stereophotography of the optic disc and macula spectral-domain OCT measurement. If spherical equivalent (SE) was available only after cataract/refractive surgery, we did not include SE in the analysis.

For this report, glaucoma is defined based on photograph-based glaucomatous optic disc damage and the existence of corresponding glaucomatous VF loss (Humphrey Field Analyzer II with 24-2 testing using the Swedish Interactive Thresholding Algorithm, Carl Zeiss Meditec Inc).[33] Glaucomatous optic disc damage was defined as focal or diffuse narrowing of the neuroretinal rim, and/or presence of RNFL defects characteristic of glaucoma on optic disc stereophotographs, diagnosed by 2 masked trained observers. Glaucomatous VF damage was defined as 2 repeatable and reliable (<33% fixation losses and false negatives, and <33% false positives) VF tests with a glaucoma hemifield test outside normal limits and/or a pattern standard deviation with a P value < .05 with a similar of pattern of defect on consecutive abnormal tests.[33]

Healthy participants had healthy-appearing optic discs and RNFL based on masked stereoscopic photograph assessement with no history of repeatable abnormal VF results and no history of elevated IOP (all IOP measurements ≤21 mm Hg) in either eye. Normal VFs were defined as those with MD and pattern standard deviation with *P* values > .05 and a glaucoma hemifield test result within normal limits.

Because of optic disc changes in highly myopic eyes, optic disc photographs of highly myopic eyes were graded independently by 2 reviewers (J.R., C.B.) after a training with a senior consultant with extensive expertise in myopia and glaucoma (J.B.J.). Diagnosis was defined by consensus among the 2 reviewers and by adjudication by the senior consultant in case of disagreement.

Healthy (nonglaucomatous) eyes and eyes with glaucoma in the American and Korean cohorts were classified into 2 groups by AL, no axial high myopia (AL ≤26 mm) and axial high myopia (AL >26 mm). In this study we defined myopia by AL, rather than SE, because it is known from previous studies that axial elongation can lead to morphologic changes in the optic disc region and the fundus and that there is a stronger correlation between axial elongation and optic disc changes than SE and optic disc changes.[4,34] In addition, with this definition, we could more accurately assess myopia status using AL in eyes after refractive or cataract surgery.

• **SPECTRAL-DOMAIN OCT IMAGING:** The Spectralis OCT (Glaucoma Module Premium Edition, version 6.10; Heidelberg Engineering Inc, Heidelberg, Germany) ONH radial circle (ONH-RC) imaging protocol was used to obtain 24 radial scans and 3 circle scans centered on the ONH. A total of 24 B-scans averaged 25 × using automatic real-time and a resolution of approximately 6 μm between A-scans (1024 A-scans per B-scan) were captured per eye. The innermost termination of the Bruch membrane was automatically identified by the instrument software as the BMO in each of the 24 radial scans. The operator then reviews and confirms or corrects the location of the BMO, and if necessary retakes the scan to improve BMO centration, the distance between the scan center and the BMO center (ΔBMOC). The scan center was based on 4 BMO locations from 2 B-scans identified by the operator during live image acquisition whereas the BMO center was defined as the center of the BMO contour based on 48 BMO locations defined on the 24 high-resolution B-scans (Supplemental Figure 1). According to the manufacturer's recommendations, ΔBMOC should be <100 μm to guarantee comparability of the computed RNFL thickness with the device normative database RNFL thickness measurements (Supplemental Figure 1).[35] In this study, eyes with ΔBMOC >100 μm were included to reflect clinical practice where it is often difficult to meet the criteria in eyes with high axial myopia.

For all eyes enrolled in this study, the 48 automatically detected BMO locations obtained were reviewed for accuracy by 2 reviewers with extensive training and experience in BMO detection in myopic eyes. The first experienced reviewer manually adjusted the BMO location as needed. If the first reviewer had difficulty in identifying the BMO location in >4 different B-scans in 1 eye (4 of 8 BMO locations, but in 4 different scans), the eye was referred to a second reviewer. The second reviewer evaluated the scans with the primary reviewer to reach consensus on the correct BMO location in that eye. If the second reviewer also determined that it was not possible to confidently detect the BMO locations in >4 B-scans (>4 of 8 BMO locations in >4 different B-scans) this eye was classified as having indiscernible BMOs.[36] BMO location was classified as follows: 1) accurate automated BMO location (Figure 1); 2) manually corrected BMO location (Figure 2); and 3) indiscernible BMO (manual correction not possible [Figure 3]). BMO was defined as indiscernible only when 2 trained and experienced reviewers could not confidently place the BMO locations in >4 B-scans. Scans with low quality (quality score <15) were also excluded.

We also qualitatively evaluated characteristics of the images and B-scans of the 27 eyes with indiscernible BMO. Two graders (J.R., S.V.) reviewed the images and 24 B-scans of each of the 27 eyes with indiscernible BMO and reached consensus on the location of the B-scans and whether there was vessel shadowing or low image quality that influenced the ability to detect the BMO location. In addition, the en-face OCT ONH image was reviewed for the existence and location of PPA.

• **OPTIC NERVE HEAD MEASUREMENTS:**

Standard software ONH measurements

BMO area, BMO-MRW, ΔBMOC, and image quality score were measured automatically by the instrument software. Specifically, the BMO-MRW is automatically computed for each radial B-scan. The resultant 48 BMO-MRW measurements (each B-scan contributed 2 BMO locations) were averaged to generate global, temporal, superotempral, superonasal, nasal, inferonasal, and inferotemporal MRWs.

Custom BMO ovality index, tilt angle and rotation angle

BMO ovality index, BMO tilt angle, and BMO rotation angle were calculated using the San Diego Automated Layer Segmentation Algorithm based on the automatic or corrected BMO location.[37,38] All custom computations were performed using 3-dimensional rectangular coordinates. The coordinate transformation of each pixel was determined by the A-scan and B-scan index, along with the scan center and the fovea–BMO angle provided by the acquisition software. Major and minor axes of a BMO fit ellipse were defined as the longest and shortest axes of the fitted ellipse.

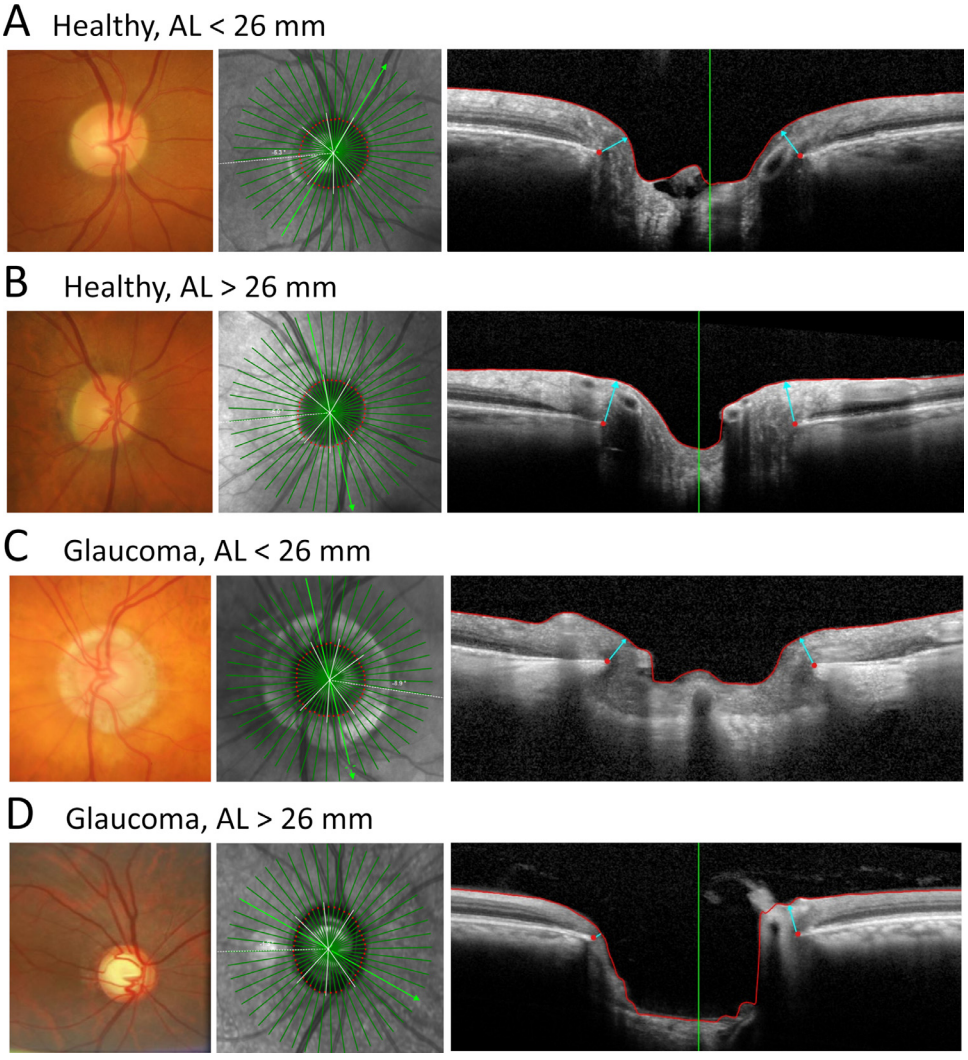

FIGURE 1. Automatically accurate Bruch membrane opening (BMO) locations in (A) a healthy non–highly myopic eye (axial length [AL] 23.4 mm), (B) a healthy highly myopic eye (AL 26.1 mm), (C) a non–highly myopic eye with glaucoma (AL 24.6 mm), and (D) a highly myopic eye with glaucoma (AL 26.2 mm). Left, Clinical photographs of the optic nerve head. Middle, En face images of the optical coherence tomography scan. Right, Radial B-scans of the optical coherence tomography scan. The red dots identify the automatic correct BMO location, the red line the internal limiting membrane segmentation, and the blue arrows indicate the BMO–minimum rim width.

The BMO ovality index was calculated by dividing the minor axis by the major axis.[38] For automated BMO-based tilt assessment, 2 BM boundary (BMB) points on the furthest outward 2 pixels on the BM contour and 2 BMO points were selected. Each BMB and BMO point was transformed into a rectangular coordinate space. One plane was fit to the BMB points and one plane to the BMO points, applying the least-squares method. BMO tilt was defined as the angle between the BMO plane and the BMB plane and computed by assessing the angle between their normal vectors.

In this study we aimed to assess the anatomically accurate 3D morphologic characteristics of the optic disc. We therefore applied a new term, "BMO rotation,"[38,39] instead of the term "optic disc torsion" used in studies that applied optic disc photographs to identify the clinical disc margin.[40] Measurements are based on the BMO, considered to be an anatomically based landmark, which has been shown to be more accurate and reliable than subjective measurements based on the clinical disc margin seen on fundus photographs.[10,36,37] In addition, the term torsion implies presence of shearing deformations in the ONH tissue, which cannot be confirmed without histologic or biomechanical analysis of the tissue. For details of BMO ovality index, BMO tilt angle, and BMO rotation angle calculations, see Rezapour and associates.[38]

For calculation of the BMO rotation angle, the center of mass of the BMO points was subtracted from each BMO

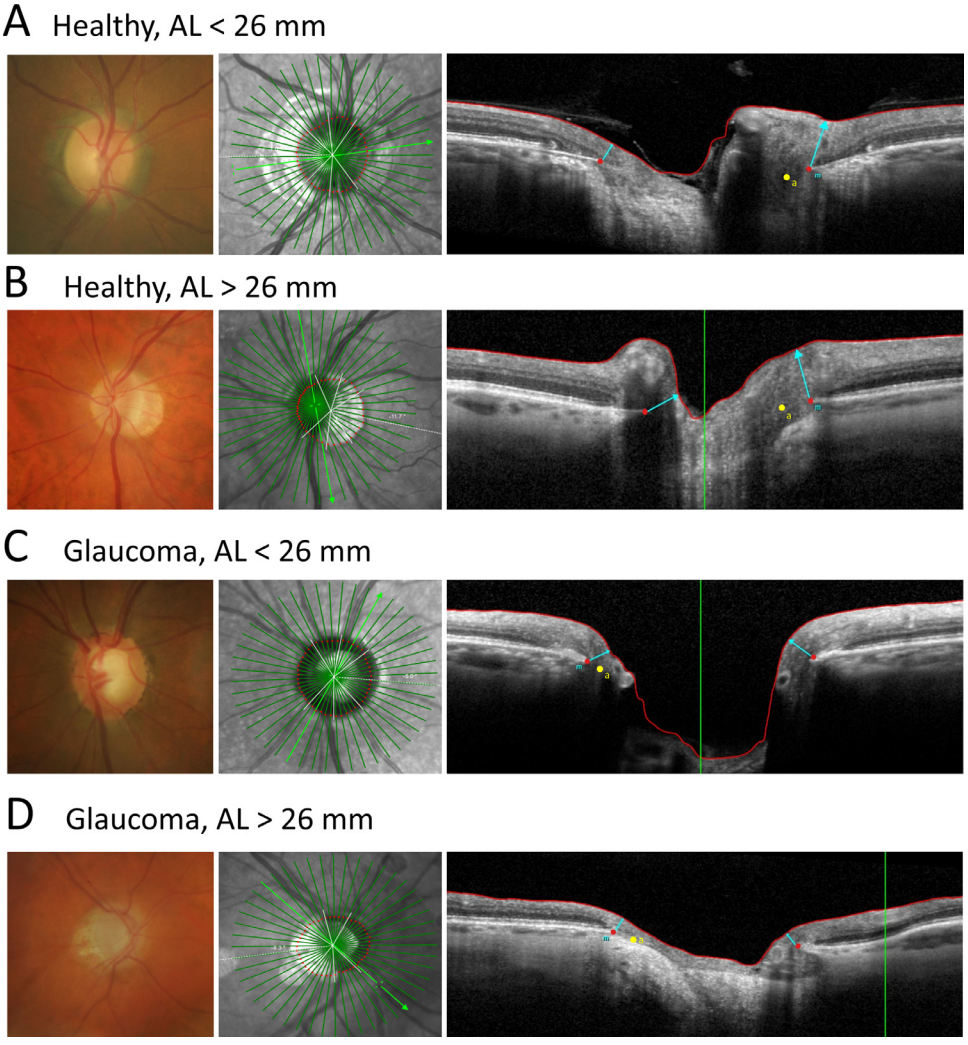

FIGURE 2. Manually corrected Bruch membrane opening (BMO) location (red dot) in (A) a healthy non–highly myopic eye (axial length [AL] 23.8 mm), (B) a healthy highly myopic eye (AL 27.2 mm), (C) a non–highly myopic eye with glaucoma (AL 23.3 mm), and (D) a highly myopic eye with glaucoma (AL 27.5 mm). Left, Clinical photographs of the optic nerve head. Middle, En face images of the optical coherence tomography scan. Right, Radial B-scans of the optical coherence tomography scan. The red dots identify the correct BMO location, the blue "m" stands for manually corrected, the yellow dots marked with an "a" illustrate the automatic inaccurate BMO location, the red line shows the internal limiting membrane segmentation, and the blue arrows indicate the BMO–minimum rim width.

point and rotated so that the fit plane lay in the xy-plane (ie, the transverse cross-section of the radial image). These points were projected on a reference plane and used to fit an ellipse in the 2D space of the reference plane. The ellipse was fit using the least-squares method by optimizing the conic equation of an arbitrary ellipse. The orientation of the ellipse was then calculated separately and added to the fit form. The major axis orientation was reported with reference to the temporal axis (fovea BMO center). All angles were reported after transforming the vectors used in their computations into physical space by scaling according to the scale X and scale Z constants in the image volume metadata. The rotation angle was calculated relative to the fovea BMO center.

• **STATISTICAL ANALYSES:** Data are presented as means (95% confidence interval [CI]) and count (percentage) for continuous and categorical variables, respectively. The statistical significance of differences in patient-level characteristics between myopia groups was determined by 2-sample *t* tests for continuous variables and the Fisher exact test for categorical variables. Eye-level characteristics were compared via generalized estimating equations, with an exchangeable working correlation assumed to account for within-patient clustering. Rates of location failure by eye classification and myopia were compared using logistic generalized estimating equations. The influence of different patient and ocular characteristics on the odds of nonaccurate location was computed via

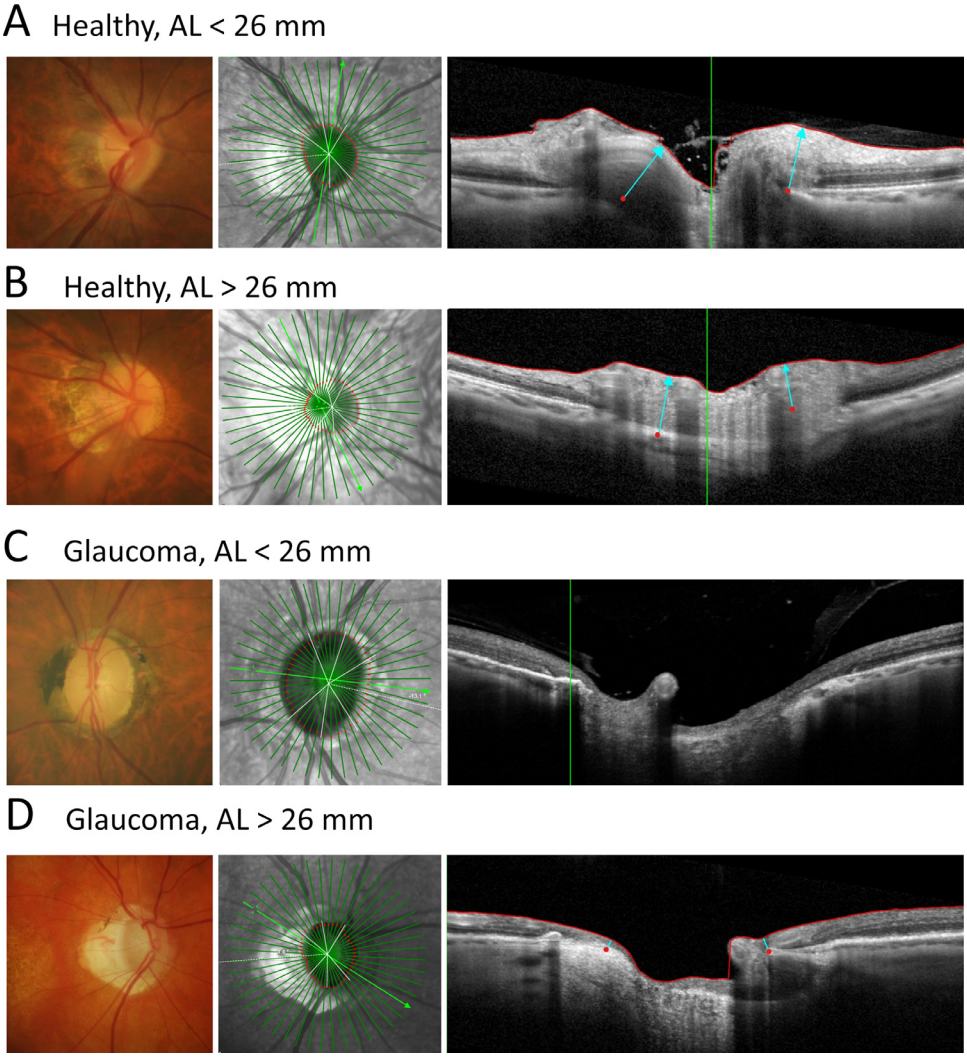

FIGURE 3. Indiscernible Bruch membrane opening (BMO) in (A) a healthy non–highly myopic eye (axial length [AL] 25.5 mm), (B) a healthy highly myopic eye (AL 29.1 mm), (C) a glaucoma non–highly myopic eye (AL 23.6 mm), and (D) a highly myopic eye with glaucoma (AL 27.2 mm). Left, Clinical photographs of the optic nerve head. Middle, En face images of the optical coherence tomography scan. Right, Radial B-scans of the optical coherence tomography scan. The red dots show the correct and incorrect automatically detected BMO locations. Incorrect BMO locations could not be manually corrected. The red line shows the internal limiting membrane segmentation, and the blue arrows indicate the BMO–minimum rim width. In part C, the software did not provide automatic BMO locations in some scans, as in this example.

univariable and multivariable logistic generalized estimating equations.

RESULTS

A total of 551 eyes (344 subjects) were included in this cross-sectional study; 438 eyes (79.5%) were classified as not highly myopic (AL ≤26 mm; 263 subjects) and 113 eyes (20.5%) as highly myopic (AL >26 mm; 81 subjects). The 154 healthy eyes included 33 (21.4%) highly myopic eyes while the 397 glaucoma eyes included 80 (20.1%) highly myopic eyes. Demographic information and eye characteristics are shown in Table 1.

Highly myopic individuals were significantly younger ($P < .001$) and more often of Asian descent ($P < .001$) than non–highly myopic individuals. There was no significant difference in the proportion of healthy eyes in the highly myopic and non–highly myopic groups (29.2% vs 27.6%, respectively; $P = .705$). The OCT quality score was slightly higher in highly myopic eyes (30.3 [29.6-30.9]) compared to non–highly myopic eyes (29.3 [28.9-29.7]; $P = .010$). The BMO-based ovality index and BMO rotation angle were significantly smaller (more oval) and BMO tilt angle significantly larger in highly myopic eyes compared with

TABLE 1. Patient and Eye Characteristics by Axial Myopia Group in American and Korean Eyes

	AL ≤26 mm (Non–Highly Myopic), n = 263 (438 Eyes)	AL >26 mm (High Myopic), n = 81 (113 Eyes)	Overall, N = 344 (551 Eyes)	*P* Value
Patient characteristics				
Age (y)	69.2 (67.5-70.9)	58.0 (54.6-61.4)	66.6 (64.9-68.2)	<.001[a]
Female (%)	54.8	42.0	51.7	
Race (n, %)				
African descent	62 (23.6)	6 (7.4)	68 (19.8)	<.001[a]
Asian descent	38 (14.4)	41 (50.6)	79 (23.0)	
European descent	156 (59.3)	32 (39.5)	188 (54.7)	
Other/not reported	7 (2.7)	2 (2.5)	9 (2.6)	
Eye characteristics				
Spherical equivalent (D)[b]	−0.91 (−1.17 to −0.65)	−4.23 (−5.08 to −3.38)	−1.51 (−1.85 to −1.17)	<.001[a]
Visual field MD (dB)[c]	−5.69 (−6.44 to −4.95)	−7.16 (−8.74 to −5.57)	−5.98 (−6.70 to −5.27)	.083
IOP (mm Hg)[b]	13.5 (13.1-14.0)	13.2 (12.2-14.2)	13.5 (13.0-13.9)	.563
Axial length (mm)	24.2 (24.1-24.3)	26.9 (26.6-27.2)	24.8 (24.6-25.0)	<.001[a]
CCT (μm)[d]	536.0 (531.2-540.8)	536.0 (527.6-544.4)	536.0 (531.5-540.5)	.999
BMO ovality index[e]	0.88 (0.87-0.89)	0.84 (0.81-0.86)	0.87 (0.86-0.88)	.001[a]
BMO rotation angle (°)[f]	34.3 (32.1-36.5)	24.2 (18.6-29.7)	32.3 (30.1-34.5)	<.001[a]
BMO tilt angle (°)[e]	2.0 (1.8-2.2)	4.8 (3.9-5.6)	2.6 (2.3-2.8)	<.001[a]
BMO area (mm^2)	2.13 (2.07-2.20)	2.30 (2.12-2.49)	2.17 (2.10-2.23)	.084
ΔBMOC (μm)	49.2 (43.9-54.5)	96.7 (81.0-112.5)	59.2 (53.4-65.0)	<.001[a]
OCT quality score	29.3 (28.9-29.7)	30.3 (29.6-30.9)	29.5 (29.1-29.8)	.010[a]
Eye diagnosis, n (%)				
Healthy	121 (27.6)	33 (29.2)	154 (27.9)	.705
Glaucoma	317 (72.4)	80 (70.8)	397 (72.1)	
Global MRW (μm)[g]	222.4 (213.7-231.0)	208.5 (195.4-221.5)	219.4 (211.3-227.6)	.038[a]
Temporal MRW (μm)[g]	169.0 (162.2-175.9)	168.5 (156.7-180.3)	168.9 (162.6-175.2)	.932
TS MRW (μm)[g]	202.1 (192.0-212.3)	198.5 (182.6-214.4)	201.4 (192.0-210.7)	.674
TI MRW (μm)	211.9 (200.0-223.7)	190.6 (173.0-208.2)	207.4 (196.4-218.3)	.023[a]
Nasal MRW (μm)	254.1 (243.5-264.6)	238.4 (220.3-256.5)	250.7 (241.2-260.2)	.130
NS MRW (μm)	249.5 (239.2-259.9)	219.3 (204.0-234.5)	243.1 (233.3-252.9)	<.001[a]
NI MRW (μm)	261.2 (248.4-274.0)	238.9 (216.7-261.0)	256.5 (245.1-267.8)	.084

AL = axial length; BMO = Bruch membrane opening; CCT = central corneal thickness; ΔBMOC = distance between the scan center and the BMO center; D = diopter; IOP = intraocular pressure; MD = mean deviation; MRW = minimum rim width; NI = nasal inferior; NS = nasal superior, OCT = optical coherence tomography; SE = spherical equivalent; TI = temporal inferior; TS = temporal superior; VF = visual field.

Data presented as mean (95% confidence interval) for continuous variables and n (%) for categorical variables. Significance is determined by a 2-sample *t* test and the Fisher exact rest for continuous and categorical patient-level variables and generalized estimating equations for eye-level variables.

[a]Statistically significant ($P < .05$).Missing values (n): 74,[b] 19,[c] 29,[d] 67,[e] 69,[f] and 1.[g]

non–highly myopic eyes (all $P < .001$). OCT ΔBMOC was significantly lower in non–highly myopic eyes (49.2 μm [43.9-54.5 μm]) compared with highly myopic eyes (96.7 μm [81.0-112.5 μm]; $P < .001$). BMO-MRW was significantly smaller in highly myopic compared with non–highly myopic eyes globally (208.5 μm [195.4-221.5 μm] and 222.4 μm [213.7-231.0 μm]), respectively; $P = .038$), in the temporal-inferior sector (190.6 μm [173.0-208.2 μm], vs 211.9 μm [200.0-223.7 μm], respectively; $P = .023$) and nasal-superior sector (219.3 μm [204.0-234.5 μm], vs 249.5 μm [239.2-259.9 μm], respectively; $P < .001$).

The proportion of eyes with accurate BMO location was significantly lower in the highly myopic healthy eyes (18/33 [54.5%]) and eyes with glaucoma (24/80 [30.0%]) than non–highly myopic healthy eyes (106/121 [87.6%]) and eyes with glaucoma (186/317 [58.7%]; Table 2). Similarly, the proportion of eyes with indiscernible BMO was significantly higher in highly myopic eyes compared to non–highly myopic eyes in both the healthy (9.1% vs 1.7%; $P = .017$) and glaucoma eyes (15.0% vs 3.2%; $P = .005$; Table 2 and Figure 4). Similar trends were found when the American and Korean datasets were analyzed separately before pooling the data across sites (data not shown).

Univariable logistic regression analysis and the associated odds ratios (ORs) assessing demographic and eye-specific predictors associated with BMO location inaccuracy (manually corrected and indiscernible combined) are shown in Table 3. Both longer AL as a continuous vari-

TABLE 2. Rates of Location Accuracy by Diagnosis and Axial Myopia Status in American and Korean Eyes

BMO Localization Status, n (%)	Healthy			Glaucoma		
	Non–High Myopia (AL ≤26 mm), n = 121	High Myopia (AL >26 mm), n = 33	*P* Value	Non–High Myopia (AL ≤26 mm), n = 317	High Myopia (AL > 26 mm), n = 80	*P* Value
Accurate automated	106 (87.6)	18 (54.5)	.017[a]	186 (58.7)	24 (30.0)	.005[a]
Manually corrected	13 (10.7)	12 (36.4)		121 (38.2)	44 (55.0)	
Indiscernible	2 (1.7)	3 (9.1)		10 (3.2)	12 (15.0)	

AL = axial length; BMO = Bruch membrane opening.

Significance is determined by logistic generalized estimating equations to adjust for both eyes of the patient in the analysis

[a]Statistically significant (*P* < .05).

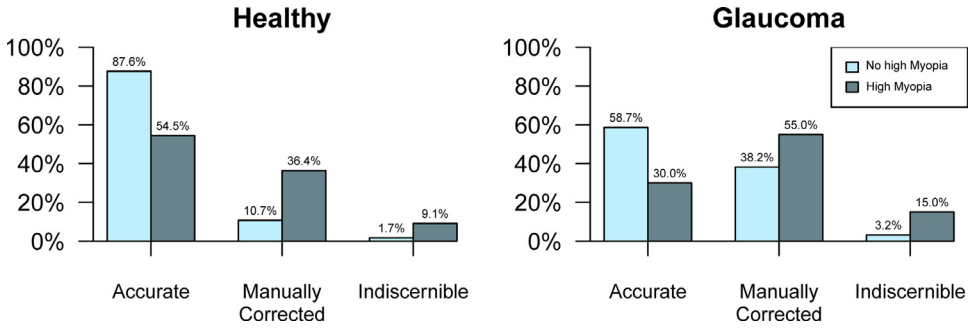

FIGURE 4. Percentage of automatic accurate, manually corrected, and indiscernible Bruch membrane opening in healthy eyes (left) and glaucoma eyes (right). "No high myopia" is defined as an axial length ≤26 mm and high myopia as an axial length >26 mm.

able and as a categorical variable (high myopia vs not high myopia) were strong predictors of higher BMO location inaccuracy. Specifically, for each 1-mm larger AL, the odds (95% CIs) of BMO location inaccuracy were 1.36 (1.20-1.54; $P < .001$). Eyes with axial high myopia were 3.38 ($P < .001$) times more likely to have initial inaccurate BMO location than eyes without axial high myopia. In addition, lower BMO ovality index (OR [95% CI] per 0.1 lower [more oval]: 1.57 [1.21-2.04]; $P < .001$), larger BMO tilt angle (OR [95% CI] per degree higher: 1.24 [1.14-1.35]; $P < .001$), larger BMO area (OR [95% CI] per 1 mm^2 higher: 1.40 [1.03-1.90]; $P = .032$), and thinner global BMO-MRW (OR [95% CI] per 10-μm thinner: 1.06 [1.03-109]; $P < .001$) were associated with location inaccuracy. Other factors associated with a higher univariable odds (OR [95% CI]) of location inaccuracy included male sex (1.56 [1.06-2.31]; $P = .025$), Asian descent (2.63 [1.42-4.88]; $P = .002$), and worse VF MD (per 1 dB lower; 1.10 [1.07-1.13]; $P < .001$).

Five multivariable models (Table 4) of BMO location error were developed for each of the 5 myopia-related parameters (SE, axial length, BMO ovality index, BMO tilt angle, and high myopia status) that were statistically significant ($P < .05$) based on the univariable analysis. The separate multivariable models were developed because the 5 myopia-related parameters were highly correlated with one another (data not shown). Glaucoma eyes were >4 times likely to have inaccurate location than healthy eyes and highly myopic eyes were 2.4 times more likely to have inaccurate BMO location than non–highly myopic eyes. Moreover, AL, BMO ovality index, BMO tilt angle, but not SE were significant predictors of BMO location inaccuracy. Specifically, the odds (95% CIs) of BMO location inaccuracy for each 1-mm larger AL were 1.20 (1.02-1.40; $P = .023$). Lower BMO ovality index (per 0.1 units lower – more oval: 1.45 [1.09-1.93]; $P = .010$), larger BMO tilt angle (per degree: 1.18 [1.07-1.30]; $P = .001$), and highly myopic eyes (AL >26 mm: 2.41 [1.36-4.25]; $P = .002$) were also associated with BMO location inaccuracy. None of the other parameters that were statistically significant in the univariable analysis were predictors of BMO location inaccuracy in the multivariable analysis.

The qualitative evaluation of characteristics of the images and b-scans of the 27 eyes with indiscernible BMO is shown in Table 5. In general, in highly myopic eyes with indiscernible BMOs, indiscernible BMOs were more often located in the temporal (43.5%) than the nasal sectors (26.3%). Vessel shadowing was visible in a relatively small proportion (21.5% and 30.3%) of B-scans in the high and non–high myopic eyes with indiscernible BMOs,

TABLE 3. Patient and Eye Characteristics by BMO Location Status in American and Korean Eyes

	BMO Location Status			Univariable Analysis		
	Accurate Automated, n = 334	Manually Corrected, n = 190	Indiscernible, n = 27	OR Units	Inaccurate BMO Location, OR (95% CI)	*P* Value
Age (y)	66.3 (64.7-67.9)	67.0 (65.4-68.6)	66.8 (65.2-68.4)	Per year older	0.99 (0.98-1.01)	.362
Sex, n (%)						
Female	191 (57.2%)	89 (46.8%)	11 (40.7%)			
Male	143 (42.8%)	101 (53.2%)	16 (59.3%)	Vs female	1.56 (1.06, 2.31)	.025[a]
Race, n (%)						
African descent	72 (21.6%)	38 (20.0%)	1 (3.7%)	(Reference)		
Asian descent	52 (15.6%)	60 (31.6%)	14 (51.9%)	Vs African descent	2.63 (1.42-4.88)	.002[a]
European descent	199 (59.6%)	89 (46.8%)	11 (40.7%)	Vs African descent	0.93 (0.54-1.58)	.784
Other/not reported	11 (3.3%)	3 (1.6%)	1 (3.7%)	Vs African descent	0.67 (0.16-2.85)	.589
Spherical equivalent (D)	−1.51 (−1.84 to −1.17)	−1.55 (−1.97 to −1.12)	−1.25 (−2.62 to 0.13)	Per D lower	1.09 (1.02-1.17)	.015[a]
VF MD (dB)	−4.54 (−5.23 to −3.84)	−7.97 (−9.20 to −6.74)	−9.91 (−12.99 to −6.82)	Per dB lower	1.10 (1.07-1.13)	<.001[a]
IOP (mm Hg)	13.8 (13.3-14.3)	13.0 (12.4-13.7)	12.3 (9.8-14.8)	Per mm Hg higher	0.94 (0.90-0.99)	.013[a]
AL (mm)	24.7 (24.5-24.8)	24.9 (24.7, 25.1)	25.4 (24.9-26.0)	Per mm higher	1.36 (1.20-1.54)	<.001[a]
CCT (μm)	536.7 (531.9-541.4)	535.2 (529.8-540.6)	534.5 (524.7-544.4)	Per μm higher	1.00 (0.99-1.00)	.445
BMO ovality index	0.88 (0.87-0.89)	0.86 (0.85-0.87)	0.83 (0.80-0.87)	Per 0.1 lower	1.57 (1.21-2.04)	<.001[a]
BMO rotation angle (°)	33.3 (30.7-35.9)	31.4 (27.8-35.0)	25.7 (17.0-34.3)	Per 10° lower	1.07 (0.97-1.17)	.159
BMO tilt angle (°)	2.2 (1.9-2.4)	3.1 (2.6-3.5)	3.5 (2.4-4.6)	Per degree higher	1.24 (1.14-1.35)	<.001[a]
BMO area (mm^2)	2.13 (2.06-2.21)	2.20 (2.11-2.28)	2.38 (1.96-2.79)	Per 1 mm^2 higher	1.40 (1.03-1.90)	.032[a]
ΔBMOC (μm)	50.6 (44.4-56.8)	61.8 (52.9-70.8)	144.8 (110.3-179.4)	Per 10 mm higher	1.06 (1.03-1.10)	<.001[a]
OCT quality score	29.5 (29.1-29.9)	29.6 (29.1-30.2)	28.4 (26.5-30.3)	Per unit lower	0.99 (0.94-1.04)	.614
Myopia group, n (%)						
Non–high myopia[b] (AL ≤26 mm)	292 (87.4)	134 (70.5)	12 (44.4)			
High myopia[b] (AL >26 mm)	42 (12.6)	56 (29.5)	15 (55.6)	Vs no myopia	3.38 (2.11-5.42)	<.001[a]
Global MRW (μm)	225.8 (216.5-235.1)	209.2 (198.8-219.6)	216.6 (189.4-243.7)	Per 10 μm thinner	1.06 (1.03-1.09)	<.001[a]
Temporal MRW (μm)	172.8 (165.5-180.1)	161.9 (153.7-170.1)	172.4 (152.1-192.8)	Per 10 μm thinner	1.04 (1.01-1.08)	.013[a]
TS MRW (μm)	209.6 (199.2-219.9)	187.2 (174.9-199.6)	204.6 (174.4-234.8)	Per 10 μm thinner	1.04 (1.02-1.06)	<.001[a]
TI MRW (μm)	219.5 (206.4-232.5)	188.9 (174.9-202.9)	195.4 (158.6-232.1)	Per 10 μm thinner	1.05 (1.03-1.07)	<.001[a]
Nasal MRW (μm)	256.9 (246.0-267.8)	242.2 (229.7-254.7)	237.0 (201.3-272.8)	Per 10 μm thinner	1.04 (1.02-1.07)	<.001[a]
NS MRW (μm)	252.1 (240.6-263.6)	228.2 (214.6-241.7)	243.4 (205.2-281.5)	Per 10 μm thinner	1.04 (1.02-1.06)	<.001[a]
NI MRW (μm)	269.0 (255.7-282.2)	235.2 (219.9-250.5)	259.3 (219.4-299.2)	Per 10 μm thinner	1.05 (1.03-1.07)	<.001[a]

AL = axial length; BMO = Bruch membrane opening; CCT = central corneal thickness; CI = confidence interval; D = diopter; IOP = intraocular pressure; MD = mean deviation; MRW = minimum rim width; NI = nasal inferior; NS = nasal superior, OCT = optical coherence tomography; OR = odds ratio; SE = spherical equivalent; TI = temporal inferior; TS = temporal superior; VF = visual field.

Data presented as mean (95% confidence interval) for continuous variables and n (%) for categorical variables. ORs indicate the odds of inaccurate locations.

[a]Statistically significant ($P < .05$). Significance is determined by logistic generalized estimating equations.

[b]AL ≤26 mm is defined as non–high myopia and AL >26 mm as high myopia.

respectively. Moreover, the majority (80%) of the highly myopic eyes with indiscernible BMO had a clinical visible PPA zone. In non–highly myopic eyes, the location of indiscernible eyes was similarly distributed in the temporal (27.1%) and nasal sectors (26.3%), but vessel shadowing was more often in the nasal sectors (72.0%) than the temporal sector (28.0%). Only 50% of the non–highly myopic eyes had a clinically visible PPA zone. The proportion of scans with indiscernible BMO due to vessel shadowing was higher (30.3%) in non–highly myopic eyes than in highly myopic eyes (21.5%). Only 4 eyes had poor-quality OCT images; the proportion of eyes with indiscernible BMO because of low image quality was only 13.3% and 16.7% in the non–highly myopic eyes and highly myopic eyes, respectively.

TABLE 4. Multivariable Logistic Generalized Estimating Equations Models Output for Predicting Inaccurate Locations With BMO Ovality Index, BMO Tilt Angle, Axial Length, Axial High Myopia, and Spherical Equivalent Included in Separate Models

	Model 1		Model 2		Model 3		Model 4		Model 5	
	OR (95% CI)	*P* Value	OR (95% CI)	*P* Value	OR (95% CI)	*P* Value	OR (95% CI)	*P* Value	OR (95% CI)	*P* Value
Male (vs female)	1.17 (0.76-1.81)	.469	1.16 (0.75-1.79)	.515	1.04 (0.67-1.62)	.853	1.09 (0.71-1.68)	.690	1.20 (0.77-1.88)	.428
Asian descent (vs African descent)	1.72 (0.89-3.32)	.107	1.29 (0.65-2.56)	.462	1.43 (0.73-2.81)	.295	1.31 (0.66-2.58)	.441	0.88 (0.40-1.91)	.739
European descent (vs African descent)	0.65 (0.36-1.15)	.136	0.60 (0.34-1.06)	.077	0.57 (0.32-1.01)	.053	0.57 (0.32-1.00)	.052	0.63 (0.36-1.09)	.096
Other race/unreported (vs African descent)	0.94 (0.20-4.46)	.937	0.94 (0.18-4.90)	.938	0.90 (0.16-5.07)	.905	0.81 (0.14-4.76)	.812	1.04 (0.22-4.87)	.959
BMO area (per mm^2)	0.94 (0.63-1.42)	.783	0.92 (0.60-1.42)	.701	0.86 (0.58-1.29)	.477	0.88 (0.59-1.32)	.529	0.98 (0.65-1.48)	.925
BMO centering (per 10 mm)	1.01 (0.98-1.05)	.484	1.01 (0.97-1.05)	.691	1.02 (0.98-1.06)	.283	1.02 (0.98-1.06)	.314	1.04 (1.00-1.08)	.033[a]
Glaucoma (vs healthy)	4.50 (2.50-8.12)	<.001[a]	4.36 (2.39-7.96)	<.001[a]	4.39 (2.45-7.86)	<.001[a]	4.67 (2.60-8.40)	<.001[a]	3.96 (2.14-7.32)	<.001[a]
BMO ovality index (per 0.1 units lower)	1.45 (1.09-1.93)	.010[a]								
BMO tilt (per degree)			1.18 (1.07-1.30)	.001[a]						
AL (per mm)					1.20 (1.02-1.40)	.023[a]				
Axial high myopia (AL >26 mm)							2.41 (1.36-4.25)	.002[a]		
Spherical equivalent (per D lower)									1.07 (0.98-1.17)	.134

AL = axial length; BMO = Bruch membrane opening; CI = confidence interval; OR = odds ratio.
[a]Statistically significant ($P < .05$).

DISCUSSION

This study assessed the accuracy of OCT BMO location in healthy eyes and eyes with glaucoma with and without axial high myopia using Spectralis ONH-RC scans. We found that BMO location inaccuracy (manually corrected and indiscernible BMOs) was significantly higher in eyes with axial high myopia compared with eyes without axial high myopia in both healthy subjects and those with glaucoma. In addition to longer AL, we found that a more oval BMO, larger BMO tilt angle, axial high myopia status, as well as having glaucoma were significantly associated with BMO location inaccuracy in multivariable analysis. These results suggest that qualitative review and manual correction of the BMO location is critical to ensure accurate assessment of OCT-based ONH morphology for glaucoma management, especially in eyes with high axial myopia.

Using OCT-based neuroretinal rim area and BMO-MRW in clinical management to diagnose and monitor glaucoma requires accurate BMO localization as the BMO based disc margin. RNFL measurements also are affected by the accuracy of BMO segmentation. If the BMO center is inaccurately identified in eyes with myopia, cpRNFL measurements will not be made in the appropriate location for comparison to internal instrument normative reference databases, which can lead to inaccurate designation of cpRNFL sectors as outside or within normal limits.

The current results are consistent with those of Zheng and associates,[21] who reported a higher proportion of indiscernible BMOs in ≥1 meridian in eyes with high axial myopia (≥26 mm) compared with eyes without high myopia in both eyes with glaucoma (32.1% and 8.2%, respectively) and healthy eyes (28.0% and 3.9%, respectively). The authors suggested that the area of β-PPA increases with the severity of glaucoma and that the BMO can be indiscernible when the interface between the BM and choroid layer becomes indistinct. This is often the case in eyes with β-PPA, where the retinal pigment epithelium, the choriocapillaris, and the choroidal vessels are atrophic.[21] The proportion of indiscernible BMOs was lower in the current study than in the study of Zheng and associates[21] in part because we classified eyes as indiscernible when the BMO was indiscernible in ≥4 meridians compared with ≥1 meridian in their study.

TABLE 5. Characteristics and Factors Associated With Indiscernible Bruch Membrane Opening

	Non–High Myopia, n = 438	High Myopia, n = 113	Total, n = 551
Total number of eyes			
No. of eyes with indiscernible BMO/no. of eyes (%)	12/438 (2.7)	15/113 (13.3)	27/551 (4.9)
No. of meridians[a] with indiscernible BMO (48 meridians per eye) (%)	307/21,024 (1.5)	503/5424 (9.3)	810/26,448 (3.1)
Eyes with indiscernible BMO	Non–high myopia, n = 12	High myopia, n = 15	Total, n = 27
Mean no. of indiscernible meridians/no. of eyes with indiscernible BMO (%)	12.8/48 (26.7)	16.8/48 (35.0)	14.8/48 (30.8)
Mean no. of indiscernible B-scans by location (%)			
Temporal	13.0/48 (27.1)	20.9/48 (43.5)	17.0/48 (35.4)
Nasal	12.6/48 (26.3)	12.6/48 (26.3)	12.6/48 (26.3)
No. of B-scans with blood vessel shadowing/no. of indiscernible B-scans (%)	93/307 (30.3)	106/493 (21.5)	199/800 (24.9)
Blood vessel shadowing location (%)			
Temporal region	26/93 (28.0)	33/106 (31.1)	59/199 (29.6)
Nasal region	67/93 (72.0)	73/106 (68.9)	140/199 (70.4)
No. of eyes with indiscernible BMO because of poor image quality (%)	2/12 (16.7)	2/15 (13.3)	4/27 (14.8)
No. of indiscernible eyes with clinically visible PPA[b] (%)	6/12 (50.0)	12/15 (80.0)	18/27 (66.7)
PPA location in indiscernible eyes with PPA (%)			
Temporal PPA only	3/6 (50.0)	6/12 (50.0)	9/18 (50.0)
Nasal PPA only	1/6 (16.7)	0/12 (0)	1/18 (5.6)
Temporal and nasal PPA	2/6 (33.3)	6/12 (50.0)	8/18 (44.4)

BMO = Bruch membrane opening; PPA = peripapillary atrophy.
[a]There are 2 BMO locations for each of the 24 B-scans
[b]Based on review of the optical coherence tomography optic nerve head en face images.

In addition, we found that the BMO was more often indiscernible because of morphology and not because of vessel shadowing or image quality in both highly myopic and non–highly myopic eyes. Moreover, indiscernible BMO locations were more often located in the temporal sectors in the highly myopic eyes, which might be in part because of the higher BMO tilt angle and/or PPA in the temporal sector. These findings are of particular interest in glaucoma diagnostics, as the temporal ONH region corresponds with the central VF.[41] The results concur with Zheng and associates,[21] where the temporal meridian was the most frequent location with indiscernible BMO.

In addition to its importance for using OCT ONH scans for clinical management, accurate BMO localization is critical for investigators who are actively developing new OCT BMO–based parameters to characterize 3D ONH morphology. For example, the neural canal's anatomy can be characterized by assessing the anatomic tilt and rotation angle of the anterior scleral canal opening relative to a BMO reference plane instead of characterizing ovality or tilt-based optic disc photographs.[39,42] For example, by analyzing the ONH anatomy using OCT BMO–based morphology, Jeoung and associates[42] were able to objectively characterize neural canal obliqueness by determining the magnitude and direction of the offset of anterior scleral canal opening relative to BMO. In summary, accurate BMO localization is not only critical for appropriate interpretation of OCT ONH scans and cpRNFL thickness in clinical management but also for research characterizing optic disc morphology. For the above-mentioned reasons, it is important to understand the challenges in identifying the BMO in highly myopic eyes.

The reasons for incorrect BMO localization by the standard OCT software are likely in part related to anatomic differences in highly myopic eyes compared with non–highly myopic eyes[42] and because the segmentation algorithms were not developed on highly myopic eyes. However, it should also be noted that the software's BMO localization relies on the manual BMO localization conducted by the operator. If this first step is not done correctly (because of a lack of expertise in high myopic eyes) the final BMO localizations provided by the software are inaccurate. Our preliminary results suggest that BMO location accuracy in highly myopic eyes can be improved by using deep learn-

ing retinal layer segmentation strategies trained on highly myopic eyes (Belghith, personal communication May 10, 2021). Future improvements in instrument retinal layer segmentation will therefore likely reduce the impact of these BMO segmentation issues.

There are several strengths of this study. First, we included 2 study populations from 2 different countries, providing evidence that indiscernible BMOs in highly myopic eyes are independent of race and that race is not a predictor of location accuracy. We found no differences in the proportion of indiscernible or inaccurate BMO location between the American and Korean populations (data not shown). We also included new OCT parameters that characterize highly myopic discs, BMO based on ovality index, tilt, and rotation angle that have not been reported previously. In addition, high myopia was defined in this study by AL rather than SE, as used in most studies. By using AL, we can better predict anatomic differences in the ONH related to axial elongation and include axially elongated eyes without relying on SE, which changes after refractive and cataract surgery. Furthermore, multivariable models indicated that AL (and parameters correlated to it) were associated with location inaccuracy, whereas SE was not.

Our study has several limitations. First, we included only Spectralis OCT for imaging the optic disc and BMO location and did not directly determine the frequency of accurate BMO detection in other OCT instruments. However, the accuracy of BMO detection also is relevant to other OCT instruments, including Cirrus (Carl Zeiss Meditec), AngioVue/RTVue (Optovue Inc, Fremont, California, USA), and the swept-source DRI and Maestro Topcon (Tokyo, Japan) OCT. These instruments rely on the identification of the innermost segment of the Bruch membrane or the Bruch membrane/retinal pigment epithelium complex for calculation of ONH parameters and cpRNFL thickness at a fixed distance from the center of the BMO. In addition, not all OCT images were reviewed by both reviewers. All highly myopic eyes were reviewed by both reviewers, but non–highly myopic eyes were only assessed by 2 reviewers if the first reviewer was not able to manually correct the BMO localization in >4 different OCT B-scans. However, extensive training and review of eyes with difficult BMO detection (both with and without axial high myopia) was completed by both reviewers, which facilitated consensus even in the most challenging eyes. Finally, we did not exclude poor-quality scans or scans in which the manufacturer's recommended distance between the BMO center of the ONH-RC scans and the center of the image (ΔBMOC) was not met. We included all acquired scans to better reflect clinical practice because it can be challenging to acquire images of highly myopic eyes that meet general quality and BMOC distance requirements. Although a significantly larger BMO/scan center distance was found in highly myopic eyes, it was a predictor for localization failure in univariate but not multivariable analysis.

In conclusion, we found that highly myopic eyes are significantly more likely to have inaccurate BMO locations and indiscernible BMOs in both healthy and glaucoma eyes than non–highly myopic eyes. In addition, we found that AL and parameters that are associated with high myopia such as a more oval BMO configuration (smaller BMO ovality index) and a higher BMO tilt angle were predictors of BMO localization inaccuracy. Moreover, we found that eyes with glaucoma were >4 times more likely to have inaccurate BMO locations than healthy eyes. Accurate BMO locations are important for calculating ONH parameters that are used for glaucoma management. For this reason, BMO localization of OCT scans should be reviewed carefully, particularly in highly myopic eyes and, if possible, manually corrected to ensure the accuracy of ONH parameters used in glaucoma management. Promising work to improve BMO localization in highly myopic eyes using deep learning strategies is underway, which may alleviate some of these issues.

All authors have completed and submitted the ICMJE form for disclosure of potential conflicts of interest. Funding/Support: The Diagnostic Innovations in Glaucoma Study is supported by National Eye Institute grants EY011008, EY019869, EY014267, EY027510, EY026574, EY029058, and P30EY022589, a University of California, San Diego School of Medicine Summer Research Fellowship, and participant retention incentive grants in the form of glaucoma medication at no cost from Novartis/Alcon Laboratories Inc, Allergan, Akorn, and Pfizer Inc. Support was also provided by an unrestricted grant from Research to Prevent Blindness (New York, New York). Financial Disclosures: J.R. has received a Research Fellowship Grant from the German Research Foundation and a grant from the German Ophthalmological Society. M.A.F. has received supported from National Eye Institute grant R01EY026574 (the African Descent and Glaucoma Evaluation Study [ADAGEs] IV: alterations of the lamina cribrosa in progression). R.N.W. has been a consultant forAerie Pharmaceuticals, Allergan, Eyenovia, Implantdata, and Unity and has received research support from Heidelberg Engineering, Carl Zeiss Meditec, Centervue, Bausch & Lomb, Genentech, Konan Medical, National Eye Institute, Optos, Optovue, and Research to Prevent Blindness. L.M.Z. has received research support from Carl Zeiss Meditec, Heidelberg Engineering, the National Eye Institute, Optovue, and Topcon Medical System Inc. The other authors indicate no conflicts of interest. All authors attest that they meet the current ICMJE criteria for authorship.

REFERENCES

1. Resnikoff S, Pascolini D, Etya'ale D, et al. Global data on visual impairment in the year 2002. *Bull World Health Organ*. 2004;82(11):844–851.
2. Harwerth RS, Carter-Dawson L, Smith 3rd EL, Barnes G, Holt WF, Crawford ML. Neural losses correlated with visual losses in clinical perimetry. *Invest Ophthalmol Vis Sci*. 2004;45(9):3152–3160.
3. Gordon MO, Kass MA. What we have learned from the Ocular Hypertension Treatment Study. *Am J Ophthalmol*. 2018;189:xxiv–xxvii.
4. Marcus MW, de Vries MM, Junoy Montolio FG, Jansonius NM. Myopia as a risk factor for open-angle glaucoma: a systematic review and meta-analysis. *Ophthalmology*. 2011;118(10):1989–1994 e2.
5. Jonas JB, Gusek GC, Naumann GO. Optic disk morphometry in high myopia. *Graefes Arch Clin Exp Ophthalmol*. 1988;226(6):587–590.
6. Leung CK, Mohamed S, Leung KS, et al. Retinal nerve fiber layer measurements in myopia: an optical coherence tomography study. *Invest Ophthalmol Vis Sci*. 2006;47(12):5171–5176.
7. Leung CK, Yu M, Weinreb RN, et al. Retinal nerve fiber layer imaging with spectral-domain optical coherence tomography: interpreting the RNFL maps in healthy myopic eyes. *Invest Ophthalmol Vis Sci*. 2012;53(11):7194–7200.
8. Kang SH, Hong SW, Im SK, Lee SH, Ahn MD. Effect of myopia on the thickness of the retinal nerve fiber layer measured by Cirrus HD optical coherence tomography. *Invest Ophthalmol Vis Sci*. 2010;51(8):4075–4083.
9. Sawada Y, Araie M, Shibata H, Ishikawa M, Iwata T, Yoshitomi T. Differences in retinal nerve fiber layer thickness as assessed on the disc center and Bruch's membrane opening center in myopic eyes. *Ophthalmol Glaucoma*. 2019;2(3):145–155.
10. Chauhan BC, O'Leary N, AlMobarak FA, et al. Enhanced detection of open-angle glaucoma with an anatomically accurate optical coherence tomography-derived neuroretinal rim parameter. *Ophthalmology*. 2013;120(3):535–543.
11. Danthurebandara VM, Sharpe GP, Hutchison DM, et al. Enhanced structure-function relationship in glaucoma with an anatomically and geometrically accurate neuroretinal rim measurement. *Invest Ophthalmol Vis Sci*. 2014;56(1):98–105.
12. Toshev AP, Lamparter J, Pfeiffer N, Hoffmann EM. Bruch's membrane opening-minimum rim width assessment with spectral-domain optical coherence tomography performs better than confocal scanning laser ophthalmoscopy in discriminating early glaucoma patients from control subjects. *J Glaucoma*. 2017;26(1):27–33.
13. Gardiner SK, Boey PY, Yang H, Fortune B, Burgoyne CF, Demirel S. Structural measurements for monitoring change in glaucoma: comparing retinal nerve fiber layer thickness with minimum rim width and area. *Invest Ophthalmol Vis Sci*. 2015;56(11):6886–6891.
14. Nakanishi H, Suda K, Yoshikawa M, et al. Association of Bruch's membrane opening and optic disc morphology to axial length and visual field defects in eyes with primary open-angle glaucoma. *Graefes Arch Clin Exp Ophthalmol*. 2018;256(3):599–610.
15. Wu Z, Vianna JR, Reis ASC, et al. Qualitative evaluation of neuroretinal rim and retinal nerve fibre layer on optical coherence tomography to detect glaucomatous damage. *Br J Ophthalmol*. 2020;104(7):980–984.
16. Bowd C, Zangwill LM, Weinreb RN, et al. Racial differences in rate of change of spectral-domain optical coherence tomography-measured minimum rim width and retinal nerve fiber layer thickness. *Am J Ophthalmol*. 2018;196:154–164.
17. Dai Y, Jonas JB, Huang H, Wang M, Sun X. Microstructure of parapapillary atrophy: beta zone and gamma zone. *Invest Ophthalmol Vis Sci*. 2013;54(3):2013–2018.
18. Jonas JB, Wang YX, Zhang Q, et al. Parapapillary gamma zone and axial elongation-associated optic disc rotation: the Beijing Eye Study. *Invest Ophthalmol Vis Sci*. 2016;57(2):396–402.
19. Manalastas PIC, Belghith A, Weinreb RN, et al. Automated beta zone parapapillary area measurement to differentiate between healthy and glaucoma eyes. *Am J Ophthalmol*. 2018;191:140–148.
20. Vianna JR, Malik R, Danthurebandara VM, et al. Beta and gamma peripapillary atrophy in myopic eyes with and without glaucoma. *Invest Ophthalmol Vis Sci*. 2016;57(7):3103–3111.
21. Zheng F, Wu Z, Leung CKS. Detection of Bruch's membrane opening in healthy individuals and glaucoma patients with and without high myopia. *Ophthalmology*. 2018;125(10):1537–1546.
22. Zhao XJ, Jiang HY, Li YH, et al. Correlations between the optic nerve head morphology and ocular biometrics in highly myopic eyes. *Int J Ophthalmol*. 2018;11(6):997–1001.
23. Hosseini H, Nassiri N, Azarbod P, et al. Measurement of the optic disc vertical tilt angle with spectral-domain optical coherence tomography and influencing factors. *Am J Ophthalmol*. 2013;156(4):737–744.
24. Brien Holden Vision Institute. A Vision for All to See. A report on global eye health and vision care. Sydney, Australia; 2013.
25. Dunaway D, Berger I. Worldwide distribution of visual refractive errors and what to expect at a particular location. Available at: https://www.scribd.com/document/161680442/Worldwide-Distribution-of-Visual-Refractive-Error1. Accessed January 5, 2022.
26. Marsh-Tootle WL, Harb E, Hou W, et al. Optic nerve tilt, crescent, ovality, and torsion in a multi-ethnic cohort of young adults with and without myopia. *Invest Ophthalmol Vis Sci*. 2017;58(7):3158–3171.
27. Fredrick DR. Myopia. *BMJ*. 2002;324(7347):1195–1199.
28. Quigley HA. Open-angle glaucoma. *N Engl J Med*. 1993;328(15):1097–1106.
29. Jonas JB, Budde WM. Optic nerve damage in highly myopic eyes with chronic open-angle glaucoma. *Eur J Ophthalmol*. 2005;15(1):41–47.
30. David R, Zangwill L, Stone D, Yassur Y. Epidemiology of intraocular pressure in a population screened for glaucoma. *Br J Ophthalmol*. 1987;71(10):766–771.
31. Wilson MR, Hertzmark E, Walker AM, Childs-Shaw K, Epstein DL. A case-control study of risk factors in open angle glaucoma. *Arch Ophthalmol*. 1987;105(8):1066–1071.
32. Leske MC, Connell AM, Wu SY, Hyman LG, Schachat AP. Risk factors for open-angle glaucoma. The Barbados Eye Study. *Arch Ophthalmol*. 1995;113(7):918–924.
33. Sample PA, Girkin CA, Zangwill LM, et al. The African Descent and Glaucoma Evaluation Study (ADAGES): design and baseline data. *Arch Ophthalmol*. 2009;127(9):1136–1145.

34. Wang Y, Xu L, Zhang L, Yang H, Ma Y, Jonas JB. Optic disc size in a population based study in northern China: the Beijing Eye Study. *Br J Ophthalmol*. 2006;90(3):353–356.
35. Heidelberg Engineering. *Spectralis Training Guide. Software Manual*. Heidelberg, Germany: Heidelberg Engineering; 2014.
36. Sung MS, Heo MY, Heo H, Park SW. Bruch's membrane opening enlargement and its implication on the myopic optic nerve head. *Sci Rep*. 2019;9(1):19564.
37. Belghith A, Bowd C, Medeiros FA, et al. Does the location of Bruch's membrane opening change over time? Longitudinal analysis using San Diego Automated Layer Segmentation Algorithm (SALSA). *Invest Ophthalmol Vis Sci*. 2016;57(2):675–682.
38. Rezapour J, Bowd C, Dohleman J, et al. The influence of axial myopia on optic disc characteristics of glaucoma eyes. *Sci Rep*. 2021;11(1):8854.
39. Wang YX, Yang H, Luo H, et al. Peripapillary scleral bowing increases with age and is inversely associated with peripapillary choroidal thickness in healthy eyes. *Am J Ophthalmol*. 2020;217:91–103.
40. How AC, Tan GS, Chan YH, et al. Population prevalence of tilted and torted optic discs among an adult Chinese population in Singapore: the Tanjong Pagar Study. *Arch Ophthalmol*. 2009;127(7):894–899.
41. Garway-Heath DF, Poinoosawmy D, Fitzke FW, Hitchings RA. Mapping the visual field to the optic disc in normal tension glaucoma eyes. *Ophthalmology*. 2000;107(10):1809–1815.
42. Jeoung JW, Yang H, Gardiner S, et al. Optical coherence tomography optic nerve head morphology in myopia I: implications of anterior scleral canal opening versus Bruch membrane opening offset. *Am J Ophthalmol*. 2020;218:105–119.

Publikation III

Rezapour J, Tran AQ, Bowd C, El-Nimri NW, Belghith A, Christopher M, Brye N, Proudfoot JA, Dohleman J, Fazio MA, Jonas JB, Weinreb RN, Zangwill LM; *Comparison of Optic Disc Ovality Index and Rotation Angle Measurements in Myopic Eyes Using Photography and OCT based Techniques*; Frontiers in Medicine; 2022 Jun 24;9:872658. doi: 10.3389/fmed.2022.872658. PMID: 35814778; PMCID: PMC9263212

frontiers | Frontiers in Medicine

ORIGINAL RESEARCH
published: 24 June 2022
doi: 10.3389/fmed.2022.872658

Comparison of Optic Disc Ovality Index and Rotation Angle Measurements in Myopic Eyes Using Photography and OCT Based Techniques

*Jasmin Rezapour[1,2], Andrew Q. Tran[1], Christopher Bowd[1], Nevin W. El-Nimri[1], Akram Belghith[1], Mark Christopher[1], Nicole Brye[1], James A. Proudfoot[1], Jade Dohleman[1], Massimo A. Fazio[1,3,4], Jost B. Jonas[5,6], Robert N. Weinreb[1] and Linda M. Zangwill[1]**

[1] Viterbi Family Department of Ophthalmology, Hamilton Glaucoma Center, Shiley Eye Institute, University of California, San Diego, San Diego, CA, United States, [2] Department of Ophthalmology, University Medical Center of the Johannes Gutenberg University Mainz, Mainz, Germany, [3] Department of Ophthalmology, School of Medicine, The University of Alabama at Birmingham, Birmingham, AL, United States, [4] Department of Biomedical Engineering, School of Engineering, The University of Alabama at Birmingham, Birmingham, AL, United States, [5] Department of Ophthalmology, Medical Faculty Mannheim, Heidelberg University, Mannheim, Germany, [6] Institute of Molecular and Clinical Ophthalmology, Basel, Switzerland

OPEN ACCESS

Edited by:
Eray Atalay,
Eskişehir Osmangazi University, Turkey

Reviewed by:
Inas Aboobakar,
Harvard Medical School, United States
Xiaodong Sun,
Shanghai Jiao Tong University, China

***Correspondence:**
Linda M. Zangwill
lzangwill@health.ucsd.edu

Specialty section:
This article was submitted to Ophthalmology, a section of the journal Frontiers in Medicine

Received: *09 February 2022*
Accepted: *24 May 2022*
Published: *24 June 2022*

Citation:
Rezapour J, Tran AQ, Bowd C, El-Nimri NW, Belghith A, Christopher M, Brye N, Proudfoot JA, Dohleman J, Fazio MA, Jonas JB, Weinreb RN and Zangwill LM (2022) Comparison of Optic Disc Ovality Index and Rotation Angle Measurements in Myopic Eyes Using Photography and OCT Based Techniques. Front. Med. 9:872658. doi: 10.3389/fmed.2022.872658

Purpose: To compare optic nerve head (ONH) ovality index and rotation angle measurements based on semi-automated delineation of the clinical ONH margin derived from photographs and automated BMO configuration derived from optical coherence tomography (OCT) images in healthy and glaucomatous eyes with high-, mild- and no axial myopia.

Methods: One hundred seventy-five healthy and glaucomatous eyes of 146 study participants enrolled in the Diagnostic Innovations in Glaucoma Study (DIGS) with optic disc photographs and Spectralis OCT ONH scans acquired on the same day were stratified by level of axial myopia (non-myopic [$n = 56$, axial length (AL) <24 mm], mild-myopic [$n = 58$, AL 24–26 mm] and high-myopic [$n = 32$, AL >26 mm]. The clinical disc margin of each photograph was manually annotated, and semi-automated measurements were recorded of the ovality index and rotation angle based on a best-fit ellipse generated using ImageJ software. These semi-automated photograph-based measurements were compared to ovality index and rotation angle generated from custom automated BMO-based analysis using segmented OCT ONH volumes. R^2 values from linear mixed effects models were used to describe the associations between semi-automated, photograph-based and automated OCT-based measurements.

Results: Average (95% CI) axial length was 23.3 (23.0, 23.3) mm, 24.8 (24.7, 25.0) mm and 26.8 (26.6, 27.0) mm in non-myopic, mild-myopic and high-myopic eyes, respectively (ANOVA, $p \leq 0.001$ for all). The R^2 association (95% CI) between semi-automated photograph-based and automated OCT-based assessment of ONH OI for all eyes was [0.26 (0.16, 0.36); $p < 0.001$]. This association was weakest in non-myopic eyes [0.09 (0.01, 0.26); $p = 0.02$], followed by mild-myopic eyes

[0.13 (0.02, 0.29); $p = 0.004$] and strongest in high-myopic eyes [0.40 (0.19, 0.60); $p < 0.001$]. No significant associations were found between photography- and OCT-based assessment of rotation angle with R^2 values ranging from 0.00 (0.00, 0.08) in non-myopic eyes to 0.03 (0.00, 0.21) in high-myopic eyes (all associations $p \geq 0.33$).

Conclusions: Agreement between photograph-based and automated OCT-based ONH morphology measurements is limited, suggesting that these methods cannot be used interchangeably for characterizing myopic changes in the ONH.

Keywords: high myopia, glaucoma, OCT, Bruch's membrane opening, axial myopia, optic nerve head morphology, clinical disc margin, OCT landmarks

INTRODUCTION

Axial myopia typically results from progressive eye enlargement, reflected in a larger axial length (AL). The prevalence of myopia has increased in the United States (1) and worldwide (2), with some populations reporting prevalence as high as 96% (3). It is now projected that ∼50% of the world's population will be myopic by 2050, with 10% being highly myopic (4). There is strong evidence linking myopia with glaucoma (5). For instance, the Blue Mountains Eye Study reported that compared to eyes with no myopia, the odds of having glaucoma in mild myopic eyes was 2.3, and this increased to 3.3 for moderate to high myopic eyes (6). This association presents significant public health concerns in the context of swiftly rising myopia prevalence. Moreover, accurate detection of glaucoma in myopic patients is challenging. Myopic eyes often develop structural changes at the optic nerve head (ONH) independent of glaucoma (7, 8), and these changes are often difficult to distinguish from those observed in glaucoma.

Many studies have reported the prevalence of ONH ovality, tilt and torsion and their associations with myopia, particularly with high myopia (9–20). However, these studies often used manual methods to measure ovality, tilt and torsion parameters based on measurements of two- dimensional fundus photographs or two-dimensional fundus photographs projected on spectral-domain optical coherence tomography (OCT) scans. Although manual or semi-automated measurement of ovality, tilt and torsion from photographs are the most common methods reported in the literature, they are not based on anatomical landmarks such as Bruch's membrane opening (BMO). Furthermore, two-dimensional viewing of the ONH at an oblique angle may lead to inaccurate observations with regard to the shape of the disc, especially its horizontal diameter (19). We previously reported an automated custom-software based method to measure ONH ovality index, tilt and rotation (torsion) angles based on the BMO assessed on OCT scans (21). The purpose of the current study is to compare semi-automated measurements of optic disc ovality index (often referred to as tilt) and rotation angle based on the manually demarcated clinical disc margin identified on optic disc stereophotographs with automated measurements based on the BMO identified from ONH-OCT scans in eyes with no axial myopia, mild axial myopia and high axial myopia, with and without glaucoma.

MATERIALS AND METHODS

This cross-sectional comparison of semi-automated photograph-based vs. automated OCT-based assessment involved healthy individuals and glaucoma patients with varying levels of axial myopia, from the Diagnostic Innovations in Glaucoma Study (DIGS). The DIGS is an ongoing prospective, longitudinal study conducted at the Hamilton Glaucoma Center, University of California, San Diego, designed to evaluate anatomical structures in glaucoma. Details of the DIGS protocol have been described elsewhere (22). All methods adhered to the tenets of the Declaration of Helsinki and the Health Insurance Portability and Accountability Act and were approved by the Institutional Review Board of the University of California, San Diego.

Participants

Study participants were a subset of glaucoma patients and healthy individuals with varying degrees of axial myopia enrolled in DIGS (clinical trials.gov identifier NCT00221897). All participants were ≥18 years old, had open anterior chamber angles, and had undergone a full ophthalmologic examination including refractometry, best-corrected visual acuity assessment, standard automated perimetry [Humphrey Field Analyzer; 24–2 Swedish interactive thresholding algorithm (SITA) standard; Carl-Zeiss Meditec], Goldmann applanation tonometry, gonioscopy, dilated fundus examination, central corneal thickness (CCT) measurement by ultrasound pachymetry (DGH Technology, Inc., Exton, PA), coherence interferometry measurement of the axial length (IOLMaster, Carl Zeiss Meditec, Dublin, CA), and simultaneous stereophotography and OCT imaging of the optic disc and macula.

Patients with primary open angle glaucoma (POAG) were clinically defined by the DIGS conventional standard of visual field loss or photograph-based optic disc damage (22)[30].

Standard automated perimetry glaucomatous visual field damage was defined as two repeatable and reliable visual field tests (rate of fixation losses and false negatives and false positives responses of <33%) with a glaucoma hemifield test (GHT) outside normal limits and/or a pattern standard deviation (PSD) with a p-value of <0.05 with a similar defect on consecutive abnormal tests (22). Healthy subjects were required to have intraocular pressure ≤21 mmHg and no structural abnormalities or functional loss. The Visual Field Assessment Center (VisFACT) Reading Center completed the quality control

of all visual fields according to standard protocols and excluded unreliable visual field tests (22).

Stereophotograph-based optic disc damage was defined as focal or diffuse narrowing of the neuroretinal rim, and/or detection of RNFL defects characteristic of glaucoma based on masked assessment by two trained reviewers (JR and CB) after a high myopia optic disc grading training with a senior consultant (JBJ). Optic disc damage was defined by consensus between both graders and in case of disagreement, diagnosis was defined by adjudication by the senior consultant. Intergrader agreement was good with agreement on 131/175 (76.6%) eyes; 41/175 (23.4%) required consensus meetings between the two graders to determine diagnosis. Adjudication by the senior consultant was needed in 3/175 (1.7%) of eyes.

Axial Myopia Categories

Elongation of the globe in the axial plane can lead to morphological changes of the optic disc and the fundus.[32,33] Such elongation and associated changes are not always directly correlated with myopia defined by the refractive error. Furthermore, refractive error is subject to change after patients undergo cataract surgery or refractive procedures. In this study we were interested in morphological changes of the optic disc due to axial elongation and for these reasons myopia was defined by axial length and not by refractive error. Based on population-based studies (23, 24), axial myopia was stratified into three groups: no axial myopia (AL <24.0 mm), mild axial myopia (AL = 24.0–26.0 mm) and high axial myopia (AL >26.0 mm). For each eye, ovality and rotation angle were measured based on: (1) stereophotographs using manual annotation of the clinical disc margin and (2) OCT images of the ONH using automated analysis of BMO.

Image Acquisition

Simultaneous stereophotographs centered on the optic disc were obtained for all participants. Poor quality images due to low lighting, haziness or otherwise obscured features of the optic disc were excluded.

ONH radical circle (ONHRC) scans from the Spectralis Glaucoma Module Premier Edition (version 6.10; Heidelberg Engineering Inc., Heidelberg, Germany) were acquired on all participants. The ONHRC scan consists of 24 high-resolution ONH radial scans and 3 RNFL circle scans. Images were electronically transferred for quality assessment to the UC San Diego Imaging Data Evaluation and Analysis (IDEA) Reading Center. Low quality images, with quality score <15, or poor centering (based on the distance between the BMO center of the ONHRC scans and the center of the image) were excluded.

Semi-automated Photograph-Based Measurement of the Clinical Optic Disc Margin and Optic Disc Ovality Index and Rotation Angle

Digital stereophotographs were reviewed through a stereo viewer and annotated manually in ImageJ (ver. 1.53a, NIH) on a touch-screen tablet. The photographs of left eyes were transformed into right eye format for all analyses. The clinical disc margin, defined as the inner margin of the scleral ring was manually demarcated by one study author (AT) and its location was confirmed by all 3 senior reviewers (JR, CB, NEN). A best-fit ellipse was generated by ImageJ. From the best-fit ellipse, the length of the major (longest) axis, minor (shortest) axis, and ultimately the angle between the major axis and the vertical axis were automatically generated by ImageJ and exported to.csv files to calculate ovality index and rotation angle and direction (**Figure 1**). Annotations were made on the image and the best-fit ellipse from which the measurements were derived and saved for later review to confirm proper selection of the disc margin as well as appropriate calculation of rotation angle and direction.

As described in our previous study (21), optic disc ovality index can be defined on a 2- or 3-dimensional level, whereas optic disc tilt is calculated on a 3-dimensional level. As photograph-based measurements can only be performed on a 2-dimensional level, we assessed the optic disc ovality index and not the optic disc tilt angle in this report. Ovality index was calculated by dividing the minor axis by the major axis, with a value closer to 0 indicating a more oval optic disc. For this report, we used the term "rotation" rather than the more commonly used term "torsion," as "torsion" implies shearing of the tissue that can only be detected at a histological level (25). The optic disc rotation angle was defined as the smaller angle formed by either the major axis or minor axis and the vertical axis extending from the center of the best-fit ellipse (**Figure 2**). We adjusted for whether a right eye or left eye was analyzed, and conserved the magnitude of the rotation angle, regardless of the direction.

Automated OCT-Based BMO Ovality Index and Rotation Angle Measurements

Ovality index and rotation angle measurements based on BMO points were calculated for the segmented Spectralis ONHRC scans using the San Diego Automated Layer Segmentation Algorithm (SALSA) Image Processing Pipeline. Details of SALSA and its validation have been described previously (21, 26, 27). In brief SALSA is a python-based automated algorithm that segments retinal layers in OCT scans. Spectralis OCT raw image (vol) files were exported to the SALSA-Image Processing Pipeline. SALSA identified the Bruch's membrane (BM) and the 2 BMO points in each scan, produced a fitted ellipse and documented the results as a.csv file. The accuracy of the BMO locations was reviewed by one of the authors (JR) on a randomly chosen subset of 30 non-, mild- and high axial myopic eyes and showed good performance. Ovality index was defined as the minor axis (shortest axis) divided by the major axis (longest axis) of the fitted BMO ellipse.

The OCT-based rotation angle is defined as the angle between the major axis and the temporal axis (0°, horizontal axes of the *enface* OCT image). In another words, we characterize rotation as the angle of rotation around the sagittal axis (z axis). Angles are reported after transforming the vectors used in their computations into physical space by scaling according to the scale x and scale z constants in the image volume metadata as described previously (26, 27). All measurements were calculated

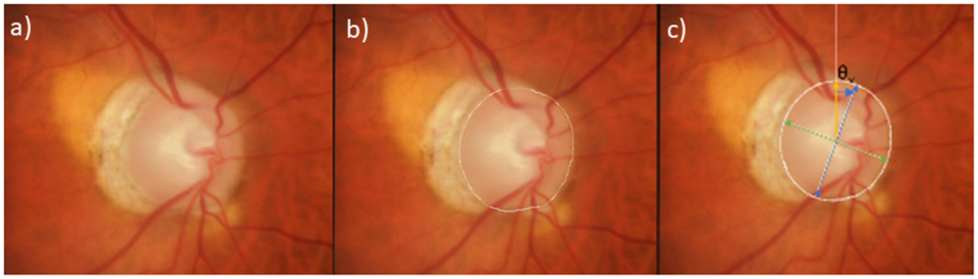

FIGURE 1 | Delineation of semi-automated measurement of ovality index and rotation angle from photographs. **(a)** Stereophotograph of a glaucomatous mild myopic eye, **(b)** Clinical disc margin manually delineated in white, **(c)** Best-fitted ellipse overlaid in white. Ovality index is calculated as the minor axis (green) divided by the major axis (blue). Rotation angle (θ_v blue arrow) is defined as the angle between the vertical axis (yellow) and major axis (blue).

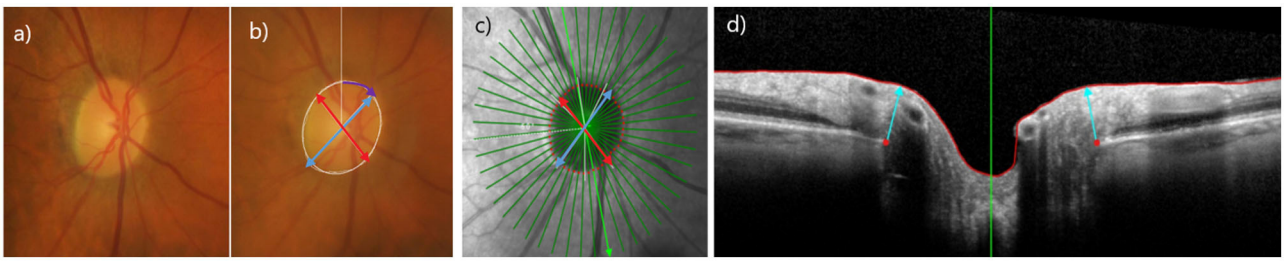

FIGURE 2 | Ovality and Rotation angle measurements on photographs and OCT. **(a)** Stereophotograph of a healthy eye, **(b)** clinical disc margin annotated in white, labeled with major axis (blue), minor axis (red), rotation angle (purple); Ovality index (minor axis/major axis), **(c)** en-face OCT optic nerve head image of Bruch's Membrane Opening (BMO) (red); Ovality index (minor axis (red)/major axis (blue). Please note as described previously, the calculations use the 3D OCT scan. (21) **(d)** b-scan of optic nerve head with BMO points in red.

with respect to individual anatomies by factoring in the Fovea-BMO center (FoBMOc) angle captured by the Spectralis OCT.

Details of how the automated BMO ovality index and rotation angle measurements were completed have been described previously (21).

Statistical Analyses

Statistical analysis was conducted to compare ONH ovality index and rotation angle values determined by semi-automated assessment of photographs and automated assessment of OCT images. Data is presented as mean (95% confidence interval) or count (percentage) for continuous and categorical variables, respectively. The statistical significance of comparisons between patient-level characteristics across myopia groups was determined by analysis of variance (ANOVA) for continuous variables and Fisher's exact test for categorical variables. For eye-level characteristics, mean and confidence interval estimates were derived from linear mixed effect models, with a random intercept to account for within-subject correlation before and after adjusting for age and visual field mean deviation. Linear mixed effect models were used to compare semi-automated-derived ovality index and rotation angle values (separately) from photographs with those automatically derived from OCT images, stratified by axial myopia. R-squared values for reported for correlation between semi-automated photograph-based and automated OCT-based ovality index and rotation angle. Bland-Altman plots were used to characterize the agreement between photograph- and OCT-based measurements of ovality index and rotation angle. We considered p-values <0.05 to indicate statistical significance throughout. All statistical analyses were performed using the R (version 3.5.2).

RESULTS

Demographics and Clinical Characteristics

One hundred and seventy-five eyes from 146 patients were included in this study, with 64 eyes (56 patients) in the no axial myopia group, 70 eyes (58 patients) in the mild axial myopia group and 41 eyes (32 patients) in the high myopia group (**Table 1**). The no myopia and mild axial groups have a larger proportion of healthy participants than the high axial myopia group (42.2, 41.4, and 26.8%, respectively). The mean (95% CI) age of the participants in the no axial myopia group was older [70.7 (67.3, 74.1)] years than those in the mild [65.2 (61.1, 69.4)] years, followed by the high [63.3 (58.0, 68.7)] years axial myopia groups ($p < 0.040$). Mean (95% CI) spherical equivalent was significantly lower in high axial myopic eyes [−4.01 (−4.78, −3.23)] D compared to that of eyes with mild [−1.51 (−2.09, −0.93)] D or no axial myopia [0.09 (−0.50, 0.69)] D (visual field MD/age adjusted; $p < 0.001$). There was no significant difference

TABLE 1 | Patient characteristics by myopia status.

	No myopia ($n = 56$)	Mild myopia ($n = 58$)	High myopia ($n = 32$)	Overall ($n = 146$)	*P*-value	MD/Age Adj. *p*-value
Patient specific data						
Age (years)	70.7 (67.3, 74.1)	65.2 (61.1, 69.4)	63.3 (58.0, 68.7)	66.9 (64.5, 69.3)	0.04	
Sex						
Female	39 (69.6%)	31 (53.4%)	12 (37.5%)	82 (56.2%)	0.01	
Male	17 (30.4%)	27 (46.6%)	20 (62.5%)	64 (43.8%)		
Race						
Asian	5 (8.9%)	6 (10.3%)	11 (34.4%)	22 (15.1%)	0.02	
Black or African American	16 (28.6%)	20 (34.5%)	4 (12.5%)	40 (27.4%)		
White	32 (57.1%)	31 (53.4%)	16 (50.0%)	79 (54.1%)		
Unknown or not reported	3 (5.4%)	1 (1.7%)	1 (3.1%)	5 (3.4%)		
Eye specific data						
BMO area (mm^2)	$n = 64$ 2.12 (1.97, 2.27)	$n = 68$ 2.20 (2.05, 2.35)	$n = 38$ 2.37 (2.17, 2.58)	$n = 170$ 2.20 (2.11, 2.30)	0.15	0.24
Axial length (mm)	$n = 64$ 23.2 (23.0, 23.3)	$n = 70$ 24.8 (24.7, 25.0)	$n = 41$ 26.8 (26.6, 27.0)	$n = 175$ 24.6 (24.4, 24.9)	<0.001	<0.001
Spherical equivalent (Dpt)	$n = 64$ 0.09 (–0.50, 0.69)	$n = 70$ –1.51 (–2.09, –0.93)	$n = 41$ –4.01 (–4.78, –3.23)	$n = 175$ –1.44 (–1.88, –1.00)	<0.001	<0.001
Eye classification	$n = 64$	$n = 70$	$n = 41$	$n = 175$	-	-
Healthy	27 (42.2%)	29 (41.4%)	11 (26.8%)	67 (38.3%)		
Glaucoma	37 (58.8%)	41 (58.5%)	30 (73.1%)	108 (61.7%)		
Visual field MD (dB)	$n = 64$ –3.14 (–4.72, –1.55)	$n = 70$ –3.89 (–5.45, –2.34)	$n = 41$ –5.29 (–7.38, –3.21)	$n = 175$ –3.91 (–4.89, –2.93)	0.27	0.08

Results are presented as mean (95% CI) or counts (percentages).

TABLE 2 | Ovality Index (closer to 0=more oval, closer to 1=more circular) and Rotation Angle by Myopia Status.

		No Myopia	*Mild Myopia*	*High Myopia*	*Overall*	*P*-value*	**Visual field MD and age adjusted *p*-value
Ovality index	Photograph-based	$n = 64$ 0.89 (0.88, 0.91)	$n = 70$ 0.90 (0.89, 0.92)	$n = 41$ 0.85 (0.83, 0.88)	$n = 175$ 0.89 (0.88, 0.90)	0.002	0.002
	OCT-based	$n = 64$ 0.88 (0.86, 0.89)	$n = 70$ 0.88 (0.86, 0.90)	$n = 41$ 0.84 (0.81, 0.86)	$n = 175$ 0.87 (0.86, 0.88)	0.01	0.008
Rotation angle (degrees)	Photograph-based	$n = 63$ 15.2 (11.8, 18.7)	$n = 69$ 19.9 (16.6, 23.3)	$n = 38$ 20.9 (16.4, 25.4)	$n =169$ 18.4 (16.2, 20.5)	0.078	0.108
	OCT-based	$n = 63$ 35.9 (31.3, 40.6)	$n = 68$ 34.4 (29.9, 39.0)	$n = 38$ 33.7 (27.6, 39.9)	$n = 169$ 34.8 (32.0, 37.7)	0.83	0.96

**p-value based on linear mixed models adjusting for both eyes in the model. **p-value based on linear mixed models adjusting for age, visual field mean deviation (MD) and both eyes in the model. Results are presented as mean (95% confidence interval).*

in the visual field MD ($p = 0.27$), pattern standard deviation (PSD) ($p = 0.37$), BMO area ($p = 0.15$), or CCT ($p = 0.12$) among myopia groups.

Ovality Index and Rotation Angle Measurements

Overall, we found that the mean ovality index values derived from photographs were similar to those derived from OCT in each myopia category (**Table 2**). Specifically, mean (95% CI) photograph-based ovality index was significantly lower (i.e., ONH was more oval) in high axial myopic eyes [0.85 (0.83, 0.88)] compared to eyes with mild [0.90 (0.89–0.92)] or no [0.89 (0.88–0.91)] axial myopia (MD/age adjusted $p = 0.002$). Similarly, mean OCT-based ovality index was significantly lower in high axial myopic eyes [0.84 (0.81, 0.86)] compared to eyes with mild [0.88

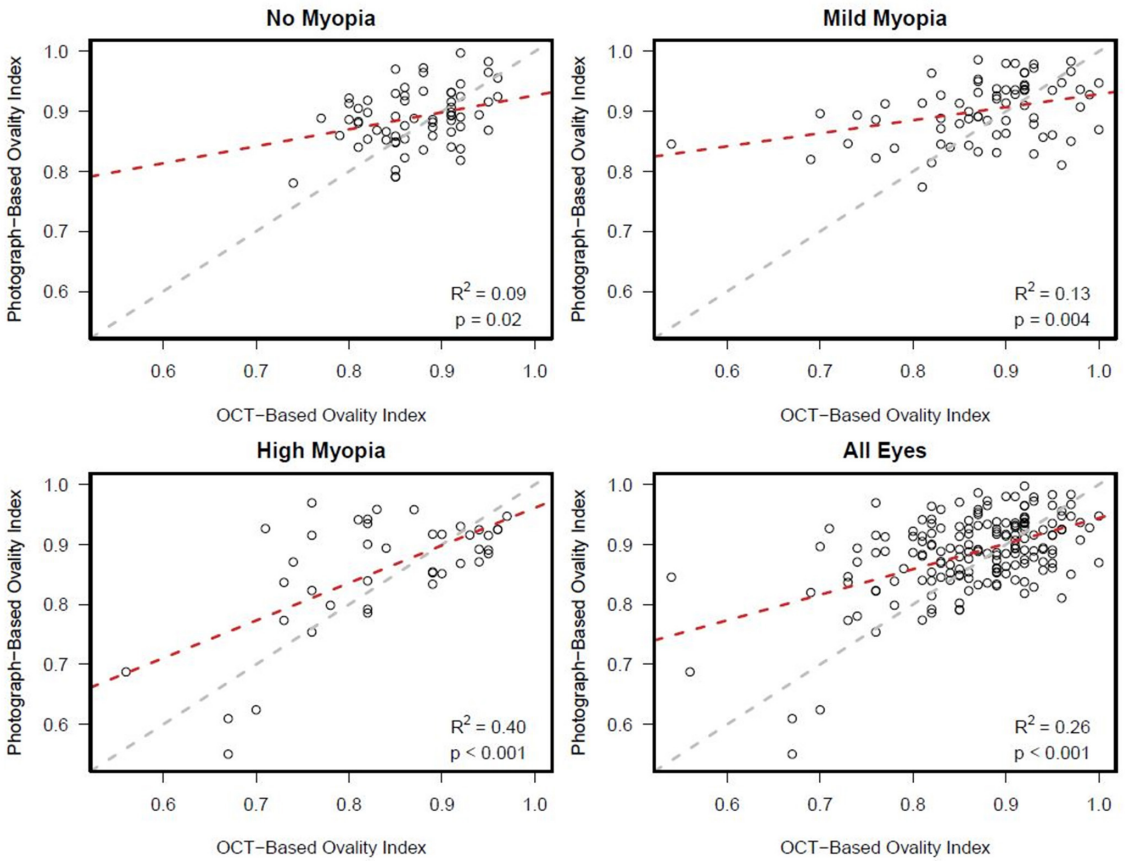

FIGURE 3 | Ovality index: Scatterplots showing stronger associations between semi-automated clinical disc margin photograph-based ovality index and automated, BMO OCT-based ovality index in eyes with axial high myopia compared to eyes with mild or no axial myopia.

(0.85–0.89)] or no [0.88 (0.88–0.90)] myopia (MD/age adjusted $p = 0.008$).

In contrast, the mean values of OCT-based rotation angles were much larger than photograph-based measures (34.8 and 18.4 degrees, respectively). Moreover, photograph-based rotation angles tended to be larger in high axial myopic eyes (20.9 degrees) compared to eyes with mild (19.9 degrees) and no myopia (15.2 degrees) (visual field MD and age-adjusted $p = 0.108$) but there was no difference in the OCT-based rotation angles across the three categories of myopia (visual field MD and age-adjusted $p = 0.96$.

Agreement Between Photograph-Based and OCT-Based Measurements of Optic Disc Ovality Index and Rotation Angle

There was a statistically significant association [R^2 (95% CI)] between semi-automated photograph-based and automated OCT-based assessment of ONH ovality index for all eyes [0.26 (0.16; 0.36); $p < 0.001$]. This association was weakest in non-myopic eyes [0.09 (0.01, 0.26); $p = 0.02$], followed by mild-axial myopic eyes [0.13 (0.02, 0.29); $p = 0.004$] and strongest in high-axial myopic eyes [0.40 (0.19, 0.60); $p < 0.001$] (**Figure 3**). In addition, Bland-Altman plots suggest that the mean difference in the photograph- and OCT-based ovality index values was close to zero and did not vary by the degree of ovality or myopia status (**Figure 4**).

There was no association between semi-automated photograph-based and automated OCT-based assessment of rotation angle with R^2 values ranging from 0.00 (0.00, 0.08) in non-myopic eyes to 0.03 (0.0, 0.21) in high-axial myopic eyes (all associations $p \geq 0.33$) (**Figure 5**). The Bland-Altman plots suggest that the difference in the photograph- and OCT-based rotation angle was close to 20 degrees and did not vary by rotation angle (**Figure 6**).

DISCUSSION

To our knowledge, this is the first study to compared semi-automated measurements of ONH ovality index and rotation angle based on the clinical disc margin manually identified on optic disc photographs to automated OCT measurements based on the BMO in healthy and glaucomatous eyes with high-, mild- and no axial myopia. We found a statistically significant, weak to moderate association between manual

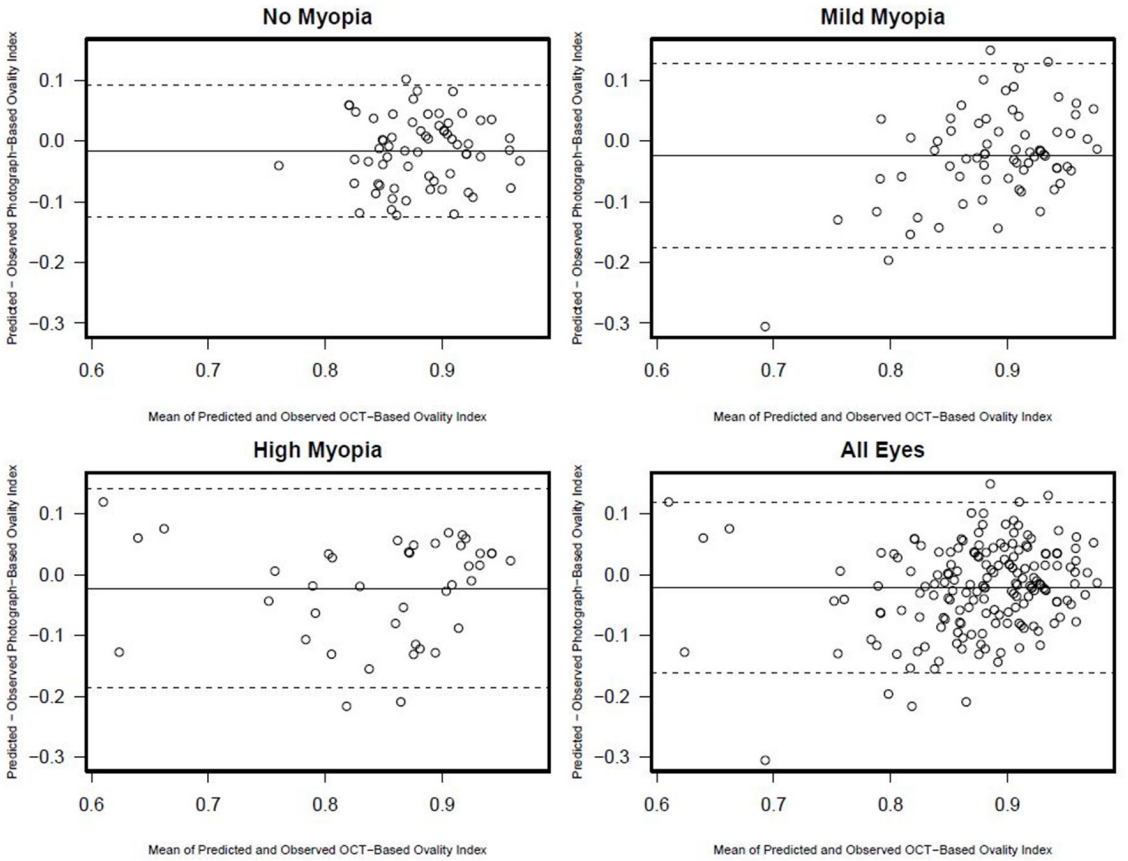

FIGURE 4 | Ovality index Bland-Altman plots documenting the agreement between photograph and OCT-based ovality index by myopia status.

photograph-based and automated OCT-based assessment of ONH ovality index ($R^2 = 0.26$), which was strongest in highly myopic eyes ($R^2 = 0.40$), followed by weaker associations in mild-myopic ($R^2 = 0.13$), and non-myopic eyes ($R^2 = 0.09$). No association was found between photograph-based and OCT-based assessment of the rotation angle with R^2 values ranging from 0.00 to 0.03 (all $p > 0.33$). The large difference between photographs and OCT-based rotation angle measurements suggests that these parameters cannot be used interchangeably, and the results should not be directly compared.

Axial elongation can cause pathological changes located at the posterior pole, such as myopic maculopathy, Bruch's membrane defects and posterior staphyloma (28). The clinical challenge to diagnose glaucoma in (highly) myopic eyes is that the appearance of the ONH can mimic changes that are pathognomonic for glaucoma. Those changes include optic disc ovality/tilt, rotation and peripapillary atrophy. At the same time, myopic changes can also mistakenly be interpreted as glaucoma (29). We hypothesize that objective characterization of the morphological characteristics of myopic disks can be used to help identify features related more to myopia than glaucoma (and vice versa). A precise characterization of the myopic optic disc is the first step to elucidate parameters that can ultimately help improve clinicians' ability to differentiate between (high) myopia and glaucoma.

We previously reported methods to characterize the myopic optic disc with an OCT based automated three-dimensional approach to characterize the ONH morphology in myopic eyes (21). We used this automated custom software to measure optic disc ovality index and rotation angle in the current study. Most previous studies characterized the myopic optic disc using manual photograph-based methods (9–13, 18, 30–35). The current study suggests that the characterization of the degree of ovality and rotation of the myopic optic disc based on photographs and OCT is not interchangeable.

It has been reported previously that optic disc features that are assessed two-dimensionally based on the clinical disc margin of optic disc photographs and three-dimensionally based on the BMO from OCT scans often do not agree (36). Based on measurements of fundus photographs relative to the clinical disc margin, myopic optic disks have been reported to have a more oval configuration (11, 18, 30–32, 34, 37), a higher degree of disc tilt (12, 13, 18, 30, 33–35) and rotation (11, 12, 18, 31, 34, 35). The current study confirms greater ovality (lower ovality index) in eyes in the high axial myopia group compared to eyes in the no and mild axial myopia groups using both semi-automated

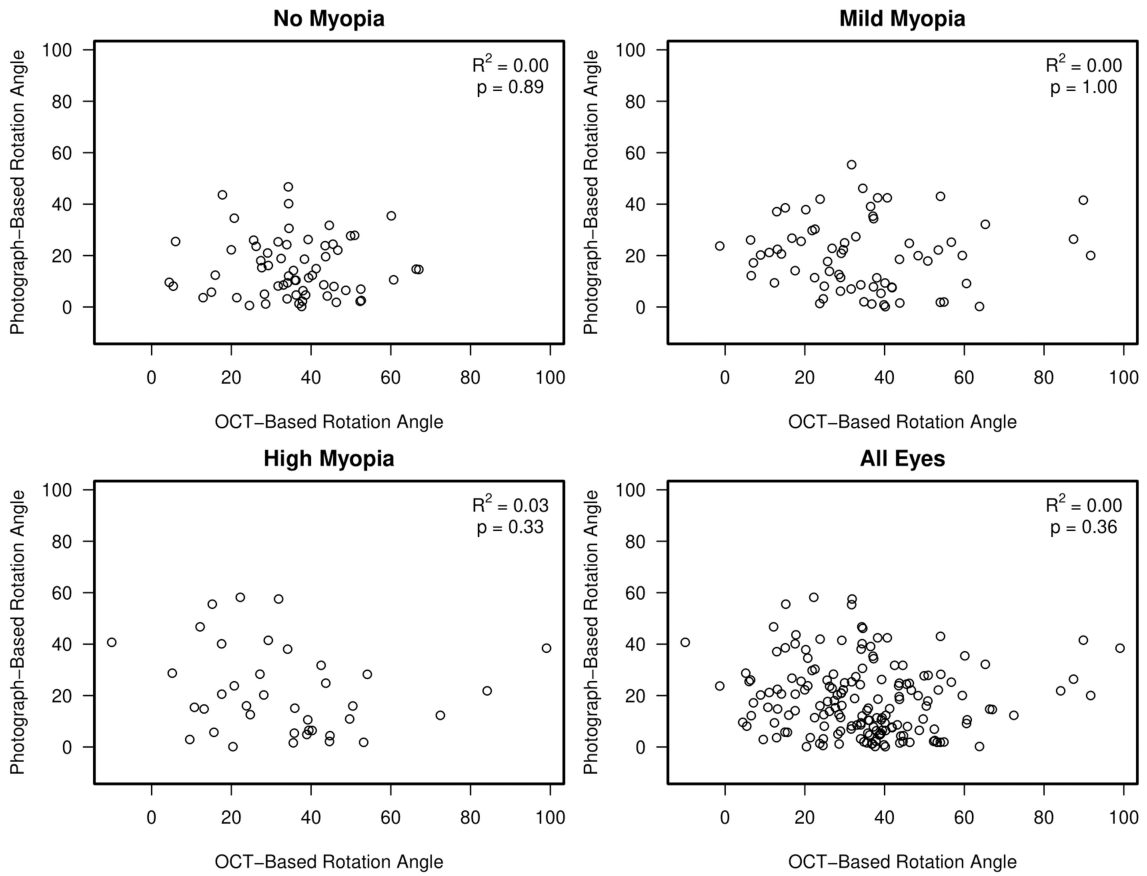

FIGURE 5 | Scatterplots showing no association between semi-automated, clinical disc margin photograph-based rotation angle and automated, BMO OCT-based rotation angle.

photograph- and automated OCT measurements. However, the rotation angle is larger in the high myopia group, but only when measured from the photographs and not when measured from OCT scans. These differences are in large part due to the fact that the features and anatomy used to delineate optic disc margins from clinical examination or fundus photography are often different from features identified in OCT as the BMO, resulting in different rotation angle values. The OCT-based rotation angle is a 3-dimensional BMO-based assessment while the 2-dimensional photographed-based rotation angle is measured relative to the clinical disc margin, which does not always correspond with the BMO, particularly in myopic eyes. Previous studies co-localized optic disc stereophotographs to OCT images of the optic disc and found that the clinically identified disc margin does not correspond to one single anatomic structure in OCT images (38). For example, in some eyes, in specific regions of the optic disc, Bruch's membrane extends beyond the clinically identified disc margin and is therefore not visible on a photograph or a clinical exam (36, 38, 39). For example in myopic eyes, OCT ONH images often show a temporal displacement of the BMO relative to the anterior scleral opening and the clinical disc margin (40). Another possible explanation for the differences in rotation angle is that there is an error in our automated OCT measurement of rotation angle. To investigate this issue, the rotation angle was calculated using an independent automated and histologically validated OCT method (41). Similar results were observed suggesting strongly that the rotation angle is not larger in eyes of the high myopic group compared to eyes in the mild and no myopia group (data not shown, personal communication with Massimo Fazio—June 2020).

A limitation of photograph-based measurements is that especially in tilted disks, which are more common in high myopic eyes (21), the optic disc is seen as more oval because of the oblique observation angle (33). It should be noted that we use the term rotation (25) instead of the more commonly used term torsion to describe the rotation of the BMO around a sagittal axis (instead of vertical axis, as measured by the 3D tilt angle) (42, 43). In contrast, measuring optic disc configuration based on an objective anatomical BMO-based feature improves our ability to obtain repeatable measurements of the ONH. However, we documented recently, objective detection of the BMO in OCT scans can also be challenging, particularly in some eyes with high axial myopia (44).

Given the results of the current study and the consistent evidence that the subjective delineation of the clinical disc margin often does not represent the anatomical BMO-based

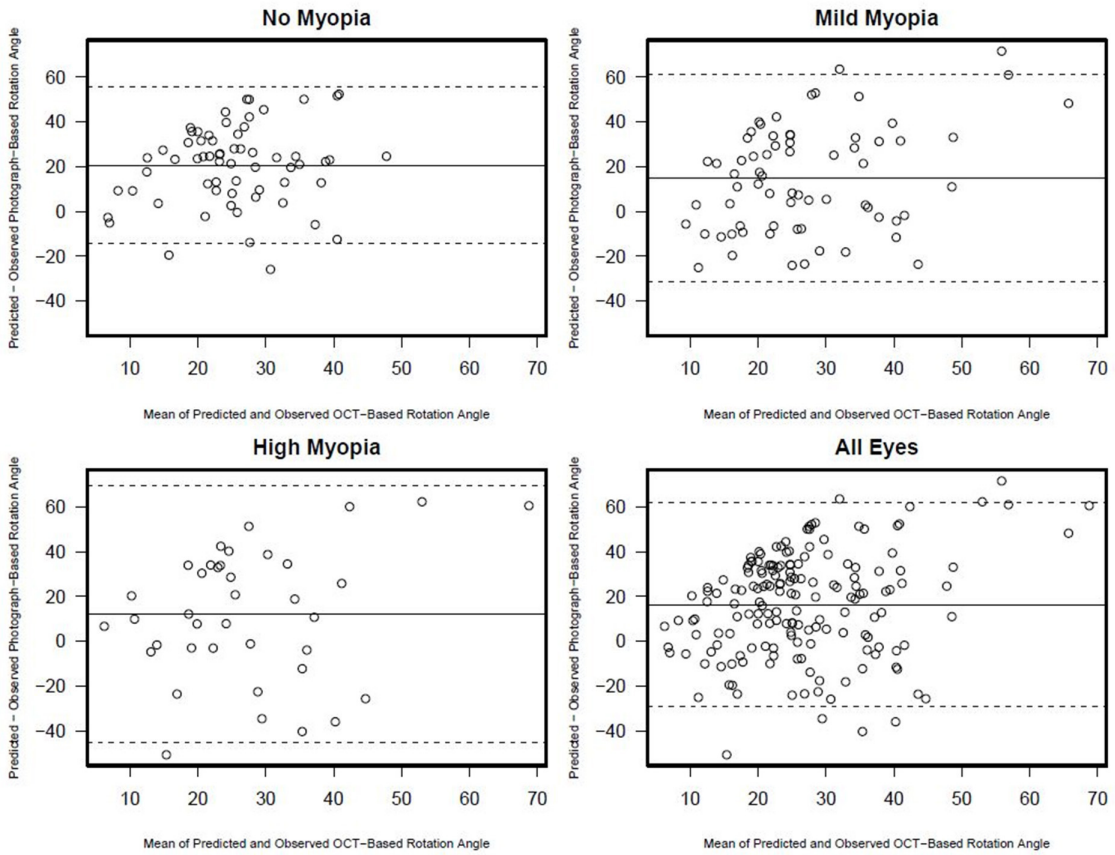

FIGURE 6 | Rotation angle Bland-Altman plots documenting the agreement between photograph and OCT based rotation angle by myopia status.

disk configuration, particularly in myopic eyes (36, 39), objective measurement and characterization of the optic disc using OCT appears to be a more appropriate tool to objectively characterize the morphology of the optic disc. Characterizing the ONH based on OCT anatomical morphology may facilitate the identification of biomarkers that can help clinicians differentiate between high myopes with and without glaucoma.

This study has several limitations. First, manual measurements were assessed by only one of the authors and we therefore did not provide interobserver variability and reproducibility. However, all measurements were re-evaluated by three expert graders. Second, OCT measurements were based only on Spectralis OCT imaging. Our results are therefore not generalizable to other OCT devices. Third, the horizontal axis for semi-automated photograph-based rotation angle calculation was not defined by the Fovea-BMO axis and therefore was not adjusted for an individual's anatomy of the eye. Fourth, there is a significant difference in age and race within the different myopia groups. However, it is unlikely that this may affect the results, as in this study two different methods were compared in the exact same eyes and results reported separately for non-, mild- and high myopic eyes. Finally, as we included both glaucoma and healthy eyes in the analysis it is possible that glaucomatous optic nerve head changes may have influenced the mean ovality index and rotation angle values. To address this issue, we adjusted for visual field MD in the analysis comparing mean ovality index and rotation angles by myopia status for both the photograph- and OCT-based measurement strategy (**Table 2**). The significant differences in ovality index across myopia status remained after this adjustment, suggesting that including glaucoma patients in the analysis is not driving the results. Moreover, as the main objective of this report is to compare photograph and OCT-based analysis strategies, regardless of diagnosis, including glaucoma patients may increase the generalizability of the results.

A strength of this study is that myopia groups were defined by AL instead of using the spherical equivalent. Axial length better represents the size of the eye and its axial elongation than spherical equivalent which changes after cataract and refractive surgery. In addition, both photograph-based and OCT-based measurements were automated to improve repeatability. Furthermore, the automated OCT-based ovality index and rotation angle measurements were validated with an independent method.

In conclusion, we found weak to moderate associations between manual photograph-based and OCT BMO-based assessment of optic disc ovality and no association between assessment of optic disc rotation angle. Our results indicate that measurements based on these methods cannot be used interchangeably and results should not be directly compared.

DATA AVAILABILITY STATEMENT

The datasets analyzed during the current study are not publicly available until the ongoing NIH funded studies are complete, but are available in a de-identified format from the corresponding author on request.

ETHICS STATEMENT

The studies involving human participants were reviewed and approved by Institutional Review Board of the University of California, San Diego, clinicaltrials.gov, identifier: NCT00221897. The patients/participants provided their written informed consent to participate in this study.

AUTHOR CONTRIBUTIONS

JR and LZ: conceptualization. JR, LZ, AT, CB, and NE-N: study design. LZ, MF, and RW: funding. JR, LZ, MF, CB, NE-N, AB, MC, JJ, and RW: data interpretation. LZ: supervision. JR, LZ, AT, and MC: data curation. JR, NB, JP, and LZ: visualization. JR, AT, CB, NE-N, MC, and LZ: writing (draft and editing). AT, CB, AB, NB, JP, MF, and NE-N: data analysis. AB, MC, NB, JP, MF, JJ, and RW: writing (editing). JP: methodology. RW: data acquisition. All authors contributed to the article and approved the submitted version.

FUNDING

Supported in part by National Eye Institute, EY027510, EY029058, EY026574, K99EY030942, P30EY022589, JR: German Research Foundation research fellowship grant recipient (RE 4155/1-1) and German Ophthalmological Society Grant, University of California, San Diego School of Medicine Summer Research Training Fellowship grant and an unrestricted grant from Research to Prevent Blindness, New York, NY.

REFERENCES

1. Vitale S, Sperduto RD, Ferris FL, 3rd. Increased Prevalence of Myopia in the United States between 1971-1972 and 1999-2004. *Arch Ophthalmol.* (2009) 127:1632–9. doi: 10.1001/archophthalmol.2009.303
2. Pan CW, Dirani M, Cheng CY, Wong TY, Saw SM. The age-specific prevalence of myopia in Asia: a meta-analysis. *Optom Vision Sci.* (2015) 92:258–66. doi: 10.1097/OPX.0000000000000516
3. Jung SK, Lee JH, Kakizaki H, Jee D. Prevalence of myopia and its association with body stature and educational level in 19-year-old male conscripts in Seoul, South Korea. *Invest Ophthalmol Visual Sci.* (2012) 53:5579–83. doi: 10.1167/iovs.12-10106
4. Holden BA, Fricke TR, Wilson DA, Jong M, Naidoo KS, Sankaridurg P, et al. Global prevalence of myopia and high myopia and temporal trends from 2000 through 2050. *Ophthalmology.* (2016) 123:1036–42. doi: 10.1016/j.ophtha.2016.01.006
5. Flitcroft DI. The complex interactions of retinal, optical and environmental factors in myopia aetiology. *Prog Retinal Eye Res.* (2012) 31:622–60. doi: 10.1016/j.preteyeres.2012.06.004
6. Mitchell P, Hourihan F, Sandbach J, Wang JJ. The relationship between glaucoma and myopia: the blue mountains eye study. *Ophthalmology.* (1999) 106:2010–5. doi: 10.1016/S0161-6420(99)90416-5
7. Verkicharla PK, Ohno-Matsui K, Saw SM. Current and predicted demographics of high myopia and an update of its associated pathological changes. *Ophthalmic Physiol Optics.* (2015) 35:465–75. doi: 10.1111/opo.12238
8. Koh V, Tan C, Tan PT, Tan M, Balla V, Nah G, et al. Myopic maculopathy and optic disc changes in highly myopic young asian eyes and impact on visual acuity. *Am J Ophthalmol.* (2016) 164:69–79. doi: 10.1016/j.ajo.2016.01.005
9. Hwang YH, Yoo C, Kim YY. Myopic optic disc tilt and the characteristics of peripapillary retinal nerve fiber layer thickness measured by spectral-domain optical coherence tomography. *J Glaucoma.* (2012) 21:260–5. doi: 10.1097/IJG.0b013e31820719e1
10. Hwang YH, Yoo C, Kim YY. Characteristics of peripapillary retinal nerve fiber layer thickness in eyes with myopic optic disc tilt and rotation. *J Glaucoma.* (2012) 21:394–400. doi: 10.1097/IJG.0b013e3182182567
11. How AC, Tan GS, Chan YH, Wong TT, Seah SK, Foster PJ, et al. Population prevalence of tilted and torted optic discs among an adult chinese population in Singapore: the Tanjong pagar study. *Arch Ophthalmol.* (2009) 127:894–9. doi: 10.1001/archophthalmol.2009.134
12. Park HL, Kim YC, Jung Y, Park CK. Vertical disc tilt and features of the optic nerve head anatomy are related to visual field defect in myopic eyes. *Sci Rep.* (2019) 9:3485. doi: 10.1038/s41598-019-38960-6
13. Seol BR, Park KH, Jeoung JW. Optic disc tilt and glaucoma progression in myopic glaucoma: a longitudinal match-pair case-control study. *Invest Ophthalmol Visual Sci.* (2019) 60:2127–33. doi: 10.1167/iovs.18-25839
14. Lim L, Gazzard G, Chan YH, Fong A, Kotecha A, Sim EL, et al. Corneal biomechanics, thickness and optic disc morphology in children with optic disc tilt. *Brit J Ophthalmol.* (2008) 92:1461–6. doi: 10.1136/bjo.2008.139113
15. Nakazawa M, Kurotaki J, Ruike H. Longterm findings in peripapillary crescent formation in eyes with mild or moderate myopia. *Acta Ophthalmol.* (2008) 86:626–9. doi: 10.1111/j.1600-0420.2007.01139.x
16. Vongphanit J, Mitchell P, Wang JJ. Population prevalence of tilted optic disks and the relationship of this sign to refractive error. *Am J Ophthalmol.* (2002) 133:679–85. doi: 10.1016/S0002-9394(02)01339-9
17. Xu L, Li Y, Wang S, Wang Y, Wang Y, Jonas JB. Characteristics of highly myopic eyes: the beijing eye study. *Ophthalmology.* (2007) 114:121–6. doi: 10.1016/j.ophtha.2006.05.071
18. Choi JA, Park HY, Shin HY, Park CK. Optic disc tilt direction determines the location of initial glaucomatous damage. *Invest Ophthalmol Visual Sci.* (2014) 55:4991–8. doi: 10.1167/iovs.14-14663
19. Guo Y, Liu LJ, Xu L, Lv YY, Tang P, Feng Y, et al. Optic disc ovality in primary school children in Beijing. *Invest Ophthalmol Visual Sci.* (2015) 56:4547–53. doi: 10.1167/iovs.15-16590
20. Marsh-Tootle WL, Harb E, Hou W, Zhang Q, Anderson HA, Weise K, et al. Optic nerve tilt, crescent, ovality, and torsion in a multi-ethnic cohort of young adults with and without myopia. *Invest Ophthalmol Visual Sci.* (2017) 58:3158–71. doi: 10.1167/iovs.16-20860
21. Rezapour J, Bowd C, Dohleman J, Belghith A, Proudfoot JA, Christopher M, et al. The influence of axial myopia on optic disc characteristics of glaucoma eyes. *Sci Rep.* (2021) 11:8854. doi: 10.1038/s41598-021-88406-1
22. Sample PA, Girkin CA, Zangwill LM, Jain S, Racette L, Becerra LM, et al. The African descent and glaucoma evaluation study (Adages): design and baseline data. *Arch Ophthalmol.* (2009) 127:1136–45. doi: 10.1001/archophthalmol.2009.187
23. Marcus MW, de Vries MM, Junoy Montolio FG, Jansonius NM. Myopia as a risk factor for open-angle glaucoma: a systematic review and meta-analysis. *Ophthalmology.* (2011) 118:1989–94 e2. doi: 10.1016/j.ophtha.2011.03.012

24. Wang Y, Xu L, Zhang L, Yang H, Ma Y, Jonas JB. Optic disc size in a population based study in northern China: the Beijing eye study. *Brit J Ophthalmol.* (2006) 90:353–6. doi: 10.1136/bjo.2005.081521
25. Wang YX, Yang H, Luo H, Hong SW, Gardiner SK, Jeoung JW, et al. Peripapillary scleral bowing increases with age and is inversely associated with peripapillary choroidal thickness in healthy eyes. *Am J Ophthalmol.* (2020) 217:91–103. doi: 10.1016/j.ajo.2020.03.050
26. Belghith A, Bowd C, Medeiros FA, Hammel N, Yang Z, Weinreb RN, et al. Does the location of bruch's membrane opening change over time? Longitudinal Analysis Using San Diego Automated Layer Segmentation Algorithm (Salsa). *Invest Ophthalmol Visual Sci.* (2016) 57:675–82. doi: 10.1167/iovs.15-17671
27. Belghith A, Bowd C, Weinreb RN, Zangwill LM. A hierarchical framework for estimating neuroretinal rim area using 3d spectral domain optical coherence tomography (Sd-Oct) Optic nerve head (Onh) images of healthy and glaucoma eyes. *Annu Int Conf IEEE Eng Med Biol Soc.* (2014) 2014:3869–72. doi: 10.1109/EMBC.2014.6944468
28. Curtin BJ, Karlin DB. Axial length measurements and fundus changes of the myopic eye. I. The Posterior Fundus. *Trans Am Ophthalmol Soc.* (1970) 68:312–34.
29. Hsu CH, Chen RI, Lin SC. Myopia and glaucoma: sorting out the difference. *Curr Opin Ophthalmol.* (2015) 26:90–5. doi: 10.1097/ICU.0000000000000124
30. Tay E, Seah SK, Chan SP, Lim AT, Chew SJ, Foster PJ, et al. Optic disk ovality as an index of tilt and its relationship to myopia and perimetry. *Am J Ophthalmol.* (2005) 139:247–52. doi: 10.1016/j.ajo.2004.08.076
31. Nakanishi H, Suda K, Yoshikawa M, Akagi T, Kameda T, Ikeda HO, et al. Association of bruch's membrane opening and optic disc morphology to axial length and visual field defects in eyes with primary open-angle glaucoma. *Graefe's Arch Clin Exp Ophthalmol.* (2018) 256:599–610. doi: 10.1007/s00417-017-3874-8
32. Zhao XJ, Jiang HY, Li YH, Liu BQ, Xu HX, Zhou J, et al. Correlations between the optic nerve head morphology and ocular biometrics in highly myopic eyes. *Int J Ophthalmol.* (2018) 11:997–1001. doi: 10.18240/ijo.2018.06.17
33. Hosseini H, Nassiri N, Azarbod P, Giaconi J, Chou T, Caprioli J, et al. Measurement of the optic disc vertical tilt angle with spectral-domain optical coherence tomography and influencing factors. *Am J Ophthalmol.* (2013) 156:737–44. doi: 10.1016/j.ajo.2013.05.036
34. Takasaki H, Higashide T, Takeda H, Ohkubo S, Sugiyama K. Relationship between optic disc ovality and horizontal disc tilt in normal young subjects. *Japan J Ophthalmol.* (2013) 57:34–40. doi: 10.1007/s10384-012-0193-9
35. Park HY, Choi SI, Choi JA, Park CK. Disc torsion and vertical disc tilt are related to subfoveal scleral thickness in open-angle glaucoma patients with myopia. *Invest Ophthalmol Visual Sci.* (2015) 56:4927–35. doi: 10.1167/iovs.14-15819
36. Reis AS, Sharpe GP, Yang H, Nicolela MT, Burgoyne CF, Chauhan BC. Optic disc margin anatomy in patients with glaucoma and normal controls with spectral domain optical coherence tomography. *Ophthalmology.* (2012) 119:738–47. doi: 10.1016/j.ophtha.2011.09.054
37. Guo X, Chen X, Li M, Li S, You R, Wang Y. Association between morphological characteristics of the optic disc and other anatomical features of the fundus in highly myopic eyes. *Eur J Ophthalmol.* (2021) 31:2329–38.
38. Chauhan BC, O'Leary N, AlMobarak FA, Reis ASC, Yang H, Sharpe GP, et al. Enhanced detection of open-angle glaucoma with an anatomically accurate optical coherence tomography-derived neuroretinal rim parameter. *Ophthalmology.* (2013) 120:535–43. doi: 10.1016/j.ophtha.2012.09.055
39. Dai Y, Jonas JB, Ling Z, Sun X. Ophthalmoscopic-Perspectively distorted optic disc diameters and real disc diameters. *Invest Ophthalmol Visual Sci.* (2015) 56:7076–83. doi: 10.1167/iovs.14-16033
40. Jeoung JW, Yang H, Gardiner S, Wang YX, Hong S, Fortune B, et al. Optical coherence tomography optic nerve head morphology in myopia i: implications of anterior scleral canal opening versus bruch membrane opening offset. *Am J Ophthalmol.* (2020) 218:105–19. doi: 10.1016/j.ajo.2020.05.015
41. Fazio MA, Gardiner SK, Bruno L, Hubbard M, Bianco G, Karuppanan U, et al. Histologic validation of optical coherence tomography-based three-dimensional morphometric measurements of the human optic nerve head: methodology and preliminary results. *Exp Eye Res.* (2021) 205:108475. doi: 10.1016/j.exer.2021.108475
42. Fan YY, Jonas JB, Wang YX, Chen CX, Wei WB. Horizontal and vertical optic disc rotation. The Beijing eye study. *PLoS ONE.* (2017) 12:e0175749. doi: 10.1371/journal.pone.0175749
43. Jonas JB, Wang YX, Zhang Q, Fan YY, Xu L, Wei WB, et al. Parapapillary gamma zone and axial elongation-associated optic disc rotation: the Beijing eye study. *Invest Ophthalmol Visual Sci.* (2016) 57:396–402. doi: 10.1167/iovs.15-18263
44. Rezapour J, Proudfoot JA, Bowd C, Dohleman J, Christopher M, Belghith A, et al. Bruch membrane opening detection accuracy in healthy eyes and eyes with glaucoma with and without axial high myopia in an American and Korean cohort. *Am J Ophthalmol.* (2022) 237:221–34. doi: 10.1016/j.ajo.2021.11.030

Conflict of Interest: RW Consultant: Abbvie, Aerie Pharmaceuticals, Allergan, Equinox, Eyenovia, Iantrek, Implandata, Ioptic, Nicox, Topcon Financial support: Carl Zeiss Meditec., Bausch & Lomb, Konan, Centervue, Optos, Heidelberg Engineering, National Eye Institute, National Institute for Minority Health and Health Disparities, Optovue, Centervue, Topcon Patent: Toromedes, Meditec-Zeiss. LZ Financial Support: National Eye Institute, Carl Zeiss Meditec Inc., Heidelberg Engineering GmbH, Optovue Inc., Topcon Medical Systems Inc. Patent: Zeiss Meditec. Abbvie (Consultant).

The remaining authors declare that the research was conducted in the absence of any commercial or financial relationships that could be construed as a potential conflict of interest.

Publisher's Note: All claims expressed in this article are solely those of the authors and do not necessarily represent those of their affiliated organizations, or those of the publisher, the editors and the reviewers. Any product that may be evaluated in this article, or claim that may be made by its manufacturer, is not guaranteed or endorsed by the publisher.

Publikation IV

Rezapour J, Bowd C, Dohleman J, Belghith A, Proudfoot JA, Christopher M, Hyman L, Jonas JB, Penteado RC, Moghimi S, Hou H, Fazio MA, Weinreb RN, Zangwill LM; *Macula structural and vascular differences in glaucoma eyes with and without high axial myopia. British Journal of Ophthalmology;* 2023; Sep;107(9):1286-1294. doi: 10.1136/bjophthalmol-2021-320430. Epub 2022 Jun 20. PMID: 35725293.

Macula structural and vascular differences in glaucoma eyes with and without high axial myopia

Jasmin Rezapour,[1,2] Christopher Bowd,[1] Jade Dohleman,[1] Akram Belghith,[1] James A Proudfoot,[1] Mark Christopher,[1] Leslie Hyman,[3] Jost B Jonas ,[4] Rafaella C Penteado,[1] Sasan Moghimi,[1] Huiyuan Hou,[1] Nevin W. El-Nimri,[1] Eleonora Micheletti,[1] Massimo A Fazio ,[5] Robert N Weinreb ,[1] Linda M Zangwill [1]

► Additional supplemental material is published online only. To view, please visit the journal online (http://dx.doi.org/10.1136/bjophthalmol-2021-320430).

[1]Hamilton Glaucoma Center, Shiley Eye Institute, Viterbi Family Department of Ophthalmology, University of California San Diego, La Jolla, California, USA
[2]Department of Ophthalmology, University Medical Center Mainz, Mainz, Germany
[3]Wills Eye Hospital, Thomas Jefferson University, Philadelphia, Pennsylvania, USA
[4]Department of Ophthalmology, Medical Faculty Mannheim, Ruprecht-Karls-University Heidelberg, Mannheim, Germany
[5]Ophthalmology and Visual Sciences, University of Alabama at Birmingham, Birmingham, Alabama, USA

Correspondence to
Dr Linda M Zangwill, Hamilton Glaucoma Center, Shiley Eye Institute and Viterbi Family Department of Ophthalmology, University of California San Diego, La Jolla, CA 92093, USA; lzangwill@ucsd.edu

Received 23 November 2021
Accepted 24 April 2022
Published Online First 20 June 2022

To cite: Rezapour J, Bowd C, Dohleman J, *et al*. *Br J Ophthalmol* 2023;**107**:1286–1294.

ABSTRACT

Aims To identify clinically relevant parameters for identifying glaucoma in highly myopic eyes, an investigation was conducted of the relationship between the thickness of various retinal layers and the superficial vessel density (sVD) of the macula with axial length (AL) and visual field mean deviation (VFMD).

Methods 270 glaucoma patients (438 eyes) participating in the Diagnostic Innovations in Glaucoma cross-sectional study representing three axial myopia groups (non-myopia: n=163 eyes; mild myopia: n=218 eyes; high myopia (AL>26 mm): n=57 eyes) who completed macular optical coherence tomography (OCT) and OCT-angiography imaging were included. Associations of AL and VFMD with the thickness of the ganglion cell inner plexiform layer (GCIPL), macular retinal nerve fibre layer (mRNFL), ganglion cell complex (GCC), macular choroidal thickness (mCT) and sVD were evaluated.

Results Thinner Global GCIPL and GCC were significantly associated with worse VFMD (R^2=34.5% and R^2=32.9%; respectively p<0.001), but not with AL (all p>0.1). Thicker mRNFL showed a weak association with increasing AL (R^2=2.4%; p=0.005) and a positive association with VFMD (global R^2=19.2%; p<0.001). Lower sVD was weakly associated with increasing AL (R^2=1.8%; p=0.028) and more strongly associated with more severe glaucoma VFMD (R^2=29.6%; p<0.001). Thinner mCT was associated with increasing AL (R^2=15.5% p<0.001) and not associated with VFMD (p=0.194). mRNFL was thickest while mCT was thinnest in all sectors of high myopic eyes.

Conclusions As thinner GCIPL and GCC were associated with increasing severity of glaucoma but were not significantly associated with AL, they may be useful for monitoring glaucoma in highly myopic eyes.

WHAT IS ALREADY KNOWN ON THIS TOPIC

⇒ Previous studies have reported that macular measurements can be used to detect glaucoma in myopic eyes; however, little is known about the topographic distributions of macular layer thickness and microvasculature (vessel density) in glaucoma eyes with and without (high) myopia.

WHAT THIS STUDY ADDS

⇒ In this study, we analysed the sectoral distribution of macular retinal layers, superficial vessel density and choroidal thickness in glaucoma eyes without axial myopia, with mild axial myopia and with high axial myopia. We found that all sectors of the ganglion cell inner plexiform layer and ganglion cell complex thickness were significantly associated with the severity of glaucomatous visual field damage but not with axial length.

HOW THIS STUDY MIGHT AFFECT RESEARCH, PRACTICE OR POLICY

⇒ These results suggest that ganglion cell layer thickness measurements can be used to monitor glaucoma in clinically challenging high axial myopic eyes.

INTRODUCTION

With its potential vision threatening risk and with its prevalence increasing globally, myopia, especially high myopia, has become increasingly problematic.[1] Although optical coherence tomography (OCT)-based measurements of peripapillary retinal nerve fibre layer (pRNFL) thickness can accurately discriminate between healthy and glaucomatous eyes,[2] there is concern that in myopic eyes (and especially those that are highly myopic), the diagnostic accuracy of OCT measures is decreased. Optic disc changes in myopic eyes such as morphologic changes in the parapapillary region and optic disc enlargement pose significant challenges to the use of optical imaging and clinical optic disc evaluation to detect and monitor glaucoma (figure 1).[1 3] In part, this is due to differences in the regional arrangement of the peripapillary retinal nerve fibres between myopic eyes and emmetropic eyes that may result in sectoral values incorrectly classified as outside normal limits by instrument-specific software analysis in healthy myopic eyes.[4 5]

Approximately 50% of the retinal ganglion cells are concentrated within 10° of the fovea.[6] As a result, the macula region is useful for diagnosing optic neuropathies including glaucoma, especially in myopic eyes because myopic axial elongation primarily affects the optic nerve head (ONH) region. Previous studies have reported that early glaucomatous damage can be detected in the macula region[7] and that measurements of the ganglion cell inner plexiform layer (GCIPL) can

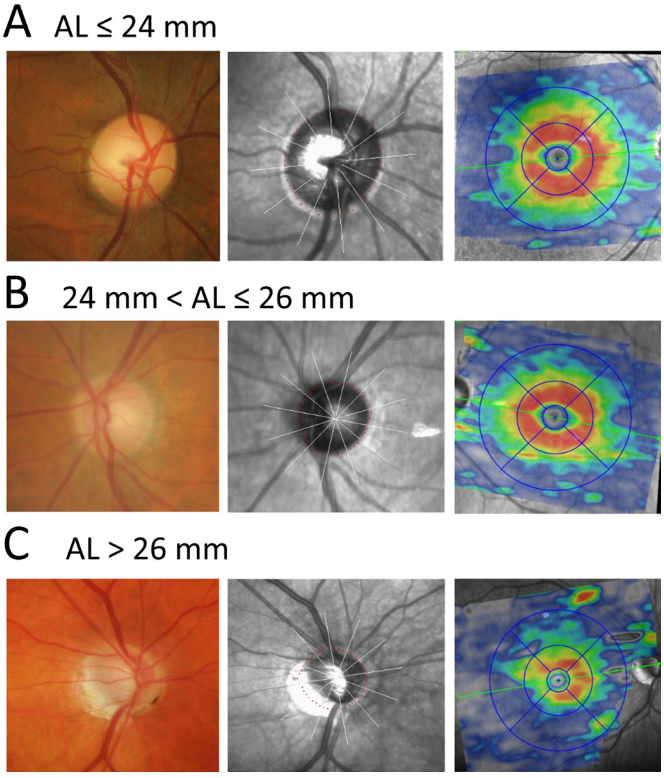

Figure 1 Optic disc photograph (left), optical coherence tomography optic nerve head en face image (middle) and optical coherence tomography macula posterior pole image (right) of an eye with (A) no axial myopia (axial length=23.8 mm), (B) mild axial myopia (axial length=24.7 mm and (C) high axial myopia (axial length=29 mm). AL, axial length.

be used for detecting glaucoma in highly myopic eyes.[8–12] However, little information is available about differences in the topographic distribution of either the thickness of the various macular retinal layers or the retinal vessel density in glaucomatous eyes with and without myopia. Sectoral measurements of the underlying macular vasculature may offer additional insight into differences in glaucomatous eyes with and without myopia.

Several studies using OCT-angiography (OCTA) have demonstrated a strong relationship between macular capillary density and the severity of glaucoma.[13 14] Furthermore, recent studies have reported the peripapillary choroid and the macula choroid to be thinner in highly myopic eyes compared with non-myopic eyes.[15 16 17 18] To date, to the best of our knowledge, the local distribution of macular choroidal thickness (mCT) in glaucomatous eyes with and without high myopia has not been reported.

The purpose of this study was to characterise the local distribution of GCIPL, ganglion cell complex (GCC), macular retinal nerve fibre layer (mRNFL), choroidal thickness (CT) and superficial vessel density (sVD) in glaucoma eyes with and without axial myopia. By better understanding, how the topographic distribution of these parameters varies with axial length (AL) and severity of disease, macula parameters that may be useful for detecting and monitoring glaucoma in myopic eyes can be identified.

METHODS

Study sample

This cross-sectional study included all glaucoma patients enrolled in the University of California, San Diego Diagnostic Innovations in Glaucoma Study (DIGS; clinicaltrials.gov identifier NCT00221897) with available AL measurements and good-quality macula OCT scans acquired between 2015 and 2020. The study was approved by the institutional review board of the University of California San Diego and according to the tenets of the Declaration of Helsinki written informed consent was obtained from all patients. As described previously,[19] participants underwent a complete ophthalmologic examination including assessment of refractive error, AL measurement (IOLMaster, Carl Zeiss Meditec, Dublin, California), visual field (VF) testing, simultaneous stereophotography of the optic disc and macula and macular OCT and OCTA imaging. Study participants were ≥18 years with best-corrected visual acuity ≥20/40 and open anterior chamber angles at baseline.

VF testing was performed using the standard Humphrey Field Analyzer 24–2 Swedish interactive thresholding algorithm. Primary open-angle glaucoma was defined as the presence of glaucomatous ONH damage based on masked assessment by two trained observers and corresponding glaucomatous VF loss in eyes with open angles. Stereo photograph-based optic disc damage was defined as focal or diffuse narrowing of the neuroretinal rim, and/or detection of retinal nerve fibre layer (RNFL) defects characteristic of glaucoma. ONH stereophotographs of highly myopic eyes were graded for glaucoma by two experts (CB and JR) after training with a senior consultant (JBJ). Diagnosis was defined by consensus between the two graders and adjudication by the senior consultant in case of disagreement. Glaucomatous VF damage was defined as two repeatable and reliable VF tests (rate of fixation losses and false-negative and false-positive responses of <33%) with a glaucoma hemifield test outside normal limits and/or a pattern standard deviation with a p value of <0.05 with a similar defect on consecutive abnormal tests.[19]

Myopia definition

Several morphological changes of the optic disc and the fundus can occur due to axial elongation.[20 21] However, myopia defined by the current refractive error does not always imply axial elongation that can lead to those morphological changes. Moreover, a change in refractive error can occur after refractive or cataract surgery in eyes that are axially elongated but do no longer appear to be (highly) myopic as defined by refractive error. For these reasons, myopia was classified by AL into the following three groups.

- No axial myopia: AL ≤24.0 mm.
- Mild axial myopia: 24.0 mm < AL ≤26.0 mm.
- High axial myopia: AL >26.0 mm.

OCT and OCT angiography imaging

OCT imaging of the macula was performed with the Spectralis OCT (V.6.10; Heidelberg Engineering, Heidelberg, Germany). Details of this instrument have been previously described.[14] Macula horizontal posterior pole (p-Pole) scans covering an area of 30°×25° (6×6 mm) were obtained. GCIPL, mRNFL and GCC (GCIPL +mRNFL) thickness measurements were generated from each retinal layer from the central 1-mm, 3-mm and 6mm circles as inner rings (1-mm and 3mm circle) and outer rings (3-mm and 6mm circle) according to the Early Treatment Diabetic Retinopathy Study defined sectors (temporal, superior, nasal and inferior).

OCTA imaging of the macula was performed with the Avanti AngioVue OCT system (V.2017.1.0.151; Optovue, Fremont California).[20] Macular whole image vessel density was calculated on a 3×3 mm² field macula scan (304 B-scans x 304 A-scans

per B-scan) centred on the fovea. Whole image vessel density of the temporal, superior, nasal and inferior sectors were reported. Macular parafoveal sVD was calculated within an annulus centred on the fovea, with an inner diameter of 1 mm and an outer diameter of 2.5 mm.

All images were reviewed by the Imaging Data Evaluation and Analysis (IDEA) Reading Center for image quality, accurate segmentation of the mRNFL, ganglion cell layer and inner plexiform layer (IPL). The automated Spectralis software segmentation was manually corrected if needed, according to the standard IDEA Reading Center protocols.[19]

Choroidal thickness measurement using deep learning

As choroidal thickness is not available from standard software, custom deep learning-based software, the San Diego Automated Layer Segmentation Algorithm—Deep, was developed to automatically measure mCT.[21] A trained grader (JR) manually segmented the Bruch's Membrane (BM)/retinal pigment epithelium (RPE) complex and the posterior boundary of the choroid in 120 p-Pole scans in the SPX software (V.1.9.204.0; Heidelberg Engineering, Heidelberg, Germany) in a subset of 20 eyes, which was used as ground truth to train a deep convolutional neural network model (BCDU-Net).[22] Two thousand two hundred fifty seven scans (753 eyes) with automated choroid segmentation were reviewed for accuracy (JR). The overall performance of the deep-learning algorithm for segmenting the choroid was very good with 400/401 (99.8%) eyes included (no myopia: 146/146 (100%), mild myopia: 208/208 (100%) and high myopia: 46/47 (97.9%)).

mCT was obtained for the inner and outer rings of the macular p-Pole scans defined above. Each ring was subdivided into temporal, superior, nasal and inferior sectors and global and sectoral choroidal thickness was calculated. The MCT was defined as the perpendicular distance between the posterior border of BM/RPE complex and the posterior boundary of the choroid.

Statistical analyses

Data are presented as mean (95% CI) and count (percentage) for continuous and categorical variables, respectively. Patient and eye characteristics were compared across myopia groups using analysis of variance and χ^2 tests for continuous and categorical patient-level variables (respectively) and linear mixed effects models for continuous eye-level variables, with a random intercept to account for within-patient correlation. Univariable and age and VFMD-adjusted multivariable models were applied to evaluate the association between AL and ocular parameters. P values less than 0.05 were considered statistically significant. All statistical analyses were performed using R (V.3.6.3).

RESULTS

Four-hundred and thirty-eight glaucoma eyes of 270 patients were included with 163 eyes (94 patients) in the non-myopic group, 218 eyes (133 patients) in the mild myopic group and 57 highly myopic eyes (36 patients) (table 1). P values are reported as age adjusted.

The participants in the high myopia group were significantly younger (mean (95% CI) 66.6 (63.2 to 70.1) years) than the members of the mild (72.6 (70.7 to 74.5) years) myopic group and the non-myopic individuals (77.1 (74.9 to 79.4) years) groups (p<0.001). There proportion of individuals of Asian descent in

Table 1 Glaucoma patient and eye characteristics by myopia group

	No axial myopia (n=94; 163 eyes)	Mild axial myopia (n=133; 218 eyes)	High axial myopia (n=36; 57 eyes)	Overall (n=270; 438 eyes)	P value	Age-adjusted p value
Age	77.1 (74.9, 79.4)	72.6 (70.7, 74.5)	66.6 (63.2, 70.1)	73.2 (71.8, 74.6)	<0.001*†‡	
Gender						
Female	59 (62.8%)	58 (43.6%)	17 (39.5%)	134 (49.6%)	0.006*†	
Male	35 (37.2%)	75 (56.4%)	26 (60.5%)	125 (50.4%)		
Race						
African Descent	21 (22.3%)	25 (18.8%)	3 (7.0%)7	49 (18.1%)	0.022†‡	
Asian Descent	8 (8.5%)	16 (12.0%)	12 (27.9%)	36 (13.3%)		
European Descent	63 (67.0%)	88 (66.2%)	25 (58.1%)	176 (65.2%)		
Axial length (mm)	23.4 (22.3, 23.5)	24.9 (24.8, 25.0)	26.6 (26.4, 26.7)	24.6 (24.4, 24.7)	<0.001	<0.001
SE (dpt)	−0.09 (−0.51, 0.34)	−1.46 (−1.84,−1.08)	−3.50 (−4.16,−2.85)	−1.16 (−1.53, −0.80)	<0.001	<0.001
CCT	536.8 (528.9, 544.6)	534.6 (527.9, 541.3)	535.4 (525.1, 547.6)	535.6 (530.2, 541.0)	0.868	0.737
VFMD (db)	−5.96 (−7.22, −4.69)	−7.19 (−8.28, −6.11)	7.17 (−9.20 to −5.14)	−6−73 (−7.53 to −5.93)	0.303	0.160
IOP (mm Hg)	14.3 (13.4, 15.1)	13.8 (13.1, 14.5)	14.3 (12.9, 15.6)	14.0 (13.5, 14.6)	0.619	0.181
Cataract surgery						
No	90 (55.2%)	132 (60.6%)	41 (71.9%)	263 (60.0%)	0.085	
Yes	73 (44.8%)	86 (39.4%)	16 (28.1%)	175 (40.0%)		
Refractive surgery						
No	163 (100.0%)	206 (94.5%)	55 (96.5%)	424 (96.8%)	0.003*	
Yes	0 (0.0%)	12 (5.5%)	2 (3.5%)	14 (3.2%)		

Results are presented as mean (95% CI) or percentage. Race was compared using a chi-squared test. Continuous variables were compared using ANOVA (for age) or linear mixed models (for eye level data).
No myopia: AL≤24.0 mm; mild myopia: AL:>24 mm and ≤26.0 mm; high myopia: AL>26.0 mm.
Missing 13a, 2b, and 8c values.
*No versus mild myopia p<0.05.
†No versus high myopia p<0.05.
‡Mild versus high myopia p<0.05.
AL, axial length; ANOVA, analysis of variance; CCT, central corneal thickness; SE, spherical equivalent; VFMD, visual field mean deviation.

the high myopia group was significantly higher compared with the no-myopic and the mild myopic group (p=0.022).

There was no significant difference in intraocular pressure (p=0.181) and central corneal thickness (p=0.737) among the three groups (table 1). Non-myopes tended (p=0.160) to have less severe glaucoma than the mild myopic group and the high myopic group (mean VF mean deviation (VFMD) −5.96 dB, −7.19 dB and −7.17 dB, respectively).

Macular thickness measurements

A total of 43 eyes were excluded from the analysis for not meeting image quality criteria (Spectralis quality score >15 dB or segmentation failure) with 14/140 (10.1%), 12/220 (5.5%) and 17/64 (26.6%) eyes excluded from the no-axial, mild-axial and high-axial myopia groups, respectively. Macular thickness measures are presented in figure 2 and online supplemental table 1.

Associations with AL

There were no statistically significant associations between global and sectoral GCC or GCPIL thickness measurements and AL except for a weak association of the GCIPL outer superior (R^2=1.1%, p=0.047) and outer nasal sector (R^2=1.9%, p=0.011). All mRNFL measurements, except for the inner temporal, inner inferior and outer inferior sector were significantly (all p<0.029) but relatively weakly (all R^2<5%) associated with AL. We found weak associations between lower global and sectoral vessel density measurements and longer AL (all $R^2 \leq 2.7\%$, all p<0.04) and stronger associations between thinner choroidal measures and longer AL (R^2 range: 9.3%–19.8%, all p<0.001) (figure 3 and online supplemental table 2).

Associations with severity of glaucoma (VFMD)

In multivariable models adjusted for age and AL, we found relatively strong associations between thinner global and sectoral GCIPL measures and worse VFMD (R^2 range: 10.3%–36.9%, all p<0.001). Thinner mRNFL was also significantly associated with worse VFMD in all sectors (R^2 range: 3.1%–27.4%, all p<0.001) with exception of the inner nasal and temporal sectors (p>0.088). Thinner global and sectoral Spectralis and Avanti GCC measures were significantly associated with worse VFMD (R^2 range: from 19.0% to 36.3% and 18.6% to 35.8%, all p<0.001, respectively). In addition, we found a relatively strong association between lower macular vessel density and worse VFMD (R^2 ranged from 17.2% to 33.5%, all p<0.001). mCT was not associated with VFMD (figure 4 and online supplemental table 3).

Secondary analysis of differences by axial myopia group

As a secondary analysis, we compared macular thickness and vascular measurement differences across the three axial myopia groups and adjusted for age and VFMD. In general, there was a trend that mRNFL was thickest in high myopic eyes in all sectors and globally (all p>0.137) and significantly thicker in the outer superior sector (p=0.013) (figure 2B), while mCT was significantly thinner in all sectors in high myopic eyes (figure 2F). The pattern of other macular thickness and vessel density measurements was less consistent across the three axial myopia groups (online supplemental table 1 and figure 2A–F.)

Specifically, global and sectoral GCC (both Spectralis and Avanti) and GCIPL thickness values were similar across myopic groups (all p>0.17) (see figure 2A,C,D). Parafoveal vessel density tended to be slightly higher in non-myopes compared with mild and high myopes, but only reached statistical significance in the nasal sector (mean (95% CI)); nasal vessel density in high myopes (43.1% (41.2% to 45.0%)), in mild myopes (42.7% (41.7% to 43.7%), in non-myopes (44.4% (43.6% to 45.3%)) (p=0.011) (figure 2E). Global and sectoral mean MCT was significantly thinner in high myopes compared with mild and non-myopes (all p<0.001, see figure 2F).

DISCUSSION

The results of this work have implications for diagnosing glaucoma in patients with high myopia. Our results suggest that macula measurements can be useful to diagnose and monitor glaucoma in myopic eyes as the GCIPL and GCC thinned with increasing severity of glaucoma but were not associated with AL. Except for choroidal thickness, all other macula thickness measures obtained in this study were associated with the severity of glaucoma. Because ganglion cell-related macular thickness measurements are strongly associated with VFMD but do not vary with AL, GCIPL and GCC show promise for detecting glaucoma in myopic eyes. However, future studies including healthy control eyes are needed to confirm our findings.

Because the macula is devoid of morphometric variations such as tilt and peripapillary atrophy, its diagnostic role in detecting glaucoma in highly myopic eyes is gaining attention r. There is evidence that myopia can lead to a high rate of false positives in the measurement of the pRNFL.[23] Earlier studies examined the diagnostic ability of GCIPL, pRNFL and GCC; they reported that GCIPL thickness has been reported as superior[8 9 24–27] or comparable to pRNFL thickness[28] for diagnosing glaucoma in myopic eyes. Shoji *et al* found that GCC parameters had high diagnostic accuracy to detect glaucoma in highly myopic eyes and that the diagnostic ability was higher than that of the pRNFL.[8] In another study, these authors reported that GCC parameters were not significantly related to refractive errors and had good accuracy to detect glaucoma in non-myopes and in high myopes.[9] Similarly, Kim *et al* determined that in highly myopic eyes, the accuracy of glaucoma detection based on the macular GCC thickness was comparable to that based on the pRNFL thickness.[29] These findings and those of other studies[8 9 27] are consistent with our results that GCIPL and GCC thickness measured using both Spectralis and Avanti showed no association between the GCIPL thickness and AL . This suggests that GCIPL thickness is less sensitive to changes due to axial elongation. Moreover, in our study, GCIPL and GCC measurements showed the strongest association with VFMD, suggesting that both are useful for measuring ganglion cell loss associated with glaucoma in both non-highly myopic and highly myopic eyes. These results are generalisable across instruments as both Spectralis GCC and Avanti GCC showed similar results.

High myopia is characterised by marked structural changes in the retina and choroid and the corresponding vasculature.[30 31] With the introduction of the non-invasive technique, OCTA images can provide a microvascular map from different retinal layers. To the best of our knowledge, this is the first study comparing both macular tissue thickness and vascular measurements in axial non-myopic, mild and high myopic glaucomatous eyes.

In the current study, the macular vessel density showed a weak association with AL and a moderate association with VFMD. Previous studies reported conflicting results. This inconsistency can be explained in part by differences in study populations and image acquisition and analysis protocols. For instance, we employed a 3×3 mm imaging area, whereas Yang *et al* employed

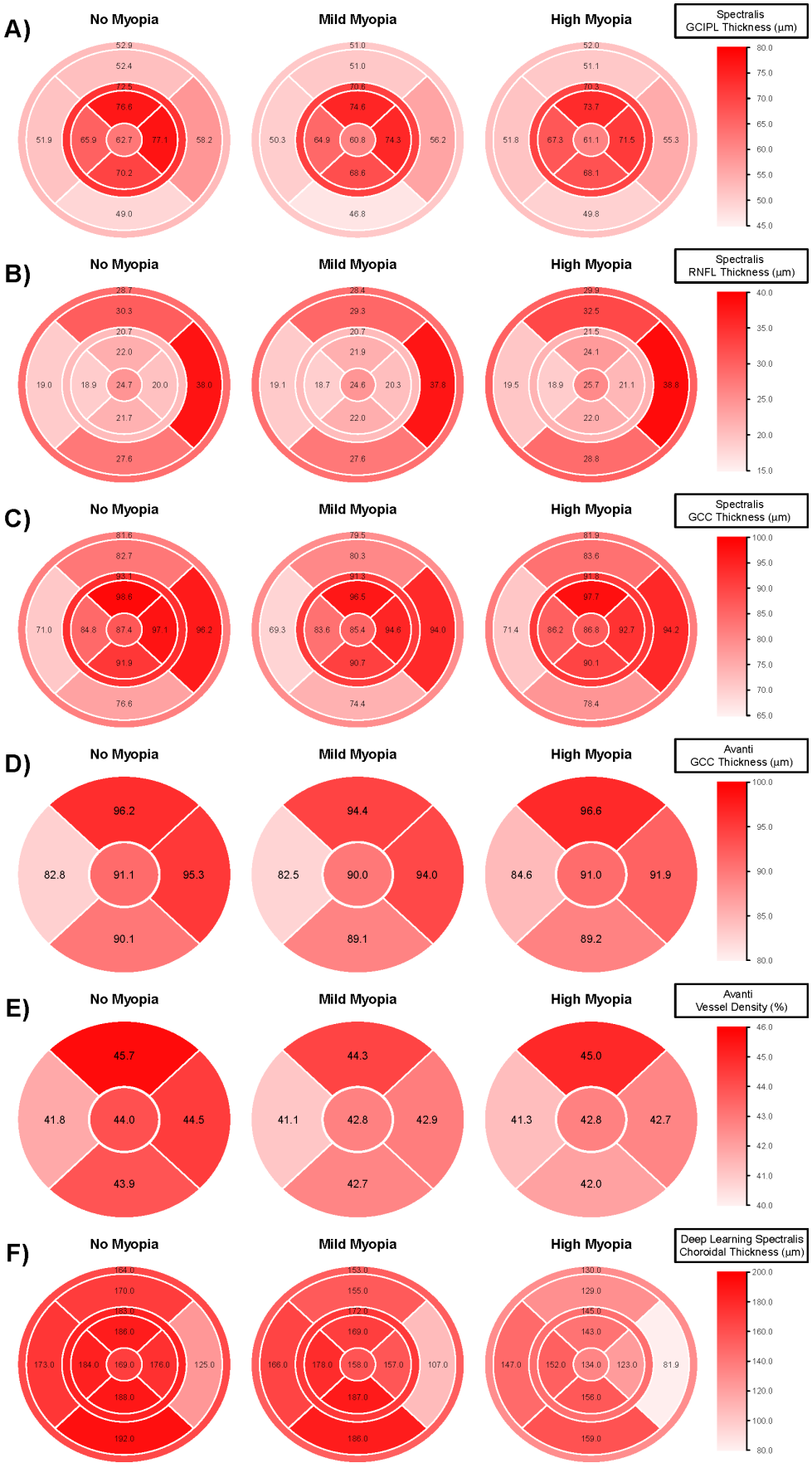

Figure 2 Sectoral and global thickness distribution of the Spectralis GCIPL thickness (A), Spectralis macular RNFL thickness (B), Spectralis GCC thickness (C), Avanti GCC thickness (D), Avanti macular vessel density (E) and Spectralis macular choroidal thickness (F) in non-myopic, mild myopic and highly myopic glaucoma eyes. GCC, ganglion cell complex; GCIPL, ganglion cell inner plexiform layer; RNFL, retinal nerve fibre layer.

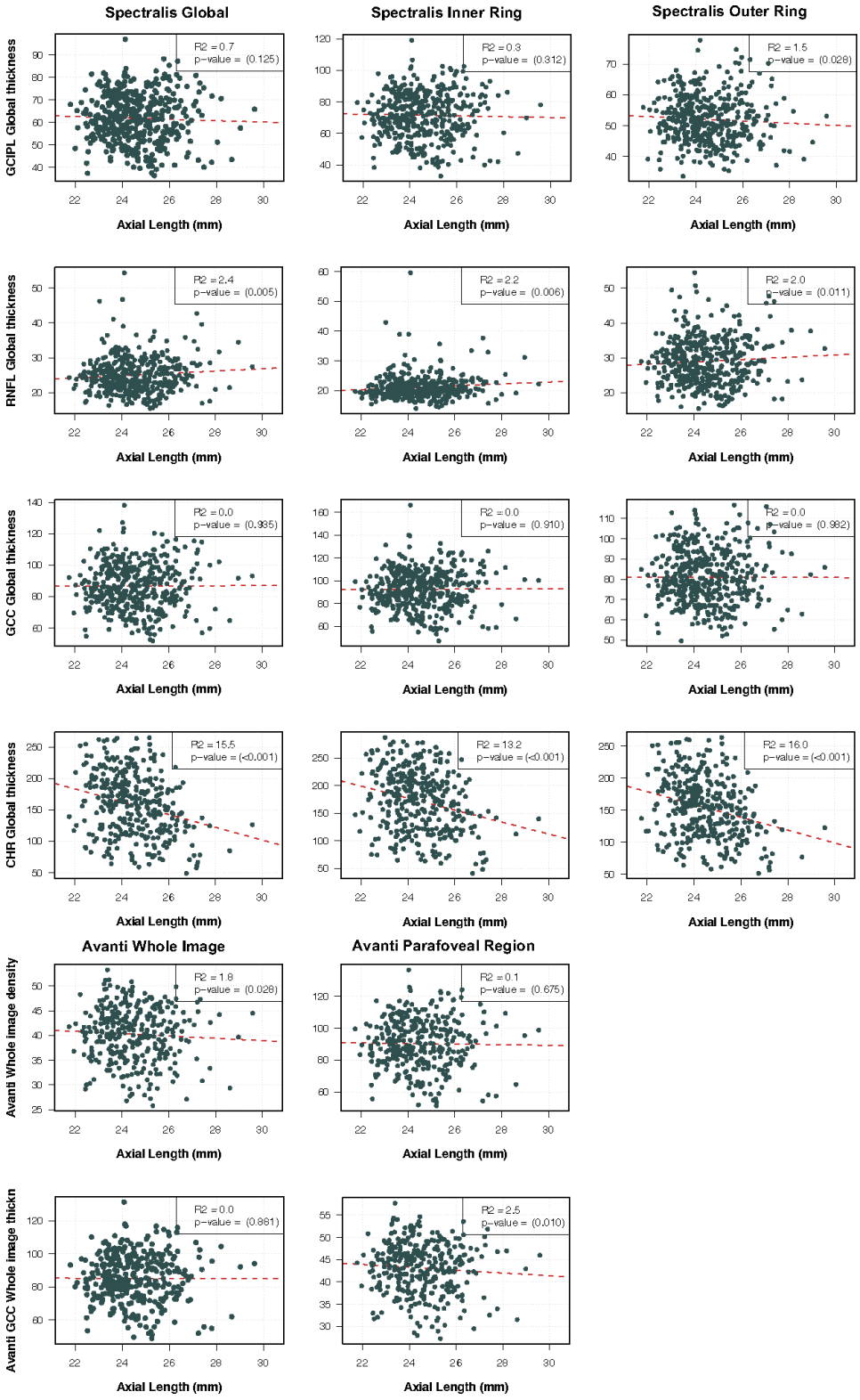

Figure 3 Scatterplots showing associations between axial length and global macula ganglion cell inner plexiform layer (GCIPL), retinal nerve fibre layer (mRNFL), ganglion cell complex (GCC) and choroidal (CHR) thickness, superficial vessel density. R^2 values are reported as percentages.

a larger 6×6 mm area.[31] A large scan size can be more sensitive to image artefacts and also may identify microvasculature dropout in outer regions.[31] We found only a weak association between superficial macula vessel density and AL but a moderate association between vessel density and VFMD. Our results suggest that although myopic changes might affect vessel density in the macula, effects due to glaucoma are much stronger as indicated by the stronger association to the VFMD. Therefore, they also may be useful for monitoring glaucoma in myopic eyes.[32]

We also examined choroidal thickness and found that as AL increased, the choroid thinned in all sectors. Previously reported results have demonstrated choroidal thinning in highly myopic

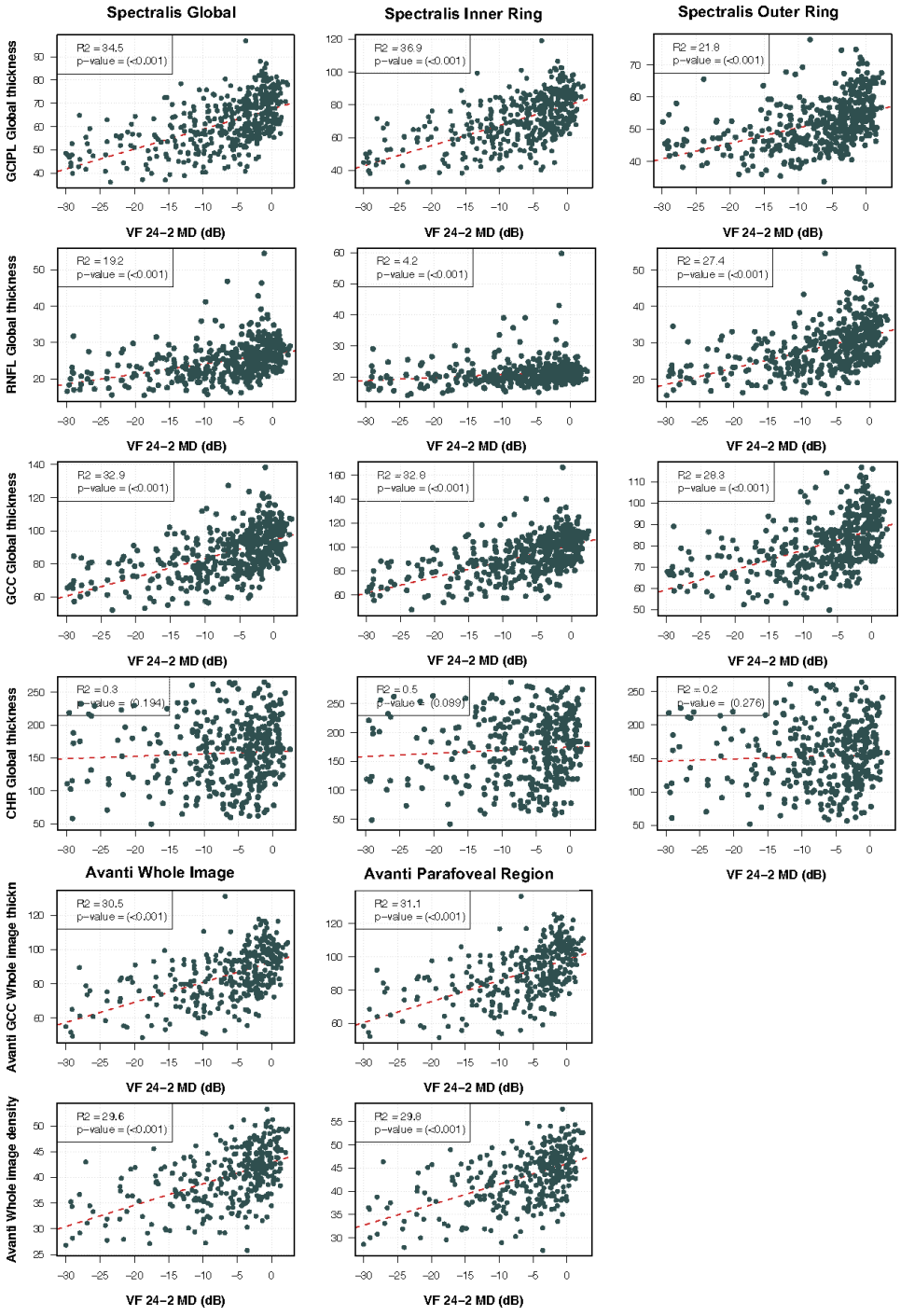

Figure 4 Scatterplots showing associations between visual field (VF) mean deviation (MD) and global macula ganglion cell inner plexiform layer (GCIPL), retinal nerve fibre layer (mRNFL), ganglion cell complex (GCC) choroidal (CHR) thickness and superficial vessel density. R^2 values are reported as percentages.

eyes.[33–35] Ho *et al*[33] reported that subfoveal choroidal thickness decreased by 6.20 µm for each diopter of myopia and was thinnest in the nasal sectors in all groups. These results are similar to the distributions of non-axial myopes, mild axial myopes and high axial myopes in our study. The choroid is a highly vascular layer. Supplied by the posterior ciliary arteries, it provides the retinal photoreceptors and the retinal pigment epithelium with oxygen and nourishment.[36] Our results did not show an association between choroidal thickness and VFMD, which suggests that choroidal thickness is not a useful metric for differentiating glaucomatous from healthy eyes or for monitoring glaucomatous progression.

The current study has several limitations. First, individuals with high myopia were younger. As retinal tissue is known to thin in older eyes,[37] we adjusted for age and VFMD in all analyses. In addition, we compared the three axial myopic groups after age-matching and found similar results (data not shown) with respect to the pattern of the retinal and vascular measurements in the three groups. Second, it has been suggested that AL might affect retinal vessel density measurements and lead to

incorrect scaling in OCTA imaging, which should be taken into account when interpreting our results.[38] Third, as vessel density measurements vary across instruments,[39] these sVD results are not necessarily generalisable to macula vessel density measurements from other OCTA instruments or to macula deep layer vessel density measurements. Furthermore, AL impacts the OCTA image magnification, which can result in differences in the retinal area measured for calculating sVD, which may affect mean vessel density measurements. However, the differences in parafoveal sVD before and after magnification correction have been shown to be less than 5%,[38] so the impact on our results is likely to be small.

In addition, axial elongation often leads to retinal layer segmentation errors and measurement failures. However, we reviewed the OCT images meticulously for segmentation errors and excluded data with uncorrectable segmentation failures. Another limitation of this study is that we did not include a healthy control group to assess if GCIPL and GCC are associated with AL in healthy eyes. It is possible that GCIPL and GCC thinning in glaucoma eyes masks associations with AL that would be found in healthy eyes. Finally, the sample size of the high myopic group was relatively small compared with the other two groups and the mean AL was only 26.6 mm. Therefore, we cannot generalise these results to eyes with longer AL.

In conclusion, GCIPL and GCC thickness may be useful measurements to monitor glaucoma in myopic eyes as they thinned with increasing severity of glaucoma but did not vary with AL.

Contributors LMZ provided overall supervision of all aspects of this work. JR and LMZ designed the study and are accountable for all aspects of the work. LMZ, RNW and MC provided funding. JR, LMZ, JAP and CB contributed to the drafting of the manuscript. JD, AB, MAF and MC contributed to the image analysis. JR, RCP, SM, HH, NEN and EM contributed to the acquisition of the data.

Funding JR: German Research Foundation research fellowship grant recipient (RE 4155/1-1) and German Ophthalmological Society Grant; MC: EY030942, K99EY030942; SM: Tobacco-Related Disease Research Program T31IP1511; RNW: National Eye Institute R01EY029058, an Unrestricted grant from Research to Prevent Blindness (New York, NY); LMZ: National Eye Institute R01EY011008, R01EY019869, R01EY027510, P30EY022589.

Competing interests RNW: Consulting: Eyenovia, Aerie Pharmaceuticals, Allergan; Research Funding or Equipment: Bausch & Lomb, Heidelberg Engineering, Carl Zeiss Meditec, Konan Medical, Optovue, Centervue; Patent: Toromedes, Carl Zeiss Meditec-Zeiss. LMZ: Research Funding and Equipment: Heidelberg Engineering; Research Equipment: Optovue Inc, Carl Zeiss Meditec Inc, Topcon Medical Systems Inc; Patent: Carl Zeiss Meditec.

Patient consent for publication Consent obtained directly from patient(s)

Ethics approval The study was approved by the institutional review board of the University of California San Diego (Ethics approval number 140276) and according to the tenets of the Declaration of Helsinki written informed consent was obtained from all patients. Participants gave informed consent to participate in the study before taking part.

Provenance and peer review Not commissioned; externally peer reviewed.

Data availability statement Data are available upon reasonable request. Data that underlie the results reported in the article and data dictionaries will be made available upon reasonable request and signed data use agreement.

ORCID iDs
Jost B Jonas http://orcid.org/0000-0003-2972-5227
Massimo A Fazio http://orcid.org/0000-0002-7489-089X
Robert N Weinreb http://orcid.org/0000-0001-9553-3202
Linda M Zangwill http://orcid.org/0000-0002-1143-5224

REFERENCES

1 Marcus MW, de Vries MM, Junoy Montolio FG, *et al*. Myopia as a risk factor for open-angle glaucoma: a systematic review and meta-analysis. *Ophthalmology* 2011;118:1989–94.
2 Leung CK-S, Cheung CY-L, Weinreb RN, *et al*. Retinal nerve fiber layer imaging with spectral-domain optical coherence tomography: a variability and diagnostic performance study. *Ophthalmology* 2009;116:63 e1-2:1257–63.
3 Jonas JB, Gusek GC, Naumann GO. Optic disk morphometry in high myopia. *Graefes Arch Clin Exp Ophthalmol* 1988;226:587–90.
4 Leung CK-S, Mohamed S, Leung KS, *et al*. Retinal nerve fiber layer measurements in myopia: an optical coherence tomography study. *Invest Ophthalmol Vis Sci* 2006;47:5171–6.
5 Leung CK-S, Yu M, Weinreb RN, *et al*. Retinal nerve fiber layer imaging with spectral-domain optical coherence tomography: interpreting the RNFL maps in healthy myopic eyes. *Invest Ophthalmol Vis Sci* 2012;53:7194–200.
6 Curcio CA, Allen KA. Topography of ganglion cells in human retina. *J Comp Neurol* 1990;300:5–25.
7 Hood DC, Raza AS, de Moraes CGV, *et al*. Glaucomatous damage of the macula. *Prog Retin Eye Res* 2013;32:1–21.
8 Shoji T, Sato H, Ishida M, *et al*. Assessment of glaucomatous changes in subjects with high myopia using spectral domain optical coherence tomography. *Invest Ophthalmol Vis Sci* 2011;52:1098–102.
9 Shoji T, Nagaoka Y, Sato H, *et al*. Impact of high myopia on the performance of SD-OCT parameters to detect glaucoma. *Graefes Arch Clin Exp Ophthalmol* 2012;250:1843–9.
10 Akashi A, Kanamori A, Nakamura M, *et al*. The ability of macular parameters and Circumpapillary retinal nerve fiber layer by three SD-OCT instruments to diagnose highly myopic glaucoma. *Invest Ophthalmol Vis Sci* 2013;54:6025–32.
11 Nakanishi H, Akagi T, Hangai M, *et al*. Effect of axial length on macular ganglion cell complex thickness and on early glaucoma diagnosis by spectral-domain optical coherence tomography. *J Glaucoma* 2016;25:e481–90.
12 Hung K-C, Wu P-C, Poon Y-C, *et al*. Macular diagnostic ability in OCT for assessing glaucoma in high myopia. *Optom Vis Sci* 2016;93:126–35.
13 Wu J, Sebastian RT, Chu CJ, *et al*. Reduced macular vessel density and capillary perfusion in glaucoma detected using OCT angiography. *Curr Eye Res* 2019;44:533–40.
14 Moghimi S, Zangwill LM, Penteado RC, *et al*. Macular and optic nerve head vessel density and progressive retinal nerve fiber layer loss in glaucoma. *Ophthalmology* 2018;125:1720–8.
15 Gupta P, Cheung CY, Saw S-M, *et al*. Peripapillary choroidal thickness in young Asians with high myopia. *Invest Ophthalmol Vis Sci* 2015;56:1475–81.
16 Yang H, Luo H, Gardiner SK, *et al*. Factors influencing optical coherence tomography peripapillary choroidal thickness: a multicenter study. *Invest Ophthalmol Vis Sci* 2019;60:795–806.
17 Flores-Moreno I, Lugo F, Duker JS, *et al*. The relationship between axial length and choroidal thickness in eyes with high myopia. *Am J Ophthalmol* 2013;155:314–9.
18 Ikuno Y, Tano Y. Retinal and choroidal biometry in highly myopic eyes with spectral-domain optical coherence tomography. *Invest Ophthalmol Vis Sci* 2009;50:3876–80.
19 Sample PA, Girkin CA, Zangwill LM, *et al*. The African descent and glaucoma evaluation study (ADAGES): design and baseline data. *Arch Ophthalmol* 2009;127:1136–45.
20 Ghahari E, Bowd C, Zangwill LM, *et al*. Macular vessel density in glaucomatous eyes with focal lamina Cribrosa defects. *J Glaucoma* 2018;27:342–9.
21 Rezapour J, Bowd C, Dohleman J, *et al*. The influence of axial myopia on optic disc characteristics of glaucoma eyes. *Sci Rep* 2021;11:8854.
22 Pyramid dilated deeper convlstm for video salient object detection. *Proceedings of the European conference on computer vision (ECCV*, 2018.
23 Biswas S, Lin C, Leung CKS. Evaluation of a myopic normative database for analysis of retinal nerve fiber layer thickness. *JAMA Ophthalmol* 2016;134:1032–9.
24 Seol BR, Jeoung JW, Park KH. Glaucoma detection ability of macular ganglion Cell-Inner plexiform layer thickness in myopic preperimetric glaucoma. *Invest Ophthalmol Vis Sci* 2015;56:8306–13.
25 Kim YK, Yoo BW, Jeoung JW, *et al*. Glaucoma-Diagnostic ability of ganglion Cell-Inner plexiform layer thickness difference across temporal raphe in highly myopic eyes. *Invest Ophthalmol Vis Sci* 2016;57:5856–63.
26 Baek SU, Kim KE, Kim YK, *et al*. Development of topographic scoring system for identifying glaucoma in myopic eyes: a spectral-domain OCT study. *Ophthalmology* 2018;125:1710–9.
27 Yang Z, Tatham AJ, Weinreb RN, *et al*. Diagnostic ability of macular ganglion cell inner plexiform layer measurements in glaucoma using swept source and spectral domain optical coherence tomography. *PLoS One* 2015;10:e0125957.

28 Choi YJ, Jeoung JW, Park KH, *et al*. Glaucoma detection ability of ganglion cell-inner plexiform layer thickness by spectral-domain optical coherence tomography in high myopia. *Invest Ophthalmol Vis Sci* 2013;54:2296–304.
29 Kim NR, Lee ES, Seong GJ, *et al*. Comparing the ganglion cell complex and retinal nerve fibre layer measurements by Fourier domain OCT to detect glaucoma in high myopia. *Br J Ophthalmol* 2011;95:1115–21.
30 Ye J, Wang M, Shen M, *et al*. Deep retinal capillary plexus decreasing correlated with the outer retinal layer alteration and visual acuity impairment in pathological myopia. *Invest Ophthalmol Vis Sci* 2020;61:45.
31 Yang D, Cao D, Zhang L, *et al*. Macular and peripapillary vessel density in myopic eyes of young Chinese adults. *Clin Exp Optom* 2020;103:830–7.
32 Lee K, Maeng KJ, Kim JY, *et al*. Diagnostic ability of vessel density measured by spectral-domain optical coherence tomography angiography for glaucoma in patients with high myopia. *Sci Rep* 2020;10:3027.
33 Ho M, Liu DTL, Chan VCK, *et al*. Choroidal thickness measurement in myopic eyes by enhanced depth optical coherence tomography. *Ophthalmology* 2013;120:1909–14.
34 Harb E, Hyman L, Gwiazda J, *et al*. Choroidal thickness profiles in myopic eyes of young adults in the correction of myopia evaluation trial cohort. *Am J Ophthalmol* 2015;160:62–71.
35 Wei WB, Xu L, Jonas JB, *et al*. Subfoveal choroidal thickness: the Beijing eye study. *Ophthalmology* 2013;120:175–80.
36 Linsenmeier RA, Padnick-Silver L. Metabolic dependence of photoreceptors on the choroid in the normal and detached retina. *Invest Ophthalmol Vis Sci* 2000;41:3117–23.
37 Hammel Na'ama, Belghith A, Bowd C, *et al*. Rate and pattern of rim area loss in healthy and progressing glaucoma eyes. *Ophthalmology* 2016;123:760–70.
38 Sampson DM, Gong P, An D, *et al*. Axial length variation impacts on superficial retinal vessel density and foveal avascular zone area measurements using optical coherence tomography angiography. *Invest Ophthalmol Vis Sci* 2017;58:3065–72.
39 Li X-X, Wu W, Zhou H, *et al*. A quantitative comparison of five optical coherence tomography angiography systems in clinical performance. *Int J Ophthalmol* 2018;11:1784–95.

	No Myopia	Low Myopia	High Myopia	Overall	p-value
Spectralis GCIPL (μm)					
	94 (163)	133 (218)	43 (57)	270 (438)	
Global thickness	62.4 (61.0, 63.9)	61.3 (59.7, 62.8)	62.1 (59.2, 65.0)	61.8 (60.8, 62.8)	0.543 ()
Inner ring thickness	72.1 (70.2, 74.0)	70.9 (68.8, 73.0)	72.3 (68.2, 76.3)	71.5 (70.2, 72.9)	0.659 ()
Outer ring thickness	52.8 (51.7, 53.9)	51.6 (50.6, 52.7)	51.9 (49.9, 54.0)	52.1 (51.4, 52.8)	0.341 ()
Inner T thickness	65.7 (63.4, 68.0)	65.2 (62.9, 67.5)	68.0 (63.9, 72.2)	65.7 (64.2, 67.3)	0.498 ()
Inner S thickness	76.3 (74.2, 78.4)	74.9 (72.7, 77.1)	76.1 (71.9, 80.3)	75.6 (74.1, 77.0)	0.647 ()
Inner N thickness	76.6 (74.5, 78.6)	74.6 (72.3, 76.9)	75.6 (70.9, 80.3)	75.5 (74.0, 76.9)	0.490 ()
Inner I thickness	69.9 (67.6, 72.2)	68.8 (66.4, 71.3)	69.4 (64.3, 74.5)	69.3 (67.7, 70.9)	0.838 ()
Outer T thickness	51.8 (50.4, 53.2)	50.9 (49.6, 52.2)	51.1 (48.6, 53.6)	51.3 (50.4, 52.2)	0.680 ()
Outer S thickness	52.4 (51.1, 53.7)	51.4 (50.3, 52.6)	51.5 (49.4, 53.7)	51.8 (51.0, 52.6)	0.527 ()
Outer N thickness	58.1 (56.7, 59.4)	56.6 (55.3, 57.8)	56.9 (54.4, 59.5)	57.2 (56.3, 58.0)	0.267 ()
Outer I thickness	48.8 (47.7, 50.0)	47.6 (46.7, 48.6)	48.1 (45.8, 50.3)	48.1 (47.4, 48.8)	0.287 ()
Spectralis RNFL (μm)					
	94 (163)	133 (218)	43 (57)	270 (438)	
Global thickness	25.0 (24.3, 25.6)	24.7 (24.0, 25.4)	26.2 (24.8, 27.5)	25.0 (24.5, 25.5)	0.137 ()
Inner ring thickness	21.0 (20.4, 21.5)	20.9 (20.4, 21.5)	22.0 (21.0, 23.1)	21.1 (20.7, 21.4)	0.148 ()
Outer ring thickness	28.9 (28.0, 29.8)	28.6 (27.6, 29.5)	30.3 (28.5, 32.1)	28.9 (28.3, 29.5)	0.194 ()
Inner T thickness	19.1 (18.6, 19.5)	18.8 (18.4, 19.3)	19.1 (18.4, 19.7)	19.0 (18.7, 19.2)	0.670 ()
Inner S thickness	22.3 (21.6, 23.0)	22.1 (21.4, 22.8)	24.6 (22.9, 26.3)	22.5 (22.0, 23.0)	0.004 ()
Inner N thickness	20.4 (19.7, 21.1)	20.5 (19.8, 21.2)	21.8 (20.2, 23.4)	20.6 (20.2, 21.1)	0.172 ()
Inner I thickness	22.1 (21.4, 22.7)	22.3 (21.6, 23.0)	22.6 (21.2, 24.0)	22.2 (21.8, 22.7)	0.791 ()
Outer T thickness	19.1 (18.8, 19.5)	19.1 (18.7, 19.5)	19.5 (18.9, 20.2)	19.2 (18.9, 19.4)	0.528 ()
Outer S thickness	30.4 (29.1, 31.6)	29.2 (28.1, 30.4)	32.9 (30.5, 35.2)	30.1 (29.3, 30.9)	0.013 ()
Outer N thickness	38.4 (37.1, 39.8)	37.8 (36.3, 39.3)	40.2 (37.4, 43.0)	38.3 (37.4, 39.3)	0.280 ()
Outer I thickness	27.9 (26.6, 29.1)	28.1 (26.9, 29.3)	28.6 (25.9, 31.4)	28.1 (27.2, 28.9)	0.842 ()
Spectralis GCC (μm)					
	94 (163)	133 (218)	43 (57)	270 (438)	
Global thickness	87.4 (85.5, 89.3)	86.0 (83.9, 88.1)	88.3 (84.4, 92.2)	86.8 (85.5, 88.2)	0.458 ()
Inner ring thickness	93.1 (90.9, 95.2)	91.8 (89.3, 94.3)	94.3 (89.7, 98.8)	92.6 (91.0, 94.2)	0.548 ()
Outer ring thickness	81.7 (79.9, 83.5)	80.2 (78.4, 82.0)	82.2 (78.7, 85.7)	81.0 (79.8, 82.2)	0.386 ()
Inner T thickness	84.8 (82.4, 87.1)	84.0 (81.6, 86.4)	87.1 (82.9, 91.4)	84.7 (83.1, 86.3)	0.461 ()
Inner S thickness	98.6 (96.1, 101.1)	97.0 (94.3, 99.6)	100.7 (95.5, 105.9)	98.1 (96.3, 99.8)	0.356 ()
Inner N thickness	96.9 (94.6, 99.3)	95.1 (92.5, 97.8)	97.4 (92.0, 102.8)	96.1 (94.4, 97.8)	0.532 ()
Inner I thickness	92.0 (89.2, 94.7)	91.1 (88.2, 94.1)	92.0 (86.0, 97.9)	91.5 (89.6, 93.5)	0.908 ()
Outer T thickness	70.9 (69.3, 72.5)	70.1 (68.5, 71.6)	70.7 (67.7, 73.6)	70.4 (69.4, 71.5)	0.738 ()
Outer S thickness	82.8 (80.5, 85.0)	80.7 (78.6, 82.7)	84.4 (80.2, 88.6)	81.9 (80.5, 83.4)	0.171 ()
Outer N thickness	96.5 (94.3, 98.7)	94.3 (91.9, 96.7)	97.1 (92.7, 101.6)	95.5 (93.9, 97.1)	0.333 ()
Outer I thickness	76.7 (74.5, 78.9)	75.7 (73.7, 77.7)	76.7 (72.3, 81.1)	76.2 (74.8, 77.6)	0.788 ()
Spectralis Choroid (μm)					
	73 (126)	119 (187)	31 (40)	223 (353)	
Global thickness	168.7 (160.0, 177.5)	158.8 (152.1, 165.5)	122.5 (109.5, 135.5)	158.2 (153.1, 163.4)	<0.001 ()
Inner ring thickness	181.8 (171.9, 191.7)	173.8 (166.1, 181.6)	132.8 (117.0, 148.5)	172.0 (166.2, 177.9)	<0.001 ()
Outer ring thickness	164.9 (156.4, 173.4)	154.3 (147.8, 160.9)	119.5 (107.2, 131.9)	154.2 (149.2, 159.1)	<0.001 ()
Inner T thickness	183.3 (174.6, 191.9)	178.1 (170.7, 185.5)	145.4 (128.1, 162.8)	176.3 (170.8, 181.7)	<0.001 ()
Inner S thickness	181.9 (171.0, 192.9)	171.4 (163.0, 179.8)	131.8 (114.5, 149.2)	170.7 (164.3, 177.1)	<0.001 ()
Inner N thickness	173.2 (161.1, 185.4)	158.8 (149.8, 167.8)	109.5 (93.6, 125.4)	158.4 (151.4, 165.3)	<0.001 ()
Inner I thickness	188.7 (178.7, 198.7)	186.9 (179.0, 194.9)	144.0 (128.1, 160.0)	182.7 (176.8, 188.6)	<0.001 ()
Outer T thickness	174.3 (167.4, 181.2)	166.2 (159.9, 172.4)	140.6 (125.7, 155.4)	166.2 (161.6, 170.7)	<0.001 ()
Outer S thickness	168.4 (157.9, 178.9)	154.7 (146.7, 162.6)	121.9 (106.4, 137.4)	155.9 (149.8, 161.9)	<0.001 ()
Outer N thickness	125.4 (115.2, 135.7)	107.5 (100.5, 114.5)	70.8 (61.5, 80.2)	109.7 (104.2, 115.3)	<0.001 ()
Outer I thickness	191.2 (182.0, 200.3)	188.9 (181.4, 196.4)	144.7 (128.9, 160.5)	184.7 (179.1, 190.3)	<0.001 ()
Avanti GCC (μm)					
	74 (125)	106 (164)	33 (40)	213 (329)	
Whole image thickness	85.5 (83.3, 87.7)	84.8 (82.3, 87.3)	84.3 (79.4, 89.3)	85.0 (83.4, 86.6)	0.882 ()
Parafovea thickness	91.0 (88.7, 93.4)	89.9 (87.2, 92.5)	89.6 (84.3, 95.0)	90.3 (88.6, 92.0)	0.797 ()
T thickness	82.9 (80.4, 85.5)	82.6 (80.0, 85.3)	83.0 (77.7, 88.3)	82.8 (81.1, 84.5)	0.984 ()
S thickness	95.8 (93.1, 98.5)	93.9 (91.0, 96.8)	95.1 (89.4, 100.8)	94.8 (92.9, 96.7)	0.652 ()
N thickness	94.8 (92.3, 97.2)	93.6 (90.8, 96.4)	92.2 (86.5, 97.8)	93.8 (92.1, 95.6)	0.655 ()
I thickness	90.3 (87.3, 93.3)	89.2 (86.0, 92.3)	87.6 (80.4, 94.7)	89.4 (87.3, 91.5)	0.730 ()
Avanti Vessel Density (%)					
	74 (125)	106 (164)	33 (40)	213 (329)	
Whole image density	40.9 (40.0, 41.7)	39.9 (39.0, 40.7)	39.9 (38.1, 41.7)	40.2 (39.7, 40.8)	0.256 ()
Parafovea density	44.0 (43.0, 44.9)	42.6 (41.7, 43.5)	42.8 (40.8, 44.8)	43.1 (42.5, 43.8)	0.127 ()
T density	41.9 (41.0, 42.9)	41.0 (40.1, 42.0)	40.9 (39.0, 42.9)	41.4 (40.7, 42.0)	0.374 ()
S density	45.5 (44.5, 46.4)	44.1 (43.1, 45.1)	45.1 (43.1, 47.2)	44.7 (44.1, 45.4)	0.141 ()
N density	44.4 (43.6, 45.3)	42.7 (41.7, 43.7)	43.1 (41.2, 45.0)	43.4 (42.8, 44.1)	0.049 ()
I density	44.0 (42.8, 45.2)	42.5 (41.4, 43.6)	41.9 (39.2, 44.6)	43.0 (42.2, 43.8)	0.141 ()

Supplemental Table 1. Results are presented as mean (95% confidence interval). Significance is determined by linear mixed models.

No myopia: AL ≤24.0mm; Mild myopia: AL: >24mm and≤26.0mm; High myopia: AL>26.0mm

[1]No vs. Mild Myopia $p < 0.05$; [2]No vs. High Myopia $p < 0.05$; [3]Mild vs. High Myopia $p < 0.05$

	Patients (eyes)	Univariable Regression		Multivariable Regression	
		Estimate	R^2 (p-value)	Estimate	$R^{2(\%)}$ (p-value)
Age	n = 270 (438)	-0.28 (-0.58, 0.02)	0.2 (0.069)	-0.27 (-0.57, 0.03)	0.1 (0.130)
VFMD	n = 270 (438)	-0.34 (-0.94, 0.26)	0.3 (0.273)	-0.52 (-1.15, 0.11)	0.7 (0.107)
Spectralis GCIPL (µm)					
Global	n = 270 (438)	-0.31 (-1.18, 0.56)	0.1 (0.488)	-0.59 (-1.34, 0.16)	0.7 (0.125)
Inner ring	n = 270 (438)	-0.25 (-1.45, 0.95)	0.1 (0.678)	-0.53 (-1.56, 0.50)	0.3 (0.312)
Outer ring	n = 270 (438)	-0.36 (-0.98, 0.26)	0.4 (0.260)	-0.65 (-1.22, -0.07)	1.5 (0.028)
Inner temporal	n = 270 (438)	0.11 (-1.20, 1.43)	0.0 (0.867)	0.07 (-1.05, 1.18)	0.0 (0.904)
Inner superior	n = 270 (438)	-0.56 (-1.83, 0.71)	0.2 (0.388)	-0.97 (-2.16, 0.23)	0.8 (0.113)
Inner nasal	n = 270 (438)	-0.32 (-1.61, 0.97)	0.1 (0.628)	-0.65 (-1.85, 0.56)	0.3 (0.292)
Inner inferior	n = 270 (438)	-0.13 (-1.52, 1.26)	0.0 (0.852)	-0.32 (-1.55, 0.90)	0.1 (0.607)
Outer temporal	n = 270 (438)	-0.42 (-1.18, 0.35)	0.3 (0.287)	-0.52 (-1.20, 0.17)	0.6 (0.140)
Outer superior	n = 270 (438)	-0.30 (-0.99, 0.40)	0.2 (0.408)	-0.70 (-1.38, -0.01)	1.1 (0.047)
Outer nasal	n = 270 (438)	-0.43 (-1.18, 0.32)	0.4 (0.260)	-0.94 (-1.66, -0.22)	1.9 (0.011)
Outer inferior	n = 270 (438)	-0.21 (-0.82, 0.40)	0.1 (0.501)	-0.34 (-0.94, 0.26)	0.4 (0.264)
Spectralis RNFL (µm)					
Global	n = 270 (438)	0.32 (-0.07, 0.72)	0.8 (0.111)	0.55 (0.17, 0.93)	2.4 (0.005)
Inner ring	n = 270 (438)	0.32 (-0.00, 0.64)	1.1 (0.053)	0.46 (0.14, 0.79)	2.2 (0.006)
Outer ring	n = 270 (438)	0.33 (-0.20, 0.87)	0.4 (0.223)	0.64 (0.15, 1.13)	2.0 (0.011)
Inner temporal	n = 270 (438)	0.02 (-0.22, 0.26)	0.0 (0.866)	0.17 (-0.08, 0.42)	0.5 (0.182)
Inner superior	n = 270 (438)	0.57 (0.14, 1.00)	1.9 (0.010)	0.73 (0.29, 1.18)	2.9 (0.001)
Inner nasal	n = 270 (438)	0.42 (-0.00, 0.84)	1.1 (0.053)	0.58 (0.14, 1.02)	1.9 (0.010)
Inner inferior	n = 270 (438)	0.26 (-0.13, 0.65)	0.5 (0.197)	0.38 (-0.02, 0.77)	1.0 (0.061)
Outer temporal	n = 270 (438)	0.09 (-0.12, 0.30)	0.2 (0.389)	0.23 (0.02, 0.43)	1.3 (0.029)
Outer superior	n = 270 (438)	0.40 (-0.29, 1.09)	0.4 (0.260)	0.76 (0.11, 1.42)	1.5 (0.024)
Outer nasal	n = 270 (438)	0.59 (-0.25, 1.43)	0.6 (0.173)	1.00 (0.20, 1.80)	1.8 (0.014)
Outer inferior	n = 270 (438)	0.24 (-0.48, 0.96)	0.1 (0.510)	0.57 (-0.10, 1.23)	0.8 (0.095)
Spectralis GCC (µm)					
Global	n = 270 (438)	0.02 (-1.16, 1.20)	0.0 (0.978)	-0.04 (-1.09, 1.00)	0.0 (0.935)
Inner ring	n = 270 (438)	0.07 (-1.31, 1.44)	0.0 (0.925)	-0.07 (-1.30, 1.16)	0.0 (0.910)
Outer ring	n = 270 (438)	-0.02 (-1.08, 1.03)	0.0 (0.967)	-0.01 (-0.97, 0.95)	0.0 (0.982)
Inner temporal	n = 270 (438)	0.14 (-1.22, 1.50)	0.0 (0.841)	0.24 (-0.92, 1.41)	0.0 (0.682)
Inner superior	n = 270 (438)	0.01 (-1.52, 1.54)	0.0 (0.989)	-0.23 (-1.70, 1.25)	0.0 (0.762)
Inner nasal	n = 270 (438)	0.10 (-1.41, 1.60)	0.0 (0.900)	-0.09 (-1.54, 1.37)	0.0 (0.905)
Inner inferior	n = 270 (438)	0.12 (-1.54, 1.78)	0.0 (0.886)	0.04 (-1.45, 1.54)	0.0 (0.955)
Outer temporal	n = 270 (438)	-0.33 (-1.21, 0.55)	0.2 (0.467)	-0.30 (-1.10, 0.51)	0.2 (0.472)
Outer superior	n = 270 (438)	0.08 (-1.17, 1.33)	0.0 (0.900)	0.03 (-1.17, 1.24)	0.0 (0.958)
Outer nasal	n = 270 (438)	0.15 (-1.23, 1.54)	0.0 (0.827)	0.06 (-1.25, 1.37)	0.0 (0.930)
Outer inferior	n = 270 (438)	0.02 (-1.20, 1.25)	0.0 (0.969)	0.21 (-0.94, 1.36)	0.0 (0.718)
Avanti GCC (µm)					
Whole image	n = 213 (329)	-0.03 (-1.41, 1.34)	0.0 (0.961)	-0.09 (-1.32, 1.14)	0.0 (0.881)
Parafovea	n = 213 (329)	-0.18 (-1.65, 1.28)	0.0 (0.810)	-0.28 (-1.59, 1.03)	0.1 (0.675)
Temporal	n = 213 (329)	-0.24 (-1.71, 1.23)	0.0 (0.748)	-0.21 (-1.45, 1.04)	0.0 (0.742)
Superior	n = 213 (329)	-0.30 (-1.92, 1.32)	0.1 (0.720)	-0.39 (-1.95, 1.17)	0.1 (0.625)
Nasal	n = 213 (329)	0.08 (-1.47, 1.63)	0.0 (0.918)	-0.08 (-1.56, 1.40)	0.0 (0.917)
Inferior	n = 213 (328)	-0.24 (-2.03, 1.54)	0.0 (0.790)	-0.41 (-2.00, 1.18)	0.1 (0.616)
Avanti Vessel Density (%)					
Whole image	n = 213 (329)	-0.24 (-0.74, 0.26)	0.3 (0.355)	-0.48 (-0.90, -0.05)	1.8 (0.028)
Parafovea	n = 213 (329)	-0.32 (-0.85, 0.21)	0.5 (0.241)	-0.59 (-1.04, -0.15)	2.5 (0.010)
Temporal	n = 213 (329)	-0.33 (-0.87, 0.21)	0.5 (0.237)	-0.47 (-0.92, -0.02)	1.5 (0.040)
Superior	n = 213 (329)	-0.20 (-0.76, 0.36)	0.2 (0.494)	-0.54 (-1.04, -0.05)	1.6 (0.033)
Nasal	n = 213 (329)	-0.30 (-0.84, 0.25)	0.4 (0.286)	-0.60 (-1.09, -0.10)	2.0 (0.020)
Inferior	n = 213 (328)	-0.48 (-1.15, 0.19)	0.7 (0.159)	-0.80 (-1.37, -0.23)	2.7 (0.006)
Spectralis Choroid (µm)					
Global	N=247 (400)	-10.95 (-14.96, -6.94)	8.9 (<0.001)	-15.17 (-18.96, -11.38)	17.3 (<0.001)
Inner Ring	N=247 (400)	-11.51 (-16.18, -6.84)	7.5 (<0.001)	-16.04 (-20.49, -11.58)	14.6 (<0.001)
Outer Ring	N=247 (400)	-10.81 (-14.70, -6.92)	9.2 (<0.001)	-14.97 (-18.64, -11.30)	17.9 (<0.001)
Inner Temporal	N=247 (400)	-8.05 (-12.53, -3.57)	4.1 (<0.001)	-12.33 (-16.64, -8.02)	9.6 (<0.001)
Inner Superior	N=247 (400)	-12.56 (-17.72, -7.40)	7.3 (<0.001)	-17.30 (-22.26, -12.34)	13.8 (<0.001)
Inner Nasal	N=247 (400)	-16.87 (-22.38, -11.36)	11.1 (<0.001)	-21.73 (-27.06, -16.41)	17.9 (<0.001)
Inner Inferior	N=247 (400)	-9.28 (-14.19, -4.37)	4.5 (<0.001)	-14.19 (-18.87, -9.51)	10.8 (<0.001)
Outer Temporal	N=247 (400)	-6.56 (-10.30, -2.83)	4.0 (<0.001)	-11.03 (-14.47, -7.60)	11.8 (<0.001)
Outer Superior	N=247 (400)	-13.07 (-17.89, -8.24)	8.9 (<0.001)	-17.45 (-22.12, -12.78)	15.5 (<0.001)
Outer Nasal	N=247 (400)	-14.37 (-18.70, -10.04)	12.8 (<0.001)	-18.10 (-22.34, -13.86)	19.3 (<0.001)
Outer Inferior	N=247 (400)	-10.15 (-14.80, -5.50)	6.0 (<0.001)	-14.92 (-19.32, -10.51)	13.1 (<0.001)

Supplemental Table 2. Ocular associations with axial length

*Linear mixed models slope estimates (with 95% confidence intervals) from univariable and multivariable models adjusted for age and VFMD. ^R^2 reported as a percentage

Abbreviations: GCC; Ganglion cell complex, GCIPL; Ganglion cell inner plexiform layer, RNFL; Retinal nerve fiber layer, VFMD; Visual field mean deviation

	Patients (eyes)	Univariable Regression		Multivariable Regression	
		Estimate	R^2 (p-value)	Estimate	$R^{2\,(\%)}$ (p-value)
Age	N=269 (438)	-0.004 (-0.023, 0.015)	0.0 (0.673)	-0.004 (-0.023, 0.014)	0.0 (0.646)
Axial length	N=269 (438)	-0.003 (-0.011, 0.006)	0.0 (0.527)	-0.004 (-0.012, 0.005)	0.1 (0.380)
Spectralis GCIPL (µm)					
Global	n = 269 (438)	0.86 (0.75, 0.96)	34.9 (<0.001)	0.84 (0.74, 0.94)	34.5 (<0.001)
Inner ring	n = 269 (438)	1.23 (1.09, 1.37)	37.4 (<0.001)	1.21 (1.07, 1.35)	36.9 (<0.001)
Outer ring	n = 269 (438)	0.48 (0.40, 0.56)	22.3 (<0.001)	0.47 (0.39, 0.55)	21.8 (<0.001)
Inner temporal	n = 269 (438)	1.36 (1.20, 1.53)	37.7 (<0.001)	1.35 (1.19, 1.52)	37.2 (<0.001)
Inner superior	n = 269 (438)	1.00 (0.83, 1.17)	22.7 (<0.001)	0.98 (0.81, 1.15)	22.0 (<0.001)
Inner nasal	n = 269 (438)	1.08 (0.92, 1.24)	25.5 (<0.001)	1.06 (0.90, 1.22)	25.0 (<0.001)
Inner inferior	n = 269 (438)	1.40 (1.22, 1.59)	34.3 (<0.001)	1.38 (1.20, 1.57)	33.7 (<0.001)
Outer temporal	n = 269 (438)	0.70 (0.60, 0.80)	29.9 (<0.001)	0.68 (0.59, 0.78)	29.2 (<0.001)
Outer superior	n = 269 (438)	0.39 (0.29, 0.50)	11.2 (<0.001)	0.37 (0.27, 0.47)	10.3 (<0.001)
Outer nasal	n = 269 (438)	0.45 (0.34, 0.55)	13.2 (<0.001)	0.42 (0.32, 0.52)	12.6 (<0.001)
Outer inferior	n = 269 (438)	0.38 (0.30, 0.47)	14.6 (<0.001)	0.37 (0.29, 0.46)	14.0 (<0.001)
Spectralis RNFL (µm)					
Global	n = 269 (438)	0.28 (0.22, 0.33)	17.9 (<0.001)	0.29 (0.23, 0.34)	19.2 (<0.001)
Inner ring	n = 269 (438)	0.10 (0.05, 0.15)	3.6 (<0.001)	0.11 (0.06, 0.16)	4.2 (<0.001)
Outer ring	n = 269 (438)	0.45 (0.38, 0.52)	26.2 (<0.001)	0.46 (0.39, 0.53)	27.4 (<0.001)
Inner temporal	n = 269 (438)	0.02 (-0.01, 0.06)	0.4 (0.226)	0.03 (-0.01, 0.07)	0.6 (0.114)
Inner superior	n = 269 (438)	0.11 (0.05, 0.18)	2.5 (<0.001)	0.12 (0.06, 0.19)	3.1 (<0.001)
Inner nasal	n = 269 (438)	0.05 (-0.02, 0.11)	0.5 (0.159)	0.06 (-0.01, 0.12)	0.7 (0.088)
Inner inferior	n = 269 (438)	0.21 (0.15, 0.27)	10.0 (<0.001)	0.22 (0.16, 0.28)	10.6 (<0.001)
Outer temporal	n = 269 (438)	0.06 (0.03, 0.10)	3.6 (<0.001)	0.07 (0.04, 0.10)	4.7 (<0.001)
Outer superior	n = 269 (438)	0.52 (0.43, 0.62)	20.8 (<0.001)	0.53 (0.44, 0.63)	21.7 (<0.001)
Outer nasal	n = 269 (438)	0.64 (0.53, 0.74)	21.2 (<0.001)	0.65 (0.55, 0.76)	22.2 (<0.001)
Outer inferior	n = 269 (438)	0.58 (0.48, 0.68)	23.8 (<0.001)	0.59 (0.50, 0.69)	24.5 (<0.001)
Spectralis GCC (µm)					
Global	n = 269 (438)	1.13 (0.99, 1.28)	33.4 (<0.001)	1.13 (0.98, 1.27)	32.9 (<0.001)
Inner ring	n = 269 (438)	1.34 (1.17, 1.50)	33.4 (<0.001)	1.33 (1.16, 1.50)	32.8 (<0.001)
Outer ring	n = 269 (438)	0.93 (0.80, 1.06)	28.8 (<0.001)	0.93 (0.79, 1.06)	28.3 (<0.001)
Inner temporal	n = 269 (438)	1.39 (1.21, 1.56)	36.7 (<0.001)	1.38 (1.21, 1.56)	36.3 (<0.001)
Inner superior	n = 269 (438)	1.12 (0.92, 1.33)	19.8 (<0.001)	1.11 (0.90, 1.32)	19.2 (<0.001)
Inner nasal	n = 269 (438)	1.14 (0.95, 1.34)	21.0 (<0.001)	1.13 (0.94, 1.33)	20.5 (<0.001)
Inner inferior	n = 269 (438)	1.62 (1.40, 1.84)	32.2 (<0.001)	1.61 (1.38, 1.83)	31.6 (<0.001)
Outer temporal	n = 269 (438)	0.76 (0.64, 0.87)	27.2 (<0.001)	0.75 (0.64, 0.87)	26.6 (<0.001)
Outer superior	n = 269 (438)	0.92 (0.74, 1.09)	19.5 (<0.001)	0.91 (0.73, 1.08)	19.0 (<0.001)
Outer nasal	n = 269 (438)	1.08 (0.91, 1.26)	22.9 (<0.001)	1.08 (0.91, 1.25)	22.4 (<0.001)
Outer inferior	n = 269 (438)	0.97 (0.80, 1.13)	23.0 (<0.001)	0.97 (0.80, 1.13)	22.7 (<0.001)
Avanti GCC (µm)					
Whole image	n = 213 (329)	1.17 (0.99, 1.35)	30.7 (<0.001)	1.17 (0.99, 1.34)	30.5 (<0.001)
Parafovea	n = 213 (329)	1.26 (1.07, 1.45)	31.3 (<0.001)	1.26 (1.07, 1.44)	31.1 (<0.001)
Temporal	n = 213 (329)	1.36 (1.17, 1.56)	36.1 (<0.001)	1.36 (1.16, 1.55)	35.8 (<0.001)
Superior	n = 213 (329)	1.08 (0.85, 1.30)	18.8 (<0.001)	1.07 (0.84, 1.30)	18.6 (<0.001)
Nasal	n = 213 (329)	1.05 (0.84, 1.25)	19.6 (<0.001)	1.04 (0.83, 1.25)	19.5 (<0.001)
Inferior	n = 213 (328)	1.57 (1.32, 1.82)	31.4 (<0.001)	1.56 (1.31, 1.81)	31.2 (<0.001)
Avanti Vessel Density (%)					
Whole image	n = 213 (329)	0.42 (0.34, 0.49)	28.9 (<0.001)	0.41 (0.34, 0.47)	29.6 (<0.001)
Parafovea	n = 213 (329)	0.44 (0.37, 0.51)	28.9 (<0.001)	0.43 (0.36, 0.50)	29.8 (<0.001)
Temporal	n = 213 (329)	0.48 (0.41, 0.56)	33.3 (<0.001)	0.48 (0.40, 0.55)	33.5 (<0.001)
Superior	n = 213 (329)	0.38 (0.29, 0.47)	19.2 (<0.001)	0.37 (0.29, 0.45)	19.7 (<0.001)
Nasal	n = 213 (329)	0.35 (0.26, 0.43)	17.1 (<0.001)	0.34 (0.26, 0.42)	17.2 (<0.001)
Inferior	n = 213 (328)	0.56 (0.47, 0.66)	29.1 (<0.001)	0.55 (0.45, 0.64)	29.7 (<0.001)
Spectralis Choroid (µm)					
Global	N=247 (400)	0.35 (-0.11, 0.80)	0.3 (0.137)	0.25 (-0.19, 0.69)	0.2 (0.262)
Inner Ring	N=247 (400)	0.51 (-0.04, 1.06)	0.5 (0.068)	0.39 (-0.13, 0.92)	0.4 (0.144)
Outer Ring	N=247 (400)	0.31 (-0.14, 0.75)	0.2 (0.177)	0.21 (-0.22, 0.63)	0.2 (0.335)
Inner Temporal	N=247 (400)	0.43 (-0.17, 1.04)	0.4 (0.159)	0.27 (-0.30, 0.85)	0.2 (0.355)
Inner Superior	N=247 (400)	0.67 (0.01, 1.33)	0.7 (0.046)	0.49 (-0.14, 1.12)	0.5 (0.127)
Inner Nasal	N=247 (400)	0.77 (0.10, 1.44)	0.8 (0.025)	0.59 (-0.05, 1.22)	0.6 (0.071)
Inner Inferior	N=247 (400)	0.48 (-0.14, 1.10)	0.4 (0.130)	0.33 (-0.26, 0.93)	0.2 (0.274)
Outer Temporal	N=247 (400)	0.40 (-0.09, 0.88)	0.5 (0.108)	0.25 (-0.20, 0.71)	0.3 (0.281)
Outer Superior	N=247 (400)	0.27 (-0.33, 0.88)	0.1 (0.376)	0.12 (-0.46, 0.69)	0.0 (0.687)
Outer Nasal	N=247 (400)	0.34 (-0.20, 0.87)	0.2 (0.217)	0.18 (-0.32, 0.69)	0.1 (0.477)
Outer Inferior	N=247 (400)	0.46 (-0.11, 1.02)	0.4 (0.118)	0.32 (-0.23, 0.86)	0.2 (0.253)

Supplemental Table 3. Ocular characteristics associations with Visual Field mean deviation
*Linear mixed models slope estimates (with 95% confidence intervals) from univariable and multivariable models adjusted for age and axial length.
^R^2 reported as a percentage
Abbreviations: GCC; Ganglion cell complex, GCIPL; Ganglion cell inner plexiform layer, RNFL; Retinal nerve fiber layer

Publikation V

Rezapour J, Walker E, Belghith A, Bowd C, Fazio MA, Jiravarnsirikul A, Hyman L, Jonas JB, Weinreb RN, Zangwill LM; *Diagnostic accuracy of optic nerve head and macula OCT parameters for detecting glaucoma in eyes with and without high axial myopia;* American Journal of Ophthalmology; 2024; Oct;266:77-91. doi: 10.1016/j.ajo.2024.04.022. Epub 2024 May 15. PMID: 38754801.

Diagnostic Accuracy of Optic Nerve Head and Macula OCT Parameters for Detecting Glaucoma in Eyes With and Without High Axial Myopia

JASMIN REZAPOUR, EVAN WALKER, AKRAM BELGHITH, CHRISTOPHER BOWD, MASSIMO A. FAZIO, ANUWAT JIRAVARNSIRIKUL, LESLIE HYMAN, JOST B. JONAS, ROBERT N. WEINREB, AND LINDA M. ZANGWILL

• PURPOSE: To characterize structural differences and assess the diagnostic accuracy of optic nerve head (ONH) and macula optical coherence tomography (OCT) parameters to detect glaucoma in eyes with and without high axial myopia.

• DESIGN: Cross-sectional study.

• METHODS: Three hundred sixty-eight glaucoma and 411 healthy eyes with no axial myopia, 393 glaucoma and 271 healthy eyes with mild axial myopia and 124 glaucoma and 85 healthy eyes with high axial myopia were included. Global and sectoral peripapillary retinal nerve fiber layer thickness (pRNFLT), Bruch's membrane opening minimum rim width (BMO-MRW), ganglion cell inner plexiform layer thickness (GCIPLT), and macula RNFLT (mRNFLT) were compared and the diagnostic accuracy for glaucoma detection was evaluated using the adjusted area under the receiver operating characteristic curve (AUC).

• RESULTS: Diagnostic accuracy for ONH and macula parameters to detect glaucoma was generally high and differed by myopia group. For ONH parameters the diagnostic accuracy was highest for global (AUC = 0.95) and inferotemporal (AUC = 0.91) pRNFLT for high myopes and global BMO-MRW for nonmyopes (AUC = 1.0) and mild myopes (AUC = 0.97). For macula parameters, the diagnostic accuracy was higher in high myopes with 6 of the 11 GCIPLT global/sectors having adjusted AUCs > 0.90 compared to nonhigh myopes with no AUCs > 0.90. In all myopia groups, mRNFLT had lower AUCs than GCIPLT.

• CONCLUSIONS: The diagnostic accuracy for pRNFL and GCIPL was high for high axial myopic eyes and shows promise for glaucoma detection in high myopes. Further analysis is needed to determine whether the high diagnostic accuracy can be confirmed in other populations. (Am J Ophthalmol 2024;266: 77–91. © 2024 Elsevier Inc. All rights are reserved, including those for text and data mining, AI training, and similar technologies.)

AJO.com Supplemental Material available at AJO.com.
Accepted for publication April 22, 2024.

From the Department of Ophthalmology (J.R.), University Medical Center of the Johannes Gutenberg University Mainz, Mainz, Germany; Viterbi Family Department of Ophthalmology (J.R., E.W., A.B., C.B., A.J., R.N.W., L.M.Z.), Hamilton Glaucoma Center, Shiley Eye Institute, UC San Diego, La Jolla, California, USA; Department of Ophthalmology and Vision Science (M.A.F.), The Heersink School of Medicine, The University of Alabama at Birmingham, Birmingham, Alabama, USA; Department of Biomedical Engineering (M.A.F.), School of Engineering, The University of Alabama at Birmingham, Birmingham, Alabama, USA; Department of Ophthalmology (A.J.), Faculty of Medicine Siriraj Hospital, Mahidol University, Bangkok, Thailand; Wills Eye Hospital, Thomas Jefferson University (L.H.), Philadelphia, Pennsylvania, USA; Department of Ophthalmology, Medical Faculty Mannheim (J.B.J.), Heidelberg University, Mannheim, Germany; Institute of Molecular and Clinical Ophthalmology Basel (J.B.J.), Basel, Switzerland

Inquiries to Linda M. Zangwill, Department of Ophthalmology, University of California San Diego, La Jolla, CA; e-mail: lzangwill@health.ucsd.edu

INTRODUCTION

Myopia is projected to affect approximately 50% of the world's population by 2050.[1] The dramatically increasing prevalence is of concern, as glaucoma is 2 to 3 times more prevalent in myopic eyes.[2,3] The glaucoma prevalence in highly myopic eyes is even 5 to 6 times higher than in nonhigh myopes.[4] The myopic eye is not only one of the fastest growing phenotypes in open-angle glaucoma (OAG) management, but with their characteristic tilted discs, large parapapillary zones, and other morphologic changes in the peripapillary region, myopic eyes are among the most challenging to correctly diagnose with the disease based on clinical optic nerve head (ONH) evaluation.[5-8] Therefore, it is not surprising that OAG is relatively often over-diagnosed in myopic eyes.[9,10]

Optical coherence tomography (OCT) based measurements of the optic nerve head (ONH) have become more and more important in the past decades in discriminating healthy and glaucoma eyes. However, there is concern that the diagnostic accuracy of OCT-based ONH measurements such as the peripapillary retinal nerve fiber thickness (pRN-

0002-9394/$36.00
https://doi.org/10.1016/j.ajo.2024.04.022

FLT) and Bruch's membrane opening minimum rim width (BMO-MRW) is reduced due to segmentation failures and a variety of different anatomic configurations of the ONH in highly myopic eyes which are typically poorly represented in the OCT devices' normative databases.[11,12] The ONH appearance such as more "tilted" discs and morphologic changes in the peripapillary region might in part explain the challenges in interpreting OCT-based imaging of the ONH and challenges in clinical optic disc evaluation to detect glaucoma in myopic eyes.

In view of the myopia-related changes in ONH morphology, macular measurements could be a useful tool to diagnose glaucoma, as the fovea contains approximately 50% of the retinal ganglion cells.[13] Previous studies have shown that macula parameters, such as the ganglion cell inner plexiform layer thickness (GCIPLT) can be used for detecting glaucoma.[14] However, little information has been available on how the topographic distribution of macular retinal layers is affected by axial elongation, especially in eyes with axial lengths of more than 26 mm. Regional variations in GCIPLT or macula retinal nerve fiber layer thickness (mRNFLT) also can have an impact on the evaluation of glaucoma in highly myopic eyes.[15] Furthermore, myopic eyes are typically not included in instruments' normative ONH or macula databases, which can result in reduced diagnostic accuracy of glaucoma detection in myopic, and in particular in highly myopic eyes.[16-18]

The purpose of this study is to characterize the local distribution of OCT-based measurements of the ONH (pRNFLT and BMO-MRW) and macula (GCIPLT and mRNFLT), in healthy and glaucoma eyes with mild axial myopia, high axial myopia and without axial myopia. Furthermore, we aimed to assess the diagnostic accuracy of ONH and macula parameters to detect glaucoma in high axial myopic eyes. The results of this study may elucidate which parameters are best for detecting and monitoring glaucoma in the rapidly growing population of myopic individuals.

METHODS

• **STUDY POPULATION:** This study included all patients enrolled in the University of California, San Diego Diagnostic Innovations in Glaucoma Study (DIGS; clinicaltrials.gov identifier NCT00221897) with available axial length measurements, visual field (VF) measurements and good quality ONH and macula OCT scans. The study was approved by the institutional review board of the University of California San Diego and according to the tenets of the Declaration of Helsinki, written informed consent was obtained from all participants. A detailed study protocol was published previously.[19] All participants underwent a complete ophthalmologic examination including assessment of refractive error, visual acuity, axial length measurement (IOLMaster, Carl Zeiss Meditec, Dublin, CA), VF testing, simultaneous stereophotography of the optic disc and macula, and ONH and macular OCT imaging. Participants were required to be ≥18 years old with best-corrected visual acuity ≥20/40 and open anterior chamber angles at baseline.

• **GLAUCOMA DEFINITION:** VF testing was performed using the standard Humphrey Field Analyzer 24-2 Swedish interactive thresholding algorithm [SITA] and the Visual Field Assessment Center (VisFACT) Reading Center completed the quality control according to standard protocols.

Glaucomatous VF damage was defined as two repeatable and reliable VF tests (rate of fixation losses and false negatives and false positives responses of <33%) with a glaucoma hemifield test (GHT) outside normal limits and/or a pattern standard deviation (PSD) with a *P*-value of <.05 with a similar defect on consecutive abnormal tests.[19] Primary open-angle glaucoma was defined as the presence of glaucomatous ONH damage and corresponding glaucomatous VF loss in open-angle eyes. Stereophotographs were assessed by two trained observers and optic disc damage was defined as focal or diffuse narrowing of the neuroretinal rim, and/or detection of RNFL defects characteristic of glaucoma. Because of morphologic ONH changes due to axial elongation stereophotographs of highly myopic eyes were graded by two experts (J.R. and C.B.) with extensive expertise after training with a senior consultant (JBJ). Diagnosis was defined by consensus between the two graders and adjudication by the senior consultant in case of disagreement.[20]

• **MYOPIA DEFINITION:** Because axial elongation can lead to several morphological changes of the optic disc and the fundus but is not necessarily represented by the refractive status, we defined myopia by axial length.[21-23] Furthermore, cataract- or refractive surgery can result in a change of refractive error in eyes that are axially elongated but do no longer appear to be (highly) myopic as defined by refractive error. We therefore classified eyes by axial length into the following groups:

- No axial myopia: axial length ≤ 24.0 mm
- Mild axial myopia: 24.0 mm < axial length ≤ 26.0 mm
- High axial myopia: axial length > 26.0 mm

• **OPTICAL COHERENCE TOMOGRAPHY IMAGING:** OCT imaging of the ONH and macula was performed with the Spectralis OCT (version 6.10; Heidelberg Engineering Inc, Heidelberg, Germany). Details of this instrument have been previously described.[24] 24 high-resolution ONH radial scans and 3 RNFL circle scans centered on the ONH were obtained using the ONH radical circle (ONHRC) scan from the Glaucoma Module Premier Edition software (version 6.10; Heidelberg Engineering Inc. Heidelberg, Germany). The Spectralis standard software was used

TABLE 1. Patient and Eye Characteristics Stratified by Diagnosis in the No Myopia, Mild Myopia, and High Myopia Group

	No Myopia			Mild Myopia			High Myopia		
	Healthy $n = 214$ (411)	Glaucoma $n = 213$ (368)	*P*-value	Healthy $n = 142$ (271)	Glaucoma $n = 225$ (393)	*P*-value	Healthy $n = 45$ (85)	Glaucoma $n = 76$ (124)	*P*-value
Age	52.7 (50.5, 54.9)	74.7 (73.1, 76.3)	<.001	51.4 (48.7, 54.2)	71.6 (70.0, 73.2)	<.001	49.0 (43.6, 54.5)	70.6 (68.3, 72.9)	<.001
Sex n (%)									
Female	157 (73.4%)	143 (67.1%)	.170	73 (51.4%)	100 (44.4%)	.200	22 (48.9%)	33 (43.4%)	.577
Male	57 (26.6%)	70 (32.9%)		69 (48.6%)	125 (55.6%)		23 (51.1%)	43 (56.6%)	
Race n (%)									
African descent	93 (43.5%)	92 (43.2%)	.095	43 (30.3%)	90 (40.0%)	.066	6 (13.3%)	11 (14.5%)	.009
Asian descent	4 (1.9%)	9 (4.2%)		3 (2.1%)	10 (4.4%)		13 (28.9%)	15 (19.7%)	
European descent	110 (51.4%)	111 (52.1%)		92 (64.8%)	123 (54.7%)		18 (40.0%)	48 (63.2%)	
Other / unknown	7 (3.3%)	1 (0.5%)		4 (2.8%)	2 (0.9%)		8 (17.8%)	2 (2.6%)	
Ethnicity n (%)									
Hispanic or Latino	10 (4.7%)	4 (1.9%)	.035	8 (5.6%)	5 (2.2%)	<.001	6 (13.3%)	2 (2.6%)	.048
Not Hispanic or Latino	172 (80.4%)	190 (89.2%)		118 (83.1%)	214 (95.1%)		35 (77.8%)	70 (92.1%)	
Unknown / Not Reported	32 (15.0%)	19 (8.9%)		16 (11.3%)	6 (2.7%)		4 (8.9%)	4 (5.3%)	
Axial length (mm)	23.2 (23.1, 23.3)	23.3 (23.3, 23.4)	.003	24.7 (24.6, 24.7)	24.8 (24.7, 24.8)	.081	26.8 (26.5, 27.1)	26.4 (26.2, 26.7)	.068
Spherical equivalent (D)	-0.22 (-0.39, -0.05)	-0.25 (-0.42, -0.08)	.775	-1.78 (-2.07, -1.49)	-1.37 (-1.60, -1.14)	.033	-6.48 (-7.49, -5.47)	-4.56 (-5.34, -3.77)	.004
Visual field MD (dB)	-0.16 (-0.76, 0.44)	-6.56 (-7.16, -5.95)	<.001	-0.11 (-0.94, 0.72)	-7.68 (-8.35, -7.01)	<.001	-1.30 (-2.91, 0.31)	-8.34 (-9.60, -7.07)	<.001
IOP (mmHg)	14.7 (14.3, 15.2)	14.6 (14.1, 15.1)	.719	14.4 (13.6, 15.2)	14.8 (14.2, 15.4)	.448	15.1 (13.9, 16.2)	13.2 (12.4, 14.1)	.013
BMO area (mm^2)	1.93 (1.81, 2.05)	2.11 (2.02, 2.19)	.024	1.96 (1.81, 2.11)	2.12 (2.03, 2.20)	.069	2.28 (2.04, 2.52)	2.14 (1.92, 2.36)	.399
Image quality score	29.2 (28.8, 29.7)	27.6 (27.1, 28.1)	<.001	29.5 (28.9, 30.0)	27.2 (26.8, 27.7)	<.001	28.7 (27.7, 29.7)	26.9 (26.2, 27.7)	.005
Cataract/refractive surgery n (%)									
No	392 (95.4%)	196 (53.3%)	<.001	253 (93.4%)	205 (52.2%)	<.001	78 (91.8%)	66 (53.2%)	<.001
Yes	19 (4.6%)	172 (46.7%)		18 (6.6%)	188 (47.8%)		7 (8.2%)	58 (46.8%)	

All values are means (95% CI) unless otherwise indicated. BMO = Bruch's membrane opening; IOP = intraocular pressure; MD = mean deviation.

Significance is determined by ANOVA / *t* tests and Fisher's exact test for patient-level continuous and categorical variables, respectively, and linear mixed models for eye-level variables.

to calculate BMO-MRW and RNFLT from ONHRC scans. The BMO-MRW was defined as the shortest distance from the BMO point to the internal limiting membrane (ILM)[25] and was automatically computed by the instrument software for each radial B-scan and then averaged for all 24 B-scans. For macula measurements, macula horizontal posterior pole (p-Pole) scans typically covering an area of 30° × 25° were obtained. GCIPLT and mRNFLT measurements were generated from each retinal layer from the central 1-, 3-, and 6-mm circles as inner rings (1- and 3-mm circle) and outer rings (3- and 6-mm circle)[26] according to the Early Treatment Diabetic Retinopathy Study defined sectors (temporal, superior, nasal, and inferior).

To avoid low quality images and segmentation failures that could bias study results, all images were reviewed by the Imaging Data Evaluation and Analysis (IDEA) Reading Center for image quality (centering, focus) and accurate segmentation of the BMO in the radial B-scans and accurate ILM, RNFL and Bruch's membrane (BM) segmentation in the circle scans. Macula p-Pole scans were reviewed for correct and accurate segmentation of the mRNFL, and GCIPL. Automated segmentations were manually cor-

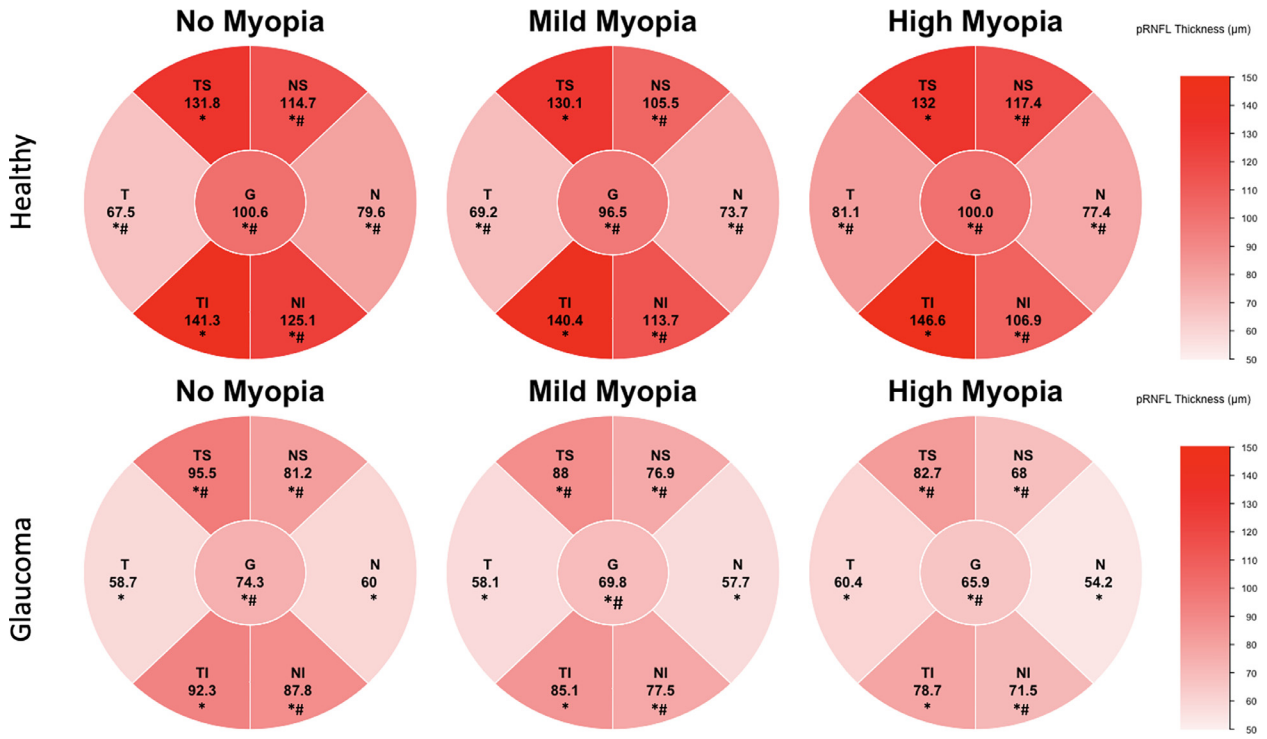

FIGURE 1. Global and sectoral distribution of peripapillary retinal nerve fiber layer thickness by diagnosis in the no myopia, mild myopia, and high myopia group. The top row presents global and sectoral peripapillary retinal nerve fiber layer thickness (pRNFLT) distribution (in µm) in the three myopia groups in healthy eyes (from left to right: no myopia, mild myopia, high myopia). The bottom row presents global and sectoral pRNFLT distribution (in µm) in the three myopia groups in glaucoma eyes (from left to right: no myopia, mild myopia, high myopia). pRNFLT values are presented as absolute values and are color coded according to the diagram on the right. * states statistical significance between healthy and glaucoma group and # states statistical significance between myopia groups. G = global; I = inferior; IR = inner ring; N = nasal; NI = inferonasal; NS = superonasal; OR = outer ring; pRNFLT = peripapillary retinal nerve fiber layer thickness; S = superior; T = temporal; TI = inferotemporal; TS = superotemporal.

rected if needed, according to standard IDEA Reading Center protocols.[19] Segmentation failures that could not be manually corrected or poor quality images (quality score <15) were excluded.

• **STATISTICAL ANALYSIS:** Patient and eye-level characteristics were presented as mean (95% confidence interval [CI]) and count (percentage) for continuous and categorical variables, respectively. Patients were stratified by diagnosis and myopia status, and demographic and clinical characteristics were compared between cohorts with statistical significance determined by ANOVA for patient-level continuous variables and chi-squared and Fisher's exact test for patient-level categorical variables. Linear mixed-effects models were applied for eye-level comparisons and included a random intercept to account for within-subject correlation between eyes. Models were adjusted for age, VF mean deviation (VFMD), and image quality, where applicable. The area under the receiver operating characteristic curve (AUC) was used to evaluate the diagnostic accuracies of ONH parameters (BMO-MRW and pRNFLT) and macula parameters (GCIPLT and mRNFLT) and adjusted for age, VFMD, and image quality.

Sensitivities at fixed specificities are reported along with the optimized sensitivities and specificities. Optimized sensitivities and specificities are defined as the highest sensitivity and specificity combinations, per optic nerve head and macula parameter. Differences in AUC were assessed using bootstrap testing, where bootstrap resampling ($n = 2000$) was clustered at the subject-level and sampled with replacement. A subanalysis was performed to evaluate proportion of eyes with pRNFLT within normal limits, outside normal limits, and borderline cases across myopia status separately for healthy and glaucoma eyes. *P*-values less than .05 were considered statistically significant. All statistical analyses were performed using the R programming language for statistical computing, version 4.2.3 (R Core Team, 2022; Vienna, Austria).[27]

RESULTS

• **STUDY POPULATION:** Eight-hundred-eighty-five glaucomatous eyes of 514 patients were included with 368 eyes (213 patients) in the nonmyopic group, 393 eyes (225 pa-

TABLE 2. Diagnostic Accuracy of Peripapillary Retinal Nerve Fiber Layer Thickness for Diagnosing Glaucoma in Different Myopia Groups

		Adjusted AUC	Sensitivity at Fixed Specificities		Optimized Sensitivity[a]	Optimized Specificity[b]
			85%. Specificity	95%. Specificity		
pRNFL Global	**All subjects**	0.90	0.75	0.59	0.86	0.76
	No myopia	0.90	0.77	0.58	0.85	0.81
	Mild myopia	0.85	0.70	0.62	0.62	0.95
	High myopia	0.95	0.94	0.73	0.91	0.88
pRNFL Temporal	**All subjects**	0.66	0.37	0.25	0.51	0.76
	No myopia	0.64	0.33	0.20	0.5	0.74
	Mild myopia	0.63	0.38	0.30	0.43	0.83
	High myopia	0.74	0.52	0.30	0.65	0.75
pRNFL TS	**All subjects**	0.81	0.57	0.36	0.78	0.70
	No myopia	0.80	0.57	0.39	0.77	0.69
	Mild myopia	0.83	0.63	0.43	0.83	0.69
	High myopia	0.79	0.47	0.45	0.83	0.62
pRNFL TI	**All subjects**	0.84	0.66	0.53	0.72	0.82
	No myopia	0.83	0.60	0.47	0.82	0.71
	Mild myopia	0.82	0.68	0.54	0.68	0.87
	High myopia	0.91	0.87	0.72	0.87	0.85
pRNFL Nasal	**All subjects**	0.78	0.54	0.31	0.61	0.82
	No myopia	0.79	0.59	0.26	0.64	0.81
	Mild myopia	0.72	0.50	0.27	0.53	0.84
	High myopia	0.82	0.63	0.51	0.69	0.82
pRNFL NS	**All subjects**	0.82	0.62	0.38	0.61	0.87
	No myopia	0.83	0.63	0.44	0.59	0.91
	Mild myopia	0.77	0.54	0.36	0.76	0.64
	High myopia	0.89	0.71	0.50	0.88	0.74
pRNFL NI	**All subjects**	0.81	0.56	0.43	0.72	0.73
	No myopia	0.82	0.58	0.37	0.79	0.71
	Mild myopia	0.80	0.56	0.46	0.71	0.76
	High myopia	0.84	0.73	0.45	0.73	0.85

Adjusted area under the receiver operating characteristic curve (AUC) with sensitivities at 85%, and 95% specificity.
NI = inferonasal; NS = superonasal; pRNFL = peripapillary retinal nerve fiber layer; TI = inferotemporal; TS = superotemporal.
AUC is adjusted for visual field mean deviation, age, and image quality score.
[a]Highest sensitivity per optic nerve head parameter.
[b]Highest specificity per optic nerve head parameter.

tients) in the mild myopic group, and 124 eyes (76 patients) in the highly myopic group. In addition, 767 healthy eyes of 401 subjects were included with 411 eyes (214 patients) in the nonmyopic group, 271 eyes (142 patients) in the mild myopic group, and 85 eyes (45 patients) in the highly myopic group (Table 1). There was no significant difference in axial length between the healthy and glaucoma eyes with high myopia (mean [95% CI] AL: (26.8 mm [26.5, 27.1] and 26.4mm [26.2, 26.7], $P = .068$)

In each of the 3 myopia groups, compared to the glaucoma patients, the healthy participants were significantly younger (all $P < .001$), had significantly better image quality scores (all $P \leq .005$) and fewer cataract/refractive surgeries (all $P < .001$). BMO area tended to be larger in glaucoma eyes compared to healthy eyes in the no myopia (mean difference glaucoma eyes – healthy eyes: 0.18 mm^2, $P = .024$) and mild myopia group (mean difference glaucoma eyes – healthy eyes: 0.16 mm2 ($P = .069$). In the high myopia group, BMO area tended to be higher in the healthy eyes (mean difference glaucoma eyes – healthy eyes: -0.16 mm^2 but did not reach statistical significance ($P = .399$). As expected, mean VFMD was significantly worse in glaucoma compared to healthy eyes. VFMD also tended to be worse in high myopia compared to no myopia and mild myopia in both the healthy (mean (95% CI) VFMD: -1.30 (−2.91, 0.31) dB, −0.16 (−0.76, 0.44) dB, and −0.11 (−0.94, 0.72) dB respectively, $P < .001$)) and glaucoma eyes (mean (95% CI) VFMD: −8.34 (−9.60, −7.02) dB, −6.56 (−7.16, −5.95) dB, and −7.68 (−8.35, −7.01) dB, respectively, $P < .001$). (Table 1).

TABLE 3. Diagnostic Accuracy of Bruch's Membrane Opening Minimum Rim Width for Diagnosing Glaucoma in Different Myopia Groups

		Adjusted AUC	Sensitivity at Fixed Specificities		Optimized Sensitivity[a]	Optimized Specificity[b]
			85% Specificity	95% Specificity		
BMO-MRW Global	**All subjects**	0.94	0.93	0.86	0.91	0.87
	No myopia	1.00	1.00	0.85	1.00	0.96
	Mild myopia	0.97	0.93	0.62	0.93	0.95
	High myopia	0.89	0.82	0.91	0.82	0.91
BMO-MRW Temporal	**All subjects**	0.87	0.84	0.51	0.84	0.86
	No myopia	0.91	0.90	0.5	0.98	0.84
	Mild myopia	0.88	0.90	0.43	0.90	0.89
	High myopia	0.83	0.76	0.65	0.74	0.91
BMO-MRW TS	**All subjects**	0.89	0.76	0.78	0.93	0.74
	No myopia	0.97	1.00	0.77	1.00	0.96
	Mild myopia	0.96	0.97	0.83	0.97	0.89
	High myopia	0.81	0.73	0.83	0.72	0.88
BMO-MRW TI	**All subjects**	0.94	0.93	0.72	0.93	0.93
	No myopia	1.00	1.00	0.82	1.00	0.98
	Mild myopia	0.97	0.97	0.68	0.95	0.98
	High myopia	0.88	0.87	0.87	0.87	0.93
BMO-MRW Nasal	**All subjects**	0.90	0.73	0.61	0.69	0.97
	No myopia	0.98	1.00	0.64	1.00	0.98
	Mild myopia	0.91	0.87	0.53	0.86	0.86
	High myopia	0.89	0.72	0.69	0.72	0.97
BMO-MRW NS	**All subjects**	0.93	0.89	0.61	0.89	0.87
	No myopia	0.99	1.00	0.59	0.91	0.99
	Mild myopia	0.96	0.94	0.76	0.93	0.92
	High myopia	0.87	0.79	0.88	0.79	0.89
BMO-MRW NI	**All subjects**	0.91	0.78	0.72	0.91	0.81
	No myopia	1.00	1.00	0.79	1.00	0.96
	Mild myopia	0.92	0.94	0.71	0.92	0.87
	High myopia	0.86	0.84	0.73	0.79	0.96

Adjusted area under the receiver operating characteristic curve (AUC) with sensitivities at 85%, and 95% specificity.
AUC is adjusted for visual field mean deviation, age, and image quality score.
NI = inferonasal; NS = superonasal; pRNFL = peripapillary retinal nerve fiber layer; TI = inferotemporal; TS = superotemporal.
[a]Highest sensitivity per optic nerve head parameter.
[b]Highest specificity per optic nerve head parameter.

• **OPTIC NERVE HEAD AND MACULA PARAMETERS BY MYOPIA GROUP:** In each of the 3 myopia groups, all global and sectoral pRNFLT and BMO-MRW values were significantly higher in healthy compared to glaucoma eyes (all $P \leq .01$, Figure 1 and 2, Supplemental Table 1). All global and sectoral GCIPLT values were also significantly thicker in healthy eyes compared to glaucoma eyes in the 3 myopia groups (all $P \leq .013$), except for the nasal sector where statistical significance was not reached in eyes with no myopia and mild myopia ($P \geq .211$, Figure 3, Supplemental Table 2). Moreover, regardless of myopia group and diagnosis, all eyes tended to have thickest GCIPL in the inner superior sector and thinnest GCIPL in the outer inferior sector. Global mRNFLT was significantly thicker in all 3 myopia groups in healthy eyes compared to glaucoma eyes ($P < .001$ Figure 4, Supplemental Table 2). In the high myopia group, all sectoral mRNFLT values were significantly thicker in the healthy compared to glaucoma eyes. In the no myopia and mild myopia group, all sectoral mRNFLT values were also significantly thicker in the healthy compared to glaucoma eyes with the exception of the inner ring mRNFLT (specifically the inner nasal in the no myopia and the inner temporal in the mild myopia group).

• **DIAGNOSTIC ACCURACY OF ONH PARAMETERS:** The diagnostic accuracy to detect glaucoma varied by specific ONH parameter, sector, and myopia group (Tables 2 and 3, Figure 5). Specifically, in high myopes, the diagnostic accuracy adjusted for baseline VFMD, age, and scan quality was highest for global pRNFLT (adjusted AUC = 0.95), and in

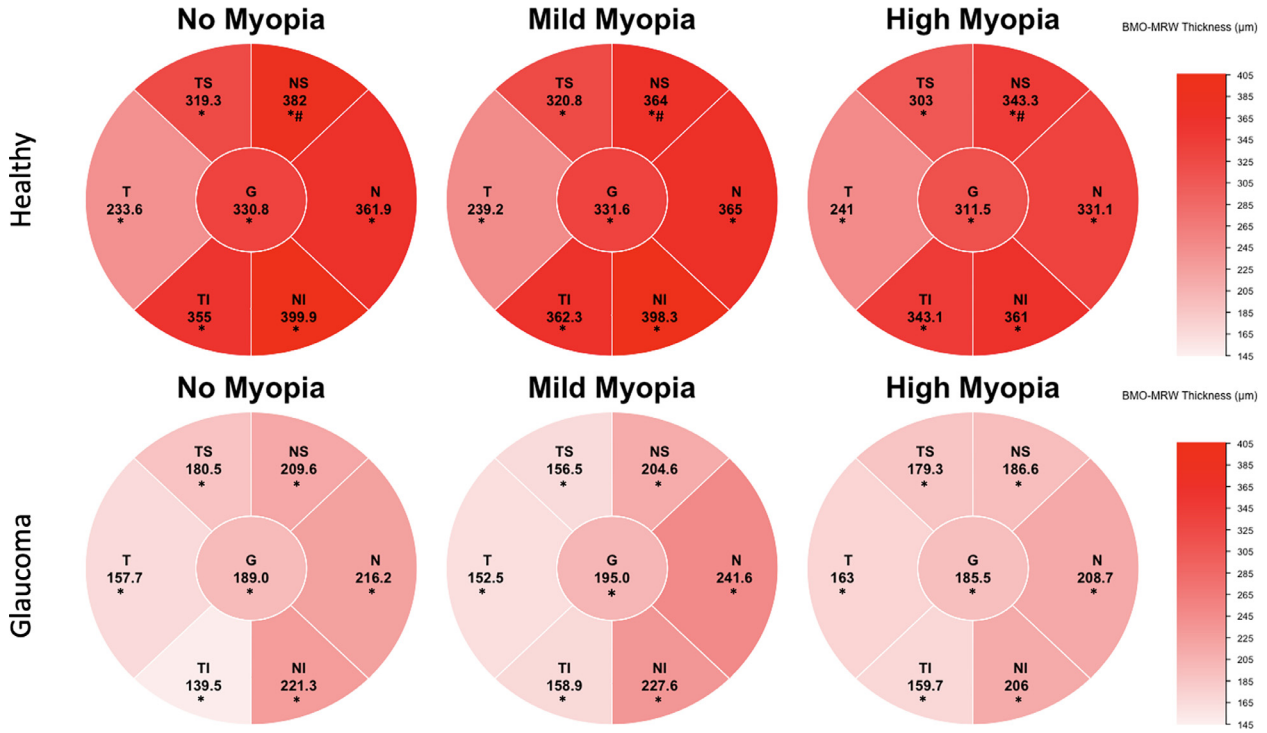

FIGURE 2. Global and sectoral distribution of Bruch's membrane opening minimum rim width by diagnosis in the no myopia, mild myopia, and high myopia group. The top row presents global and sectoral distribution of Bruch's membrane opening minimum rim width (BMO-MRW) (in µm) in the three myopia groups in healthy eyes (from left to right: no myopia, mild myopia, high myopia). The bottom row presents global and sectoral BMO-MRW distribution (in µm) in the three myopia groups in glaucoma eyes (from left to right: no myopia, mild myopia, high myopia). BMO-MRW values are presented as absolute values and are color coded according to the diagram on the right. * states statistical significance between healthy and glaucoma group and # states statistical significance between myopia groups. BMO-MRW = Bruch's membrane opening minimum rim width; G = global; I = inferior; IR = inner ring; N = nasal; NI = inferonasal; NS = superonasal; OR = outer ring; S = superior; T = temporal; TI = inferotemporal; TS = superotemporal.

the infero-temporal sector (adjusted AUC = 0.91) (Supplemental Figure 1A). In contrast, the diagnostic accuracy in eyes without myopia and with mild myopia was highest for global BMO-MRW (adjusted AUC = 1.00 and 0.97, respectively) (Supplemental Figure 1B) but not in eyes with high myopia (adjusted AUC = 0.89) (Table 3).

The diagnostic accuracy of sectoral pRNFLT was highest for high myopic eyes (adjusted AUC ranged from 0.74 to 0.91) followed by nonmyopic eyes and mild myopic eyes (adjusted AUC ranged from 0.64 to 0.83 and from 0.63 to 0.83, respectively) (Table 2, Supplemental Figure 1).

• **DIAGNOSTIC ACCURACY OF MACULA PARAMETERS:** The diagnostic accuracy to detect glaucoma also varied by specific macula parameter, sector, ring, and myopia group (Tables 4 and 5, Figure 5). In general, in each of the myopia groups, the diagnostic accuracy for detecting glaucoma based on the global GCIPLT and sectoral values was higher than the accuracy based on mRNFLT. For example, in high myopic eyes, the diagnostic accuracy for glaucoma detection of global GCIPLT overall and in the inner and outer circles (Supplemental Figure 1C) tended to be higher (adjusted AUC = 0.91, 0.90, 0.91, respectively) than the diagnostic accuracy of global mRNFLT (Supplemental Figure 1D) overall and in the inner and outer circles (adjusted AUC = 0.84, 0.71, and 0.89, respectively). There were however exceptions. With the exception of the outer nasal and outer inferior sectors, sectoral GCIPLT had higher diagnostic accuracy (adjusted AUCs ranged from 0.79 to 0.92) than sectoral mRNFLT (adjusted AUCs ranged from 0.52 to 0.89). In addition, the diagnostic accuracy for detecting glaucoma of global outer ring GCIPLT (Supplemental Figure 1E) was similar to mRNFLT (Supplemental Figure 1F) in each of the myopia groups. Compared to the diagnostic accuracy in high myopic eyes (adjusted AUCs ranged from 0.52 to 0.92), the diagnostic accuracy of GCIPLT and mRNFLT for detecting glaucoma tended to be lower in nonmyopic and mild myopic eyes (adjusted AUCs ranged from 0.59 to 0.83 and from 0.52 to 0.80, (Tables 4 and 5, Supplemental Figures 1C-1F).

The overall diagnostic accuracy of mRNFLT was lower for all eyes compared to other macula and ONH parameters.

TABLE 4. Diagnostic Accuracy of Ganglion Cell Inner Plexiform Layer Thickness for Diagnosing Glaucoma in Different Myopia Groups

		Adjusted AUC	Sensitivity at Fixed Specificities		Optimized Sensitivity[a]	Optimized Specificity[b]
			85% Specificity	95% Specificity		
GCIPL Global	**All subjects**	0.83	0.68	0.56	0.68	0.85
	No myopia	0.83	0.59	0.55	0.55	0.95
	Mild myopia	0.78	0.56	0.52	0.77	0.66
	High myopia	0.91	0.85	0.84	0.82	0.97
GCIPL Inner	**All subjects**	0.81	0.65	0.54	0.65	0.87
	No myopia	0.79	0.58	0.53	0.55	0.93
	Mild myopia	0.77	0.57	0.48	0.56	0.87
	High myopia	0.90	0.84	0.84	0.84	0.95
GCIPL Outer	**All subjects**	0.83	0.66	0.50	0.66	0.85
	No myopia	0.83	0.62	0.46	0.89	0.64
	Mild myopia	0.79	0.56	0.47	0.66	0.76
	High myopia	0.91	0.83	0.80	0.79	0.99
GCIPL Inner T	**All subjects**	0.83	0.67	0.56	0.66	0.89
	No myopia	0.83	0.62	0.54	0.60	0.92
	Mild myopia	0.80	0.59	0.55	0.62	0.83
	High myopia	0.92	0.87	0.87	0.87	0.95
GCIPL Inner S	**All subjects**	0.75	0.56	0.42	0.56	0.86
	No myopia	0.73	0.53	0.46	0.50	0.89
	Mild myopia	0.70	0.46	0.35	0.33	0.99
	High myopia	0.85	0.73	0.68	0.72	0.92
GCIPL Inner N	**All subjects**	0.72	0.50	0.35	0.65	0.76
	No myopia	0.70	0.45	0.33	0.45	0.85
	Mild myopia	0.67	0.37	0.29	0.48	0.78
	High myopia	0.86	0.79	0.63	0.77	0.92
GCIPL Inner I	**All subjects**	0.82	0.67	0.56	0.65	0.88
	No myopia	0.81	0.58	0.54	0.54	0.96
	Mild myopia	0.80	0.60	0.59	0.59	0.96
	High myopia	0.91	0.85	0.79	0.85	0.90
GCIPL Outer T	**All subjects**	0.86	0.68	0.59	0.59	0.96
	No myopia	0.87	0.67	0.55	0.66	0.92
	Mild myopia	0.80	0.60	0.46	0.60	0.85
	High myopia	0.92	0.85	0.76	0.75	0.99
GCIPL Outer S	**All subjects**	0.79	0.63	0.45	0.66	0.83
	No myopia	0.79	0.62	0.41	0.62	0.85
	Mild myopia	0.75	0.49	0.45	0.42	0.99
	High myopia	0.86	0.74	0.69	0.69	0.95
GCIPL Outer N	**All subjects**	0.74	0.48	0.33	0.50	0.84
	No myopia	0.74	0.37	0.25	0.87	0.51
	Mild myopia	0.73	0.45	0.38	0.38	0.96
	High myopia	0.79	0.64	0.62	0.62	0.95
GCIPL Outer I	**All subjects**	0.81	0.63	0.48	0.61	0.88
	No myopia	0.82	0.69	0.35	0.69	0.85
	Mild myopia	0.79	0.57	0.46	0.70	0.78
	High myopia	0.86	0.82	0.68	0.82	0.85

I = inferior; N = nasal; S = superior; T = temporal.

Adjusted area under the receiver operating characteristic curve (AUC) with sensitivities at 85%, and 95% specificity.

AUC is adjusted for visual field mean deviation, age, and image quality score.

[a]Highest sensitivity per macula parameter.

[a]Highest specificity per macula parameter.

TABLE 5. Diagnostic Accuracy of Macular Retinal Nerve Fiber Layer Thickness for Diagnosing Glaucoma in Different Myopia Groups

		Adjusted AUC	Sensitivity at Fixed Specificities		Optimized Sensitivity[a]	Optimized Specificity[b]
			85% Specificity	95% Specificity		
mRNFL Global	**All subjects**	0.78	0.57	0.45	0.48	0.93
	No myopia	0.76	0.46	0.31	0.50	0.83
	Mild myopia	0.74	0.60	0.52	0.58	0.90
	High myopia	0.84	0.71	0.62	0.62	0.95
mRNFL Inner	**All subjects**	0.62	0.36	0.22	0.40	0.83
	No myopia	0.59	0.23	0.21	0.29	0.80
	Mild myopia	0.60	0.35	0.28	0.30	0.94
	High myopia	0.71	0.37	0.35	0.40	0.78
mRNFL Outer	**All subjects**	0.83	0.63	0.50	0.68	0.82
	No myopia	0.81	0.53	0.39	0.50	0.90
	Mild myopia	0.78	0.61	0.55	0.55	0.96
	High myopia	0.89	0.79	0.67	0.79	0.85
mRNFL Inner T	**All subjects**	0.63	0.26	0.12	0.68	0.60
	No myopia	0.68	0.41	0.22	0.55	0.75
	Mild myopia	0.63	0.29	0.14	0.50	0.80
	High myopia	0.52	0.27	0.09	0.27	0.91
mRNFL Inner S	**All subjects**	0.63	0.37	0.26	0.37	0.85
	No myopia	0.61	0.24	0.14	0.44	0.76
	Mild myopia	0.59	0.40	0.30	0.40	0.91
	High myopia	0.68	0.34	0.34	0.60	0.70
mRNFL Inner N	**All subjects**	0.55	0.18	0.18	0.50	0.71
	No myopia	0.51	0.17	0.17	0.17	0.97
	Mild myopia	0.52	0.18	0.11	0.11	0.96
	High myopia	0.66	0.31	0.22	0.63	0.67
mRNFL Inner I	**All subjects**	0.71	0.39	0.31	0.39	0.90
	No myopia	0.68	0.34	0.24	0.24	0.96
	Mild myopia	0.70	0.52	0.42	0.42	0.97
	High myopia	0.75	0.50	0.46	0.44	0.99
mRNFL Outer T	**All subjects**	0.69	0.49	0.25	0.49	0.85
	No myopia	0.66	0.24	0.07	0.66	0.74
	Mild myopia	0.62	0.45	0.27	0.45	0.80
	High myopia	0.79	0.45	0.30	0.45	0.90
mRNFL Outer S	**All subjects**	0.78	0.56	0.44	0.55	0.87
	No myopia	0.77	0.49	0.40	0.40	0.95
	Mild myopia	0.75	0.56	0.48	0.47	0.97
	High myopia	0.80	0.63	0.55	0.63	0.91
mRNFL Outer N	**All subjects**	0.76	0.49	0.36	0.59	0.76
	No myopia	0.73	0.38	0.28	0.50	0.78
	Mild myopia	0.71	0.53	0.45	0.52	0.90
	High myopia	0.82	0.65	0.42	0.65	0.90
mRNFL Outer I	**All subjects**	0.85	0.70	0.64	0.64	0.95
	No myopia	0.81	0.66	0.61	0.61	0.96
	Mild myopia	0.83	0.65	0.62	0.60	0.98
	High myopia	0.92	0.80	0.72	0.80	0.90

Adjusted area under the receiver operating characteristic curve (AUC) with sensitivities at 85%, and 95% specificity.
AUC is adjusted for visual field mean deviation, age, and image quality score.
mRNFL = macular retinal nerve fiber layer; I = inferior; N = nasal; S = superior; T = temporal.
[a]Highest sensitivity per macula parameter.
[b]Highest specificity per macula parameter.

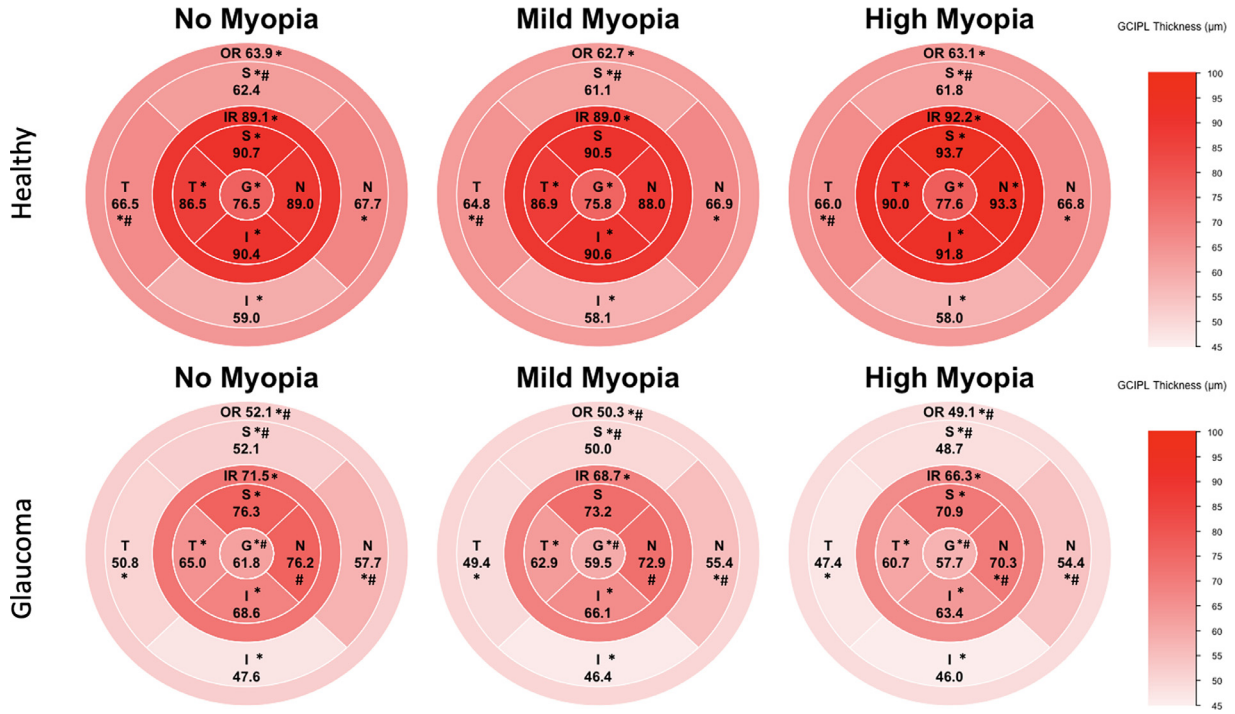

FIGURE 3. Global and sectoral distribution of ganglion cell inner plexiform layer thickness by diagnosis in the no myopia, mild myopia, and high myopia group. The top row presents global and sectoral distribution of ganglion cell inner plexiform layer thickness (GCIPLT) (in µm) in the three myopia groups in healthy eyes (from left to right: no myopia, mild myopia, high myopia). The bottom row presents GCIPLT (in µm) in the three myopia groups in glaucoma eyes (from left to right: no myopia, mild myopia, high myopia). GCIPLT values are presented as absolute values and are color coded according to the diagram on the right. * states statistical significance between healthy and glaucoma group and # states statistical significance between myopia groups. G = global; GCIPLT = ganglion cell inner plexiform layer thickness; I = inferior; IR = inner ring; N = nasal; OR = outer ring; S = superior; T = temporal.

Specifically, global mRNFLT was highest for high myopic eyes (AUC = 0.84) compared to nonmyopic (AUC = 0.76) and mild myopic eyes (AUC = 0.74) (Supplemental Figure 1D). In high myopic eyes the AUCs of mRNFLT vary significantly by sector and range between 0.52 (inner temporal sector) and 0.92 (outer inferior sector) (Supplemental Figure 1F). The AUCs range in nonmyopic eyes between 0.51 and 0.81 and between 0.52 and 0.83 in mild myopic eyes. (Table 5). All AUCs were adjusted for age, VFMD and image quality.

DISCUSSION

The current study characterized topographic differences in ONH and macula parameters and found that the diagnostic accuracy for detecting glaucoma in nonaxial myopic eyes, mild axial myopic eyes, and high axial myopic eyes varied by myopia status. As expected, we found that global ONH pRNFLT, BMO-MRW, mRNFLT, and GCIPLT values were significantly lower in glaucoma compared to healthy eyes within each myopia group. Most importantly, we found specific ONH and macula parameters that had good diagnostic accuracy for glaucoma detection in each of the myopic groups (adjusted AUC > 0.85 or 0.90). However, the parameters with the highest diagnostic accuracy varied by myopia status and topographic location of the measurement. In general, pRNFLT and GCIPLT measures had the highest diagnostic accuracy in eyes with high myopia, whereas BMO-MRW had the highest diagnostic accuracy in the no-myopia and mild myopia groups.

Our study shows that pRNFLT, mRNFLT, and GCIPLT have similar diagnostic accuracy to predict glaucoma in eyes across all myopia ranges. Peripapillary RNFL is an established OCT parameter for predicting glaucoma and widely used to detect and monitor glaucoma. The peripapillary RNFL represents the axons of almost all retinal ganglion cells axons (except for those few ganglion cells which are located between the measurement ring and the optic disc border), and it has been assumed that it is not affected by macular pathologies and therefore a good marker for glaucoma assessment.[28] Because of changes in ONH configuration secondary to axial elongation such as disc "tilting," ovalization

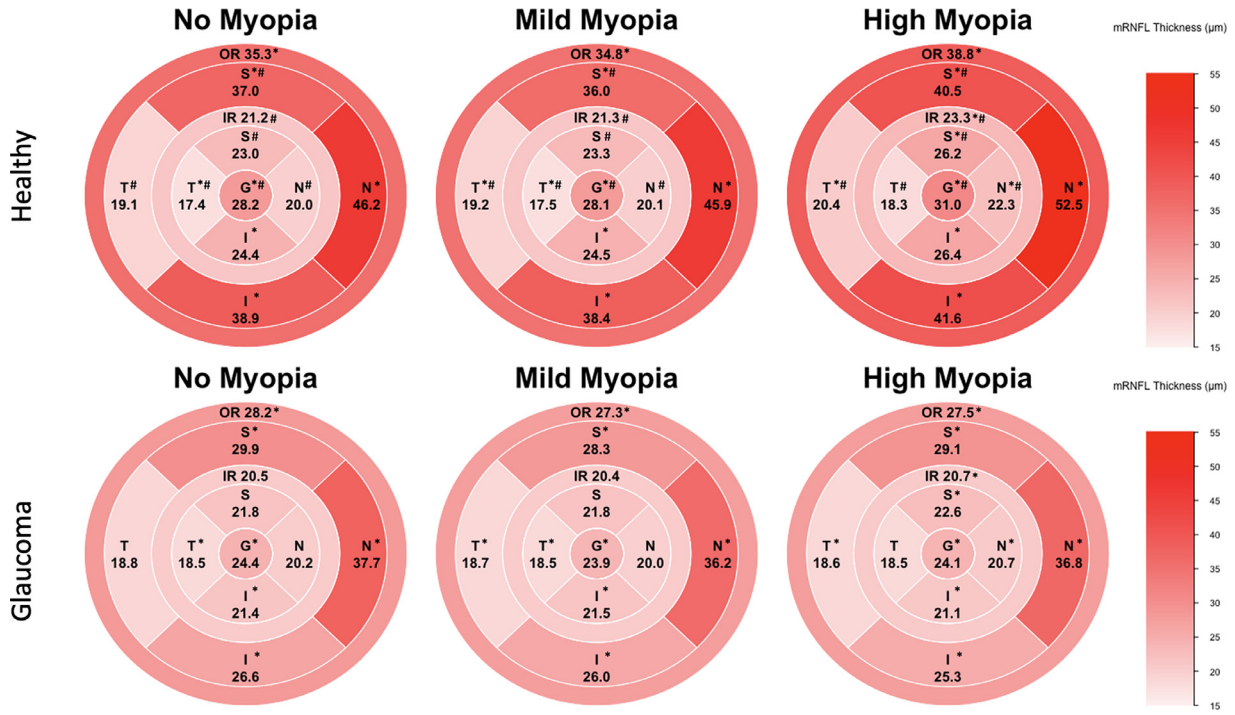

FIGURE 4. Global and sectoral distribution of macular retinal nerve fiber layer thickness by diagnosis in the no myopia, mild myopia, and high myopia group. The top row presents global and sectoral distribution of macular retinal nerve fiber layer thickness (mRNFLT) (in µm) in the three myopia groups in healthy eyes (from left to right: no myopia, mild myopia, high myopia). The bottom row presents mRNFLT (in µm) in the three myopia groups in glaucoma eyes (from left to right: no myopia, mild myopia, high myopia). mRNFLT values are presented as absolute values and are color coded according to the diagram on the right. * states statistical significance between healthy and glaucoma group and # states statistical significance between myopia groups. G = global; mRNFLT = macula retinal nerve fiber layer thickness; I = inferior; IR = inner ring; N = nasal; OR = outer ring; S = superior; T = temporal.

of the disc shape and increased size of parapapillary zones, it was unclear whether these changes affect the diagnostic accuracy of both pRNFLT and BMO-MRW. We found that in highly myopic eyes, pRNFLT had better diagnostic accuracy for glaucoma detection than BMO-MRW. In contrast, in the no-myopia and mild myopia group, BMO-MRW tended to have higher diagnostic accuracy than pRNFLT. This lower diagnostic accuracy of BMO-MRW in highly myopic eyes is likely due to the ONH morphologic changes associated with axial elongation. It is unclear why the diagnostic accuracy of BMO-MRW was so high in the nonhigh myope groups.[29] It was previously shown that the neuroretinal rim performs well in diagnosing glaucoma in nonhigh myopic eyes. One possible reason it performs worse in high myopes could be, that due to morphologic changes in high myopes as disc tilting, the neuroretinal rim measurements are not as sensitive as other parameters.

These axial elongation-related morphologic changes can also lead to a change in the distribution of pRNFLT profile, with a dislocation of the temporal superior and temporal inferior pRNFLT peaks into the temporal region in myopic eyes,[20,30,31] which can result in eyes incorrectly classified outside normal limits. Additionally, It remains unknown whether retinal ganglion cell axon loss that is responsible for RNFL bundle defects proceeds or follows retinal ganglion cell body loss.[32] It is therefore of interest to examine the retinal ganglion cells and with more than 50% of the retinal ganglion cells concentrated in the perifoveal region, the macula is of special interest.[13] It has been assumed that the macula is less affected by morphologic changes due to axial elongation and that the examination of macula parameters like the GCIPLT and ganglion cell complex (GCC; the sum of the GCIPLT and mRNFLT) can be useful parameters to detect glaucomatous changes.[20,33] We found that the diagnostic ability of GCIPLT was similar to that of pRNFLT and not superior in the high axial myopia group.

Previous studies comparing the diagnostic accuracy of GCIPLT and pRNFLT showed conflicting results. Choi and associates found similar results to the current study and stated that inferior RNFL (AUC 0.906) and inferotemporal GCIPLT (AUC 0.852) were the best parameters for discriminating healthy from glaucomatous highly

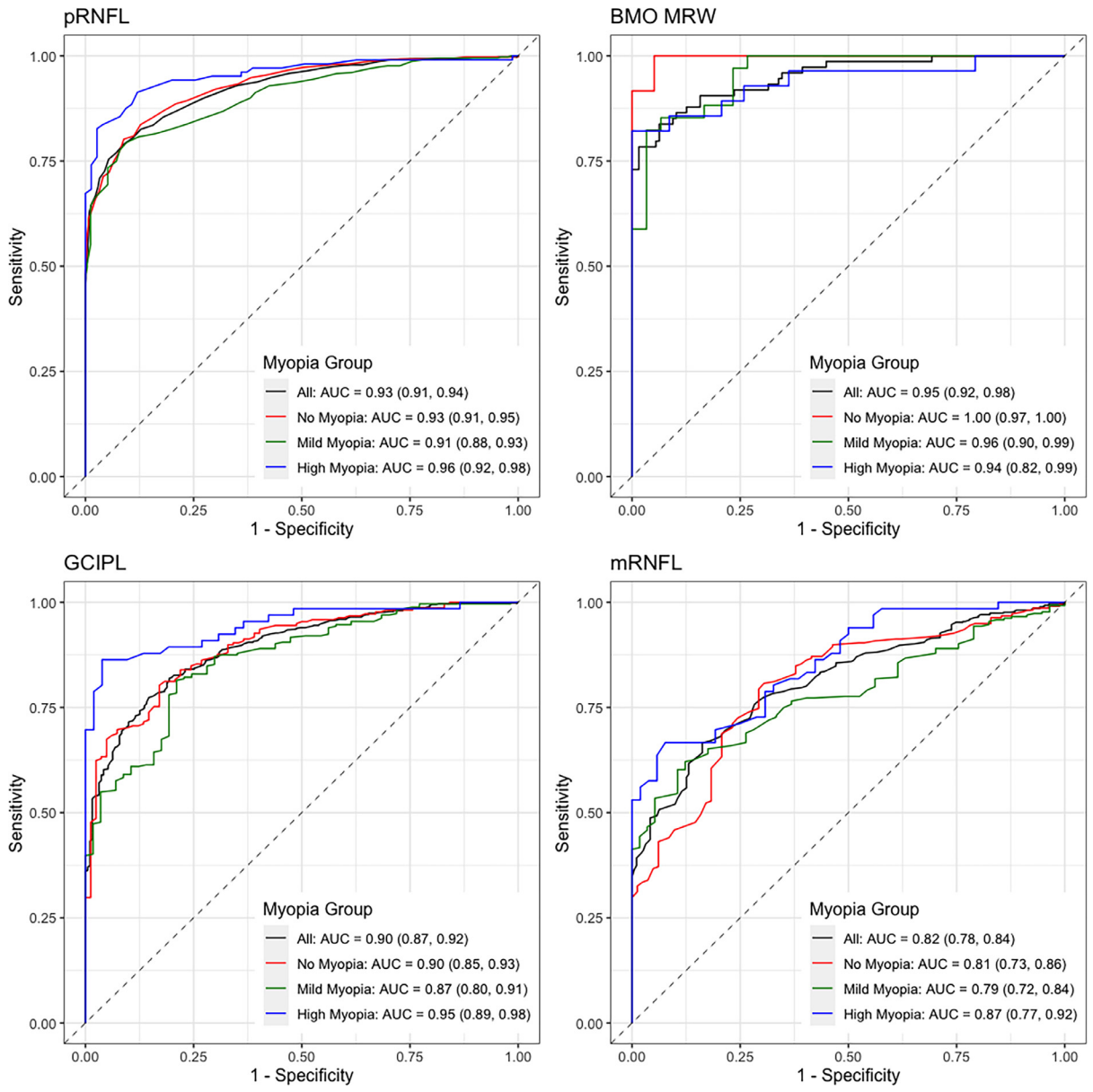

FIGURE 5. Diagnostic accuracy of ONH- and macula parameters in predicting glaucoma in the no myopia, mild myopia, and high myopia group. Top left presents the diagnostic accuracy of the peripapillary retinal nerve fiber layer thickness to detect glaucoma as the area under the receiver operating characteristic curve (AUC, (95%CI)) in no myopia- (red line), mild myopia- (green line), high myopia (blue line)- and all eyes (black line). Top right presents the diagnostic accuracy of the Bruch's membrane opening minimum rim width to detect glaucoma as the AUC in no myopia- (red line), mild myopia- (green line), high myopia (blue line)- and all eyes (black line). Bottom left presents the diagnostic accuracy of the ganglion cell inner plexiform layer thickness to detect glaucoma as the area under the AUC in no myopia- (red line), mild myopia- (green line), high myopia (blue line)- and all eyes (black line). Bottom right presents the diagnostic accuracy of the macular retinal nerve fiber layer thickness to detect glaucoma as the AUC in no myopia- (red line), mild myopia- (green line), high myopia (blue line)- and all eyes (black line). AUC = area under the receiver operating characteristic curve; BMO-MRW = Bruch's membrane opening minimum rim width; GCIPLT = ganglion cell inner plexiform layer thickness; mRNFLT = macula retinal nerve fiber layer thickness; pRNFLT = peripapillary retinal nerve fiber layer thickness.

myopic eyes with no statistically significant difference between both parameters.[28] In our study the inferotemporal pRNFLT also had the best diagnostic accuracy (adjusted AUC = 0.91) among the pRNFLT parameters for high myopes. For GCIPLT, the sectors with best diagnostic accuracy for glaucoma detection in high myopes were the inner inferior, the inner temporal and the outer temporal sectors (all adjusted AUC> 0.91). Similar results were obtained by Kim and associates with higher AUC for GCC (0.89) than for pRNFLT (0.83) to detect glaucomatous changes in highly myopic eyes, however with no statistical significance ($P = .442$) between both parameters.[34] The pRNFLT might generally be a good marker for glaucomatous changes, as the axonal fibers of almost all retinal ganglion cells converge towards the ONH, where RNFL loss can be detected, whereas the perifoveal region only comprises information only on ganglion cell loss located in that region.[34,35] However Shoji and colleagues compared the diagnostic ability of the GCC and pRNFLT in highly myopic eyes and found that GCC was the best OCT parameter to diagnose glaucoma in a highly myopic eye.[36] Because the RNFL is included in the GCC, the diagnostic ability of the GCC is dependent on that of the RNFL. Both GCIPL and RNFL have different sectoral diagnostic accuracy and it is important to consider the topographic distribution of nerve fiber bundles when interpreting the results, especially in high myopic eyes, which are reported to have a more temporally located peak of the RNFLT.[30,34] The region inferotemporal to the fovea is reported to be affected prior to other sectors by glaucoma[37] and also in our study the temporal and inferior GCIPLT had a higher diagnostic accuracy compared to other GCIPLT sectors.

In this study, we found high diagnostic accuracy for both pRNFLT and GCIPLT parameters in high myopic eyes. One possible reason for the high diagnostic accuracy could be the selection bias we had for high myopic eyes as these eyes underwent a separate grading process where diagnosis was defined by consensus between two graders and adjudication by a senior consultant based on assessment of optic disc photographs. By having a separate grading process for high myopic eyes, we likely included fewer "borderline cases" in the high myopia group compared to the other two myopia groups. The borderline cases were mostly graded as healthy high myopic eyes. This could explain in part the high AUCs, however only a few high myopic eyes (5 in total) were excluded because of unclassified diagnosis.

There are several possible limitations to this study. First, Individuals with healthy eyes were significantly younger than those with glaucomatous eyes, which could lead to an overestimate of the diagnostic accuracy of both ONH and macula parameters. For these reasons, we adjusted for age in our analysis. Second, it is possible that selection bias led to an overestimate of the diagnostic accuracy in the highly myopic group, as these eyes were more challenging to detect glaucoma based on our standard definition using consensus between two graders reviewing optic disc photographs, or in cases of disagreement, adjudication by a third expert grader. For the highly myopic eyes, the same process of grading of optic disc photographs was completed, except adjudication was conducted by a senior consultant (J.J.) who is an expert on the myopic disc. It is possible that our study includes eyes that were mistakenly identified as glaucomatous, resulting in false positive or overcalling of glaucoma. To minimize the possibility of false positive cases of glaucoma, the two independent graders trained with a senior consultant (J.J.) with extensive expertise in high myopic eyes, and the protocol required consensus on the determination of glaucoma with adjudication by the same senior consultant when necessary. If there is indeed a substantial number of individuals mistakenly identified as having glaucoma, then any differences identified would be conservative as they would underestimate true differences between groups. It should be noted, that in contrast to other studies,[38] highly myopic glaucoma eyes did not have more severe glaucoma, as measured by VFMD, than the glaucoma eyes in the no-myopia and mild myopia groups, suggesting that possible selection bias of more severe glaucoma in the highly myopic eyes may be limited. Third, the majority of individuals in our study were of African and European descent. Consequently, the generalizability of our findings to other populations may be limited. This limitation should be considered when interpreting the results.

In conclusion, the diagnostic ability of the GCIPLT and pRNFLT was high for high axial myopic eyes and both OCT parameters can be used in glaucoma management in high myopes. Further studies with larger sample sizes for healthy high myopic eyes are needed to determine which combination of parameters is best in glaucoma management of high myopic eyes.

CREDIT AUTHORSHIP CONTRIBUTION STATEMENT

JASMIN REZAPOUR: Writing – review & editing, Writing – original draft, Validation, Methodology, Investigation, Conceptualization. **EVAN WALKER:** Writing – review & editing, Visualization, Validation, Methodology, Formal analysis, Data curation. **AKRAM BELGHITH:** Writing – review & editing, Software, Data curation. **CHRISTOPHER BOWD:** Writing – review & editing, Validation, Methodology. **MASSIMO A. FAZIO:** Writing – review & editing, Methodology. **ANUWAT JIRAVARNSIRIKUL:** Writing – review & editing, Methodology. **LESLIE HYMAN:** Writing – review & editing. **JOST B. JONAS:** Writing – review & editing, Methodology. **ROBERT N. WEINREB:** Writing – review & editing, Resources, Conceptualization. **LINDA M. ZANGWILL:** Writing – review & editing, Validation, Supervision, Resources, Project administration, Methodology, Investigation, Funding acquisition, Data curation, Conceptualization.

Funding/Support: JR: Research Fellowship Grant (RE4155/1-1) of the German Research Foundation (DFG) and German Ophthalmological Society (DOG) Grant (no grant number).

EW: None.

AB: None.

CB: None.

MAF: National Eye Institute, EyeSight Foundation of Alabama, Research to Prevent Blindness (New York, NY), Heidelberg Engineering GmbH, Topcon and Wolfram Research.

AJ: None.

LH: None.

JBJ: None.

RNW: Consultant: Abbvie, Aerie Pharmaceuticals, Alcon, Allergan, Amydis, Balance, Equinox, Eyenovia, Iantrek, Implandata, iSTAR Medical, Nicox, Topcon Medical; Research support: Centervue, National Eye Institute, National Institute for Minority Health and Health Disparities, Research to Prevent Blindness (New York, NY); Patents: licensed by UCSD to Toromedes, Carl Zeiss Meditec; co-Founder: Toromedes;

LMZ: Consultant: Abbvie Inc., Topcon; F: The Glaucoma Foundation grant (no grant number), National Institutes of Health (OT2OD032644), National Eye Institute, Carl Zeiss Meditec Inc., Heidelberg Engineering GmbH, Optovue Inc., Topcon Medical Systems Inc., AISight Health; and Nonfinancial Support (equipment): from Carl Zeiss Meditec, Optovue, Icare, Optomed, and Topcon.

Funding/Support: National Institutes of Health grants R01EY011008, R01EY019869, U10EY014267, R01EY027510, R01EY026574, R01EY029058, and Core grant P30EY022589; an Unrestricted grant from Research to Prevent Blindness (New York, NY) and participant retention incentive grants in the form of glaucoma medication at no cost from Novartis/Alcon Laboratories Inc, Allergan, Akorn, and Pfizer Inc.

Financial Disclosures: Dr. Zangwill has been a consultant for Abbvie Inc. Topcon Medical Systems and received funding from Heidelberg Engineering GmbH, and equipment from Heidelberg Engineering GmbH, Optovue Inc., Topcon Medical Systems Inc. ICare Inc. Optomed Inc. Dr. Zangwill is cofounder, inventor, board member and equity holder of AISight Health Inc.

Dr. Robert Weinreb is a consultant for Abbvie, Aerie Pharmaceuticals, Alcon, Allergan, Amydis, Balance, Equinox, Eyenovia, Iantrek, Implandata, iSTAR Medical, Nicox, Topcon Medical. Dr. Robert Weinreb has patents licensed by UCSD to Toromedes, Carl Zeiss Meditec; cofounder: Toromedes. All authors attest that they meet the current ICMJE criteria for authorship.

Other Acknowledgements: None.

REFERENCES

1. Holden BA, Fricke TR, Wilson DA, et al. Global prevalence of myopia and high myopia and temporal trends from 2000 through 2050. *Ophthalmology*. 2016;123:1036–1042.
2. Leske MC, Connell AM, Wu SY, Hyman LG, Schachat AP. Risk factors for open-angle glaucoma. The Barbados Eye Study. *Arch Ophthalmol*. 1995;113:918–924.
3. Mitchell P, Hourihan F, Sandbach J, Wang JJ. The relationship between glaucoma and myopia: the Blue Mountains Eye Study. *Ophthalmology*. 1999;106:2010–2015.
4. Xu L, Wang Y, Wang S, Wang Y, Jonas JB. High myopia and glaucoma susceptibility the Beijing Eye Study. *Ophthalmology*. 2007;114:216–220.
5. Tan NYQ, Sng CCA, Jonas JB, Wong TY, Jansonius NM, Ang M. Glaucoma in myopia: diagnostic dilemmas. *Br J Ophthalmol*. 2019;103:1347–1355.
6. Chang RT, Singh K. Myopia and glaucoma: diagnostic and therapeutic challenges. *Curr Opin Ophthalmol*. 2013;24:96–101.
7. Jeoung JW, Yang H, Gardiner S, et al. Optical coherence tomography optic nerve head morphology in myopia I: implications of anterior scleral canal opening versus Bruch membrane opening offset. *Am J Ophthalmol*. 2020;218:105–119.
8. Burgoyne CF, Wang YX, Jeoung JW, et al. OCT optic nerve head morphology in myopia II: peri-neural canal scleral bowing and choroidal thickness in high myopia-an american ophthalmological society thesis. *Am J Ophthalmol*. 2023;252:225–252.
9. Lee JY, Sung KR, Han S, Na JH. Effect of myopia on the progression of primary open-angle glaucoma. *Invest Ophthalmol Vis Sci*. 2015;56:1775–1781.
10. Hsu CH, Chen RI, Lin SC. Myopia and glaucoma: sorting out the difference. *Curr Opin Ophthalmol*. 2015;26:90–95.
11. Rezapour J, Proudfoot JA, Bowd C, et al. Bruch membrane opening detection accuracy in healthy eyes and eyes with glaucoma with and without axial high myopia in an American and Korean cohort. *Am J Ophthalmol*. 2022;237:221–234.
12. Yilmaz H, Yeşiltaş YS, Aydemir E, et al. A myopic normative database for retinal nerve fiber layer thickness using optical coherence tomography. *J Glaucoma*. 2022;31:816–825.
13. Curcio CA, Allen KA. Topography of ganglion cells in human retina. *J Comp Neurol*. 1990;300:5–25.

14. Hood DC, Raza AS, de Moraes CG, Liebmann JM, Ritch R. Glaucomatous damage of the macula. *Prog Retin Eye Res*. 2013;32:1–21.
15. Lam DS, Leung KS, Mohamed S, et al. Regional variations in the relationship between macular thickness measurements and myopia. *Invest Ophthalmol Vis Sci*. 2007;48:376–382.
16. Chen HS, Ling XC, Lu DW, et al. Glaucoma diagnostic performance of macular ganglion cell complex thickness using regular and long axial length normative databases. *Sci Rep*. 2022;12:11263.
17. Biswas S, Lin C, Leung CK. Evaluation of a myopic normative database for analysis of retinal nerve fiber layer thickness. *JAMA Ophthalmol*. 2016;134:1032–1039.
18. Song Y, Li F, Chong RS, et al. High myopia normative database of peripapillary retinal nerve fiber layer thickness to detect myopic glaucoma in a Chinese population. *Ophthalmology*. 2023;130:1279–1289.
19. Sample PA, Girkin CA, Zangwill LM, et al. The African descent and glaucoma evaluation study (ADAGES): design and baseline data. *Arch Ophthalmol*. 2009;127:1136–1145.
20. Rezapour J, Bowd C, Dohleman J, et al. Macula structural and vascular differences in glaucoma eyes with and without high axial myopia. *Br J Ophthalmol*. 2022;107:1286–1294.
21. Jonas JB, Ohno-Matsui K, Panda-Jonas S. Optic nerve head histopathology in high axial myopia. *J Glaucoma*. 2017;26:187–193.
22. Shen L, You QS, Xu X, et al. Scleral and choroidal volume in relation to axial length in infants with retinoblastoma versus adults with malignant melanomas or end-stage glaucoma. *Ophthalmologie*. 2016;254:1779–1786.
23. Rezapour J, Bowd C, Dohleman J, et al. The influence of axial myopia on optic disc characteristics of glaucoma eyes. *Sci Rep*. 2021;11:8854.
24. Moghimi S, Zangwill LM, Penteado RC, et al. Macular and optic nerve head vessel density and progressive retinal nerve fiber layer loss in glaucoma. *Ophthalmology*. 2018;125:1720–1728.
25. Kromer R, Spitzer MS. Bruch's membrane opening minimum rim width measurement with SD-OCT: a method to correct for the opening size of Bruch's Membrane. *J Ophthalmol*. 2017;2017:8963267.
26. Rezapour J, Bowd C, Dohleman J, et al. Macular thickness and vessel density in glaucoma eyes with and without high axial myopia. *Invest Ophthalmol Vis Sci*. 2021;62:2431.
27. Team RC. *A Language and Environment for Statistical Computing*. Vienna: R Foundation for Statistical Computing; 2016.
28. Choi YJ, Jeoung JW, Park KH, Kim DM. Glaucoma detection ability of ganglion cell-inner plexiform layer thickness by spectral-domain optical coherence tomography in high myopia. *Invest Ophthalmol Vis Sci*. 2013;54:2296–2304.
29. Chauhan BC, O'Leary N, AlMobarak FA, et al. Enhanced detection of open-angle glaucoma with an anatomically accurate optical coherence tomography-derived neuroretinal rim parameter. *Ophthalmology*. 2013;120:535–543.
30. Leung CK, Yu M, Weinreb RN, et al. Retinal nerve fiber layer imaging with spectral-domain optical coherence tomography: interpreting the RNFL maps in healthy myopic eyes. *Invest Ophthalmol Vis Sci*. 2012;53:7194–7200.
31. Leung CK, Mohamed S, Leung KS, et al. Retinal nerve fiber layer measurements in myopia: an optical coherence tomography study. *Invest Ophthalmol Vis Sci*. 2006;47:5171–5176.
32. Mwanza JC, Durbin MK, Budenz DL, et al. Profile and predictors of normal ganglion cell-inner plexiform layer thickness measured with frequency-domain optical coherence tomography. *Invest Ophthalmol Vis Sci*. 2011;52:7872–7879.
33. Nakanishi H, Akagi T, Hangai M, et al. Effect of axial length on macular ganglion cell complex thickness and on early glaucoma diagnosis by spectral-domain optical coherence tomography. *J Glaucoma*. 2016;25:e481–e490.
34. Kim NR, Lee ES, Seong GJ, et al. Comparing the ganglion cell complex and retinal nerve fibre layer measurements by Fourier domain OCT to detect glaucoma in high myopia. *Br J Ophthalmol*. 2011;95:1115–1121.
35. Xu XY, Xiao H, Luo JY, Liu X. Evaluation of spectral domain optical coherence tomography parameters in discriminating preperimetric glaucoma from high myopia. *Int J Ophthalmol*. 2019;12:58–65.
36. Shoji T, Sato H, Ishida M, Takeuchi M, Chihara E. Assessment of glaucomatous changes in subjects with high myopia using spectral domain optical coherence tomography. *Invest Ophthalmol Vis Sci*. 2011;52:1098–1102.
37. Takayama K, Hangai M, Durbin M, et al. A novel method to detect local ganglion cell loss in early glaucoma using spectral-domain optical coherence tomography. *Invest Ophthalmol Vis Sci*. 2012;53:6904–6913.
38. Christopher M, Nakahara K, Bowd C, et al. Effects of study population, labeling and training on glaucoma detection using deep learning algorithms. *Transl Vis Sci Technol*. 2020;9:27.

Supplemental Table 1 Mean (95% CI) Peripapillary Retinal Nerve Fiber Layer (pRNFL) Thickness, and Bruch's Membrane Opening Minimum Rim Width (BMO-MRW) by Diagnosis in the No Myopia, Mild Myopia and High Myopia Group

	No Myopia			Mild Myopia			High Myopia			p-value* comparing Glaucoma subgroups	p-value* comparing Healthy subgroups
	Glaucoma n=213 (368 eyes)	Healthy n = 214 (411 eyes)	p-value*	Glaucoma n=225 (394 eyes)	Healthy n = 142 (271 eyes)	p-value*	Glaucoma n = 76 (125 eyes)	Healthy n = 45 (85 eyes)	p-value*		
pRNFL											
Global	74.3 (72.7, 75.9)	100.6 (99.1, 102.2)	< 0.001	69.8 (68.0, 71.5)	96.5 (94.4, 98.7)	< 0.001	65.9 (62.6, 69.2)	100.0 (95.8, 104.2)	< 0.001	0.003	0.013
Temporal	58.7 (57.1, 60.2)	67.5 (66.0, 69.1)	< 0.001	58.1 (56.2, 60.1)	69.2 (66.8, 71.6)	0.013	60.4 (56.0, 64.9)	81.1 (75.5, 86.7)	0.002	0.119	< 0.001
Temporal Superior	95.5 (92.8, 98.3)	131.8 (129.0, 134.5)	< 0.001	88.0 (85.2, 90.8)	130.1 (126.6, 133.6)	< 0.001	82.7 (76.2, 89.3)	132.0 (123.7, 140.3)	< 0.001	0.010	0.846
Temporal Inferior	92.3 (88.9, 95.6)	141.3 (137.9, 144.6)	< 0.001	85.1 (81.4, 88.8)	140.4 (135.8, 145.0)	< 0.001	78.7 (72.3, 85.2)	146.6 (138.6, 154.6)	< 0.001	0.080	0.359
Nasal	60.0 (58.3, 61.8)	79.6 (77.9, 81.3)	< 0.001	57.7 (56.0, 59.4)	73.7 (71.5, 75.8)	< 0.001	54.2 (50.8, 57.5)	77.4 (73.2, 81.7)	< 0.001	0.082	< 0.001
Nasal Superior	81.2 (78.6, 83.9)	114.7 (112.0, 117.3)	< 0.001	76.9 (74.1, 79.6)	105.5 (102.1, 108.9)	< 0.001	68.0 (62.4, 73.6)	117.4 (110.3, 124.5)	< 0.001	0.001	< 0.001
Nasal Inferior	87.8 (84.8, 90.7)	125.1 (122.2, 128.1)	< 0.001	77.5 (74.7, 80.3)	113.7 (110.2, 117.2)	< 0.001	71.5 (65.9, 77.0)	106.9 (99.9, 114.0)	< 0.001	< 0.001	< 0.001
BMO-MRW											
Global	189.0 (141.6, 236.5)	330.8 (303.5, 358.1)	< 0.001	195.0 (171.5, 218.5)	331.6 (306.5, 356.6)	< 0.001	185.5 (164.1, 206.8)	311.5 (294.8, 328.2)	< 0.001	0.288	0.539
Temporal	157.7 (119.8, 195.7)	233.6 (211.8, 255.5)	0.010	152.5 (132.3, 172.8)	239.2 (217.6, 260.8)	< 0.001	163.0 (144.4, 181.6)	241.0 (226.7, 255.3)	< 0.001	0.475	0.604
Temporal Superior	180.5 (130.7, 230.4)	319.3 (290.6, 347.9)	0.002	156.5 (134.2, 178.8)	320.8 (297.0, 344.6)	< 0.001	179.3 (151.4, 207.1)	303.0 (281.5, 324.5)	< 0.001	0.479	0.222
Temporal Inferior	139.5 (80.0, 199.0)	355.0 (320.9, 389.1)	< 0.001	158.9 (128.9, 188.9)	362.3 (330.3, 394.3)	< 0.001	159.7 (128.4, 191.1)	343.1 (318.8, 367.3)	< 0.001	0.143	0.728
Nasal	216.2 (163.3, 269.0)	361.9 (331.5, 392.3)	< 0.001	241.6 (209.0, 274.2)	365.0 (330.2, 399.7)	0.003	208.7 (183.4, 234.0)	331.1 (311.2, 350.9)	< 0.001	0.725	0.319
Nasal Superior	209.6 (150.3, 268.9)	382.0 (347.8, 416.1)	< 0.001	204.6 (179.6, 229.5)	364.0 (337.4, 390.7)	< 0.001	186.6 (154.2, 218.9)	343.3 (318.0, 368.6)	< 0.001	0.097	0.010
Nasal Inferior	221.3 (164.6, 278.1)	399.9 (367.3, 432.5)	< 0.001	227.6 (191.4, 263.8)	398.3 (359.7, 436.8)	< 0.001	206.0 (176.7, 235.3)	361.0 (338.9, 383.0)	< 0.001	0.660	0.403

*Significance is determined by linear mixed models. Models are adjusted for visual field mean deviation, age and image quality score.

Supplemental Table 2. Mean (95% CI) Ganglion Cell Inner Plexiform Layer (GCIPL) Thickness and Macular Retinal Nerve Fiber Layer (mRNFL) Thickness by Diagnosis

	No Myopia			Mild Myopia			High Myopia			p-value* comparing Glaucoma subgroups	p-value* comparing Healthy subgroups
	Glaucoma n = 119 (197 eyes)	Healthy n = 39 (71 eyes)	p-value*	Glaucoma n=157 (267 eyes)	Healthy n = 33 (61 eyes)	p-value*	Glaucoma n = 55 (84 eyes)	Healthy 36 (59 eyes)	p-value*		
GCIPL											
Global	61.8 (60.4, 63.2)	76.5 (74.3, 78.8)	< 0.001	59.5 (58.0, 61.0)	75.8 (72.6, 79.1)	< 0.001	57.7 (55.3, 60.2)	26.2 (24.5, 27.8)	< 0.001	0.029	0.098
Inner Ring	71.5 (69.7, 73.3)	89.1 (86.2, 92.1)	< 0.001	68.7 (66.6, 70.8)	89.0 (84.5, 93.5)	0.002	66.3 (63.0, 69.6)	92.2 (88.2, 96.2)	< 0.001	0.098	0.163
Outer Ring	52.1 (51.0, 53.2)	63.9 (62.0, 65.7)	< 0.001	50.3 (49.2, 51.4)	62.7 (60.4, 65.0)	< 0.001	49.1 (47.3, 50.9)	63.1 (60.9, 65.3)	< 0.001	0.006	0.253
Inner Temporal	65.0 (63.0, 67.0)	86.5 (83.2, 89.8)	< 0.001	62.9 (60.7, 65.1)	86.9 (82.3, 91.6)	< 0.001	60.7 (57.2, 64.3)	90.0 (85.8, 94.3)	< 0.001	0.649	0.619
Inner Superior	76.3 (74.2, 78.3)	90.7 (87.3, 94.0)	0.024	73.2 (71.0, 75.4)	90.5 (85.9, 95.2)	0.056	70.9 (67.3, 74.5)	93.7 (89.3, 98.0)	0.003	0.113	0.501
Inner Nasal	76.2 (74.3, 78.2)	89.0 (85.7, 92.2)	0.126	72.9 (70.5, 75.2)	88.0 (83.0, 93.0)	0.211	70.3 (66.5, 74.1)	93.3 (88.7, 97.9)	0.001	0.040	0.111
Inner Inferior	68.6 (66.4, 70.7)	90.4 (86.9, 93.9)	< 0.001	66.1 (63.7, 68.5)	90.6 (85.6, 95.6)	< 0.001	63.4 (59.7, 67.1)	91.8 (87.4, 96.2)	< 0.001	0.295	0.388
Outer Temporal	50.8 (49.6, 52.1)	66.5 (64.4, 68.5)	< 0.001	49.4 (48.2, 50.7)	64.8 (62.1, 67.5)	< 0.001	47.4 (45.3, 49.4)	66.0 (63.5, 68.5)	< 0.001	0.100	0.006
Outer Superior	52.1 (50.8, 53.5)	62.4 (60.1, 64.6)	< 0.001	50.0 (48.9, 51.1)	61.1 (58.7, 63.5)	< 0.001	48.7 (46.9, 50.6)	61.8 (59.5, 64.0)	< 0.001	0.005	0.047
Outer Nasal	57.7 (56.4, 59.1)	67.7 (65.4, 69.9)	0.006	55.4 (54.0, 56.7)	66.9 (64.1, 69.7)	0.005	54.4 (52.0, 56.7)	66.8 (63.9, 69.6)	0.013	0.003	0.365
Outer Inferior	47.6 (46.5, 48.8)	59.0 (57.2, 60.9)	< 0.001	46.4 (45.4, 47.4)	58.1 (55.9, 60.3)	< 0.001	46.0 (44.1, 47.9)	58.0 (55.8, 60.3)	< 0.001	0.272	0.204
mRNFL											
Global	24.4 (23.8, 24.9)	28.2 (27.3, 29.2)	< 0.001	23.9 (23.2, 24.5)	28.1 (26.7, 29.4)	< 0.001	24.1 (22.9, 25.3)	31.0 (29.6, 32.5)	< 0.001	0.330	0.009
Inner Ring	20.5 (20.1, 20.9)	21.2 (20.5, 21.8)	0.806	20.4 (20.0, 20.9)	21.3 (20.5, 22.2)	0.402	20.7 (19.8, 21.7)	23.3 (22.2, 24.4)	0.006	0.193	< 0.001
Outer Ring	28.2 (27.4, 29.1)	35.3 (33.9, 36.7)	< 0.001	27.3 (26.4, 28.2)	34.8 (32.9, 36.8)	< 0.001	27.5 (25.8, 29.1)	38.8 (36.8, 40.7)	< 0.001	0.530	0.069
Inner Temporal	18.5 (18.2, 18.7)	17.4 (16.9, 17.8)	0.005	18.5 (18.2, 18.8)	17.5 (16.9, 18.1)	0.009	18.5 (17.8, 19.2)	18.3 (17.5, 19.1)	0.238	0.483	< 0.001
Inner Superior	21.8 (21.3, 22.4)	23.0 (22.0, 23.9)	0.675	21.8 (21.2, 22.4)	23.3 (22.1, 24.5)	0.267	22.6 (21.2, 23.9)	26.2 (24.5, 27.8)	0.002	0.085	< 0.001
Inner Nasal	20.2 (19.6, 20.8)	20.0 (19.0, 20.9)	0.491	20.0 (19.5, 20.5)	20.1 (19.1, 21.2)	0.727	20.7 (19.5, 21.9)	22.3 (20.8, 23.8)	0.043	0.093	< 0.001
Inner Inferior	21.4 (20.9, 21.9)	24.4 (23.5, 25.2)	0.005	21.5 (20.9, 22.1)	24.5 (23.3, 25.8)	0.035	21.1 (20.0, 22.2)	26.4 (25.1, 27.7)	< 0.001	0.755	0.056
Outer Temporal	18.8 (18.5, 19.1)	19.1 (18.6, 19.6)	0.102	18.7 (18.4, 19.0)	19.2 (18.6, 19.9)	0.041	18.6 (18.1, 19.2)	20.4 (19.7, 21.0)	< 0.001	0.501	< 0.001
Outer Superior	29.9 (28.7, 31.0)	37.0 (35.1, 38.9)	< 0.001	28.3 (27.2, 29.5)	36.0 (33.5, 38.4)	0.003	29.1 (26.9, 31.3)	40.5 (37.9, 43.1)	< 0.001	0.327	0.005
Outer Nasal	37.7 (36.4, 39.0)	46.2 (44.0, 48.4)	0.002	36.2 (34.7, 37.7)	45.9 (42.7, 49.1)	0.002	36.8 (34.0, 39.5)	52.5 (49.2, 55.9)	< 0.001	0.420	0.056
Outer Inferior	26.6 (25.4, 27.7)	38.9 (37.0, 40.8)	< 0.001	26.0 (24.8, 27.1)	38.4 (35.9, 40.8)	< 0.001	25.3 (23.2, 27.4)	41.6 (39.1, 44.1)	< 0.001	0.930	0.817

*Significance is determined by linear mixed models. Models are adjusted for visual field mean deviation, age and image quality score.

Supplemental Figure 1 Legend: Diagnostic accuracy of selected optic nerve head and macula OCT parameters for detecting glaucoma in eyes with and without high axial myopia

Supplemental Figure 1 presents the diagnostic accuracy (AUC (95% CI)) of selected global and sectoral optic nerve head (peripapillary retinal nerve fiber layer (pRNFL) thickness and Bruchs Membrane Opening- Minimum Rim Width (BMO-MRW)) and macula (ganglion cell inner plexiform layer (GCIPL) and macula RNFL (mRNFL) thickness to predict glaucoma in no myopia- (red line), mild myopia- (green line), high myopia (blue line)- and all eyes (black line), which is highest for high myopic eyes.

Supplemental Figure 1a. Diagnostic accuracy (AUC) of the infero-temporal sector of the peripapillary retinal nerve fiber layer thickness to predict glaucoma in no myopia-, mild myopia-, high myopia- and all eyes

Supplemental Figure 1b. Diagnostic accuracy of global Bruch's membrane opening minimum rim width to predict glaucoma in no myopia-, mild myopia-, high myopia- and all eyes

Supplemental Figure 1c. Diagnostic accuracy of the inner temporal ganglion cell inner plexiform layer thickness sector to predict glaucoma in no myopia-, mild myopia-, high myopia- and all eyes

Supplemental Figure 1d. Diagnostic accuracy of global macular retinal nerve fiber layer thickness to predict glaucoma in no myopia-, mild myopia-, high myopia- and all eyes

Supplemental Figure 1e. Diagnostic accuracy of the outer nasal ganglion cell inner plexiform layer thickness sector to predict glaucoma in no myopia-, mild myopia-, high myopia- and all eyes

Supplemental Figure 1f. Diagnostic accuracy of the outer nasal macular retinal nerve fiber layer thickness sector to predict glaucoma in no myopia-, mild myopia-, high myopia- and all eyes

A)

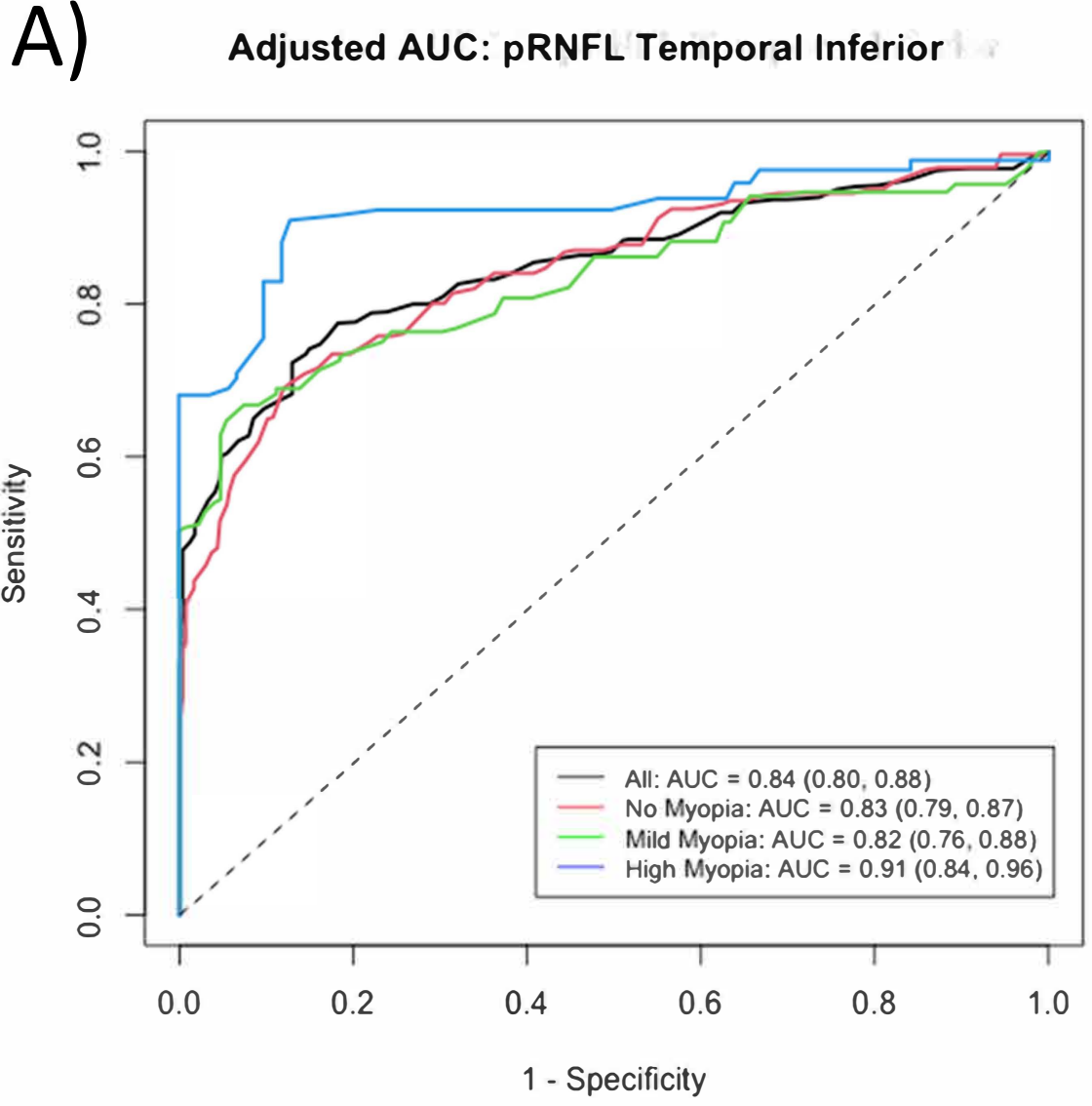
Adjusted AUC: pRNFL Temporal Inferior
Sensitivity
1 - Specificity
0.0
0.2
0.4
0.6
0.8
1.0
All: AUC = 0.84 (0.80, 0.88)
No Myopia: AUC = 0.83 (0.79, 0.87)
Mild Myopia: AUC = 0.82 (0.76, 0.88)
High Myopia: AUC = 0.91 (0.84, 0.96)

B)

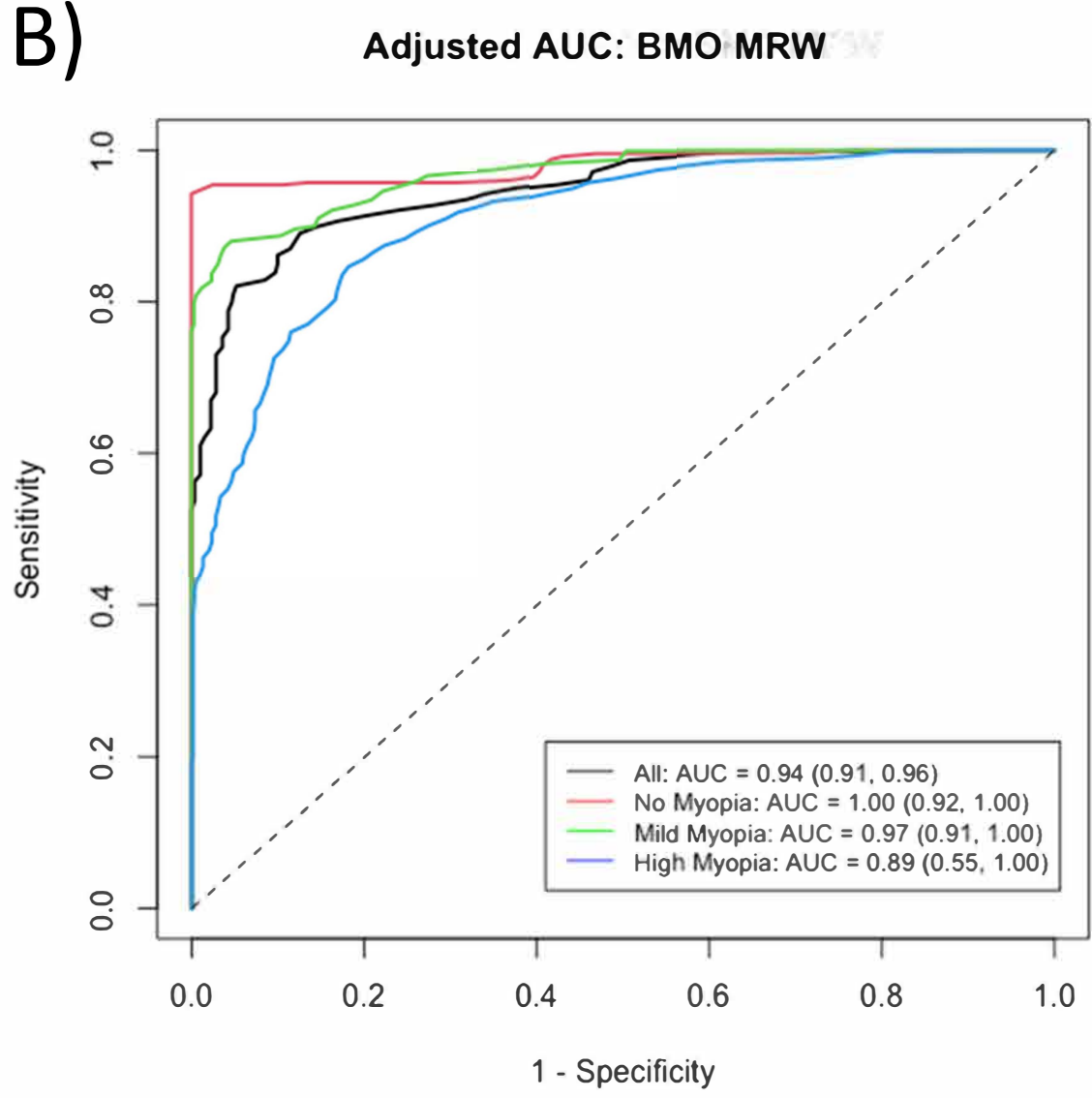
Adjusted AUC: BMO MRW
Sensitivity
1 - Specificity
0.0
0.2
0.4
0.6
0.8
1.0
All: AUC = 0.94 (0.91, 0.96)
No Myopia: AUC = 1.00 (0.92, 1.00)
Mild Myopia: AUC = 0.97 (0.91, 1.00)
High Myopia: AUC = 0.89 (0.55, 1.00)

C)

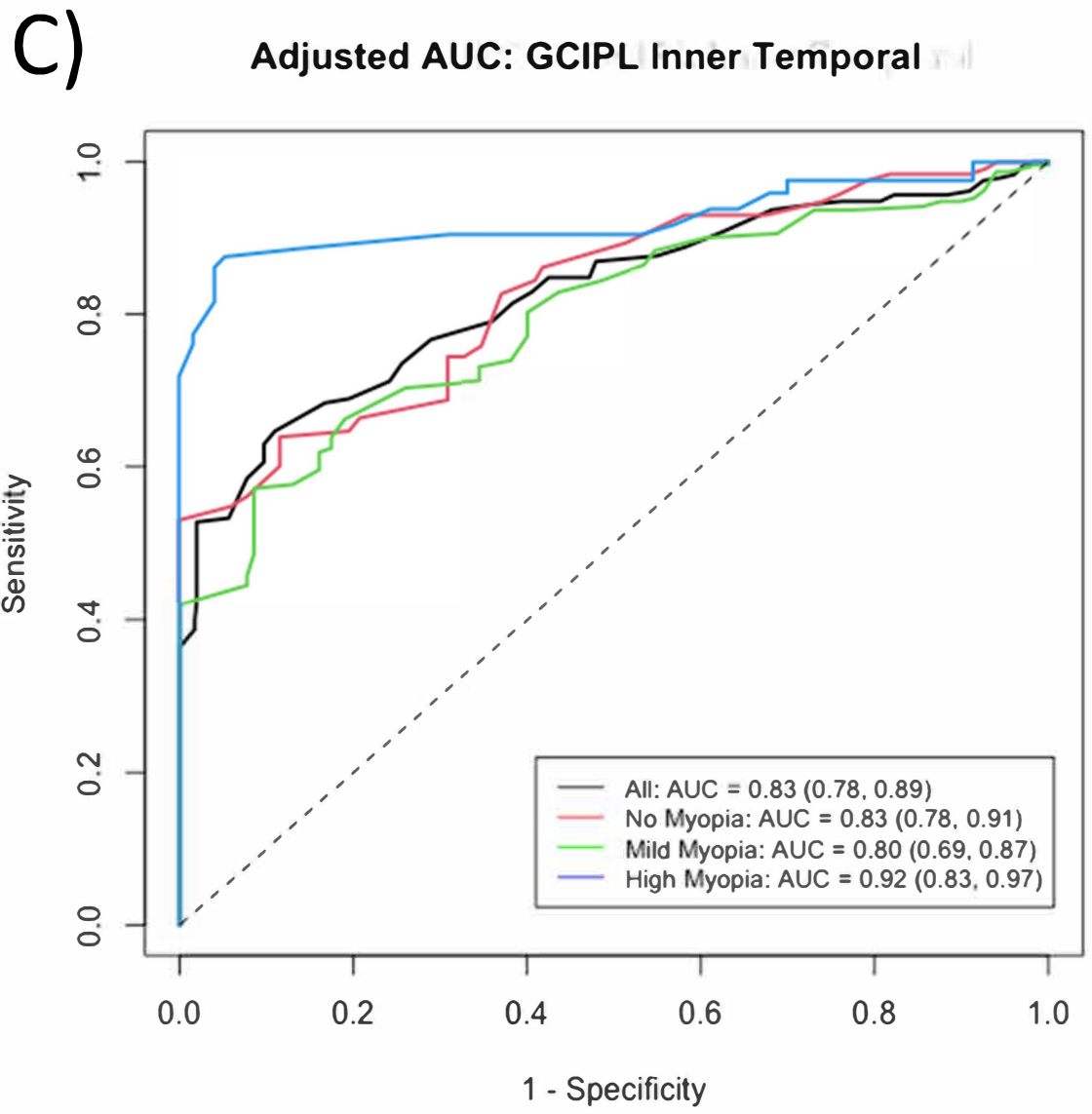
Adjusted AUC: GCIPL Inner Temporal
Sensitivity
1 - Specificity
0.0
0.2
0.4
0.6
0.8
1.0
All: AUC = 0.83 (0.78, 0.89)
No Myopia: AUC = 0.83 (0.78, 0.91)
Mild Myopia: AUC = 0.80 (0.69, 0.87)
High Myopia: AUC = 0.92 (0.83, 0.97)

D)

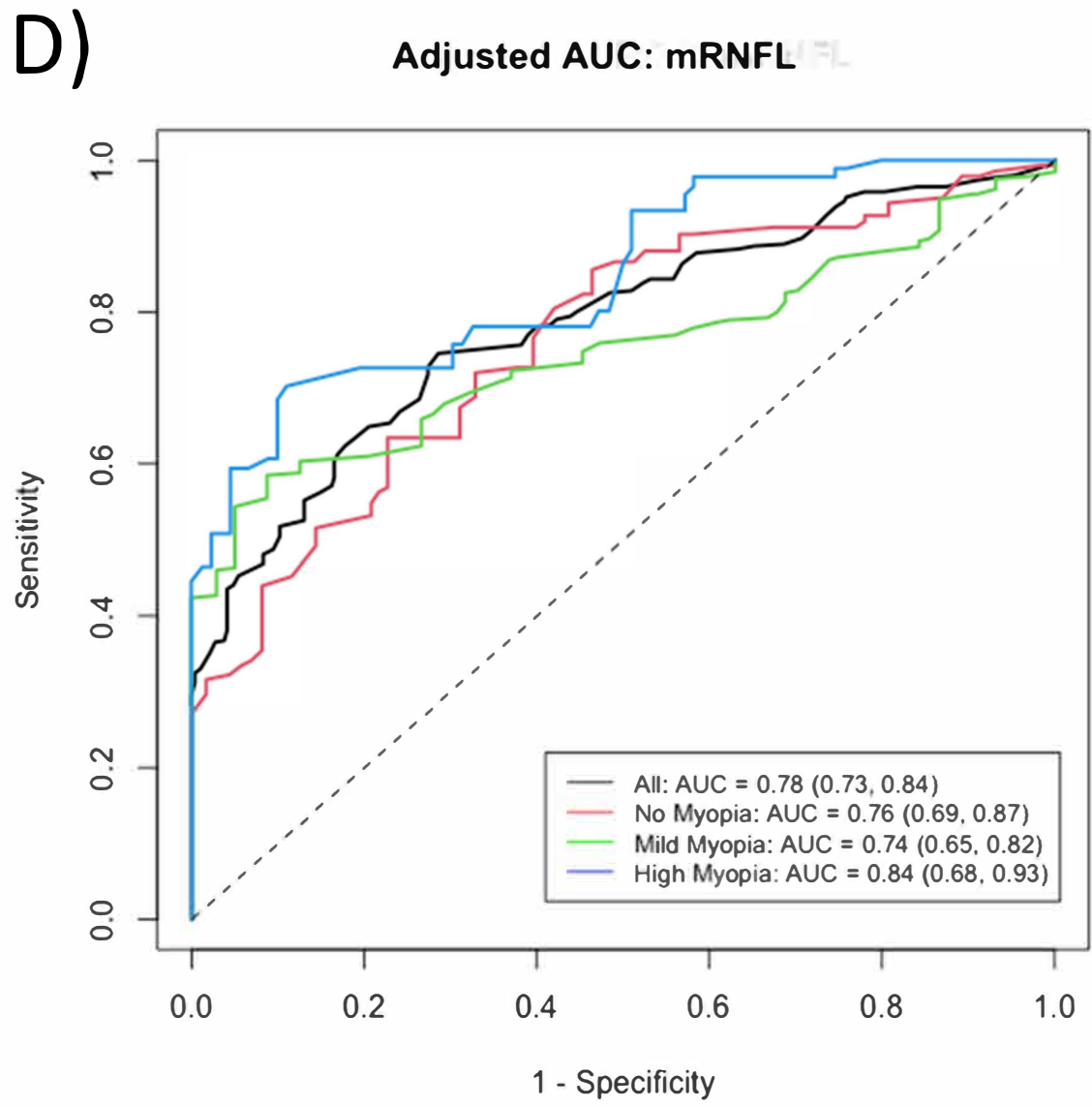
Adjusted AUC: mRNFL
Sensitivity
1 - Specificity
0.0
0.2
0.4
0.6
0.8
1.0
All: AUC = 0.78 (0.73, 0.84)
No Myopia: AUC = 0.76 (0.69, 0.87)
Mild Myopia: AUC = 0.74 (0.65, 0.82)
High Myopia: AUC = 0.84 (0.68, 0.93)

E)

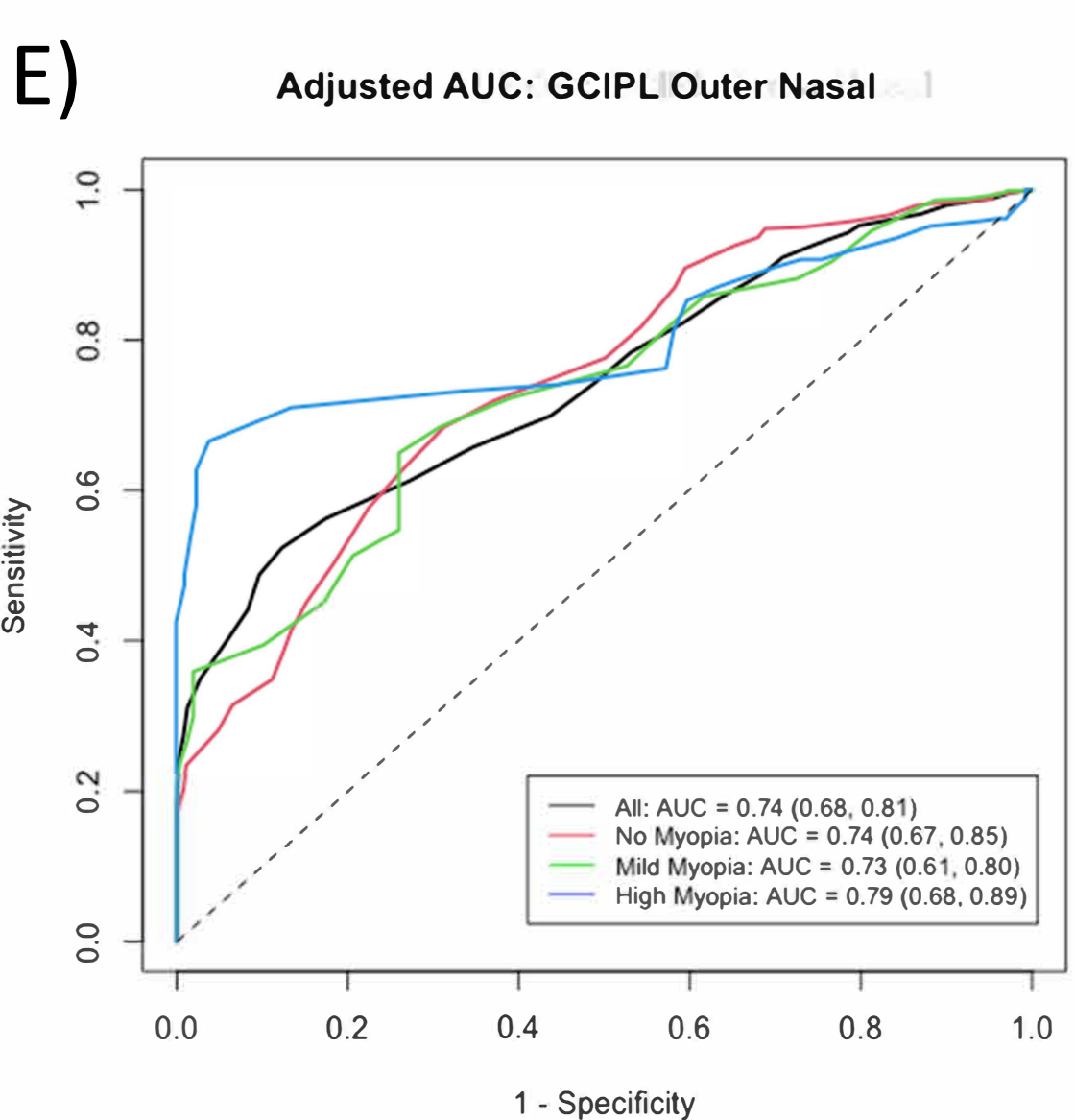
Adjusted AUC: GCIPL Outer Nasal
Sensitivity
1 - Specificity
0.0
0.2
0.4
0.6
0.8
1.0
All: AUC = 0.74 (0.68, 0.81)
No Myopia: AUC = 0.74 (0.67, 0.85)
Mild Myopia: AUC = 0.73 (0.61, 0.80)
High Myopia: AUC = 0.79 (0.68, 0.89)

F)

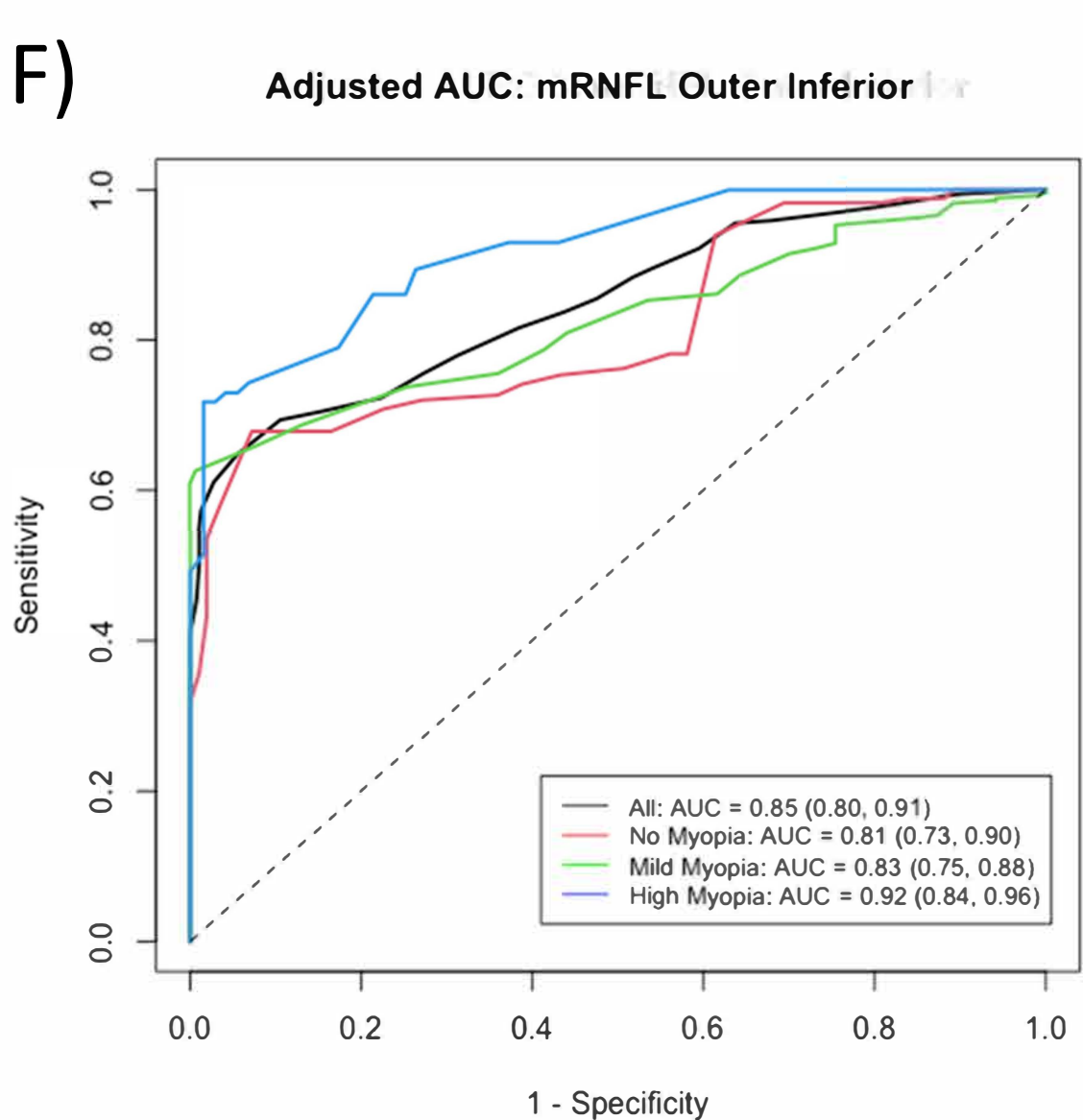
Adjusted AUC: mRNFL Outer Inferior
Sensitivity
1 - Specificity
0.0
0.2
0.4
0.6
0.8
1.0
All: AUC = 0.85 (0.80, 0.91)
No Myopia: AUC = 0.81 (0.73, 0.90)
Mild Myopia: AUC = 0.83 (0.75, 0.88)
High Myopia: AUC = 0.92 (0.84, 0.96)

5. Literaturverzeichnis

1. Holden BA, Fricke TR, Wilson DA, et al. Global Prevalence of Myopia and High Myopia and Temporal Trends from 2000 through 2050. Ophthalmology 2016;123:1036-42.
2. Marcus MW, de Vries MM, Junoy Montolio FG, Jansonius NM. Myopia as a risk factor for open-angle glaucoma: a systematic review and meta-analysis. Ophthalmology 2011;118:1989-1994 e2.
3. Xu L, Wang Y, Wang S, Wang Y, Jonas JB. High myopia and glaucoma susceptibility the Beijing Eye Study. Ophthalmology 2007;114:216-20.
4. Suh MH, Zangwill LM, Manalastas PI, et al. Deep Retinal Layer Microvasculature Dropout Detected by the Optical Coherence Tomography Angiography in Glaucoma. Ophthalmology 2016;123:2509-2518.
5. Suh MH, Jung DH, Weinreb RN, Zangwill LM. Optic Disc Microvasculature Dropout in Glaucoma Detected by Swept-Source Optical Coherence Tomography Angiography. American journal of ophthalmology 2022;236:261-270.
6. Micheletti E, El-Nimri N, Nishida T, et al. Central visual field damage in glaucoma eyes with choroidal microvasculature dropout with and without high axial myopia. The British journal of ophthalmology 2023.
7. Kwon JM, Weinreb RN, Zangwill LM, Suh MH. Parapapillary Deep-Layer Microvasculature Dropout and Visual Field Progression in Glaucoma. American journal of ophthalmology 2019;200:65-75.
8. Park HL, Kim YC, Jung Y, Park CK. Vertical disc tilt and features of the optic nerve head anatomy are related to visual field defect in myopic eyes. Scientific reports 2019;9:3485.
9. Wang YX, Panda-Jonas S, Jonas JB. Optic nerve head anatomy in myopia and glaucoma, including parapapillary zones alpha, beta, gamma and delta: Histology and clinical features. Progress in retinal and eye research 2020:100933.
10. Huang D, Swanson EA, Lin CP, et al. Optical coherence tomography. Science 1991;254:1178-81.
11. Realini T, Zangwill LM, Flanagan JG, et al. Normative Databases for Imaging Instrumentation. Journal of glaucoma 2015;24:480-3.
12. Rezapour J, Bowd C, Dohleman J, et al. The influence of axial myopia on optic disc characteristics of glaucoma eyes. Scientific reports 2021;11:8854.
13. Rezapour J, Bowd C, Dohleman J, et al. Macula structural and vascular differences in glaucoma eyes with and without high axial myopia. The British journal of ophthalmology 2022.
14. Early Treatment Diabetic Retinopathy Study design and baseline patient characteristics. ETDRS report number 7. Ophthalmology 1991;98:741-56.
15. Hwang YH, Yoo C, Kim YY. Myopic optic disc tilt and the characteristics of peripapillary retinal nerve fiber layer thickness measured by spectral-domain optical coherence tomography. Journal of glaucoma 2012;21:260-5.
16. Vongphanit J, Mitchell P, Wang JJ. Population prevalence of tilted optic disks and the relationship of this sign to refractive error. American journal of ophthalmology 2002;133:679-85.
17. Xu L, Li Y, Wang S, Wang Y, Wang Y, Jonas JB. Characteristics of highly myopic eyes: the Beijing Eye Study. Ophthalmology 2007;114:121-6.
18. Marsh-Tootle WL, Harb E, Hou W, et al. Optic Nerve Tilt, Crescent, Ovality, and Torsion in a Multi-Ethnic Cohort of Young Adults With and Without Myopia. Investigative ophthalmology & visual science 2017;58:3158-3171.
19. Rezapour J, Tran AQ, Bowd C, et al. Comparison of Optic Disc Ovality Index and Rotation Angle Measurements in Myopic Eyes Using Photography and OCT Based Techniques. Frontiers in medicine 2022;9:872658.
20. Rezapour J, Proudfoot JA, Bowd C, et al. Bruch Membrane Opening Detection Accuracy in Healthy Eyes and Eyes With Glaucoma With and Without Axial High Myopia in an American and Korean Cohort. American journal of ophthalmology 2022;237:221-234.

21. Wu J, Sebastian RT, Chu CJ, McGregor F, Dick AD, Liu L. Reduced Macular Vessel Density and Capillary Perfusion in Glaucoma Detected Using OCT Angiography. Current eye research 2019;44:533-540.
22. Moghimi S, Zangwill LM, Penteado RC, et al. Macular and Optic Nerve Head Vessel Density and Progressive Retinal Nerve Fiber Layer Loss in Glaucoma. Ophthalmology 2018;125:1720-1728.
23. Rezapour J, Bowd C, Dohleman J, et al. Macular thickness and vessel density in glaucoma eyes with and without high axial myopia. Investigative ophthalmology & visual science 2021;62:2431-2431.
24. Rezapour J, Walker E, Belghith A, et al. Diagnostic accuracy of optic nerve head and macula OCT parameters for detecting glaucoma in eyes with and without high axial myopia. American journal of ophthalmology 2024.
25. Rada JA, Shelton S, Norton TT. The sclera and myopia. Experimental eye research 2006;82:185-200.
26. Grytz R, Yang H, Hua Y, Samuels BC, Sigal IA. Connective tissue remodeling in myopia and its potential role in increasing risk of glaucoma. Current Opinion in Biomedical Engineering 2020;15:40-50.
27. Guo Y, Liu LJ, Xu L, et al. Optic Disc Ovality in Primary School Children in Beijing. Investigative ophthalmology & visual science 2015;56:4547-53.
28. Choi JA, Park HY, Shin HY, Park CK. Optic disc tilt direction determines the location of initial glaucomatous damage. Investigative ophthalmology & visual science 2014;55:4991-8.
29. How AC, Tan GS, Chan YH, et al. Population prevalence of tilted and torted optic discs among an adult Chinese population in Singapore: the Tanjong Pagar Study. Archives of ophthalmology (Chicago, Ill : 1960) 2009;127:894-9.
30. Takasaki H, Higashide T, Takeda H, Ohkubo S, Sugiyama K. Relationship between optic disc ovality and horizontal disc tilt in normal young subjects. Japanese journal of ophthalmology 2013;57:34-40.
31. Nakanishi H, Suda K, Yoshikawa M, et al. Association of Bruch's membrane opening and optic disc morphology to axial length and visual field defects in eyes with primary open-angle glaucoma. Graefe's archive for clinical and experimental ophthalmology = Albrecht von Graefes Archiv fur klinische und experimentelle Ophthalmologie 2018;256:599-610.
32. Zhao XJ, Jiang HY, Li YH, et al. Correlations between the optic nerve head morphology and ocular biometrics in highly myopic eyes. International journal of ophthalmology 2018;11:997-1001.
33. Tay E, Seah SK, Chan SP, et al. Optic disk ovality as an index of tilt and its relationship to myopia and perimetry. American journal of ophthalmology 2005;139:247-52.
34. Seol BR, Park KH, Jeoung JW. Optic Disc Tilt and Glaucoma Progression in Myopic Glaucoma: A Longitudinal Match-Pair Case-Control Study. Investigative ophthalmology & visual science 2019;60:2127-2133.
35. Nakanishi H, Akagi T, Hangai M, et al. Sensitivity and specificity for detecting early glaucoma in eyes with high myopia from normative database of macular ganglion cell complex thickness obtained from normal non-myopic or highly myopic Asian eyes. Graefe's archive for clinical and experimental ophthalmology = Albrecht von Graefes Archiv fur klinische und experimentelle Ophthalmologie 2015;253:1143-52.
36. Park HY, Choi SI, Choi JA, Park CK. Disc Torsion and Vertical Disc Tilt Are Related to Subfoveal Scleral Thickness in Open-Angle Glaucoma Patients With Myopia. Investigative ophthalmology & visual science 2015;56:4927-35.
37. Hosseini H, Nassiri N, Azarbod P, et al. Measurement of the optic disc vertical tilt angle with spectral-domain optical coherence tomography and influencing factors. American journal of ophthalmology 2013;156:737-44.
38. Dai Y, Jonas JB, Ling Z, Sun X. Ophthalmoscopic-Perspectively Distorted Optic Disc Diameters and Real Disc Diameters. Investigative ophthalmology & visual science 2015;56:7076-83.

39. Kim MJ, Lee EJ, Kim TW. Peripapillary retinal nerve fibre layer thickness profile in subjects with myopia measured using the Stratus optical coherence tomography. The British journal of ophthalmology 2010;94:115-20.
40. Vernon SA, Rotchford AP, Negi A, Ryatt S, Tattersal C. Peripapillary retinal nerve fibre layer thickness in highly myopic Caucasians as measured by Stratus optical coherence tomography. The British journal of ophthalmology 2008;92:1076-80.
41. Bowd C, Belghith A, Rezapour J, et al. Diagnostic Accuracy of Macular Thickness Map and Texture En Face Images for Detecting Glaucoma in Eyes With Axial High Myopia. American journal of ophthalmology 2022;242:26-35.
42. Curcio CA, Allen KA. Topography of ganglion cells in human retina. The Journal of comparative neurology 1990;300:5-25.
43. Yang Z, Tatham AJ, Weinreb RN, Medeiros FA, Liu T, Zangwill LM. Diagnostic ability of macular ganglion cell inner plexiform layer measurements in glaucoma using swept source and spectral domain optical coherence tomography. PloS one 2015;10:e0125957.
44. Shoji T, Sato H, Ishida M, Takeuchi M, Chihara E. Assessment of glaucomatous changes in subjects with high myopia using spectral domain optical coherence tomography. Investigative ophthalmology & visual science 2011;52:1098-102.
45. Shoji T, Nagaoka Y, Sato H, Chihara E. Impact of high myopia on the performance of SD-OCT parameters to detect glaucoma. Graefe's archive for clinical and experimental ophthalmology = Albrecht von Graefes Archiv fur klinische und experimentelle Ophthalmologie 2012;250:1843-9.
46. Kim NR, Lee ES, Seong GJ, et al. Comparing the ganglion cell complex and retinal nerve fibre layer measurements by Fourier domain OCT to detect glaucoma in high myopia. The British journal of ophthalmology 2011;95:1115-21.
47. Gupta P, Cheung CY, Saw SM, et al. Peripapillary choroidal thickness in young Asians with high myopia. Investigative ophthalmology & visual science 2015;56:1475-81.
48. Yang H, Luo H, Gardiner SK, et al. Factors Influencing Optical Coherence Tomography Peripapillary Choroidal Thickness: A Multicenter Study. Investigative ophthalmology & visual science 2019;60:795-806.
49. Flores-Moreno I, Lugo F, Duker JS, Ruiz-Moreno JM. The relationship between axial length and choroidal thickness in eyes with high myopia. American journal of ophthalmology 2013;155:314-319 e1.
50. Ikuno Y, Tano Y. Retinal and choroidal biometry in highly myopic eyes with spectral-domain optical coherence tomography. Investigative ophthalmology & visual science 2009;50:3876-80.
51. Yang D, Cao D, Zhang L, et al. Macular and peripapillary vessel density in myopic eyes of young Chinese adults. Clinical & experimental optometry 2020;103:830-837.
52. Ho M, Liu DT, Chan VC, Lam DS. Choroidal thickness measurement in myopic eyes by enhanced depth optical coherence tomography. Ophthalmology 2013;120:1909-14.
53. Harb E, Hyman L, Gwiazda J, et al. Choroidal Thickness Profiles in Myopic Eyes of Young Adults in the Correction of Myopia Evaluation Trial Cohort. American journal of ophthalmology 2015;160:62-71 e2.
54. Hirooka K, Tenkumo K, Fujiwara A, Baba T, Sato S, Shiraga F. Evaluation of peripapillary choroidal thickness in patients with normal-tension glaucoma. BMC ophthalmology 2012;12:29.
55. Tanabe H, Ito Y, Terasaki H. Choroid is thinner in inferior region of optic disks of normal eyes. Retina (Philadelphia, Pa) 2012;32:134-9.
56. Leung CK, Mohamed S, Leung KS, et al. Retinal nerve fiber layer measurements in myopia: An optical coherence tomography study. Investigative ophthalmology & visual science 2006;47:5171-6.
57. Leung CK, Yu M, Weinreb RN, et al. Retinal nerve fiber layer imaging with spectral-domain optical coherence tomography: interpreting the RNFL maps in healthy myopic eyes. Investigative ophthalmology & visual science 2012;53:7194-200.
58. Kang SH, Hong SW, Im SK, Lee SH, Ahn MD. Effect of myopia on the thickness of the retinal nerve fiber layer measured by Cirrus HD optical coherence tomography. Investigative ophthalmology & visual science 2010;51:4075-83.

59. Sawada Y, Araie M, Shibata H, Ishikawa M, Iwata T, Yoshitomi T. Differences in Retinal Nerve Fiber Layer Thickness as Assessed on the Disc Center and Bruch's Membrane Opening Center in Myopic Eyes. Ophthalmology Glaucoma 2019;2:145-155.
60. Chauhan BC, O'Leary N, AlMobarak FA, et al. Enhanced detection of open-angle glaucoma with an anatomically accurate optical coherence tomography-derived neuroretinal rim parameter. Ophthalmology 2013;120:535-543.
61. Zheng F, Wu Z, Leung CKS. Detection of Bruch's Membrane Opening in Healthy Individuals and Glaucoma Patients with and without High Myopia. Ophthalmology 2018;125:1537-1546.
62. Jeoung JW, Yang H, Gardiner S, et al. Optical Coherence Tomography Optic Nerve Head Morphology in Myopia I: Implications of Anterior Scleral Canal Opening Versus Bruch Membrane Opening Offset. American journal of ophthalmology 2020;218:105-119.
63. Reis AS, Sharpe GP, Yang H, Nicolela MT, Burgoyne CF, Chauhan BC. Optic disc margin anatomy in patients with glaucoma and normal controls with spectral domain optical coherence tomography. Ophthalmology 2012;119:738-47.
64. Guo X, Chen X, Li M, Li S, You R, Wang Y. Association between morphological characteristics of the optic disc and other anatomical features of the fundus in highly myopic eyes. European journal of ophthalmology 2021;31:2329-2338.
65. Choi YJ, Jeoung JW, Park KH, Kim DM. Glaucoma detection ability of ganglion cell-inner plexiform layer thickness by spectral-domain optical coherence tomography in high myopia. Investigative ophthalmology & visual science 2013;54:2296-304.
66. Kim HJ, Park KH, Kim YK, Jeoung JW. Evaluation of Layer-by-Layer Segmented Ganglion Cell Complex Thickness for Detecting Early Glaucoma According to Different Macular Grids. Journal of glaucoma 2017;26:712-717.
67. Xu XY, Xiao H, Luo JY, Liu X. Evaluation of spectral domain optical coherence tomography parameters in discriminating preperimetric glaucoma from high myopia. International journal of ophthalmology 2019;12:58-65.

6. Abkürzungsverzeichnis

AL	Achsenlänge
AUC	*engl.* Area under the curve
BMB	*engl.* Bruch's membane boundary
BMO	Bruch'sche Membranöffnung *engl.* Buch's membrane opening
BMO-MRW	Bruch'sche Membranöffnung – minimale Randsaumweite, *engl.* Bruch's membrane opening minimum rim width
D	Dioptrien
GCC	Ganglienzellkomplex, *engl.* ganglion cell complex
GCIPL	innere plexiforme Schicht der Gaglienzellen, *engl.* ganglion cell inner plexiform layer
OCT	Optische Kohärenztomographie
OCTA	Optische Kohärenztomographie-Angiographie
POWG	Primäres Offenwinkelglaukom
PPA	peripapilläre Atrophiezone
mRNFL	makuläre retinale Nervenfaserschicht
pRNFL	peripapilläre retinale Nervenfaserschicht
RNFL	retinale Nervenfaserschicht, *engl.* Retinal nerve fiber layer
ROC	*engl.* Receiver operating characteristic
SALSA	San Diego Automated Layer Segmentation Algorithm
SÄ	Sphärisches Äquivalent
VFMD	*engl.* visual field mean deviation
vs.	im Vergleich zu, *engl.* versus

7. Abbildungsverzeichnis

8. Danksagung

Im Folgenden möchte ich die Gelegenheit nutzen, mich bei allen Menschen zu bedanken, die mich in den letzten Jahren auf meinem beruflichen Weg begleitet und maßgeblich dazu beigetragen haben, dass diese Arbeit entstehen konnte.

Mein aufrichtiger Dank gilt folgenden Personen:

Herzlich bedanken möchte ich mich bei Herrn Professor Dr. Norbert Pfeiffer, der mich von Beginn an in meiner klinischen und wissenschaftlichen Tätigkeit motiviert und unterstützt hat und mir über all die Jahre immer beratend zur Seite stand. Sein Vertrauen ermöglichte mir einen zweijährigen Forschungsaufenthalt in San Diego, Kalifornien und seiner Expertise verdanke ich die Förderung dieses Projektes durch die Deutsche Forschungsgemeinschaft. Nicht zuletzt wäre mein Habilitationsvorhaben ohne seine uneingeschränkte Unterstützung nicht möglich gewesen.

Mein ganz besonderer Dank gilt Professorin Dr. Esther Hoffmann, die meinem Forschungsvorhaben stehts offen gegenüberstand und früh den Anstoß gab, meine wissenschaftliche Arbeit im Rahmen eines DFG-geförderten Forschungsaufenthaltes im Ausland fortzusetzen. Dank ihrer Unterstützung und ihres wertvollen Inputs konnte dieses Forschungsprojekt am Hamilton Glaucoma Center in San Diego unter der Leitung von Professorin Dr. Linda Zangwill verwirklich werden. Ihre langjährige Unterstützung ehrt und motiviert mich sehr auf meinem beruflichen Weg.

In diesem Zusammenhang möchte ich auch Professorin Dr. Linda Zangwill herzlich danken, die mein DFG-Forschungsprojekts am Hamilton Glaucoma Center in San Diego betreut hat. Sie zeigte von Beginn an großes Interesse an diesem Projekt und stand mir sowohl wissenschaftlich als auch persönlich immer beratend zur Seite und förderte meine wissenschaftliche Entwicklung. Insbesondere während der Covid-

Pandemie ist es ihrem unermüdlichen Einsatz zu verdanken, dass dieses Projekt fortgeführt werden konnte.

Mein Dank gilt auch Frau Professorin Dr. Dr. Monika Daubländer, die mich beim Erstellen der Habilitationsschrift stets motiviert hat und mir mit wertvollen Ratschlägen beratend zur Seite stand.

Die Finalisierung meiner Habilitation wäre ohne die Unterstützung meiner Familie und Freunde nicht möglich gewesen, die mir neben der intensiven Arbeit stets einen privaten Ausgleich boten.

Mein aufrichtiger Dank gilt meinem Vater, Herrn Dr. Hamid Rezapour, der mir in allen Lebenslagen sowohl beruflich als auch persönlich immer beratend zur Seite stand. Ihm verdanke ich meinen Ehrgeiz und mein Durchhaltevermögen. Ich möchte mich auch besonders bei meiner Mutter Sedigheh Maadi Roodsari und meiner Schwester, Sophie Rezapour, für Ihre Unterstützung und Begleitung bedanken.

Insbesondere Meinem Ehemann Herrn Dr. Sören Reinhard, möchte ich für das Vertrauen, die Motivation und Unterstützung meiner wissenschaftlichen Arbeit über viele Jahre danken. Zu keinem Zeitpunkt sah er meine beruflichen Ambitionen in Konkurrenz zu unserer persönlichen Beziehung, was mir ein unabhängiges Arbeiten in den USA trotz langjähriger Fernbeziehung sowohl in den USA, als auch in Deutschland, ermöglichte. Für sein Verständnis, seine Geduld und seine Hilfe danke ich ihm von Herzen.

Damit findet ein langjähriges Forschungsprojekt seinen vorläufigen Abschluss.

Mainz, im Oktober 2024

Dr. med. Jasmin Rezapour